Étude du comportement mécanique et de l'endommagement de divers matériaux composites smc soumis à des chargements de type dynamique, fatigue et dynamique post-fatigue

Mohammadali Shirinbayan

ParisTech
INSTITUT DES SCIENCES ET TECHNOLOGIES
PARIS INSTITUTE OF TECHNOLOGY

ARTS ET MÉTIERS ParisTech

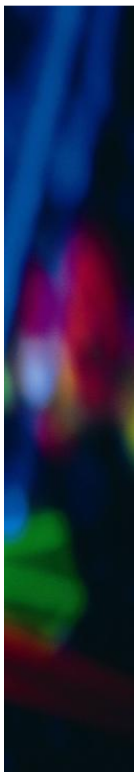

2017-ENAM-0013

École doctorale n° 432 : Sciences des Métiers de l'Ingénieur

Doctorat ParisTech

T H È S E

pour obtenir le grade de docteur délivré par

l'École Nationale Supérieure d'Arts et Métiers

Spécialité "Mécanique et Matériaux"

présentée et soutenue publiquement par

Mohammadali SHIRINBAYAN

le 04 Avril 2017

ÉTUDE DU COMPORTEMENT MÉCANIQUE ET DE L'ENDOMMAGEMENT DE DIVERS MATÉRIAUX COMPOSITES SMC SOUMIS À DES CHARGEMENTS DE TYPE DYNAMIQUE, FATIGUE ET DYNAMIQUE POST-FATIGUE

Directeur de thèse :	**Abbas**	**TCHARKHTCHI**
Co-encadrement de la thèse :	**Joseph**	**FITOUSSI**
Co-encadrement de la thèse :	**Fodil**	**MERAGHNI**

Jury

M. Jacques RENARD, Professeur, Centre des Matériaux, Mines ParisTech	Président
M. Nadia BAHLOULI, Professeur, MMB, Université de Strasbourg	Rapporteur
M. Patrick ROZYCKI, Maître de Conférences (HDR), GeM, Ecole Centrale de Nantes	Rapporteur
M. Zouhaier JENDLI, Maître de Conférences, ESTACA	Examinateur
M. Benjamin SUROWIEC, Docteur, Auto Exterior Division, Plastic Omnium	Examinateur
M. Michel BOCQUET, Professeur, PIMM, Arts et Métiers ParisTech	Invité
M. Abbas TCHARKHTCHI, Professeur, PIMM, Arts et Métiers ParisTech	Examinateur
M. Joseph FITOUSSI, Maître de Conférences, PIMM, Arts et Métiers ParisTech	Examinateur
M. Fodil MERAGHNI, Professeur, LEM3, Arts et Métiers ParisTech - Metz	Examinateur

T H È S E

Arts et Métiers ParisTech - Centre de Paris
PIMM - Procédés et Ingénierie en Mécanique et Matériaux

À Golrokh et Meïgol

En souvenir de mon père

REMERCIEMENTS

Ce travail de thèse est réalisé pour et en collaboration avec le centre de recherche et de développement Sigmatech de Plastic Omnium. Ce travail s'est déroulé au sein du PIMM du Campus ENSAM de Paris avec la participation active du LEM3 du Campus ENSAM de Metz.

J'exprime ma grande reconnaissance et mes sincères remerciements à mon directeur de thèse, Monsieur Abbas TCHARKHTCHI, Professeur aux Arts et Métiers ParisTech-Paris ainsi qu'à mes co-directeurs Monsieur Joseph FITOUSSI, Maître de conférences aux Arts et Métiers ParisTech-Paris et Monsieur Fodil MERAGHNI, Professeur aux Arts et Métiers ParisTech-Metz, pour leur disponibilité, leur excellent encadrement, leur dévouement ainsi que leurs conseils avisés qu'ils m'ont prodigués tout au long de ce travail.

Je souhaite également et vivement remercier Monsieur Benjamin SUROWIEC, encadrant industriel à l'origine de ce projet, pour la confiance qu'il m'a accordée dès le début pour mener à bien cette étude passionnante.

Mes remerciements s'adressent aussi à l'ensemble des membres du jury qui ont accepté de juger ce travail de thèse. Je remercie particulièrement Monsieur Jacques RENARD d'avoir accepté de présider ce jury. Merci également à Madame Nadia BAHLOULI et Monsieur Patrick ROZYCKI pour avoir rapporté ces travaux de thèse. Enfin un grand merci à Monsieur Zouhaier JENDLI pour avoir examiné ce travail. Je tiens à vous remercier pour les échanges pertinents et constructifs tenus lors de la soutenance.

Mes remerciements vont aussi à Madame Sedigheh FARZANEH et Monsieur Michel BOCQUET pour leur aide dans les différentes étapes de ce travail. Je leur dit un grand merci pour leurs encouragements et leur soutien ainsi que pour les précieux conseils qu'ils m'ont donnés.

Merci aussi à Monsieur Gilles REGNIER, directeur, et à son adjoint Monsieur Frédéric VALES de m'avoir accueilli au sein de leur laboratoire des Procédés et Ingénierie en Mécanique et Matériaux (PIMM) des Arts et Métiers ParisTech - Paris.

Je ne pourrais oublier de remercier tous les membres du laboratoire PIMM, laboratoire où j'ai réalisé principalement mes travaux de recherche, pour tous les bons moments passés avec vous pendant

ces trois années. En particulier, je tiens à remercier Messieurs Albert LUCAS et Paulo FERREIRA pour leur aide et leur disponibilité.

Je voudrais remercier ma famille : mes beaux-parents, mes sœurs et mes frères, pour m'avoir toujours soutenu.

Je voudrais adresser un remerciement tout particulier à mes parents, Iran et Abbas : je n'oublierai jamais le soutien que vous m'avez apportez pendant toute ma vie.

Je finis cette longue liste en remerciant mon épouse Golrokh pour sa patience inaltérable et son soutien indéfectible.

Merci ma jolie fille, Meïgol !

SOMMAIRE

TABLE DES FIGURES

Introduction générale

La recherche d'une sécurité accrue dans les véhicules automobiles est devenue une préoccupation sociétale et scientifique à la fois pour les fabricants et pour les utilisateurs. Dans la pratique, pour mieux protéger les occupants d'une automobile lors d'un accident, des essais de collision doivent être effectués en laboratoire afin d'étudier le comportement des structures lors d'un impact réel. Par ailleurs, on peut noter que les équipements automobiles ne sont pas toujours en bon état. En fait, dans de nombreuses applications et tout particulièrement dans ce secteur, les véhicules et les matériaux constitutifs sont soumis à des vibrations mécaniques induisant une dégradation progressive des performances nominales (dégradation principalement liées à des vibrations dues au revêtement des routes, plus rarement à des dos d'âne, nid de poule etc.). Un essai de fatigue peut alors être considéré comme une « simple » application d'un chargement cyclique sur un échantillon. Par la suite, il s'agira de corréler les informations recueillies en laboratoire à celles obtenues dans des conditions similaires lors d'une utilisation réelle. Finalement, une combinaison optimale entre structure et matière, associée à une connaissance du comportement couplé en fatigue-dynamique rapide s'avère nécessaire.

Dans le cadre de ce travail, l'étude du comportement est définie par une analyse permettant la caractérisation mécanique du matériau sur une gamme de vitesse allant du régime quasi-statique jusqu'au régime dynamique moyen. Nous considèrerons, dans ce qui suit, comme vitesses moyennes ou vitesses intermédiaires, les vitesses comprises entre celles relativement lentes, dites quasi-statiques et appliquées à l'échelle de la minute, et celles rapides appliquées à l'échelle de la milliseconde ; le phénomène de dynamique rapide se situe typiquement dans cette catégorie.

Également, en raison de leur forte capacité d'absorption en énergie, les SMC sont d'un emploi intéressant pour les structures automobiles surtout lorsqu'elles sont soumises malencontreusement à des accidents de type collision. Les matériaux utilisés pour cette étude sont des composites à renforts discontinus de type Sheet Molding Compounds (SMC) et dont la microstructure est particulière. Il s'agit de matériaux désignés comme : Advanced Sheet Molding Compounds (A-SMC) et Low Density SMC (LD-SMC). Ces deux matériaux sont mis en œuvre et fournis par notre partenaire industriel PLASTIC OMNIUM Auto Extérieur Services (PO). Les Sheet Molding Compounds (SMC) sont des pré-imprégnés

(semi-produits) thermodurcissables renforcés par des fibres ou des mèches de fibres courtes ou discontinues, mis en œuvre par un procédé de thermo-compression. Récemment, un nouveau composite qualifié d'Advanced SMC (A-SMC) a été développé par Plastic Omnium. Il s'agit d'un matériau innovant pour certaines composantes automobiles telles que les nouvelles générations de hayon ou le nouveau module de plancher avant d'automobile. Les résines vinylester utilisées pour l'Advanced SMC (A-SMC) présentent de nombreuses caractéristiques intéressantes à la fois désirées et attendues : des propriétés mécaniques comparables à celles de l'époxy, une excellente résistance chimique, une bonne résistance à la traction ainsi que des coûts très compétitifs.

Actuellement, la tendance est de réduire le poids des composants utilisés dans les véhicules (questions d'économie d'énergie et de pollution). Cette problématique d'allégement est primordiale pour l'emploi des composites dans l'industrie automobile. Elle se doit donc de répondre à deux critères : réduire les coûts et maintenir des performances conformes aux exigences. Dans ce sens, l'emploi de billes de verre creuses (en plus des fibres), non seulement réduit le poids des SMC, mais fournit un moulage plus précis, une plus grande stabilité dimensionnelle et améliore la résistance aux déformations d'origine thermique.

Le présent travail de thèse est une contribution à l'analyse expérimentale de la fatigue, du comportement dynamique rapide et du couplage fatigue/dynamique rapide des composites SMC. Dans le cas de la tenue en fatigue, il est important de tenir compte de divers paramètres influents comme l'orientation des fibres, la température d'essai, la fréquence et de son éventuelle implication dans des phénomènes d'auto-échauffement liés au caractère viscoélastique de la matrice et de l'interface fibre-matrice. A notre connaissance, on peut noter qu'une telle étude sur l'effet couplé de la fréquence de chargement et de son amplitude n'a jamais été abordée pour les SMC et encore moins pour les A-SMC.

Le comportement mécanique des composites SMC est sensible à la vitesse à laquelle ils sont sollicités. Par conséquent, pour une utilisation efficace de ces composites, leur réponse sous différentes vitesses de déformation doit être clairement connue et maitrisée. Au cours des essais à grande vitesse, le composite est généralement soumis initialement à des accélérations importantes. En effet, avant d'atteindre un régime stabilisé (vitesse constante), des phénomènes transitoires du type inertiel et de propagation d'ondes se produisent au sein des matériaux et des structures. Ces phénomènes transitoires,

caractérisés par des variations spatio-temporelles des champs de contrainte et de déformation non homogènes, rendent l'analyse plus difficile. Il sera donc nécessaire de minimiser en termes d'amplitude et de durée cette phase transitoire.

En accord avec les industriels et pour être représentatif des différents types de collisions routières en termes de sollicitation (traction, compression), de vitesse et de durée de vie (fatigue) d'un véhicule, nous ne retiendrons, pour les essais en laboratoire, qu'une configuration de test dont la vitesse de sollicitation est comprise dans la gamme 10^{-3} - 80 s^{-1}. Ainsi, pour une meilleure prédiction du comportement du composite SMC lors d'un accident, des études sur la réponse de la matière pré-endommagée par fatigue, puis soumise à des chargements à différentes vitesses sont nécessaires.

Contrairement aux matériaux métalliques pour lesquels l'absorption d'énergie est assurée par déformation plastique ; les structures en composites SMC font appel à plusieurs mécanismes d'endommagement diffus et progressifs qui se produisent à l'échelle locale, comme des microfissures dans la matrice, des ruptures de fibre, des décohésions à l'interface fibre-matrice et du délaminage ou du pseudo-délaminage. De plus, plusieurs études antérieures ont montré que la capacité d'absorption de l'énergie des polymères et des matériaux composites est fortement dépendante des paramètres de la microstructure comme la teneur en fibres, leur orientation et leur longueur ainsi que du type de matrice. Malgré tout, le matériau doit posséder une certaine résistance aux chocs (énergie modérée : lors d'un stationnement par exemple) pour ne pas faire apparaître des lésions locales irréversibles. Dans le cas d'une collision plus violente et pour favoriser un développement d'endommagement diffus, une bonne connaissance et une compréhension des mécanismes d'endommagement, susceptibles de se produire lors d'un chargement important à vitesse de déformation élevée, sont nécessaires. Une non-prise en compte de cette influence de la vitesse de chargement élevée sur les mécanismes d'endommagement locaux pourrait conduire à une conception incomplète et non optimale de la structure. Elle négligerait un aspect important de l'absorption de l'énergie de choc et par conséquent elle serait préjudiciable à la sécurité des passagers du véhicule, à l'optimisation des coûts ainsi qu'à la réduction d'émission de gaz à effet de serre. Le choix des lois de comportement des matériaux utilisées dans les calculs par éléments finis lors de la conception, l'influence des paramètres de la microstructure et de la vitesse de déformation sur le seuil et la cinétique des endommagements sont d'une importance primordiale.

Ce travail est réalisé pour et en collaboration avec le centre de recherche et de développement Sigmatech de Plastic Omnium. Il a été réalisé au sein du PIMM du Campus ENSAM de Paris avec la participation active du LEM3 du Campus ENSAM de Metz.

Le manuscrit est divisé en deux parties : le résumé étendu en français (Partie I) ; puis les articles publiés ou en cours de publication dans des revues internationales de rang A en anglais (Partie II). L'organisation des différentes parties du résumé étendu respecte la démarche suivante :

- **U**ne description des matériaux composites SMC standards, A-SMC et LD-SMC et de leur comportement mécanique notamment vis à vis de l'endommagement,
- **L'**analyse expérimentale du comportement en fatigue des matériaux,
- **L'**étude de l'effet de la vitesse de déformation sur le comportement mécanique des composites SMC étudiés. Une analyse multi-échelle de l'endommagement y est systématiquement proposée.
- **U**ne investigation expérimentale des propriétés dynamiques post-essais de fatigue du matériau A-SMC.

Ci-après la liste des articles publiés lors de cette étude ou en cours de publication. Ils sont cités dans le texte sous la forme de « Article N°-- ».

Article N°1: Shirinbayan M, Fitoussi J, Meraghni F, Surowiec B, Bocquet M, Tcharkhtchi A. High strain rate visco-damageable behavior of Advanced Sheet Molding Compound (A-SMC) under tension. Composites Part B: Engineering. 2015; 3670(82): 30-41.

Article N°2: Shirinbayan M, Fitoussi J, Bocquet M, Meraghni F, Surowiec B, Tcharkhtchi A. Multi-scale experimental investigation of the viscous nature of damage in Advanced Sheet Molding Compound (A-SMC) submitted to high strain rates. Composites Part B: Engineering. 2016.

Article N°3: Shirinbayan M, Fitoussi J, Meraghni F, Surowiec B, Laribi M, Tcharkhtchi A. Coupled effect of loading frequency and amplitude on the fatigue behavior of advanced sheet molding compound (A-SMC). Journal of Reinforced Plastics and Composites. 2017; 36(4): 271-82.

Article N°4: Shirinbayan M, Fitoussi J, Abbasnezhad N, Meraghni F, Surowiec B, Tcharkhtchi A. Mechanical characterization of a Low Density Sheet Molding Compound (LD-SMC): Multi-scale damage analysis and strain rate effect. Composites Part B: Engineering. 2017.

Article N°5: Shirinbayan M, Fitoussi J, Meraghni F, Farzaneh S, Surowiec B, Tcharkhtchi A. Post-fatigue residual dynamic behavior of advanced-SMC composites. Article in progress.

1. Matériaux SMC (Sheet Molding Compound) : procédé-microstructure-propriétés mécaniques

Les composites SMC font l'objet de la présente étude. Ils sont utilisés pour diverses applications dans l'industrie automobile, notamment pour des pièces de structure comme les absorbeurs avant et arrière, les pare-chocs, les boucliers, mais aussi comme des pièces de structure et d'habillage telles que les bandeaux latéraux, capots moteur, hayons, custodes, plancher et calandres [1–6].

Ce chapitre est consacré à une description du matériau composite SMC : son procédé d'élaboration, ses différentes familles et ses relations procédé-microstructure-propriétés mécaniques. Ensuite, les mécanismes d'endommagement à différents types de sollicitations seront présentés.

1.1. Composition du composites SMC : Matrice, Renforts et Charges

Les composites SMC sont constitués de trois phases : la résine, les charges minérales et les renforts fibreux. Quelques additifs sont rajoutés afin de faciliter la mise en œuvre.

1.1.1. La matrice

Les résines thermodurcissables ont des propriétés mécaniques élevées. Les matrices utilisées pour les composite SMC sont essentiellement des résines polyester ou vinylester. A ce composant essentiel, on rajoute des charges et des additifs dans le but d'améliorer les caractéristiques mécaniques et physico-chimiques de la matrice [4].

1.1.2. Le renfort

Les renforts utilisés pour les SMC étudiés sont des fibres de verre assemblées sous forme de mèche contenant de l'ordre de 200 fibres ayant un diamètre de 15 µm de et une longueur de 25 mm en moyenne [7]. Il existe par ailleurs, des composites SMC à renforts de carbone récemment développés par notre partenaire (PO) pour des applications fatigue.

1.1.3. Les charges, adjuvants et additifs

De forts taux de charges minérales sont introduits afin d'augmenter la rigidité et la viscosité. Ces charges ont aussi pour objectif de réduire les coûts tout en gardant une tenue mécanique optimale. Les particules de carbonate de calcium (craie) ou de silicate de magnésium (talc) sont en général utilisées. Des billes de verre creuses sont parfois ajoutées à la pâte de SMC pour diminuer le poids volumique [8-10]. Des adjuvants et additifs facilitent également le façonnage du composite ainsi que son moulage. Ils permettent aussi d'améliorer son aspect extérieur ainsi que sa protection vis-à-vis de la photo-oxydation. On peut rajouter également d'autres éléments d'addition comme des : lubrifiants, agents de démoulage, stabilisants, agents anti-retrait, pigments et colorants [4,6,11].

1.2. Procédé d'élaboration des SMC

Le procédé d'élaboration des SMC consiste à fabriquer des semi-produits sous forme de feuilles continues composées d'une pâte épaissie et non polymérisée dans laquelle sont dispersées et imprégnées des fibres ou des mèches de fibres [4,11,12].

1.2.1. Mélange de la matrice (pâte mère) et élaboration des feuilles pré-mix

Généralement, la matrice est mélangée dans au moins deux malaxeurs distincts alimentés de façon continue (figure 1) par les matières premières : la résine, les charges minérales (généralement constituées de particules de $CaCO_3$) et les additifs. Lorsque l'homogénéité des mélanges est atteinte dans chacun des deux malaxeurs, l'ensemble est combiné en ligne pour former une pâte [4].

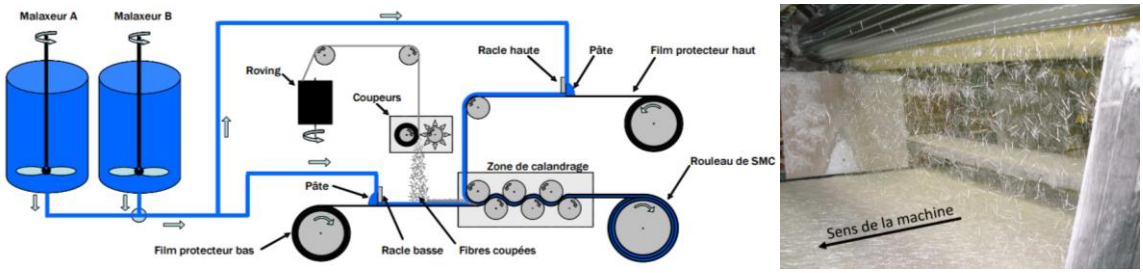

Figure 1 Schéma simplifié d'une ligne de production SMC classique.

1.2.2. Elaboration du pré-imprégné

La pâte est appliquée sur des films de protection (en polyéthylène), imperméables et déroulés en continu au-dessus et en dessous du mélange matrice, décrit plus haut. Les fibres ou les mèches de fibres tombent ensuite sur la pâte qui avance sur un tapis roulant de façon à former un mat sec de fibres. Cette étape contrôle l'agencement des fibres sur la pâte. Elle est primordiale et doit être effectuée avec minutie car elle détermine en grande partie l'architecture du renfort fibreux des futures feuilles SMC avant leur mise en forme.

1.3. Mise en forme par compression des SMC

La seconde étape de la fabrication du composite consiste à le mouler sur une presse à chaud (figure 2). Cette opération se déroule sous une température de l'ordre de 150°C et une pression moyenne de 100 à 120 bars. Ces conditions permettent de fluidifier la matrice et facilitent l'écoulement et la mise en place (orientation) des renforts. Cette étape dure de 2 à 3 minutes [13-25].

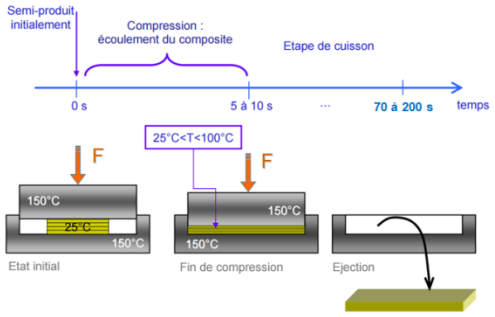

Figure 2 Moulage et mise en forme du SMC composite.

1.4. Les différentes familles de composites SMC

1.4.1. SMC standard

La matrice utilisée pour le composite SMC standard est généralement composée d'une résine polyester chargée de particules de carbonate de calcium ($CaCO_3$). Il est constitué 50% en masse de la pâte mère. Le SMC standard est renforcé par des mèches de fibres de verre discontinues d'une longueur

de l'ordre de 25 mm (30% en masse du composite). La masse volumique du composite est de l'ordre de 1,88 g/cm^3 [4,11]

1.4.2. SMC haut performance (A-SMC)

Le A-SMC, ou Advanced SMC, est un SMC à base de résine vinylester permettant l'imprégnation d'un taux élevé en fibres de verre (> 50% de la masse), ce qui permet d'obtenir de hautes performances mécaniques [26,27].

1.4.3. SMC basse densité (LD-SMC)

Cette classe de SMC a été développée pour répondre à un besoin croissant en termes de réduction de poids sur les véhicules. Les SMC basse densité (LD-SMC : Low Density SMC) ont été développés en y introduisant des billes de verre creuses afin de réduire la masse des pièces de structure [28]. On peut alors atteindre des masses volumiques de l'ordre de 1,22 g/cm^3 soit 30% inférieures à celle d'un SMC standard.

1.4.4. SMC étudiés

Pour cette étude, deux types de classe de composites SMC ont été étudiés : A-SMC et LD-SMC. Les deux SMC ont été fournis par PLASTIC OMNIUM Auto Extérieur Services. Deux configurations de renfort ont été investiguées : Orientation Aléatoire (Randomly Oriented - RO) et à forte Orientation (Highly Oriented - HO). Les plaques de SMC HO ont été obtenues en disposant une charge de pré-imprégné composite dans la partie gauche d'un moule rectangulaire (30 x 40 cm^2) ce qui permet un fort fluage lors de la phase de thermo-compression. Cette phase conduit à une forte orientation des renforts.

Les plaques RO ont été obtenues sans orientation particulière des fibres en remplissant complètement le moule avant thermo-compression de façon globalement uniforme.

1.5. Relations procédé-microstructure-propriétés mécaniques

Le comportement mécanique et l'endommagement des composites SMC est directement dépendant et gouverné par la microstructure, qui pour cette dernière est le produit du choix d'une

formulation et de paramètres procédé [4,11,12,24,25]. Il est donc important, si l'on veut maîtriser le dimensionnement des structures, de comprendre les relations existant entre le procédé d'élaboration, les microstructures et le comportement mécanique des matériaux SMC.

1.5.1. Microstructures des SMC

Les observations microscopiques et l'analyse d'image ont été réalisées d'une part, à l'aide d'un microscope électronique à balayage (HITACHI 4800 SEM) et d'autre part par micro-tomographie à rayons X (EasyTom nano setup). La première méthode donne accès à des images 2D alors que la seconde permet de visualiser l'intérieur de la structure en 3D. Par ailleurs, une méthode ultrasonore originale a été développée et permet de déterminer rapidement une éventuelle anisotropie [28] en mettant en évidence les orientations privilégiées des renforts au sein du matériau. Cette méthode est décrite dans l'article N°4.

La figure 3 montre des résultats typiques de ces trois méthodes de caractérisations de la microstructure pour les deux des composites SMC (A-SMC et LD-SMC) de notre étude.

Analyse de la microstructure			
MEB	Micro-tomographie	Ultrasonore	
		Plaque RO	Plaque HO
Le composite A-SMC			
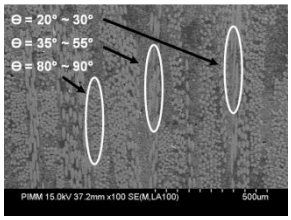	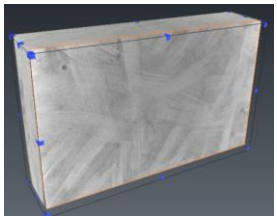	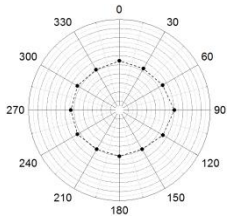	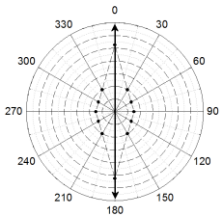
Le composite LD-SMC			
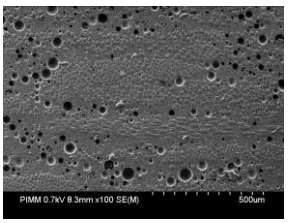	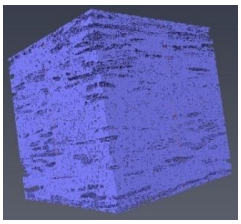	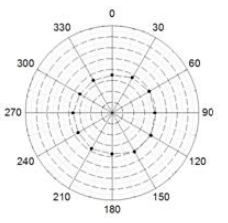	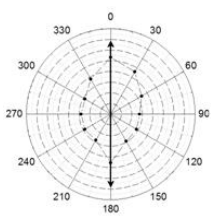

Figure 3 Résultats des analyses de la microstructure [26-28].

Les renforts de fibres de verre de longueur constante et égale à 25 mm apparaissent clairement sous forme d'une stratification locale de mèches unidirectionnelles à orientation variable. Chacune d'entre-elles contient environ 200 à 250 fibres de verre ayant un diamètre de l'ordre de 15 µm. A une certaine échelle, on peut donc définir les composites SMC comme des pseudo-stratifiés. Cet aspect de pseudo-empilement pourra expliquer un des modes d'endommagement de ces matériaux (pseudo-délaminage) ; cet aspect sera discuté ultérieurement. Par ailleurs, les diagrammes polaires de vitesses des ondes ultrasonores en fonction de l'angle d'orientation de l'échantillon montrent clairement une anisotropie du matériau dans le cas des plaques ayant subi un fluage lors de la mise en forme (HO).

L'axe principal de la courbe polaire indique la direction privilégiée des renforts et sa forme plus ou moins allongée indique une orientation des renforts plus ou moins marquée. Cette dernière est d'ailleurs caractérisée par un coefficient dit de «biréfringence acoustique» [28]. Dans le cas de la plaque RO, le diagramme polaire presque circulaire indique que les fibres sont orientées de manière quasi-aléatoire dans l'échantillon. On peut noter par ailleurs que les différentes phases (résine, renforts et billes creuses) sont réparties de façon macroscopiquement homogène, même si localement, on peut trouver des zones appauvries en renforts par endroits, surtout pour les SMC de type standard ou à faible densité (Article N°4).

1.5.2. Propriétés physico-chimiques et mécaniques

Afin d'évaluer les principales températures de transitions, des tests thermomécaniques (DMTA) ont été réalisés (uniquement sur des échantillons RO) en utilisant l'équipement DMA Q800, de la Société TA. Les tests ont été réalisés dans les conditions suivantes: fréquence de 1 Hz, variation de température de -100°C à 250°C avec une vitesse de montée en température de 2°C/min [26-28]. Par ailleurs, des essais de traction à basse vitesse (quasi-statique) ont été réalisés sur une machine hydraulique MTS 830 sur les deux SMC de l'étude mettant en évidence un comportement de type bilinéaire bien connu pour les SMC [11]. Un tableau récapitulatif regroupe les principales caractéristiques des deux SMC de notre étude ainsi que celles de composite standard issu de la littérature. On peut déjà conclure de façon évidente que la distribution d'orientation des renforts influence fortement les propriétés mécaniques des matériaux SMC (tableau 1).

Comportement mécanique en traction uni-axiale

Composite		'E' (GPa)	'σ_{seuil}' (MPa)	'ε_{seuil}' (%)	'σ_{ultime}' (MPa)	'ε_{ultime}' (%)	T_α (°C)	T_β (°C)
SMC standard [11]		11.3	22	~ 0,24	67	1.20	-	-
A-SMC	HO-0°	~ 18.5	-	-	-	-	-	-
	RO	~ 14.5	-	-	-	-	130°C	45°C
	HO-90°	~ 12	-	-	-	-	-	-
LD-SMC	HO-0°	~ 12	-	-	-	-	-	-
	RO	~ 10	-	-	-	-	60°C	Inexistante
	HO-90°	~ 9	-	-	-	-	-	-

Tableau 1 Propriétés mécaniques des A-SMC et LD-SMC en traction uni-axiale [26–28].

1.5.3. Influence de la température

Les résultats de traction quasi-statique à différentes températures (20°C, 80°C et 135°C) pour A-SMC composite sont présentés à la figure 4.

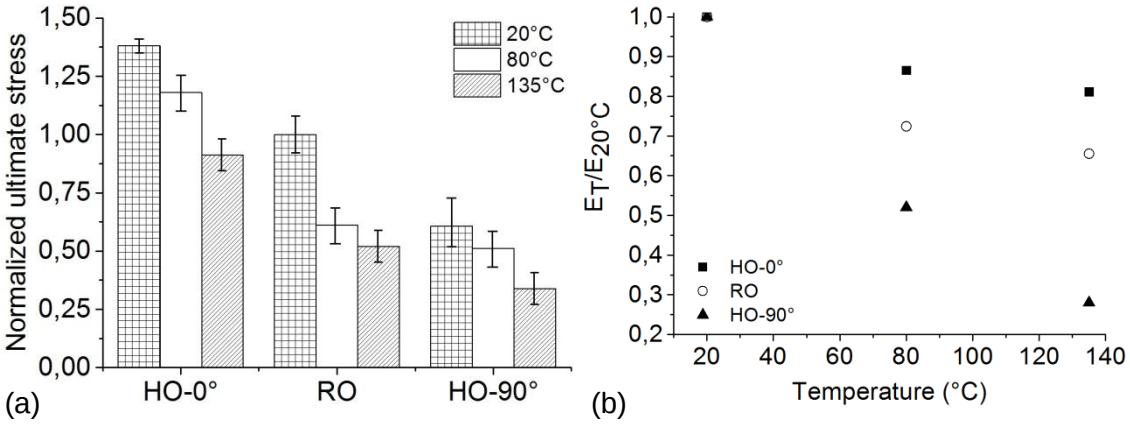

Figure 4 σ_{ultime} des échantillons HO-0°, RO et HO-90° à 20°C, 80°C et 135°C (a), et évolutions du E relatif à différentes températures (b), ($\sigma_{r(normalisée)} = \sigma_r / \sigma_{r(RO) \text{ à } 20°C}$).

L'analyse des résultats conduit aux remarques suivantes :

- Pour les échantillons HO-0°, l'effet de la température sur le module de Young est relativement faible en raison de la présence des fibres orientées parallèlement à la direction de chargement. Le module de Young diminue de 18,7 GPa à 15 GPa lorsque la température augmente de 20°C à 135°C (figure 4-a). En ce qui concerne la contrainte à la rupture, cet effet n'a pas été clairement établi en raison du glissement de l'échantillon lors des essais de traction effectués au 135°C.

- Pour les échantillons HO-90°, l'effet de la température sur le module de Young, ainsi que sur la contrainte et la déformation à la rupture est significative. Pour ce matériau, évolutions du E relatif est étroitement lié à l'effet de la température (figure 4-b).

  Une variation de la température de 20°C à 135°C, conduit à une diminution brutale du module de Young de 12,5 GPa à 3,33 GPa alors que la contrainte à la rupture diminue de 40% et que la déformation à la rupture augmente de 60%. Il est important de noter que, lorsque l'échantillon est chargé, à une température de 135°C, la matrice est à l'état caoutchouteux. Cette variation indique également que le rôle de la matrice vinylester dans les échantillons HO-90° est très important. L'observation macroscopique de la rupture (figure 5) montre qu'un pseudo-délaminage entre les faisceaux de fibres semble être favorisé. On peut voir que, dans le cas d'échantillon HO-90°.

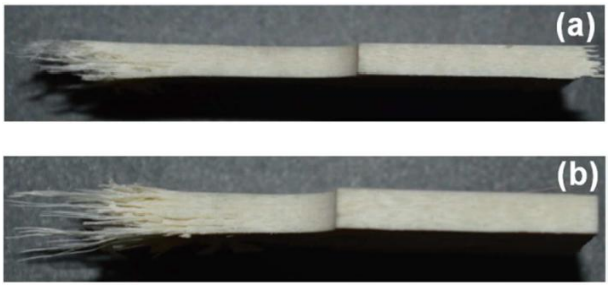

Figure 5 Aspects macroscopiques de la rupture pour HO-90° chargé à 20°C (a), et 135°C (b).

- Comme prévu pour les échantillons RO, l'influence de la température sur la rigidité et les propriétés en rupture est à mi-chemin entre les deux autres orientations (HO-0° et HO-90°). Le module de Young diminue de 14,5 GPa à 9,5 GPa lorsque la température passe de 20°C à 135°C.

1.5.4. Variabilité des microstructures au sein d'une pièce / plaque

Lors du fluage de la matière au moment de la mise en forme par compression à chaud (Sheet molding), les renforts s'orientent avec plus ou moins d'intensité en fonction du plan de chargement (façon de remplir le moule), des paramètres du procédé (schémas de pression et de température) et de la géométrie de la pièce. Cela conduit systématiquement à une dispersion des microstructures au sein de la pièce d'un endroit à l'autre. Cette variation spatiale des microstructures peut être facilement appréhendée

par notre méthode ultrasonore. On en donne une illustration, à la figure 6, le cas d'un hayon développé par PO pour un constructeur automobile.

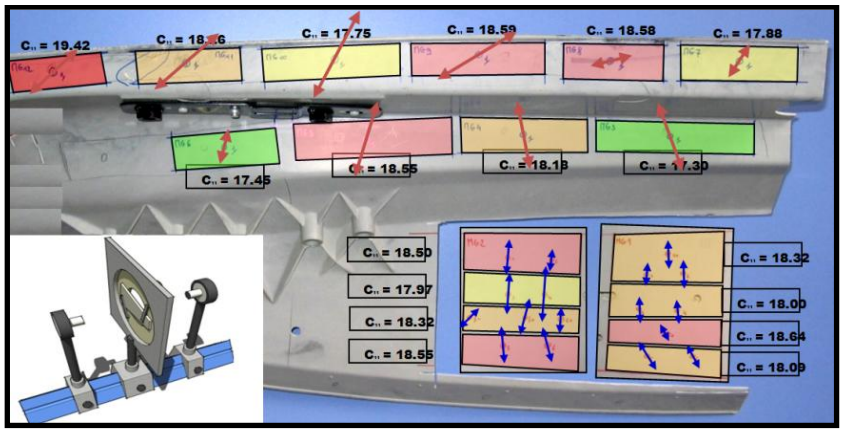

Figure 6 Mise en évidence de la dispersion des microstructures au sein d'un hayon développé par PO.

Hayon réalisé en SMC standard.

Le même type de cartographie des microstructures peut être défini dans le cas de plaques « laboratoire » fournies par PO pour les besoins de cette étude (figures 7 et 8).

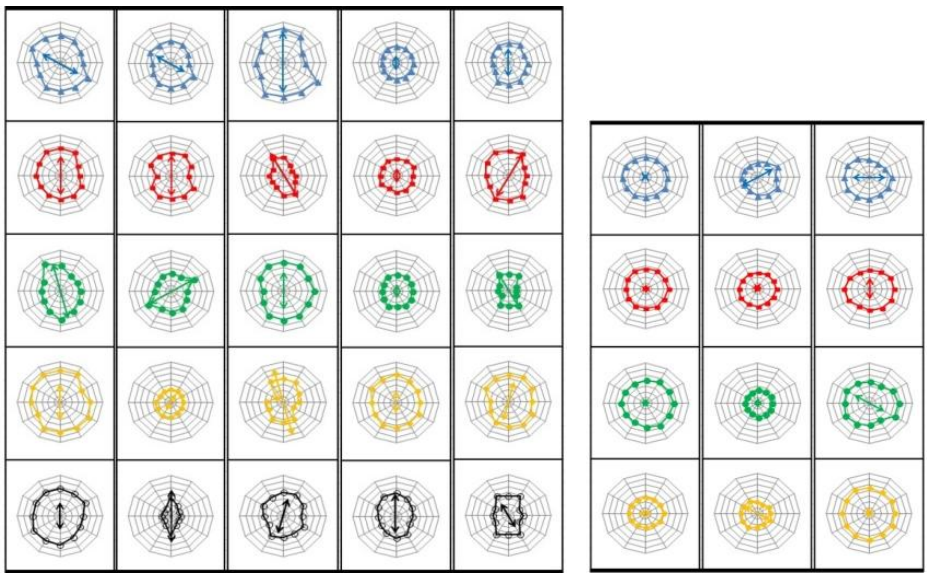

Figure 7 Mise en évidence de la dispersion des microstructures au sein d'une plaque.

Plaques fournies par PO : (a) HO-A-SMC et (b) RO-A-SMC

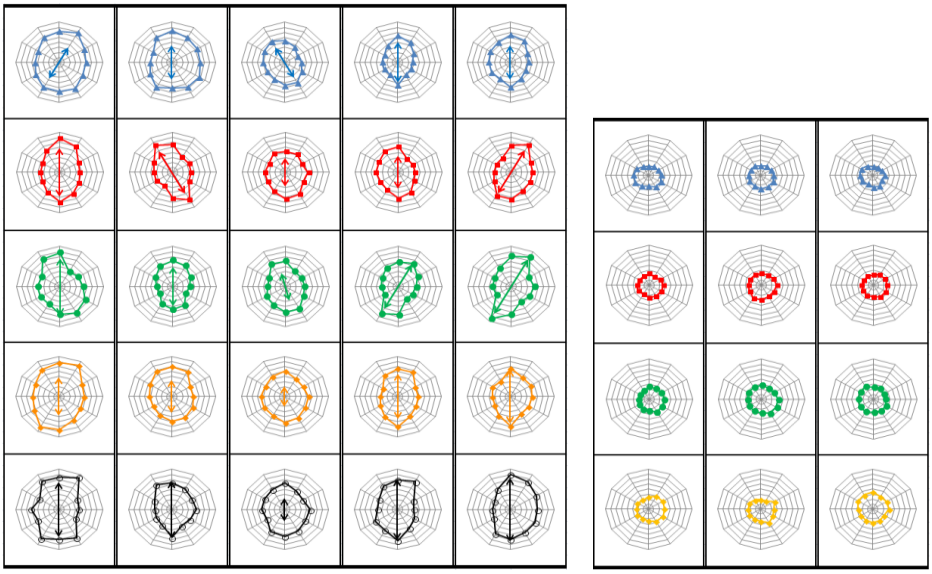

(a) (b)

Figure 8 Mise en évidence de la dispersion des microstructures au sein d'une plaque.

Plaques fournies par PO : (a) HO-LD-SMC et (b) RO-LD-SMC

Ces résultats mettent clairement en évidence le phénomène de dispersion des microstructures à l'origine des dispersions connues des propriétés mécaniques des SMC [11,28].

1.5.5. Anisotropie induite par la variabilité de microstructure

Dans cette étude, un intérêt particulier est porté aux aspects liés à la variabilité des microstructures du composite SMC induite par le procédé de fabrication. En effet, ces aspects (variabilité de fraction volumique et de distribution d'orientation des renforts) influencent fortement les propriétés mécaniques du matériau dans la phase élastique mais aussi dans la phase non linéaire liée au développement de phénomènes d'endommagement. En effet, l'orientation plus ou moins privilégiée des renforts conditionne la répartition des contraintes locales entre les renforts et la matrice. Le degré d'anisotropie qui en découle conditionnera à son tour les propriétés mécaniques élastiques d'une part et les mécanismes de dégradation d'autre part. Or, le comportement des composites SMC est généralement de type élastique-endommageable. D'où la nécessité d'une caractérisation précise et représentative de la microstructure afin de mieux maîtriser le comportement mécanique et l'endommagement des structures des SMC [4,11].

1.6. Mécanismes d'endommagement des composites à renforts discontinus

Soumis à une sollicitation mécanique, les matériaux composites à renforts discontinus se dégradent et plusieurs mécanismes d'endommagement sont mis en jeux. Le développement de cet endommagement intervient assez tôt. Dans le cas des matériaux composites SMC, ils peuvent apparaître dès 20 à 30% de la charge à rupture à l'échelle microscopique, lorsque les contraintes locales ont atteint la limite de rupture d'un des constituants [30-35]. Ces endommagements deviennent rapidement le moteur de la déformation anélastique développée jusqu'à la rupture par coalescence des microfissures. L'initiation et la propagation de l'endommagement se fait de façon diffuse [30-35]. Pour les composites à fibres courtes et pour les composites SMC en particulier, quatre types d'endommagement locaux sont susceptibles de se développer [31,32,35-44] :

- **La fissuration matricielle :** l'interface charge-matrice ou les porosités présentes dans la matrice sont le siège d'initiation de microfissures. Celles-ci se développent et se propagent selon la direction perpendiculaire à la sollicitation (dans le cas d'une sollicitation en traction).
- **Décohésion à l'interface fibre-matrice :** La rupture de l'interface fibre matrice est le mécanisme d'endommagement le plus souvent rencontré. Cette décohésion est associée à la qualité d'adhésion entre les surfaces.
- **Rupture de fibre :** Lorsque l'interface est résistante et que les fibres sont bien orientées selon la direction principale du chargement, on peut voir des ruptures voire des fragmentations des fibres. Cependant, dans le cas des SMC, ce type de phénomène n'intervient qu'à la fin du chargement juste avant la rupture finale.
- **Mécanisme de rupture par pseudo-délaminage :** en raison de la microstructure pseudo-stratifiée, un délaminage local entre les faisceaux de fibres peut avoir lieu avant la séparation totale en deux (ou plus) parties distinctes. Ce phénomène peut grandement contribuer à l'absorption d'énergie lors d'un accident.

Il est à noter que dans le cas de composites à matrice thermoplastique, l'endommagement est couplé à la déformation viscoplastique de la matrice [35]. Dans le cas de composite à matrice thermodurcissable, on parle en général d'un comportement élastique-endommageable [45-49].

1.6.1. Endommagement des SMC standards

- ***Endommagement des SMC en traction unidirectionnelle monotone***

Dans le cas d'un composite SMC standard, on peut mettre directement en relation l'évolution macroscopique du comportement mécanique du composite SMC standard et les mécanismes indiqués précédemment. On constate sur la courbe de la figure 9 trois phases distinctes [32].

La première phase est linéaire et correspond au comportement élastique réversible du matériau composite. La phase suivante étant non linéaire, elle est associée à l'amorçage des mécanismes d'endommagement. L'amorçage de microfissures au niveau des interfaces fibre/matrice suivi de leurs coalescences reste le phénomène prépondérant au cours de cette phase. L'endommagement produit alors une baisse des raideurs du composite. La troisième phase est anélastique et plus ou moins linéaire. Elle décrit la multiplication des microfissures, puis leur propagation en macrofissures. Cette dégradation progressive provoque un phénomène de pseudo-délaminage juste avant la ruine du matériau. Il est à noter que d'autres études mettent en évidence des mécanismes d'endommagement différents tels que la fissuration matricielle présentée comme étant le moteur de l'endommagement en traction [27].

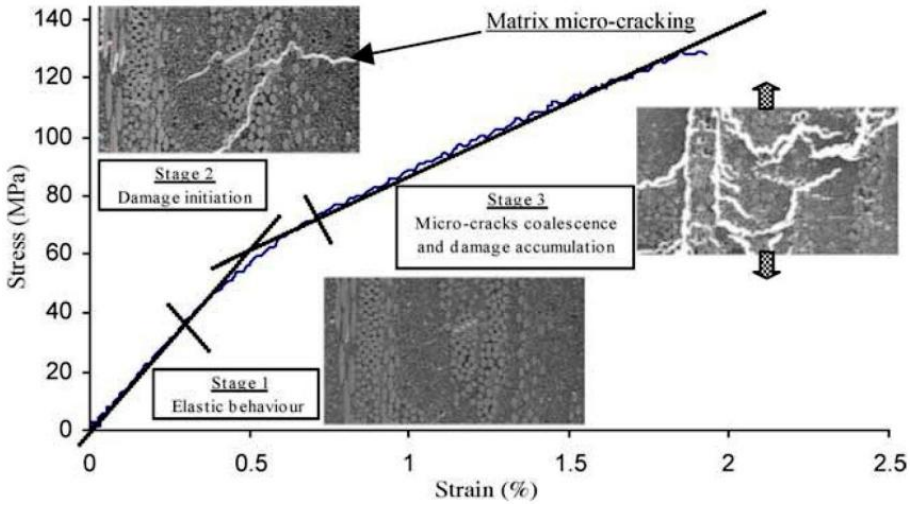

Figure 9 Courbe typique de traction du composite SMC standard [32].

- ***Endommagement des SMC en fatigue***

La grande majorité des phénomènes de rupture des pièces composites de structure en service est en général attribué à l'accumulation de l'endommagement en fatigue. Du fait de la complexité des phénomènes mis en jeu et le grand nombre de paramètres affectant la microstructure, l'endommagement

en fatigue des composites à renforts discontinus fait l'objet de nombreuses études [30,50-55]. Cependant, il existe peu d'études expérimentales du comportement des composites SMC sollicités en fatigue [55]. Nous rapportons ici l'étude réalisée par Tamboura et al [55]. Ce travail présente un intérêt particulier du fait qu'il met en relation de façon quantitative l'évolution des densités de fissure à l'interface fibre-matrice et les propriétés macroscopiques résiduelles du composite. Là encore, l'interface fibre-matrice apparaît comme le point faible du composite à partir duquel l'endommagement se développe progressivement suivant toutes les directions des renforts (figure 10).

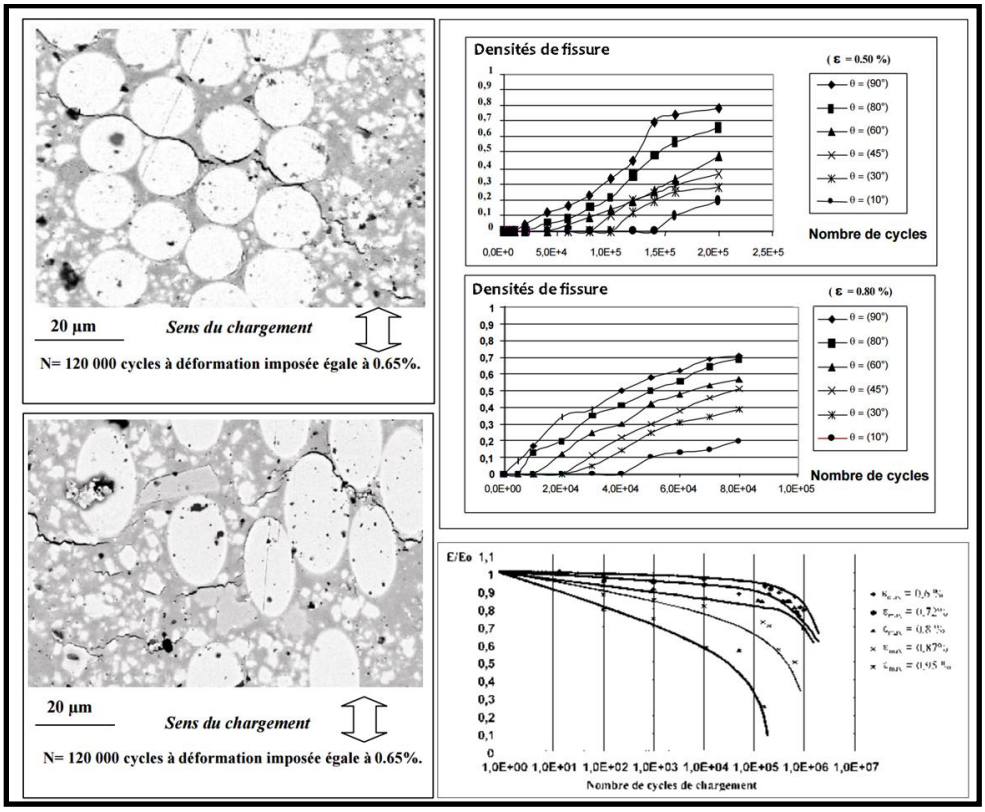

Figure 10 Etude expérimentale multi-échelle de l'endommagement d'un SMC standard sollicité en fatigue [55].

Fatigue thermomécanique et endommagement

Le phénomène d'auto-échauffement est bien connu dans les polymères et composites thermoplastiques. Le couplage thermomécanique complexe qui en découle rend difficile la maîtrise du dimensionnement des structures. On parle alors de compétition entre fatigue thermique et fatigue mécanique [30,56,57]. La première concerne les phénomènes d'auto-échauffement et la seconde est liée

aux phénomènes d'endommagement [30,56,57]. Le phénomène d'auto-échauffement est lié d'une part à la nature viscoélastique du polymère relative au frottement des chaînes macromoléculaires et d'autre part à des échauffements locaux par friction induits par des endommagements sous forme de création de micro-discontinuités (microfissures, décohésion d'interfaces, …). Ces dernières sont localisées à l'interface fibre-matrice, mais aussi entre les lèvres des microfissures lors des cycles ouverture-fermeture lors de leur propagation et aussi lors du cisaillement. L'augmentation de température modifie localement l'état des contraintes locales ce qui influence la cinétique des phénomènes d'endommagement. Par ailleurs, l'échauffement local aux interfaces fibre-matrice peut atteindre des températures de transition, ce qui peut conduire à des déformations locales extrêmement ductiles et ainsi engendrer une sorte de transition fragile-ductile localisée à l'interphase (figure 11-a). Un couplage fort entre auto-échauffement et endommagement peut alors se développer. Lorsque l'endommagement débute, on peut noter des variations de cinétique lors de l'augmentation de la température (figure 11-b).

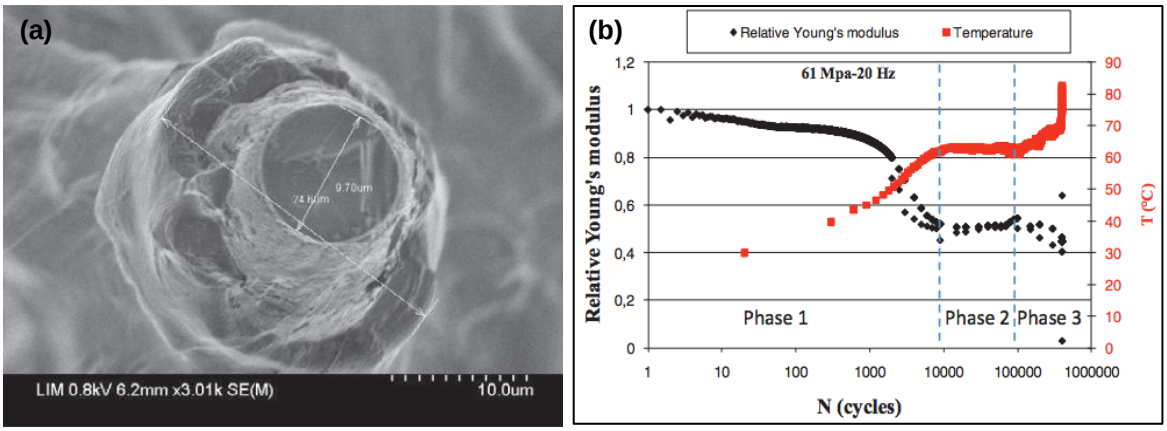

Figure 11 Etude expérimentale multi-échelle de l'endommagement d'un SMC standard sollicité en fatigue [30].

Enfin, l'amplitude de la contrainte et la fréquence des sollicitations conditionnent également les phénomènes moteur de déformation et d'endommagement [30,56,57]. On montrera au prochain chapitre que sous certaines conditions d'amplitude et de fréquence, le même couplage thermomécanique et endommagement peut être observé dans le cas de composites à matrice thermodurcissable de type SMC (Article N°3).

- ***Endommagement des SMC sous sollicitation rapide***

Il existe peu d'études expérimentales concernant le comportement en dynamique rapide des composites SMC [11,27,32-34,37,59,60]. Ceci tient tout d'abord à la difficulté expérimentale liée aux phénomènes inertiels et de propagation d'ondes venant perturber fortement la mesure. Divers systèmes de mise en charge peuvent être envisagés [11,27,32-34,37,59,60]. Cependant, dans le domaine des vitesses intermédiaires (jusqu'à 200 s^{-1}), les machines de traction dynamiques restent l'outil dédié. En effet, les systèmes standards de barres d'Hopkinson ne permettent pas d'imposer des vitesses de déformation constantes. Malgré tout, une optimisation de l'essai est alors nécessaire afin de minimiser les effets perturbateurs cités plus haut. Ceci est rendu possible grâce à une méthodologie détaillée dans [11,27,32-34,37,59,60] et est utilisées dans cette étude (Article N°1, 2, 4 et 5).

Dans le cas des composites SMC standards, on peut noter une forte influence de la vitesse de déformation sur les propriétés mécaniques macroscopiques (figure 12).

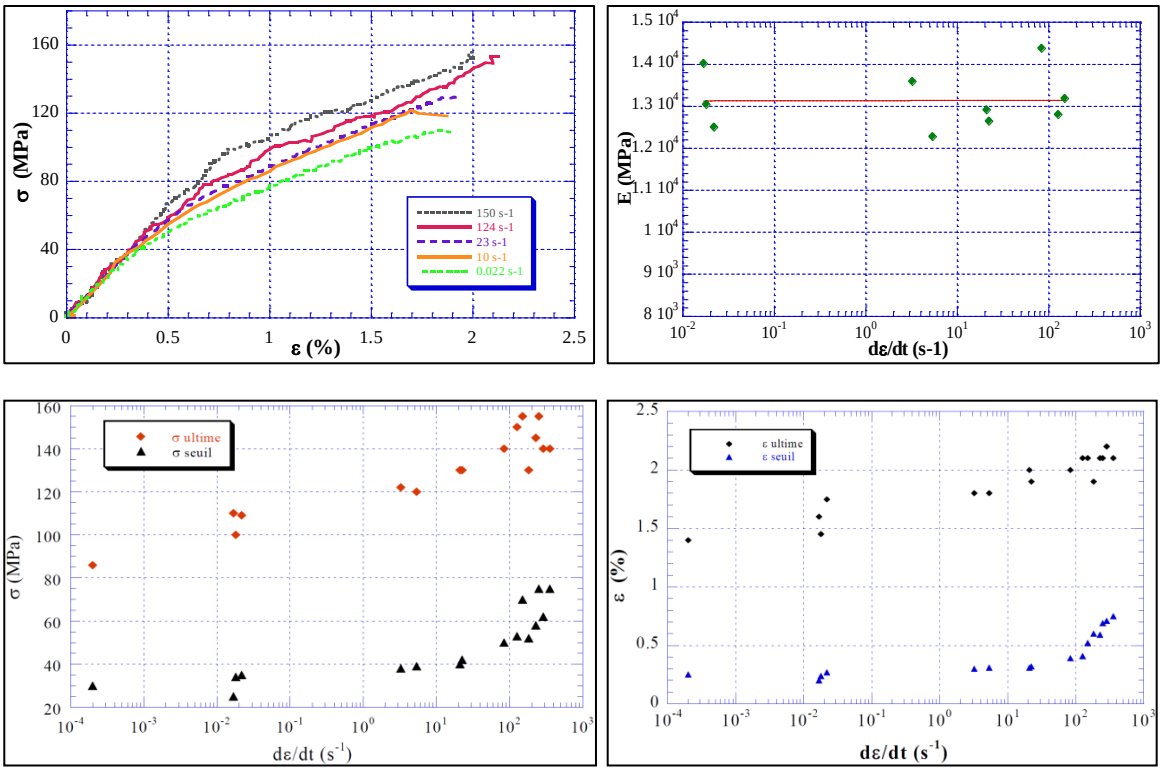

Figure 12 Influence de la vitesse de déformation sur les propriétés mécaniques macroscopiques [11].

Des essais interrompus ont permis de mettre en évidence la nature visqueuse de l'endommagement à l'interface fibre-matrice. En effet, une augmentation de la vitesse de déformation

conduit d'une part à un décalage du seuil d'endommagement et d'autre part à une baisse de la cinétique d'endommagement. Ces effets sont directement corrélés avec les seuils et cinétiques d'endommagement à l'interface fibre-matrice [11].

1.6.2. Indicateurs de l'endommagement

L'évolution du comportement mécanique d'un matériau, à partir de son état initial jusqu'à sa ruine, est décrite par la théorie de l'endommagement. Cette théorie conduit à la définition d'indicateur macroscopique de l'endommagement sous forme scalaire ou tensorielle [40,42,46,59–64]. La réduction de la rigidité en traction est un indicateur scalaire d'endommagement macroscopique souvent utilisé pour les matériaux composites. Il est facilement évalué à l'occasion d'essais de traction charge-décharge avec augmentation progressive de la charge. Une mesure de la pente résiduelle permet de définir une variable d'endommagement macroscopique [27,67-69] comme suit :

$$\mathbf{D_{macro}} = \mathbf{1} - \frac{\mathbf{E^D}}{\mathbf{E^0}} \qquad \text{Equation 1}$$

E_0 et E_D sont respectivement, les modules de matière vierge et endommagé.

L'un des objectifs de notre étude étant de comprendre les relations multi-échelles, il est intéressant de définir à l'échelle microscopique, un indicateur d'endommagement directement lié à l'évolution de la densité des microfissures [11,32–34]. Les mécanismes d'endommagement à l'échelle microscopique peuvent être identifiés au moyen d'observations au MEB, effectuées sur des surfaces d'échantillons polies [11,32–34]. On peut notamment définir une densité relative d'endommagement à l'interface fibre-matrice au travers de la variable locale suivante [27,34] :

$$\mathbf{d_{micro}} = \frac{\mathbf{f_d}}{\mathbf{f_v}} \qquad \text{Equation 2}$$

Où f_d est la fraction volumique des fibres décollées à l'interface et f_v est la teneur en volume de fibres dans le Volume Elémentaire Représentatif (VER). Dans le cas des SMC, d_{micro} peut être directement mesuré sur les micrographies MEB en dénombrant le nombre de fibres présentant une défaillance de l'interface à l'intérieur des mèches. En outre, on peut étudier l'influence de l'orientation relative des renforts par rapport à la direction principale du chargement, θ, en définissant un paramètre intermédiaire

local d(θ) ; ce dernier décrivant les seuils et cinétiques d'endommagement des renforts orientés à θ comme suit [27,34] :

$$\mathbf{d}_{\theta} = \frac{\mathbf{f}_{\mathbf{d}}^{\theta}}{\mathbf{f}_{\theta}} \qquad \text{Equation 3}$$

Où f_d^{θ} et f_{Θ} sont respectivement, la fraction volumique (ou nombre) de renforts endommagés sur l'interface au sein des mèches orientés à θ° et la fraction volumique des mèches orientées à θ° (ou nombre total des fibres contenues dans les mèches orientées à θ°).

Les évolutions de ces deux indicateurs d'endommagement peuvent être corrélés et donner des indications précises sur les seuils et les cinétiques d'endommagement lors de sollicitations rapides et/ou en fatigue [11,32–34]. Une illustration présentée à la figure 13 montre bien que pour les composites SMC standards, c'est la nature visqueuse de l'endommagement à l'interface fibre-matrice qui est à l'origine des variations de propriétés mécaniques à l'échelle macroscopique. On constate également qu'une évolution du seuil d'endommagement à l'interface fibre-matrice conduit à la même évolution du seuil de première non-linéarité. On peut parler de la nature visqueuse de l'endommagement [[11,32–34] et Article N°2] ou de la notion de « visco-endommagement » introduite en 2005 [11,34].

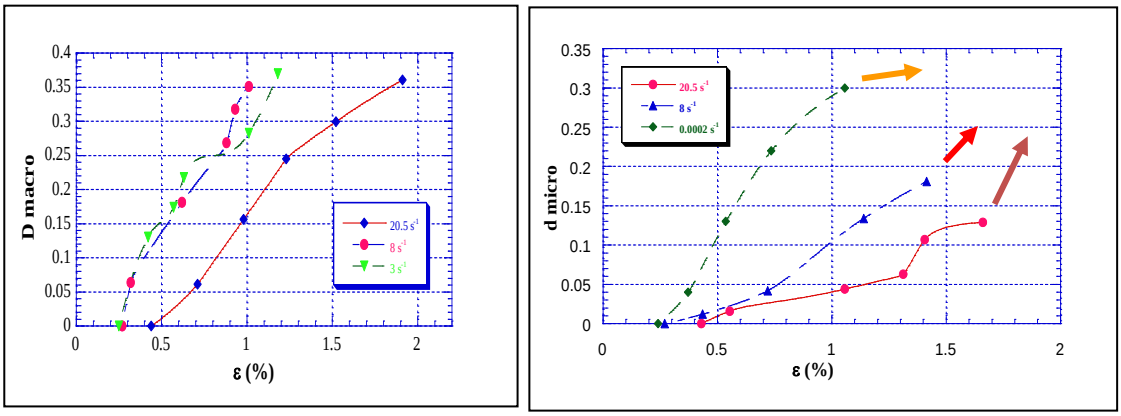

Figure 13 Evolution de l'endommagement quantifié : (a) à l'échelle macroscopique et (b) à l'échelle microscopique [11,34].

1.7. Conclusion

L'intérêt recherché par les industriels de l'automobile dans l'utilisation des SMC tient essentiellement en leurs bons rapports qualités/poids et qualités/coût [4]. Leur facilité de mise en œuvre,

leur bonne résistance thermique, leur stabilité dimensionnelle, ainsi que leur aptitude à élaborer des pièces minces voire de géométrie complexe et en moyenne série sont aussi des atouts majeurs. D'autre part, ce type de composite offre une bonne résistance mécanique à la corrosion ainsi qu'une bonne adaptabilité de ses propriétés mécaniques à des sollicitations spécifiques telles que les chargements dynamiques rapides et la fatigue. Tout particulièrement, On apprécie également ces matériaux pour leur capacité élevée à l'absorption d'énergie lors d'événement de type crash automobile. Ils sont par ailleurs soumis lors de leur usage (conduite routière entre autre) à des chargements de type fatigue. On doit donc s'intéresser aux propriétés dynamiques post-fatigue. C'est une des finalités de notre étude. Cependant, le dimensionnement des structures réalisées en composite SMC soumis à ce type de chargement dynamique (grande vitesse et fatigue) pose un certain nombre de difficultés spécifiques. Ces difficultés peuvent mettre en défaut l'introduction de ces matières au sein des structures automobiles. En effet, une mauvaise compréhension des phénomènes à l'origine des réponses mécaniques des matériaux et structures SMC conduisent souvent à de mauvais choix de modélisation et très souvent à des modélisations des structures peu ou pas prédictives.

Une exploration dans la littérature et dans ce domaine permet de lister les différentes sources de difficultés rencontrées lors du dimensionnement des structures en SMC :

- Anisotropie liée à l'orientation plus ou moins marquée des renforts du fait du fluage de la matière lors de la mise en forme [4,12] ;
- Variabilité des microstructures d'un endroit à l'autre de la pièce de structure du fait du fluage de la matière lors du procédé [4,12] ;
- Difficulté à prévoir les distributions de microstructure au sein de la pièce. Il n'existe pas aujourd'hui d'outils fiables pour modéliser le procédé SMC [4,12] ;
- Difficulté expérimentale à décrire la présence d'une multitude de microstructures au sein de la pièce. Microstructures caractérisées par des variations spatiales de la fraction volumique et de la distribution d'orientation des renforts. En d'autres termes, nécessité d'établir la cartographie microstructurale de la pièce [4,12,26,27] ;
- Présence de phénomènes d'endommagement multiples qui s'expriment à l'échelle de la microstructure et qui conditionnent le comportement macroscopique du composite. Notamment,

on peut citer la rupture de l'interface fibre-matrice comme mécanisme généralement prédominant ; mais aussi la microfissuration de la matrice qui peut parfois devenir moteur [4,11,12,30,56] ;

- Variabilité des phénomènes d'endommagement en fonction des microstructures et des types de chargement [4,12,55] ;
- Sensibilité à la vitesse de chargement. A titre indicatif, les propriétés mécaniques d'un composite de ce type peuvent doubler lors d'un chargement à grande vitesse [11,31,37,38] ;
- Influence du type de chargement : différence entre traction et compression, comportement en fatigue [11,40,41,68] ;
- Nécessité de développer une loi de comportement par microstructure ou par type de microstructure [11] et par type de chargement, (décrire le comportement et les critères limites sous sollicitations complexes tridimensionnelles) [11,32–34,55].

Le point essentiel ressortant des études bibliographiques est le fait que la compréhension et la prise en compte des modes de dégradation intervenant lors de sollicitations complexes telles que les grandes vitesses de sollicitation ou les chargements répétés (fatigue) sont essentiels lors de l'élaboration de lois de comportement. Cependant, ces dernières varient fortement en fonction de la microstructure et du type de chargement. La description faite précédemment concerne uniquement un SMC standard à orientation aléatoire. Cependant, une variation du type d'architecture du composite (fraction volumique, distribution d'orientation, présence ou non de billes de verre creuses, etc.) est susceptible de modifier sensiblement d'une part les mécanismes d'endommagement mis en jeu et d'autre part, leurs seuils et leurs cinétiques. Il en est de même pour une variation du type de sollicitation et de son orientation relative par rapport à la microstructure (traction, compression, cisaillement). Par ailleurs, l'historique de la dégradation à l'échelle locale pourra être fortement modifié lors de sollicitations rapides ou lors de sollicitations répétées (fatigue).

L'étude des relations microstructure-propriétés mécaniques sous chargement dynamique et fatigue est donc au centre des préoccupations de cette étude. Afin de compléter la connaissance du comportement des SMC, on s'intéressera à deux types de matériaux peu étudiés : les matériaux : A-SMC et LD-SMC. Une analyse multi-échelles des phénomènes d'endommagement et de leurs conséquences sur les réponses mécaniques macroscopiques sera systématiquement réalisée afin de mettre en relation

les phénomènes se produisant à l'échelle microscopique avec les réponses mécaniques macroscopiques de ces composites. On s'intéressera au chargement de type fatigue et à la sollicitation dynamique raide. Enfin, une étude des propriétés dynamiques post-fatigue permettra de mettre en évidence l'effet des sollicitations répétées sur le comportement mécanique dynamique résiduel dans le cas du composite A-SMC.

2. Etude du comportement des composites SMC en fatigue

La fatigue est une action de contraintes ou déformations variables dans le temps qui peut modifier les propriétés locales d'un matériau. La fatigue peut entraîner la formation de fissures aboutissant à la rupture de la pièce. La progression de l'endommagement en fatigue peut suivre différentes étapes [30,51,55,72–75] :

- La création de sites de nucléations
- La formation de microfissures
- La croissance et la coalescence de fissures microscopiques dominantes
- La propagation et la percolation de macros fissures dominantes
- La rupture

Les principales caractéristiques et propriétés régissant le comportement en fatigue d'un composite à matrice polymère, sont les suivantes :

1) La nature de la matrice : sa composition chimique, sa morphologie, l'état physique et la rhéologie
2) Les additifs et les charges : billes de verre …
3) La nature des renforts : architecture et dimensions
4) L'état de l'interface : l'ensimage, l'adhésion chimique, physique ou mécanique entre matrice et fibres
5) Le type et la condition de sollicitation (température, amplitude des contraintes ou des déformations, fréquence, rapport de charge …)

Dans le cadre de ce travail, des essais de fatigue en traction-traction ont été réalisés sur une machine hydraulique MTS 830 (Elastomère Test System) avec application d'une force. Ces essais ont été réalisés à différentes fréquences, à savoir 10, 30, 50 et 100 Hz. Afin de mesurer la réduction de la rigidité due à la première étape de chargement (endommagement initial éventuel « contrôlé »), chaque test de fatigue est précédé d'une étape de chargement en traction quasi-statique puis de déchargement-rechargement.

2.1. Influence des paramètres du chargement cyclique

2.1.1. Amplitude de sollicitation

L'amplitude de sollicitation affecte directement la durée de vie du matériau de façon conséquente [54,56]. On peut constater dans certains cas un auto-échauffement lié au changement de l'amplitude [73]. Cependant, cet effet est peu étudié pour les SMC ce qui conduit à une littérature assez pauvre. La figure 14 montre les courbes de Wöhler obtenues à la fréquence de 10 Hz pour les échantillons RO, HO-0° et HO-90° de A-SMC [73].

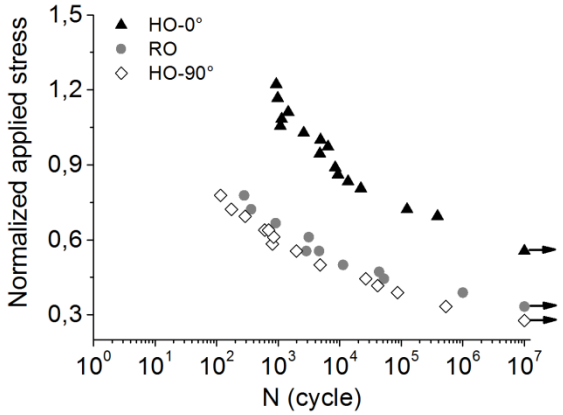

Figure 14 Courbes de Wöhler pour les éprouvettes RO, HO-0° et HO-90° à 10 Hz ($\sigma_{normalisée} = \sigma / \sigma_{r(RO)}$).

On peut remarquer que pour les échantillons RO, quand la contrainte appliquée est égale à 0.44 $\sigma_{r(RO)}$, la durée de vie est d'environ 50 000 cycles, tandis que la durée de vie est d'environ 10^6 cycles pour une contrainte appliquée de 0.39 $\sigma_{r(RO)}$. Ainsi, une diminution de 12% de la contrainte appliquée conduit à une durée de vie environ 20 fois plus élevée. Cependant, dans le cas des échantillons RO-A-SMC, pour l'essai de fatigue réalisé à 0.34 $\sigma_{r(RO)}$, aucune rupture n'a été observée en dessous de 10^7 cycles.

2.1.2. Distribution d'orientation des fibres

On note que pour une contrainte appliquée correspondant à la valeur limite « d'endurance conventionnelle » de HO-0° (soit 0.55 $\sigma_{r(RO)}$), les éprouvettes en RO et/ou HO-90° peuvent rompre entre 500 et 1000 cycles. Ce constat démontre clairement que la durée de vie est fortement influencée par l'orientation des fibres. Toutefois, la figure 14 montre également que RO et HO-90° présentent pratiquement le même comportement en fatigue. Les courbes de Wöhler des échantillons RO et HO à

10 Hz montrent une forme bilinéaire définissant deux zones différentes liées au comportement en fatigue en charge d'amplitude faible et élevée [30]. Pour le RO et le HO-90°, la zone de forte amplitude (> 0.47 $\sigma_{r(RO)}$) correspond à un nombre de cycles à la rupture inférieur à 10^4 cycles. Tandis que pour les échantillons HO-0°, la durée de vie est au moins de 30 000 cycles pour une valeur de contrainte allant jusqu'à 0.75 $\sigma_{r(RO)}$. Compte tenu de ces valeurs, les courbes commencent à dévier et tendent à une évolution que l'on pourrait qualifié d'asymptotique définissant ainsi une limite d'endurance conventionnelle pour laquelle aucune rupture n'est observée jusqu'à 10^7 cycles.

2.1.3. Fréquence de sollicitation

La fréquence de sollicitation est un paramètre important en fatigue, particulièrement pour l'établissement d'un équilibre thermique. Des fréquences élevées engendrent généralement un phénomène d'auto-échauffement qui résulte de la dissipation d'énergie [56,72–74]. Handa et al [75] ont comparé deux fréquences, 5 et 50 Hz, et ils ont observé qu'avec l'augmentation de la fréquence la durée de vie diminue. D'après Dentsoras et Kouvaritakis [76], les propriétés mécaniques des matériaux viscoélastiques dépendent de la fréquence de sollicitation. La fréquence élevée et l'auto-échauffement généré lors d'un essai de fatigue ont un effet sur la rigidité et sur la vitesse de propagation des fissures en fatigue. Les courbes de Wöhler normalisées obtenues à partir des essais de fatigue pour des fréquences de 10, 30, 50 et 100 Hz dans le cas d'échantillons de RO [73], sont présentées sur la figure 15.

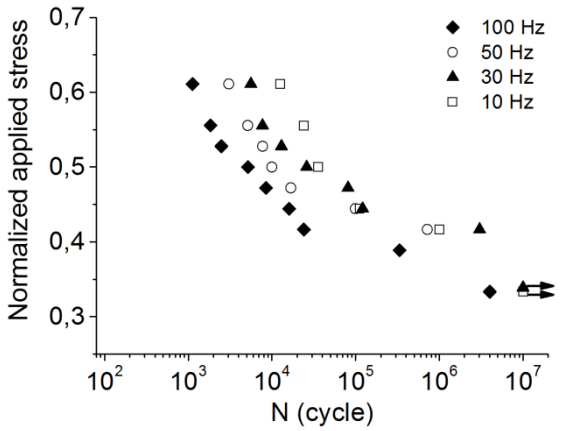

Figure 15 Courbes de Wöhler pour différentes fréquences (échantillons RO, $\sigma_{normalisée} = \sigma / \sigma_{r(RO)}$).

Comme on peut le constater, il y a peu de différence entre les courbes réalisées à 10, 30 et 50 Hz avec une faible amplitude, alors que pour une amplitude de charge élevée, l'augmentation de la fréquence conduit à des courbes de Wöhler décalées. Ce phénomène est sans aucun doute lié au phénomène d'auto-échauffement de la matrice organique induit par les effets visqueux. A des amplitudes fortes et à des fréquences élevées, l'auto-échauffement généré par un fort frottement intermoléculaire du polyester insaturé est la cause de cette baisse de la rigidité et de cette diminution de la durée de vie en fatigue du matériau. Ce phénomène est encore plus significatif si l'auto-échauffement fait basculer, au voisinage de la température de transition vitreuse (transition fragile-ductile), le polymère depuis un état rigide vers un état caoutchoutique.

2.2. Mécanisme d'endommagement des A-SMC en fatigue

Lors d'un essai de fatigue, lorsqu'une fissure coalesce, il se forme en tête de fibre, une zone où il y a une variation de la densité et de l'orientation des fibres. Le processus de propagation des fissures implique de nombreux phénomènes tels que la rupture des fibres, la déformation plastique et la rupture de la matrice, la nucléation et la coalescence de cavités, la bifurcation des fissures, le pseudo-délaminage et le déchaussement des fibres [53,72,77]. L'endommagement débute par l'amorçage des fissures. Dans le cas des composites SMC, cet amorçage se passe, en général, d'abord à l'interface fibre/matrice. Dans son évolution, ce phénomène se transforme en formation des microfissures à la décohésion fibre/matrice. Les premières apparitions de cette décohésion (figures 16-17) concernent plus particulièrement les fibres perpendiculaires à la direction de sollicitation.

En effet, les fibres orientées à 90° sont sollicitées, sur leurs interfaces, en contrainte normale pure tandis que la contrainte de cisaillement est quasi nulle au pôle (en tête de fibre). Les fibres d'orientations différentes commencent à se déchausser tardivement du fait de l'évolution des champs de contraintes et de déformations locales. Les décohésions des interfaces fibre/matrice constatées constituent des micro-discontinuités qui évoluent brutalement le long des contours des fibres pour former des vides. Une redistribution des contraintes locales s'opère à chaque fois qu'une nouvelle micro-discontinuité apparaît.

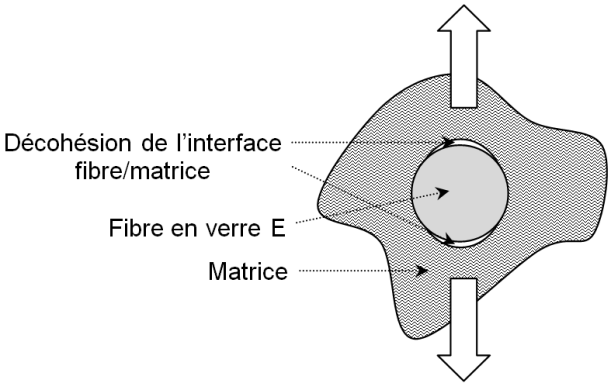

Figure 16 Initiation de décohésions interfaciales induisant des microdiscontinuités (microvides) entre la fibre et la matrice.

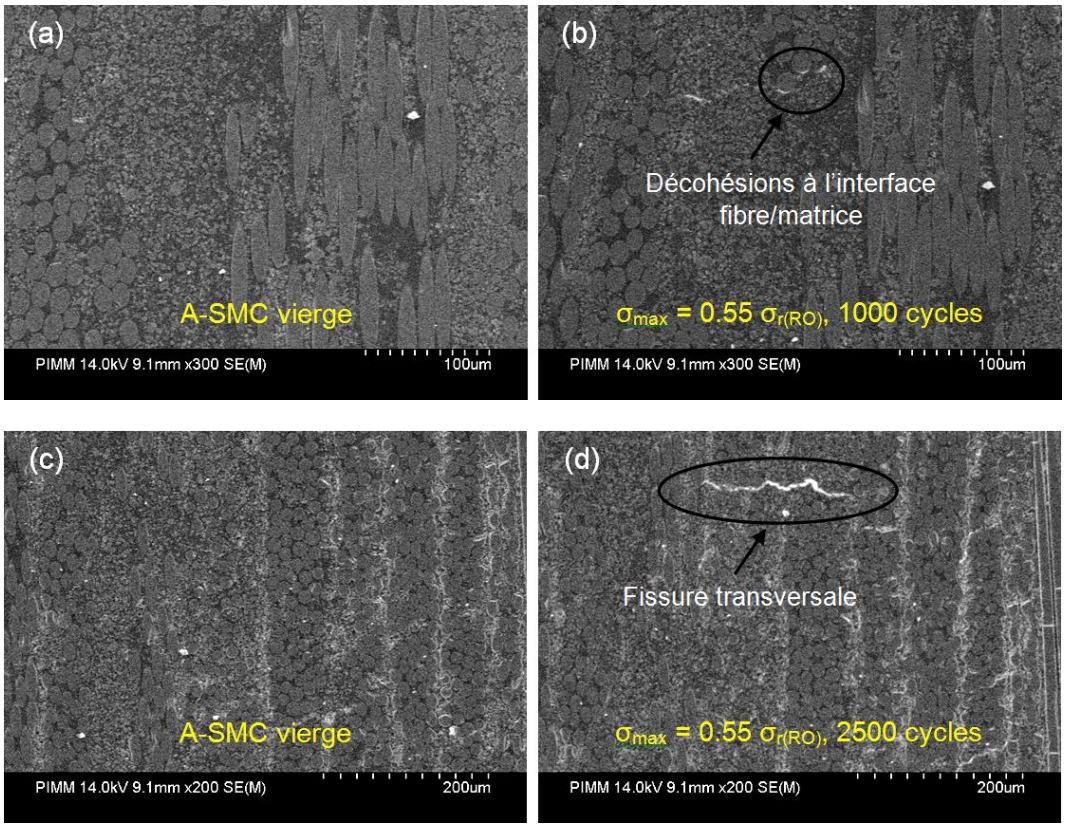

Figure 17 Microstructure de l'échantillon vierge et l'échantillon après 1000 cycles et 2500 cycles d'essai de fatigue à une contrainte appliquée de 0.55 $\sigma_{r(RO)}$ et une fréquence de 30 Hz.

2.3. Fatigue Thermique Induite (ITF) et Fatigue Mécanique (MF)

La mesure de la température induite par l'auto-échauffement d'un matériau lors d'un essai de fatigue est très importante pour déterminer la part de la fatigue thermique dans la durée de vie totale.

A basse fréquence et à faible amplitude de sollicitation, l'auto-échauffement est pratiquement négligeable et la durée de vie est gouvernée essentiellement par La fatigue mécanique. Une haute fréquence combinée à une contrainte appliquée élevée conduit à l'apparition du phénomène d'auto-échauffement [77-79]. Ce phénomène qui provoque une diminution de la durée de vie est généralement connu sous la désignation « Fatigue Thermique Induite » (ITF en anglais). La durée de vie totale est le résultat de l'effet combiné entre la fatigue thermique et la fatigue mécanique.

Dans les deux cas, l'endommagement peut se présenter sous la forme de la décohésion à l'interface fibre-matrice, du pseudo-délaminage entre les faisceaux de fibres et de la microfissuration de la matrice.

En absence d'auto-échauffement, la température de l'échantillon ne change pas et l'essai de fatigue est considéré comme isotherme. En présence d'auto-échauffement, la température de l'échantillon augmente ce qui est la cause du changement des propriétés mécaniques (module d'Young, résistance, ductilité,…) de l'échantillon. On peut supposer que dans les deux cas, l'essai de fatigue est réalisé sur deux matériaux de comportement mécanique différent.

Les résultats de différents essais et dans différentes conditions de sollicitation sont montrés sur la figure 18. Il s'agit de 4 conditions d'essais suivantes :

- Fréquence faible (10Hz) et amplitude basse ($0.40\ \sigma_{r(RO)}$), figure 18-a
- Fréquence faible (10 Hz) et amplitude élevée ($0.55\ \sigma_{r(RO)}$), figure 18-b
- Fréquence élevée (100Hz) et amplitude basse ($0.40\ \sigma_{r(RO)}$), figure 18-c
- Fréquence élevée (100Hz) et amplitude élevée ($0.55\ \sigma_{r(RO)}$), figure 18-d

Certaines caractéristiques de ces résultats sont portées dans le tableau 2. A partir de ces résultats, nous pouvons fournir les commentaires suivants :

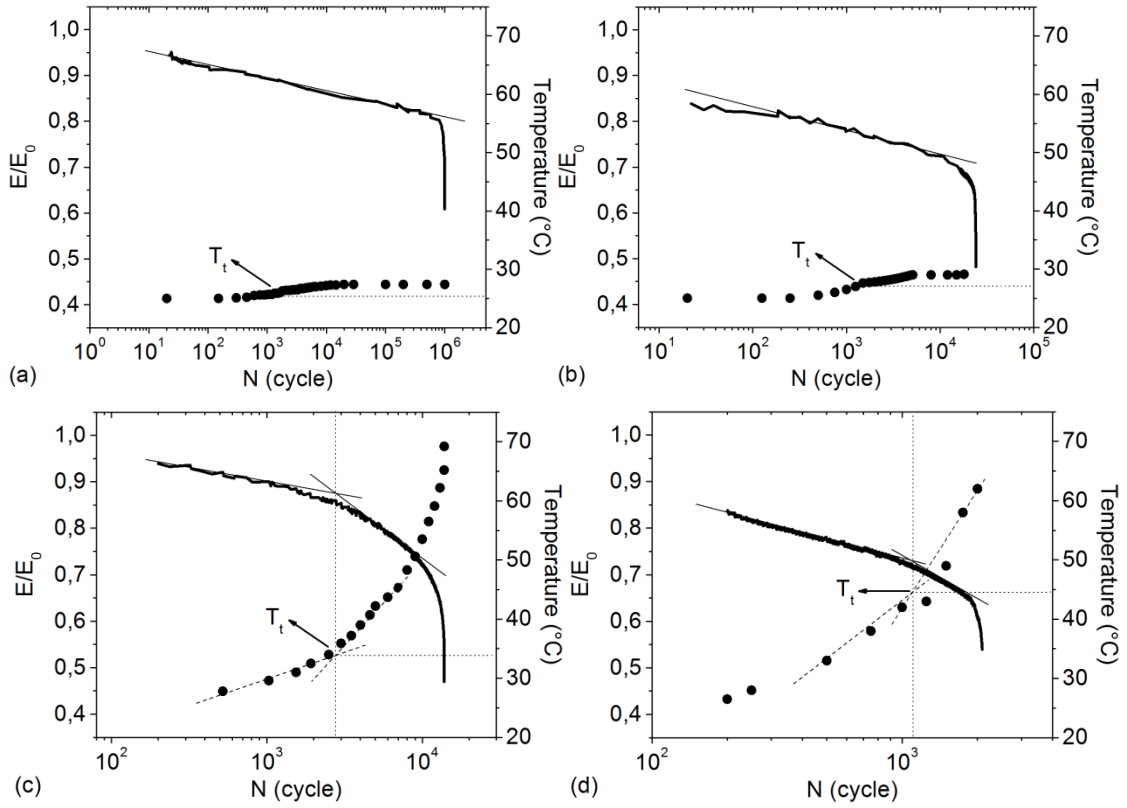

Figure 18 Evolution du module de Young (E/E_0) et de la température lors des essais de fatigue sur RO-A-SMC à différentes amplitudes et fréquences de sollicitation : (a) f = 10 Hz et σ_{max} = 0.40 $\sigma_{r(RO)}$, (b) f = 10 Hz et σ_{max} = 0.55 $\sigma_{r(RO)}$, (c) f = 100 Hz et σ_{max} = 0.40 $\sigma_{r(RO)}$ et (d) f = 100 Hz et σ_{max} = 0.55 $\sigma_{r(RO)}$.

Figure 18	T de transition (°C)	T échauffement à la rupture (°C)	Nombre de cycle à la rupture
Figure 18-a : f = 10 Hz et σ_{max} = 0.40 $\sigma_{r(RO)}$	25	27	1×10^6
Figure 18-b : f = 10 Hz et σ_{max} = 0.55 $\sigma_{r(RO)}$	27	29	$2{,}2 \times 10^4$
Figure 18-c : f = 100 Hz et σ_{max} = 0.40 $\sigma_{r(RO)}$	35	> 60	$1{,}2 \times 10^4$
Figure 18-d : f = 100 Hz et σ_{max} = 0.55 $\sigma_{r(RO)}$	44	> 60	2×10^3

Tableau 2 Quelques caractéristiques relatives aux résultats présentés sur la figure 18.

i) Pour une faible amplitude et une basse fréquence (figure 18-a), le changement de la température est très faible et le matériau RO-A-SMC présente un comportement en fatigue principalement régi par la fatigue mécanique (MF). Dans cette condition la durée de vie est relativement élevée ($N_r = 1 \times 10^6$).

ii) Pour une grande amplitude et haute fréquence (figure 18-d), la température augmente de façon conséquente (de la température ambiante jusqu'à une température supérieure à 62°C). Dans cette condition de sollicitation, la durée de vie en fatigue diminue. Cette diminution de la durée de vie est essentiellement liée à l'auto-échauffement et à Fatigue thermique induite (ITF).

iii) La comparaison entre la figure 18-a et la figure 18-b d'une part et entre la figure 18-c et la figure 18-d d'autre part montre l'importance de la fréquence de la sollicitation. Pour des essais à 10 Hz, le nombre de cycles à la rupture change de 2×10^3 à 12×10^3 quand l'amplitude de contrainte varie respectivement de 0.55 $\sigma_{r(RO)}$ à 0.40 $\sigma_{r(RO)}$, tandis que pour des essais à 100 Hz le nombre de cycles à la rupture change de $2{,}2 \times 10^4$ à 1×10^6 quand l'amplitude de contrainte varie respectivement de 0.55 $\sigma_{r(RO)}$ à 0.40 $\sigma_{r(RO)}$.

iv) Lorsque l'amplitude et la fréquence sont élevées (figure 18-d), l'effet combiné de ces deux paramètres engendre des phénomènes d'auto-échauffement et de dégâts intensifs. Dans ce cas, la température augmente jusqu'à 62°C. Température qui est supérieure à la température de transition β (45°C). Cet auto-échauffement est la cause du changement de comportement ; du vitreux-fragile au vitreux-ductile. La rigidité du matériau diminue lors de ce changement du comportement.

v) Pour les hautes fréquences et les amplitudes élevées, le comportement en fatigue est entraîné à la fois par la fatigue thermique induite (ITF) et la fatigue mécanique (MF).

vi) Les courbes de baisse de raideur pour les quatre conditions de sollicitation ne montrent pas le même régime. Quand la fréquence et l'amplitude sont faibles (figure 18-a), les courbes présentent deux régime distincts : une diminution progressive faible et une chute brutale respectivement liés à l'amorçage et l'accumulation lente des microfissures et la propagation rapide des fissures et la rupture.

3. Etude du comportement mécanique des SMC sous sollicitation dynamique

Le terme ‘dynamique’ englobe souvent diverses notions assez variées, que ce soit de mécanique, de thermodynamique ou de physique [11,80-81]. Il est alors important de situer le contexte du régime dynamique afin de mieux appréhender les phénomènes mis en jeu. En ce qui concerne le comportement mécanique qui est l’objet de notre étude, on a l’habitude de distinguer trois régimes dynamiques : lent, moyen et rapide. Le régime dynamique lent concerne des vitesses de déformation comprises entre 10^{-1} et 10 s^{-1}, il est proche du processus quasi-statique (figure 19). Dans ce régime, il est souvent question, d’événement comme les chutes d’objets. Le régime dynamique moyen (entre 1 et 5 × 10^2 s^{-1}) se caractérise par une échelle temporelle de l’ordre de la milliseconde. C’est dans ce type de régime que se situe la présente étude des phénomènes dynamiques. Le régime dynamique rapide (au-delà de 10^3 s^{-1}), à l’échelle de la microseconde, est caractérisé par le phénomène de propagation d’ondes mécaniques, et en particulier d’ondes de choc. Il s’agit, dans ce cas, d’impacts balistiques ou d’explosion.

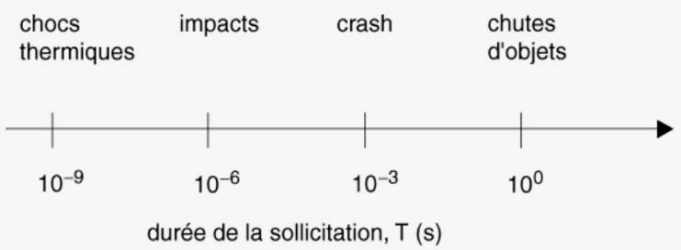

Figure 19 Classification des phénomènes dynamiques en fonction d’un temps caractéristique de variation de chargement [11].

Lorsqu’on s’intéresse au comportement des matériaux et des structures sollicités à grande vitesse, il faut distinguer les phénomènes de type inertiel de ceux liés à la propagation des ondes ou encore des variations des réponses mécaniques des matériaux du fait de leur sensibilité à la vitesse de sollicitation. Au sens strict, on ne peut parler de phénomène dynamique que lorsqu’il y a variation spatio-temporelle des champs de contrainte et de déformation. Si, comme dans notre étude, on ne s’intéresse qu’à la sensibilité des matériaux aux grandes vitesses de sollicitation afin d’identifier des lois de comportement pour le calcul des structures, on se doit de s’affranchir des effets liés aux propagations d’ondes. Dans l’absolu, toute variation spatio-temporelle des champs est considérée comme une

perturbation à éviter lors de la caractérisation mécanique. Toutefois, il est courant dans la littérature d'utiliser le terme de « comportement dynamique » pour parler de comportement à grande vitesse de sollicitation [11].

Nous considèrerons, dans ce qui suit, comme vitesses moyennes ou vitesses intermédiaires, les vitesses comprises entre celles relativement lentes, dites quasi-statiques et appliquées à l'échelle de la minute ou de la seconde. Celles appliquées à l'échelle de la milliseconde seront considérées comme rapide.

3.1. Machine de traction à grande vitesse et les mesures associées

Il existe donc différents régimes de vitesse de sollicitation que l'on peut classifier dans la figure suivante qui inclut les moyens expérimentaux classiquement dédiés par domaine de vitesse.

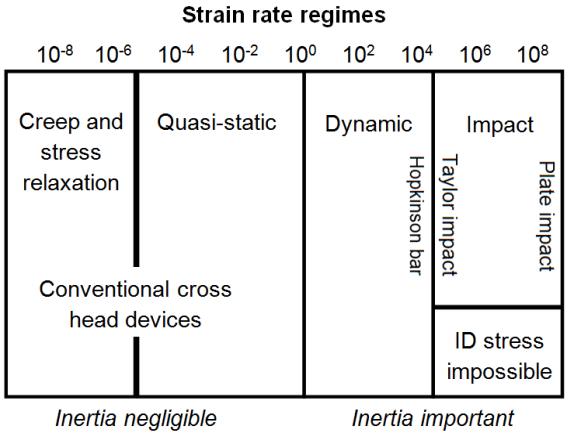

Figure 20 Classification des régimes dynamiques en fonction de la vitesse de déformation atteinte et des moyens développés pour accéder aux chargements correspondants [11].

Dans le cadre de ce travail, on vise l'analyse du comportement mécanique des SMC sur une gamme de vitesse de déformation allant du régime quasi-statique jusqu'au régime dynamique moyen soit de 10^{-4} s^{-1} à 100 s^{-1}. Ce domaine correspond en effet au domaine que l'on doit décrire pour la simulation d'événement de choc et crash dans l'automobile.

Des essais de traction à grande vitesse ont été réalisés sur une machine Schenk Hydropuls VHS 5020 (figure 21). Cet équipement permet de faire varier la vitesse de déplacement du vérin dans une plage allant de 10^{-4} m/s (quasi-statique) à 20 m/s. L'effort est mesuré par une cellule piézo-électrique

située en amont entre la traverse et le mors supérieur ; la capacité est de 50 kN. Le serrage est réalisé mécaniquement de sorte à minimiser les effets d'inertie.

La déformation locale est mesurée par une technique sans contact en utilisant une caméra à grande vitesse : deux points (taches circulaires) sont déposés sur la surface de la zone utile à ses extrémités. La distance entre ces marquages définit la longueur initiale sur laquelle la déformation est mesurée. Elle est d'un peu moins de 20 mm. Une caméra à grande vitesse (FASTCAM-APX RS) ayant une capacité d'acquisition de 250.000 images par seconde a été utilisée pour enregistrer le déplacement relatif de ces marques. Le traitement d'image est effectué à l'aide du logiciel ImageJ. Celui-ci consiste à suivre le déplacement du centre géométrique (barycentre) de chacune des taches et de calculer, à tout instant, la distance les séparant. Cette distance correspond à l'allongement de l'échantillon et permet de déterminer la déformation en fonction du temps (voir figure 22).

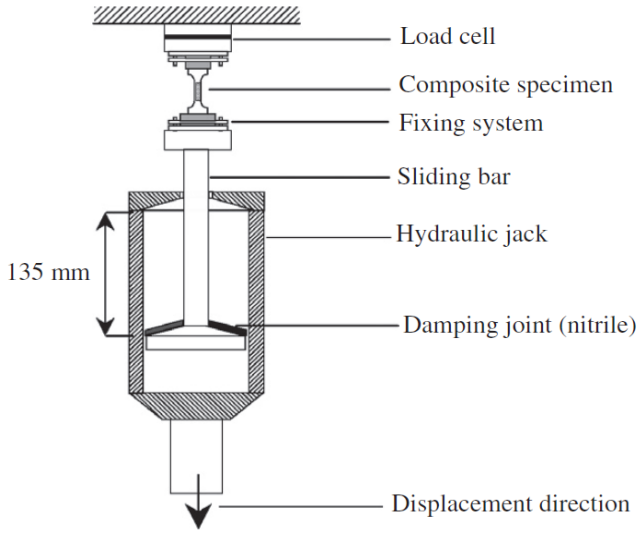

Figure 21 La machine de traction à grande vitesse.

3.2. Méthodologie d'optimisation des essais de traction à grande vitesse

3.2.1. Principe général et problématique

Lors d'un test à vitesse de sollicitation quasi-statique, on considère que le corps sollicité est en équilibre. En effet, le temps caractéristique de la sollicitation est extrêmement long, ce qui permet de stabiliser les champs de déformation. Dans le cas d'un essai de traction quasi-statique, on peut

considérer que le champ de déformation est homogène et que la vitesse de déformation est constante dans la zone utile dès le début du test. Par contre, lors d'un test aux vitesses moyennes, on utilise un système tube-piston afin d'appliquer la vitesse constante de déplacement désirée après la phase d'accélération du piston. Le choc tube-piston en fin de course implique une augmentation extrême de la vitesse de sollicitation appliquée au système. Des ondes mécaniques vont donc se propager et effectuer plusieurs allers-retours notamment dans l'échantillon. On considère qu'une dizaine d'aller-retour peut suffire à stabiliser le champ et la vitesse de déformation. Or, la durée de la sollicitation est relativement courte, le matériau peut se rompre alors que l'équilibre n'est pas encore établi. L'échantillon en matériau composite peut se trouver exposé à l'effet de propagation d'ondes de traction/compression tout au long de l'essai. Ces ondes provoquent des oscillations perturbant le chargement uniforme souhaité et la mesure. La mécanique des milieux continus est applicable dans cette gamme de vitesses en prenant toutefois quelques précautions. Par conséquent, le contrôle de l'effet de la propagation des ondes dues au choc lors du chargement devient un challenge important pour assurer la validité de l'analyse du comportement mécanique des matériaux sollicités à grande vitesse [31,32,35-37].

Comme nous l'avons précisé l'ensemble des effets cités représente des effets de « structure » que nous devons absolument découpler des effets propres au changement de comportement mécanique du composite sollicité à grande vitesse. En effet, à travers l'approche présentée ci-après, nous tendons à limiter ces effets de structure éventuels afin de n'avoir que les effets matériau, ce qui est notre objectif principal.

3.2.2. Géométrie optimisées

D'une façon générale, l'utilisation de machines servo-hydrauliques pose le problème des variables de contrôle de l'essai dynamique du fait de l'inertie propre de la machine et de la propagation de l'onde de choc. L'amplitude des perturbations de mesure conjuguée aux effets de structure liés à la géométrie de l'éprouvette et à la chaîne cinématique peut engendrer, au sein de l'éprouvette, des champs de contraintes et de déformations non homogènes au cours du chargement rapide [31,32,35-37]. C'est dans ce sens, que l'essai de traction dynamique a été optimisé afin d'obtenir des champs de déformations homogènes et une vitesse de déformation élevée et constante dans la zone utile de l'éprouvette testée.

Avant contact entre le piston (sliding bar, figure 21) et le vérin hydraulique (hydraulic jack), ce dernier peut être accéléré (en fonction de la vitesse d'essai choisie) sur une distance ou course libre allant jusqu'à 135 mm (135 mm pour la vitesse de déformation maximum). Une fois que le contact se produit, l'échantillon est ensuite soumis à l'effort de traction. Un joint d'amortissement (damping) placé entre la coulisse et le vérin hydraulique a été expérimentalement optimisé (choix du matériau, géométrie et épaisseur) afin de minimiser les perturbations dues aux effets inertiels mécaniques causés par la vitesse de mise en application de l'effort et de l'onde provoquée par le choc (tube-piston). En effet, le joint idéal doit pouvoir absorber l'onde à son premier passage lors de sa phase d'écrasement entre le tube et le coulisseau. Il est alors question de minimiser les écarts entre la contrainte maximale et minimale. Toutefois, la phase d'écrasement du joint affecte la vitesse de déformation dans l'échantillon au tout début du test. La stabilisation de la vitesse de déformation intervient alors bien avant la limite d'élasticité du matériau. Il s'agit donc, d'une part, de choisir le matériau constitutif de ce joint et d'autre part de le dimensionner de sorte que la vitesse de déformation dans la zone utile de l'échantillon soit constante avant la fin de la phase élastique du comportement. Le choix du matériau constitutif et la géométrie du joint ont été optimisés expérimentalement [11,34] (Article N°1, 2, 4 et 5). La géométrie des échantillons doit être optimisée afin de réduire les effets indésirables liés aux aspects inertiels d'une part et de propagation d'onde de choc d'autre part. Pour les essais de traction à grande vitesse, l'idée est de créer, dans l'échantillon, des changements de section (plus ou moins brutaux) afin de piéger (ou du moins limiter) ces deux phénomènes à travers une rupture brutale d'impédance mécanique. L'optimisation de la géométrie de l'éprouvette a été menée en utilisant le logiciel ABAQUS avec une résolution de type explicite afin de prendre en compte les effets d'inertie. Pour respecter le Volume Elémentaire Représentatif (VER) et tout en limitant leur volume, les éprouvettes sont du type haltère et présentent une zone utile d'étude d'une longueur de 20 mm et d'une largeur de 10 mm. Le rayon de raccordement entre la zone utile et les parties où vont se faire les prises en mors est de 6 mm [26].

3.2.3. Validation de la méthodologie des essais à grand vitesse

Après avoir testé plusieurs matériaux et plusieurs géométries, des joints en Nitrile d'épaisseur 1.5 mm ont été choisis pour remplir le rôle de joint amortisseur. Dans la figure 22-a [26], l'évolution de la

vitesse de déformation dans la zone utile obtenue par l'étude numérique est superposée à celle obtenue par des essais de traction réalisés à la même vitesse de chargement pour un composite A-SMC. Ce résultat est obtenu après avoir optimisé les dimensions de l'échantillon comme décrit plus haut.

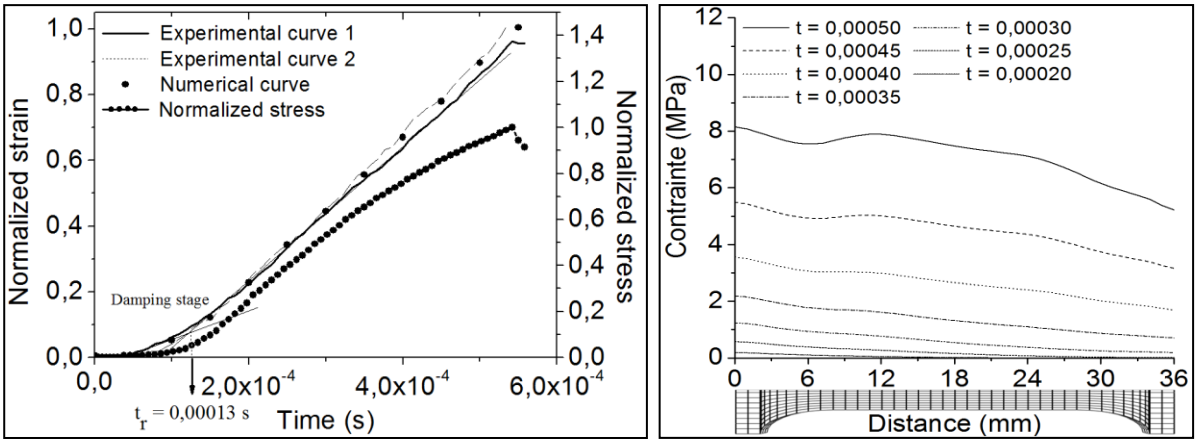

Figure 22 Evolution de la déformation au sein de l'éprouvette (a), et évolutions du champ de déformation à différents temps (b).

D'un point de vue expérimental, il est primordial que les propriétés mécaniques recueillies soient représentatives du comportement du composite étudié. La simulation numérique du chargement de l'éprouvette retrace donc une caractérisation expérimentale comparable à une caractérisation sous sollicitation quasi-statique. En effet, la vitesse de déformation se stabilise à partir d'une valeur temporelle de $1,3 \times 10^{-4}$ s correspondant au temps de montée (t_r). Sachant que le temps de montée se limite au tout début de la partie élastique du comportement mécanique, il est alors possible de déterminer correctement et avec certitude les propriétés élastiques du matériau. On vérifie d'ailleurs (figure 22-b) [26] que la stabilité est atteinte dès 4 MPa appliqué à l'échantillon dans la zone utile. On peut donc affirmer que cette géométrie permet d'obtenir rapidement un champ homogène de déformation et une vitesse de déformation constante dans la zone utile.

3.3. Effet de la vitesse de déformation

Le comportement mécanique des composites SMC est sensible à la vitesse de déformation [11,34]. Par conséquent, pour l'utilisation efficace de ces composites, leur réponse sous différentes vitesses de déformation devrait être clairement comprise. Une première étude sur un composite SMC

[31,32,35-37] standard renforcé par 30% de fibres de verre a montré que le module d'élasticité reste insensible à la vitesse de déformation pour la gamme de vitesse explorée (de quasi-statique à un maximum de 200 s^{-1}). Malgré quelques variations due à la dispersion des microstructures [11,34], le module d'Young reste stable autour d'une valeur moyenne de l'ordre de 13 GPa. Plusieurs études ont montré que le mécanisme d'endommagement prédominant pour les composites SMC standards est la décohésion à l'interface fibre-matrice. Dans le cas d'un composites SMC-R26, il a été démontré que lorsque la vitesse de déformation augmente, les phénomènes d'endommagement sont retardés et suivent une cinétique d'endommagement de plus en plus réduite avec l'augmentation de la vitesse.

A titre d'exemple, les courbes de contrainte-déformation (σ-ε) tracées pour différentes vitesses de déformation pour les composites A-SMC et LD-SMC [26,28] sont montrées dans la figure 23-a et 23-b, respectivement dans le cas de microstructure à orientation aléatoire. Ces évolutions sont à comparer avec celle de la figure obtenue pour un SMC standard (figure 12). On peut clairement noter que les comportements globaux de ces courbes de traction sont très dépendants de la vitesse de déformation. En d'autres termes, les vitesses de déformation élevées jouent un rôle important en termes de propriétés mécaniques. De même que pour les SMC standards, on observe un module élastique similaire quelle que soit la vitesse de déformation.

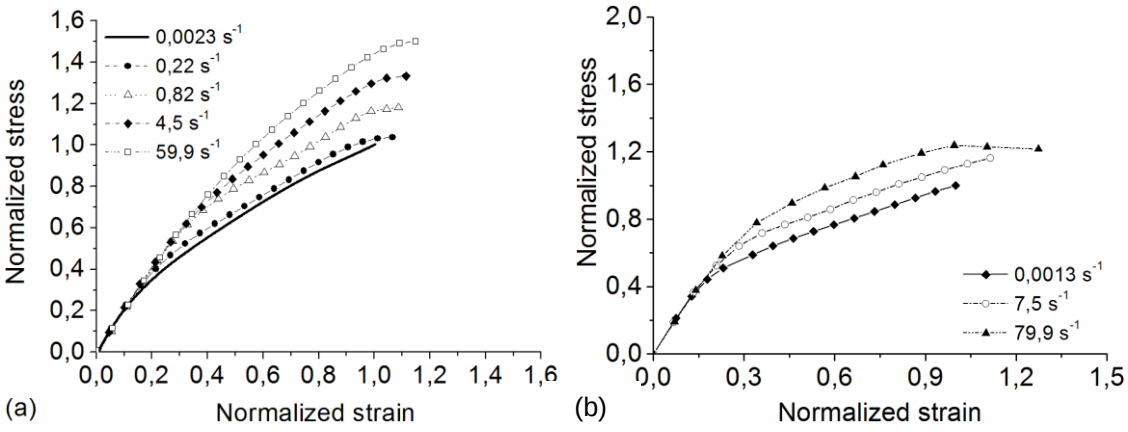

Figure 23 Courbe de traction aux vitesses de déformation différentes : RO-A-SMC (a) et RO-LD-SMC (b), (($\sigma_{normalisée} = \sigma / \sigma_{r(RO\ en\ QS)}$) et ($\varepsilon_{normalisée} = \varepsilon / \varepsilon_{r(RO\ en\ QS)}$)).

Les caractéristiques du matériau, à savoir seuils d'endommagement correspondant à la première non-linéarité ($\sigma_{threshold}$; $\varepsilon_{threshold}$) ainsi que la contrainte et la déformation ultime ($\sigma_{ultimate}$; $\varepsilon_{ultimate}$) sont

représentées sur les figures 24 et 25. Ces évolutions ont été tracées pour les trois configurations : RO, HO-0° et HO-90°. On peut noter que le seuil d'endommagement (figure 24-a, 24-b, 25-a et 25-b), en termes de contrainte et de déformation, augmente avec la vitesse de déformation. Par exemple dans le cas du HO-0°-A-SMC, on note une augmentation de 63% du seuil d'endommagement en terme de contrainte lorsque la vitesse de déformation passe du quasi-statique à 60 s^{-1}. D'autre part, la contrainte à la rupture augmente de 34% par rapport au cas quasi-statique. Il est intéressant de remarquer que les valeurs au seuil obtenues pour les plus grandes vitesses sont du même ordre de grandeur que les caractéristiques ultimes obtenues dans le cas de sollicitation quasi-statique. On peut aussi noter que quelle que soit l'orientation de la microstructure, la déformation ultime ne semble pas évoluer de façon significative avec la vitesse.

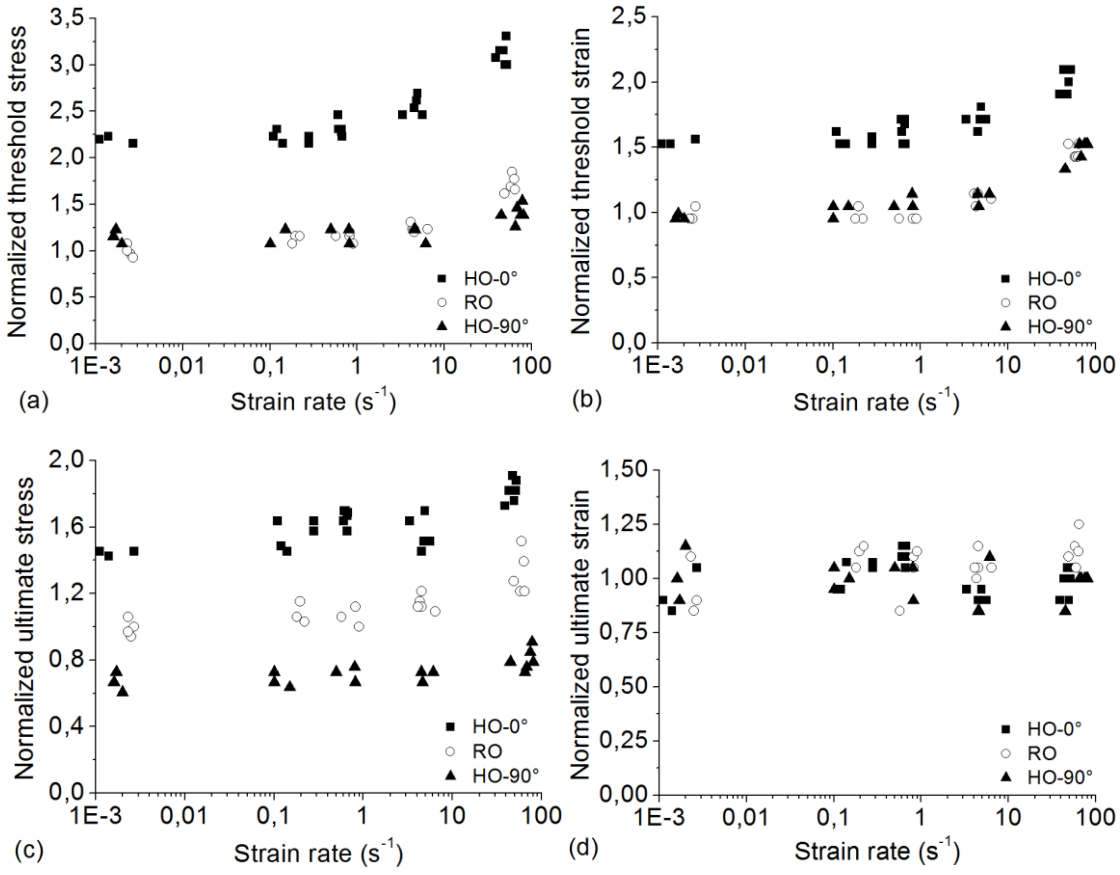

Figure 24 Influence de la vitesse de déformation : la déformation de seuil (a), la contrainte seuil (b), déformation ultime (c) et la contrainte ultime (d) (pour A-SMC composite).

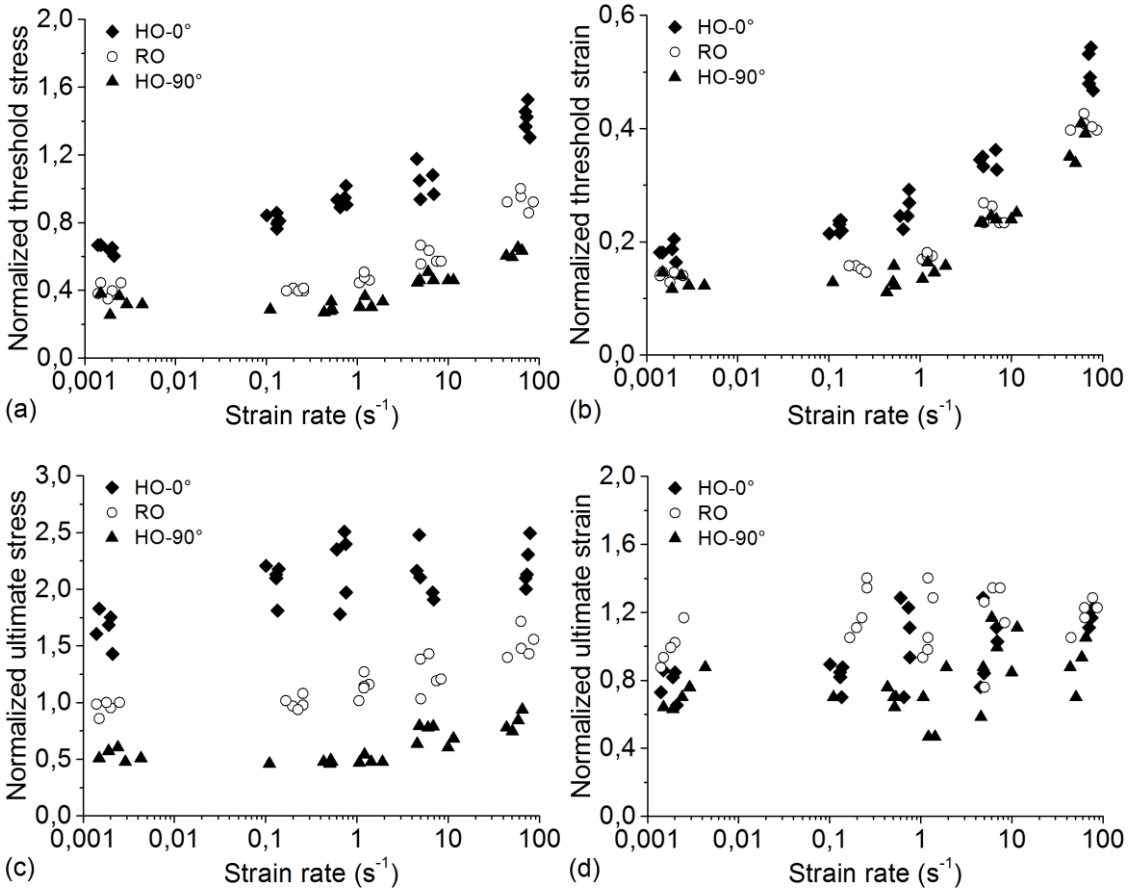

Figure 25 Influence de la vitesse de déformation : la déformation de seuil (a), la contrainte seuil (b), déformation ultime (c) et la contrainte ultime (d) (pour A-SMC composite).

Dans le cas du LD-SMC, la valeur du seuil d'endommagement en terme de contrainte augmente de plus de 120%, 130% et 114% pour les configurations HO-0°, R0 et HO-90° respectivement quand la vitesse varie du quasi-statique à 80 s^{-1}. De même que pour le A-SMC et le SMC standard, l'augmentation des contraintes ultimes est moins marquée (33%, 58% and 55% respectivement). Ci-après un tableau montre toutes les évolutions relatives des seuils et des valeurs à rupture pour les trois types de SMC.

Ces résultats mettent en évidence une forte influence de la vitesse de déformation sur les propriétés mécaniques des différents SMC. En effet, de même que pour les SMC standards, l'effet retard à l'initiation de l'endommagement est observé pour les A-SMC et le LD-SMC. En effet, dans le cas du SMC standard, il a été mis en évidence la nature visqueuse de l'endommagement qui s'exprime lors de l'initiation par un retard et lors de la propagation par une diminution de la cinétique d'endommagement. On peut alors parler d'un comportement visco-endommageable ; notion introduite par Fitoussi et al [35].

Type de SMC		Augmentation relative du seuil de non-linéarité en contrainte (%)	Augmentation relative de la contrainte à rupture (%)
SMC standard (RO) [11,34]		100	70
A-SMC [26]	HO-0°	45	40
	RO	70	45
	HO-90°	50	41
LD-SMC [28]	HO-0°	120	33
	RO	130	58
	HO-90°	114	55

Tableau 3 Valeur des seuils d'endommagement et des contraintes ultimes pour les trois types de SMC.

L'objet du paragraphe suivant est de mettre en évidence ces variations de façon expérimentale dans le cas du A-SMC qui devrait être utilisé pour des applications de type crash automobile.

3.4. Analyse expérimentale multi-échelles de l'endommagement et de la rupture à différentes vitesses de déformation

Dans le cas des SMC standards, la mise en œuvre d'essais interrompus avec suivi de l'endommagement à l'échelle microscopique et macroscopique a permis de mettre en évidence l'effet de la vitesse de déformation [31,32,35-37]. Quelle que soit la vitesse de déformation jusqu'à 100 s^{-1}, c'est toujours la rupture à l'interface fibre-matrice qui est le moteur de l'endommagement [31,32,35-37]. Une augmentation de la vitesse produit d'une part un retard à l'initiation de l'endommagement et d'autre part une diminution de la cinétique d'endommagement [31,32,35-37]. On parle alors de comportement visco-endommageable caractéristique du comportement dynamique du composite SMC standard. Par ailleurs, on montre que l'effet de vitesse sur l'endommagement de l'interface fibre-matrice est anisotrope [35]. Les résultats établis expérimentalement dans le cas du SMC standard ont permis de proposer et d'identifier une modélisation micromécanique prédictive du comportement mécanique du composite [34].

Nous proposons d'utiliser la technique des essais interrompues dans le cas du composite A-SMC afin d'une part, de déterminer les mécanismes d'endommagement à l'échelle microscopique et d'autre part de les corréler avec la réponse macroscopique à différentes vitesses de déformation. Une comparaison des mécanismes d'endommagement entre les différents types de SMC est aussi proposée.

3.4.1. Technique des essais interrompus

La technique des essais interrompus permet, pour une vitesse de sollicitation élevée, de déterminer les états d'endommagement successifs d'une éprouvette au cours d'un essai de traction dynamique. Un suivi de l'évolution des mécanismes d'endommagement à l'échelle microscopique et de la raideur résiduelle est rendu possible pour différents niveaux de contraintes. Pour cela, il est nécessaire d'interrompre l'essai à grande vitesse. La mise en série d'un fusible avec l'échantillon permet de procéder à la décharge de l'échantillon à une force de traction donnée définie par la taille du ligament de l'entaille réalisée sur le fusible (figure 26). Afin de définir des niveaux croissants de forces maximales, le ligament est optimisé pour se rompre à une vitesse donnée et à un niveau de force donné. Ces fusibles sont réalisés dans des tiges filetées en acier. Ainsi, à la rupture du fusible, l'échantillon est déchargé. Il est alors possible d'analyser au microscope les mécanismes d'endommagement pour chaque niveau croissant d'effort. Le même échantillon est alors sollicité avec un nouveau fusible dont le ligament est plus large et permet ainsi la recharge de l'échantillon jusqu'à un niveau de charge plus important. Le module d'Young est alors déterminé lors de la recharge. Ce processus est répété un certain nombre de fois jusqu'à la rupture de l'éprouvette. On peut alors corréler de façon quantitative l'évolution des propriétés macroscopiques avec celle des mécanismes d'endommagement.

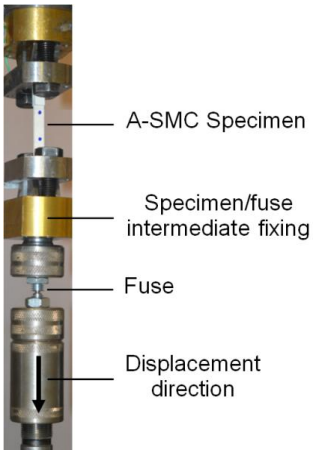

Figure 26 Dispositif échantillon-fusible pour essai interrompus en traction dynamique.

Des éprouvettes rectangulaires droites de RO-A-SMC avec talon ont été polies sur l'épaisseur afin de permettre l'observation au microscope électronique MEB. Pour une même vitesse de sollicitation, une même éprouvette sera examinée à différents niveaux de contraintes.

3.4.2. Comparaison des mécanismes d'endommagement en dynamique et en quasi-statique

- ***SMC standard et LD-SMC : Initiation et développement de l'endommagement par décohésion d'interfaces***

Dans le cas des SMC standards, c'est en général la rupture de l'interface fibre-matrice qui est la cause première de la dégradation progressive du composite. Dans le cas des LD-SMC, il a été montré (Article N°4) que l'endommagement de l'interface fibre-matrice est en compétition avec l'endommagement de l'interface bille de verre creuse-matrice (figure 27). Dans le cas où les fibres sont globalement orientées dans la direction de traction, c'est l'interface fibre-matrice qui s'endommage majoritairement. Dans le cas d'une orientation perpendiculaire, c'est plutôt l'interface bille de verre creuse-matrice qui devient le moteur de l'endommagement. Qualitativement, il n'a pas été noté de différences entre les faciès de rupture des échantillons testés en quasi-statique et ceux testés à grande vitesse. Nous n'avons pas réalisé d'essais interrompus à grande vitesse pour le cas des LD-SMC. Toutefois, les seuils et les cinétiques d'endommagement devraient varier avec la vitesse.

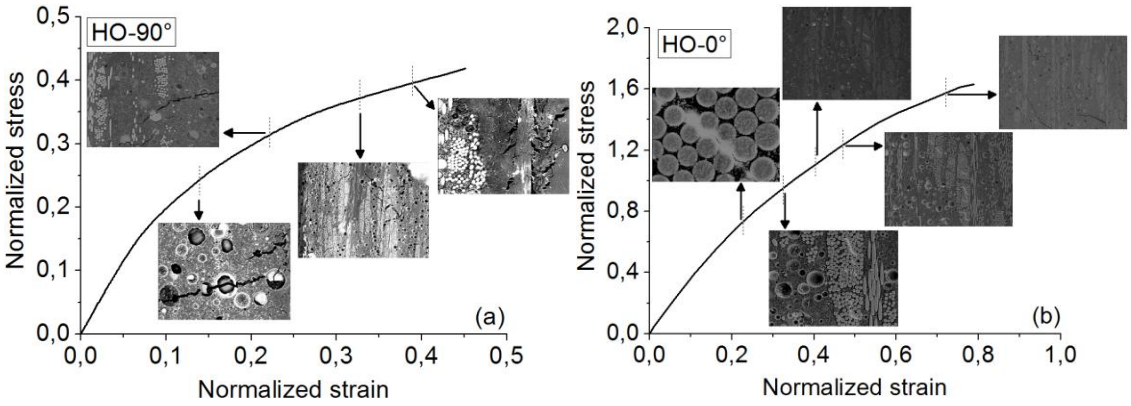

Figure 27 Mécanismes d'endommagement observés lors d'essais in-situ au MEB réalisés sur un composite LD-SMC (HO-90° et HO-0°).

- ***A-SMC : Initiations par décohésion d'interface et développement de l'endommagement par propagation de fissures***

Dans le but d'analyser les mécanismes d'endommagement lors de la traction des A-SMC à différentes vitesses, des essais de charge-décharge sous sollicitation quasi-statique et de traction interrompue sous sollicitation rapide ont été menés sur des échantillons de matériaux A-SMC. Dans le

cas du RO-A-SMC, une analyse de la chronologie des événements d'endommagement a été réalisée de la quasi-statique à 40 s^{-1}. Quelle que soit la vitesse, le premier phénomène d'endommagement observé correspond à la décohésion de l'interface fibre-matrice. Ce phénomène est le mécanisme prédominant d'initiation des microfissures. Il apparaît dès la première non-linéarité. Ce phénomène démarre tout d'abord sur les interfaces des renforts les plus désorientés et se propage progressivement à travers le volume global de la matière sur les fibres plus orientées. En effet, les fibres les plus désorientées par rapport à la direction de traction sont soumises à une contrainte normale locale élevée à l'interface. A l'intérieur de chaque faisceau de fibres, une défaillance de l'interface fibre-matrice se propage d'une fibre à sa voisine et tend rapidement à se propager d'une mèche à l'autre à travers la matrice. Lorsque la fissure rencontre une autre mèche, elle est déviée ou traverse la mèche selon l'orientation des renforts de la mèche rencontrée. Ainsi, un réseau de fissures globalement perpendiculaires à la direction de traction se développe. Les fissures déviées font apparaître des fissures globalement orientées dans la direction de traction. Ce phénomène d'initiation à l'interface fibre-matrice suivi d'une propagation progressive de fissure apparaît progressivement plusieurs fois sur chaque faisceau (figure 28).

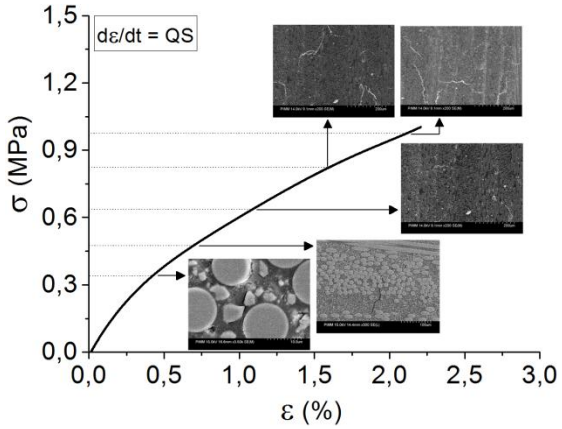

Figure 28 Chronologie des mécanismes d'endommagement en traction quasi-statique du A-SMC.

Enfin, à l'approche de la contrainte ultime, la coalescence des fissures situées entre les faisceaux induit du pseudo-délaminage des mèches justes avant rupture finale. Malgré des seuils et des cinétiques différents (voir paragraphe suivant), les mêmes phénomènes sont observés de la quasi-statique aux plus grandes vitesses (figure 29). Toutefois, on peut observer que lorsque l'on augmente la vitesse de déformation, les dégâts d'interface semblent être moins diffus. De plus, on peut observer que

l'augmentation de la vitesse de déformation favorise la propagation des microfissures transversales dans la matrice et le pseudo-délaminage [27] (voir paragraphe 3.4.4).

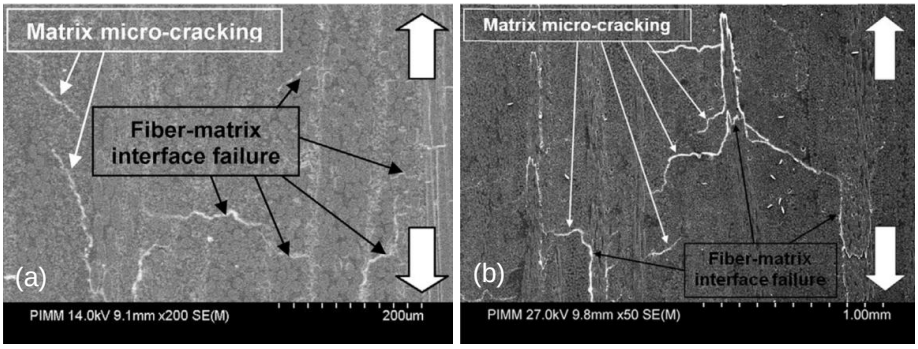

Figure 29 Observations de la microstructure après essai de traction pour RO-A-SMC: chargement quasi-statique (a), et chargement dynamique (b) [27].

On peut donc conclure pour les A-SMC que quelle que soit la vitesse de déformation imposée ;

- Le mécanisme initiateur de l'endommagement reste la décohésion à l'interface fibre-matrice (d'abord sur les fibres à 90° puis sur les fibres plus orientées (jusqu'à 30°),
- L'endommagement se développe simultanément par de nouvelles initiations à l'interface et la propagation de ces microfissures dans la matrice,
- Le pseudo-délaminage conduit à la rupture finale. Cependant, il semble bien plus développé à grande vitesse.

3.4.3. Analyse quantitative multi-échelles de l'endommagement

A) Échelle macroscopique

- Effet de l'orientation des fibres

La figure 30 montre, pour le A-SMC, l'évolution du paramètre macroscopique d'endommagement D, lors d'essais de traction charge-décharge quasi-statique, en fonction de la contrainte appliquée. On peut noter que dans le cas de l'échantillon HO-0°, les valeurs de ce paramètre macroscopique restent très faibles. Cette défaillance limitée de l'interface conduit à un comportement plus linéaire (comme on le voit sur la figure 29-b) tandis que le pseudo-délaminage est favorisé pour une valeur de D critique très faible.

De part une forte contrainte normale à l'interface fibre-matrice dans le cas de HO-90°, la cinétique d'endommagement est supérieure à celle du composite RO. D'autre part, on peut également observer sur les échantillons RO une inclinaison de la courbe (à partir de D = 0,18), indiquant une saturation de la défaillance de l'interface fibre-matrice. Enfin, la valeur critique de D à la rupture de ces deux microstructures semble être du même ordre de grandeur ; ce qui indique un état d'endommagement similaire.

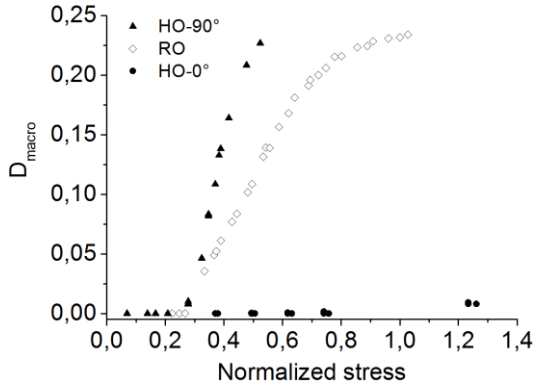

Figure 30 Evolution macroscopique de l'endommagement pour RO, HO-0° et HO-90° A-SMC.

- Effet de la vitesse de sollicitation

Les résultats expérimentaux des essais de traction interrompue réalisés à trois différentes vitesses de déformation (figure 31) variant de quasi-statique à 40 s^{-1} confirment que l'augmentation de la vitesse de déformation conduit à une initiation d'endommagement macroscopique retardé pour le A-SMC.

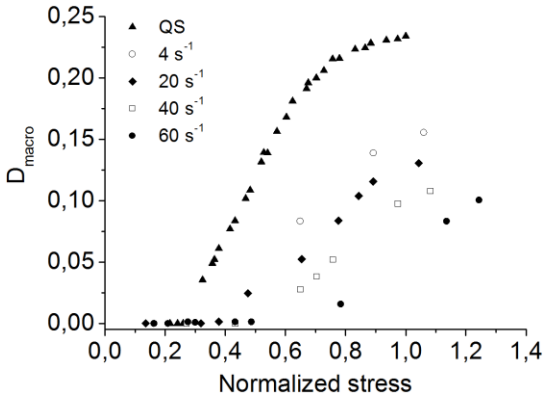

Figure 31 Evolution de l'endommagement macroscopique à différentes vitesses de déformation.

En effet, en quasi-statique la perte macroscopique de la rigidité commence à un niveau de 0.30 $\sigma_{r(RO)}$, alors que pour une vitesse de 40 s^{-1}, la première réduction de rigidité apparaît autour d'une contrainte d'environ 0.58 $\sigma_{r(RO)}$ qui correspond à une augmentation de 75% du seuil d'endommagement. En outre, il convient d'indiquer que les cinétiques d'endommagement sont plus de trois fois réduites lorsque la vitesse de déformation augmente de quasi-statique à 40 s^{-1} [27].

B) Échelle microscopique

- Effet de la vitesse de sollicitation

L'analyse de l'évolution de la microstructure lors des essais interrompus permet de comprendre l'origine physique des endommagements retardés et de quantifier, à l'échelle microscopique, les seuils et cinétiques d'endommagement. La figure 32 illustre l'évolution du paramètre d'endommagement d'interface (d_{micro}) en fonction de la contrainte appliquée à différentes vitesses de déformation [27].

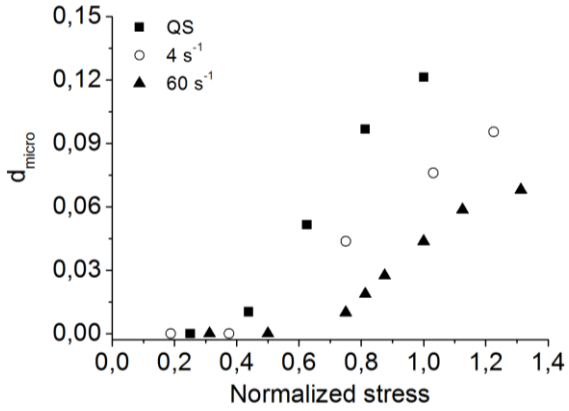

Figure 32 Evolution microscopique globale des endommagements en fonction de la vitesse.

Conformément à l'évolution macroscopique des indicateurs comme le seuil d'endommagement analysé à l'échelle microscopique est décalé vers des valeurs plus élevées et la cinétique des endommagements est réduite lorsque l'on augmente la vitesse de déformation. Ces aspects représentent l'effet du visco-endommagement déjà mis en évidence pour les SMC standards. Cependant, on doit remarquer que, comparé à ces derniers, l'endommagement microscopique à l'interface est bien plus limité dans le cas des A-SMC. En effet, les valeurs du paramètre local d'endommagement d'interface restent autour de 10% alors qu'elles atteignent déjà 20 à 30% jusqu'à 50% de la phase non linéaire

d'endommagement pour les SMC standards. Des valeurs de l'ordre de 80% ont été enregistrées dans le cas d'une sollicitation quasi-statique d'un SMC standard (figure 33).

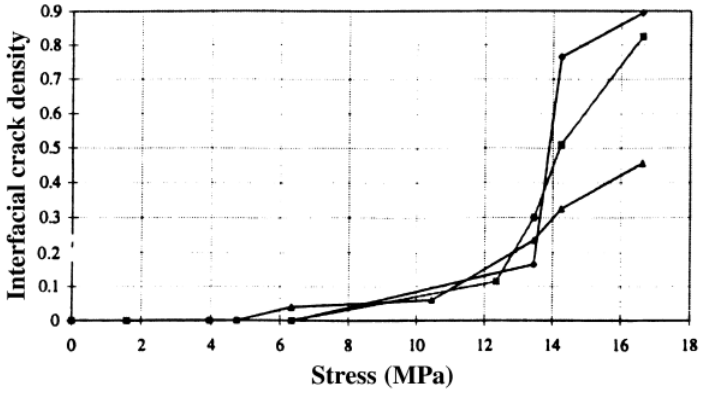

Figure 33 Evolution du paramètre local d'endommagement d'interface pour les renforts orientés à 90° lors d'une sollicitation de traction sur un SMC standard [88].

On peut donc conclure que l'augmentation du taux de renfort conduit à une diminution de l'endommagement à l'interface fibre-matrice qui reste toutefois le mécanisme initiateur mais qui est rapidement relayé par la fissuration matricielle transverse.

C) Effets anisotropes de la vitesse de déformation sur la décohésion à l'interface fibre-matrice

La figure 34 montre l'évolution de l'indicateur d'endommagement interfacial local, pour chaque famille [27].

On peut noter que, indépendamment de la vitesse de déformation appliquée, l'augmentant de l'orientation des fibres conduit à une diminution du seuil d'endommagement tandis que les cinétiques d'endommagement augmentent. En effet, la décohésion à l'interface fibre-matrice peut se produire quand la combinaison d'une contrainte normale et d'un cisaillement local se produit à l'interface. Toutefois, l'interface fibre-matrice des fibres orientées à 90° se rompt plus facilement sous l'effet d'une contrainte normale pure.

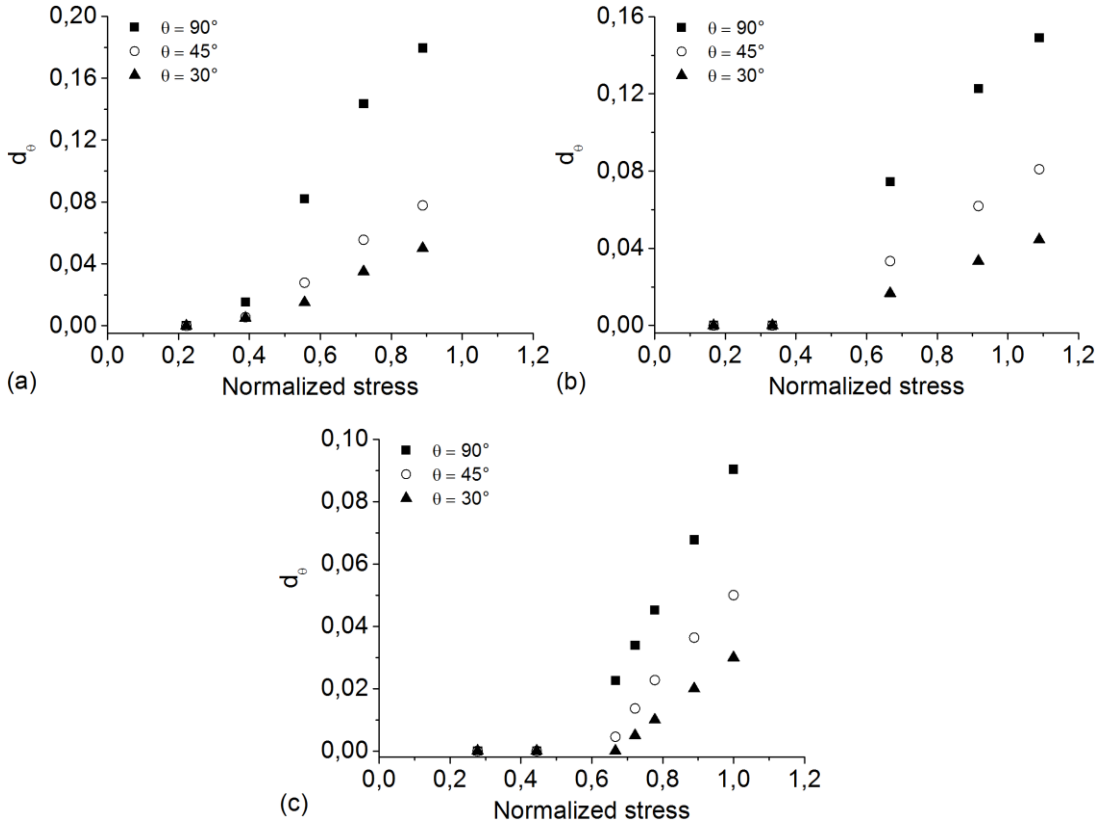

Figure 34 Evolution du d_Θ en fonction de la contrainte appliquée ; quasi-statique (a), 4 s^{-1} (b), et 40 s^{-1} (c).

3.4.4. Effet de la vitesse et de l'orientation sur le mécanisme de rupture par pseudo-délaminage

Dans cette section, l'influence de la vitesse et de l'orientation des fibres sur le phénomène de pseudo-délaminage sont étudiées pour le A-SMC composite [26]. La figure 35-a montre une évolution typique de la déformation de traction jusqu'à la séparation totale en deux parties par délaminage local entre différents faisceaux de fibres. On note une augmentation brutale de la vitesse de déformation typique des phénomènes de localisation et traduisant ici le pseudo-délaminage.

Pour les essais de traction à grande vitesse, la durée de la phase de pseudo-délaminage semble être très courte (environ 10^{-4} s) par rapport aux phases d'endommagement et élastique (environ 5,5 × 10^{-4} s). La vitesse de déformation pendant la phase de délaminage est plus de 15 fois supérieure aux autres phases. Les courbes de contrainte-déformation en traction peuvent également être représentées comme sur la figure 35-b. La surface sous la courbe contrainte-déformation correspond à l'énergie de déformation

totale par unité de volume absorbée par le composite jusqu'à une séparation complète en deux. On constate que l'énergie dissipée lors de la phase de délaminage peut être jusqu'à sept fois supérieure à l'énergie dissipée lors de l'endommagement. Ce phénomène est largement favorisé par l'orientation des renforts dans la direction de la traction et par l'augmentation de la vitesse de déformation (Article N°2). En effet, nous avons montré précédemment que l'augmentation de ces deux paramètres (orientation des renforts et vitesses) participe à l'inhibition de l'endommagement à l'interface fibre-matrice (seuil retardé et cinétique amoindrie). Le matériau développe donc une fissuration matricielle plutôt à l'extérieure des mèches qui rapidement s'endommagent sur leur interface, ce qui conduit à un fort délaminage inter-mèche.

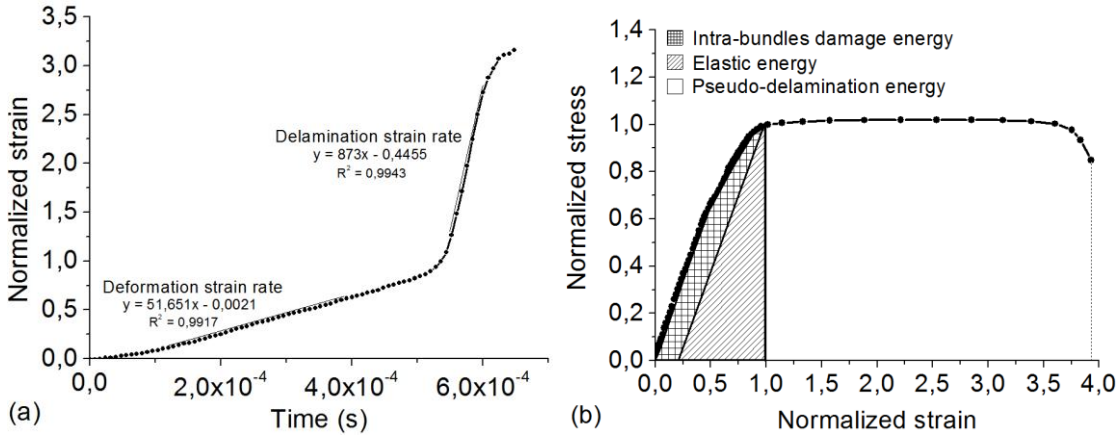

Figure 35 Déformation en fonction du temps (a), et courbe de traction pour HO-0°-A-SMC obtenue pour l'essai effectué à la vitesse de déformation de 52 s^{-1} (b).

Par conséquent, le pseudo-délaminage peut participer fortement à la dissipation d'énergie lors d'un crash automobile. Aussi, ce mécanisme ne peut être négligé.

4. Etude du comportement dynamique résiduel post-fatigue

La question posée dans ce chapitre peut être formulée de la façon suivante : Quel est l'effet d'une sollicitation de type fatigue sur le comportement dynamique résiduel du matériau A-SMC ?

Répondre à cette question nécessite de définir l'échelle de l'analyse que l'on veut proposer. En effet, on peut s'intéresser à ce couplage à différentes échelles : macroscopique, microscopique voire nanométrique. Du point de vue macroscopique, on doit s'intéresser à l'évolution de la réponse dynamique post-fatigue, ce qui permettrait de se doter de lois de comportement plus représentatif pour le dimensionnement au crash des structures automobiles réelles. En effet, les structures automobiles sont jusqu'alors toujours dimensionnées sur la base de caractérisations mécaniques réalisées sur des matériaux n'ayant subi aucune sollicitation. Or, la plupart des structures automobiles sont soumises à des sollicitations de type fatigue avant de subir un crash. En effet, les composants automobiles mis en service depuis plusieurs mois, voire quelques années ont généralement subi des sollicitations cycliques (fatigue ou vibratoire) post-impact ou crash. On pourra citer à titre d'exemple les cycles ouverture fermeture d'un hayon, la vibration transmise au plancher lors du roulage, etc. Ainsi, le dimensionnement au crash des structures et des composants automobiles au crash devra intégrer l'histoire du chargement subi et l'endommagement associé. Il est à noter que la prise en compte du comportement dynamique post-fatigue n'a pas été traitée dans la littérature ouverte et encore moins sur les composites de type SMC. Ainsi, il apparaît donc nécessaire d'évaluer les propriétés résiduelles sous sollicitation rapide des matériaux ayant subi des sollicitations partielles de type fatigue.

A une échelle plus fine les phénomènes locaux de déformation et d'endommagement sont à l'origine des réponses macroscopiques. Y-a-il à cette échelle des phénomènes spécifiques développés lors de la fatigue qui viendraient modifier la réponse attendue sous sollicitation rapide post-fatigue. Par exemple, dans le cas des matériaux composites à matrice thermoplastique, il a été montré [30,56,81] que les sollicitations répétées peuvent produire une accumulation progressive de la déformation plastique voire viscoplastique et/ou des phénomènes d'endommagements spécifiques au niveau des interfaces / interphases fibre-matrice. Enfin, à une échelle encore plus fine, on peut aussi se poser la question de l'effet des modifications microstructurales du polymère en fatigue.

Quel est l'impact de ces différents types d'évolution sur le comportement résiduel sous sollicitation rapide. Il est clair que cette thématique pourrait faire l'objet de plusieurs années de travail de recherche. Dans le cadre de ce travail, nous jetons les bases de cette thématique à travers une comparaison des propriétés dynamiques post-fatigue avec celle du même matériau vierge. Comme il a été mentionné plus haut, cette comparaison est une première étape dans l'objectif d'intégrer les effets d'un chargement cyclique sur le comportement dynamique afin d'assurer un dimensionnement réaliste.

4.1. Proposition d'une méthodologie

Afin de mettre en évidence l'effet spécifique de la fatigue sur le comportement dynamique, il nous faut définir un état de référence auquel nous comparerons le comportement dynamique post-fatigue. Etant donné qu'il a largement été démontré que l'endommagement est le moteur du comportement des composites SMC, on peut fixer l'évolution de la rigidité comme indicateur de l'endommagement. Du point de vue phénoménologique, la rigidité relative, (E/E_0), évolue au cours de la sollicitation pour les deux types de chargement : fatigue et traction (monotone croissante quasi-statique ou dynamique). Considérons un essai de charge-décharge réalisé sur un composite SMC jusqu'à une valeur de contrainte σ_1. Si l'on dépasse le seuil de non-linéarité, σ_0, des microfissures se développent à l'échelle locale définissant un état endommagé caractérisé par un module d'Young réduit. Si l'on recharge à nouveau, une nouvelle valeur du seuil de non-linéarité sera observée proche de σ_1 et une rupture pour une valeur équivalente à celle du matériau vierge (voir figure 36). Ainsi, quelle que soit la vitesse de déformation, le seuil de non-linéarité correspondra toujours à une valeur proche de la contrainte maximale précédemment atteinte. Par ailleurs, la rupture devrait toujours se produire pour une valeur proche de la contrainte à rupture du matériau vierge (figure 36).

Considérons maintenant des courbes de traction à différentes vitesses ainsi qu'un état endommagé donné du matériau caractérisé par un module E inférieur au module du matériau non endommagé E_0. Si on considère cet état d'endommagement de référence (module E) comme étant celui obtenu en traction monotone, l'évolution du seuil d'endommagement pour cet état de référence peut être tracée par construction comme dans la figure 37. Cette courbe d'évolution du seuil d'endommagement en

fonction de la vitesse de déformation peut être tracée pour différents états d'endommagement (module E différent).

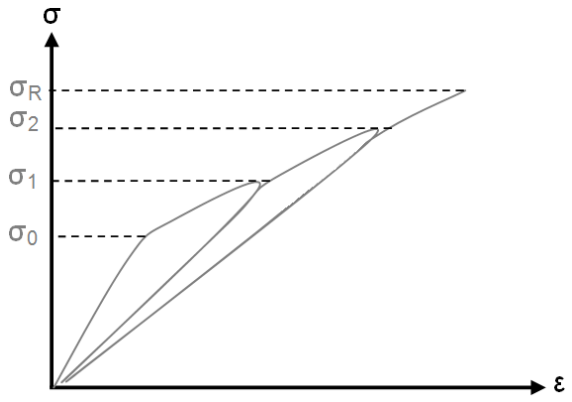

Figure 36 Schématisation de l'évolution du seuil d'endommagement apparent au cours de la sollicitation de charge-décharge.

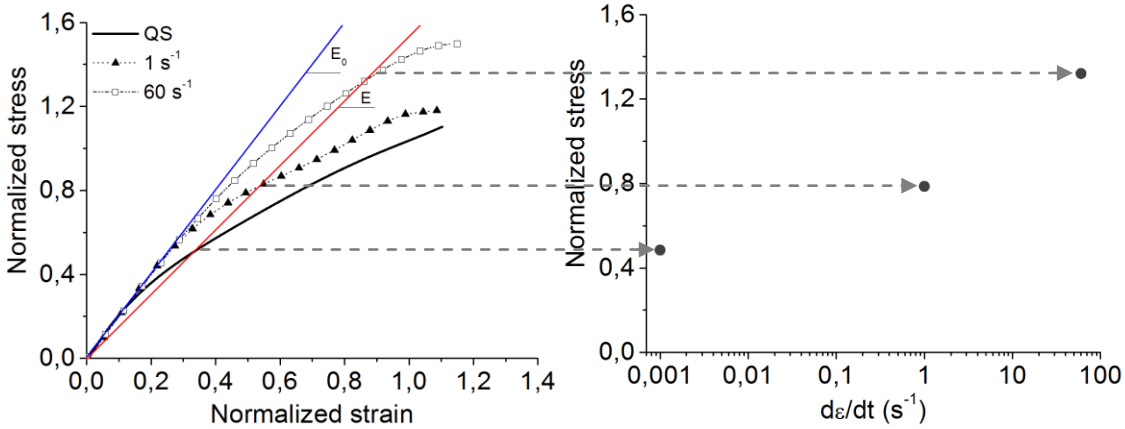

Figure 37 Évolution du seuil d'endommagement apparent en fonction de la vitesse de déformation pour un état d'endommagement donné (iso-endommagement).

On peut donc définir une courbe référence d'évolution du seuil en fonction de la vitesse par état d'endommagement considéré, autrement dit, une courbe d'évolution des seuils en fonction de la vitesse à iso-endommagement.

Toutefois, cet état d'endommagement macroscopique (module E) peut aussi être atteint par une sollicitation partielle de type fatigue (figure 38 et 39). La méthodologie proposée dans cette étude consiste à comparer les courbes d'évolution à iso-endommagement (module E) obtenues à l'issue d'essais dynamiques post-fatigue à celles qu'on peut obtenir en traction dynamique monotone (comme dans la

figure 37). La comparaison sera faite sur des états d'endommagement E équivalents successifs correspondants à différentes valeurs de la fraction de durée de vie, N/N_r. On compare alors, à différentes vitesses de sollicitation, le potentiel restant d'un échantillon pré-fatigué à celui pré-endommagé en traction monotone. Les écarts observés entre les évolutions post-fatigue et celles de référence obtenues en traction monotone seront attribuées aux phénomènes spécifiques développés en fatigue. Par exemple, l'écart observé sur le seuil d'endommagement pourra être calculé pour différentes condition (Amplitude, N/N_r, ε) par l'expression suivante :

$$\text{Écart}_{\sigma_{seuil}} = \frac{\sigma_{seuil}^{référence} - \sigma_{seuil}^{post-fatigue}}{\sigma_{seuil}^{référence}} \qquad \text{Equation 4}$$

Cette méthodologie permet donc de mettre en évidence, pour des états d'endommagement macroscopiques (E) équivalents, des différences d'état structural de la matière endommagée. En d'autres termes, cette étude s'attache à répondre à la question suivante : un pré-endommagement réalisé en traction monotone produit-il, du point de vue des propriétés macroscopiques sous sollicitation rapide, les mêmes effets que le même niveau de pré-endommagement qui serait obtenu en fatigue ? Où énoncé sous une autre forme, quel serait l'effet de la fatigue sur le potentiel restant à différentes vitesses de sollicitation.

Les paramètres de variabilité choisis seront d'une part la fraction de durée de vie en fatigue N/N_r directement liée à l'état d'endommagement (Ce dernier est caractérisé en fatigue par la baisse de raideur relative E/E_0 (figure 38 et 39)) et d'autre part, l'amplitude de la contrainte appliquée en fatigue. Trois valeurs ont été définies : 0.38 $\sigma_{r(RO)}$, 0.45 $\sigma_{r(RO)}$ et 0.55 $\sigma_{r(RO)}$. Dans ce chapitre, les essais de fatigue ont été réalisés sur le matériau RO-A-SMC, à la température ambiante (20°C) et à une fréquence de 30 Hz.

Les essais de fatigue ont été interrompus à différentes valeurs de fraction de durée de vie N/N_r, soit autour de 3%, 15%, 35% et 50% selon le tableau suivant.

On peut aisément vérifier sur les courbes de baisse de raideur relative la bonne répétabilité des essais de fatigue interrompus à différents niveaux de fraction de vie (figure 38).

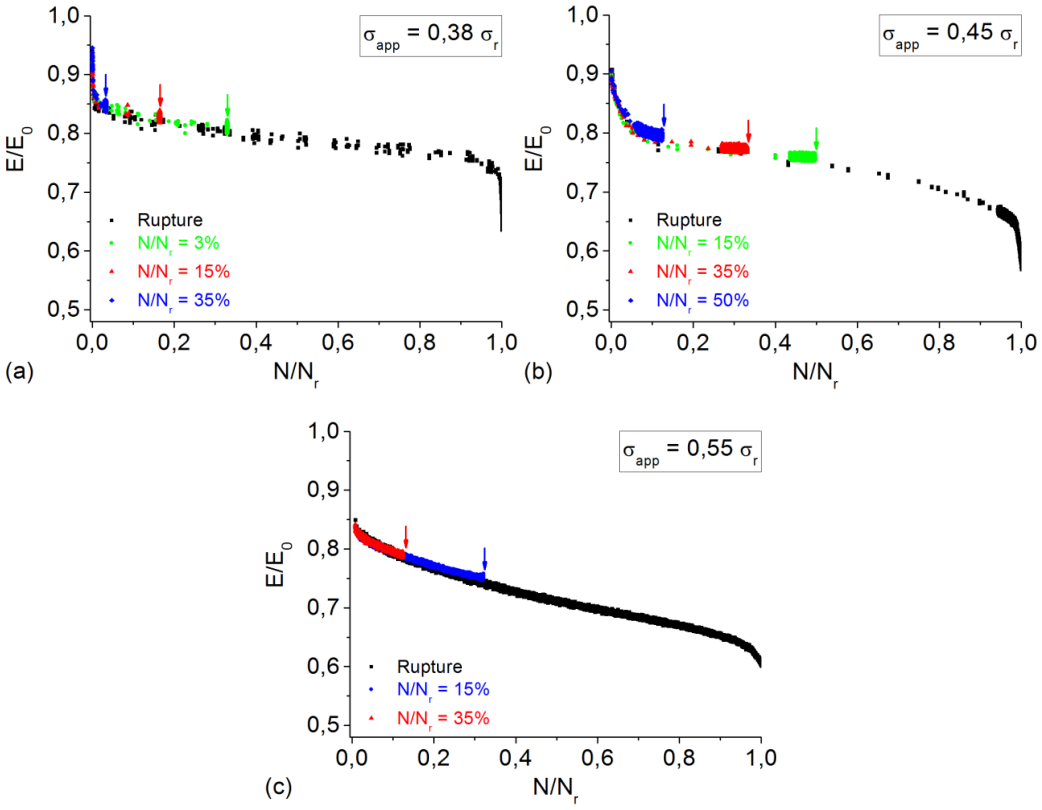

Figure 38 Evolutions du module de Young relatif pour différentes contraintes appliquées et certains cycles définis pour le matériau RO-A-SMC ; 0.38 $\sigma_{r(RO)}$ (a), 0.45 $\sigma_{r(RO)}$ (b), et 0.55 $\sigma_{r(RO)}$ (c).

Les courbes représentative $E/E_0 = f(N/N_r)$ sont regroupées sur la figure 39 pour les trois amplitudes de travail.

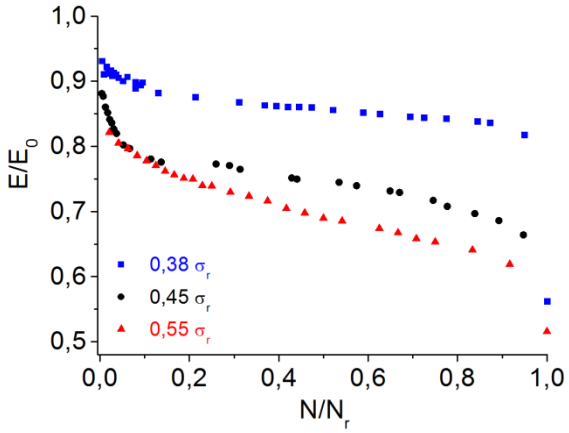

Figure 39 Evolution de la raideur relative en fonction de la fraction de durée de vie.

A la suite de l'interruption du test de fatigue (figure 38), des essais de traction monotones sont réalisés à trois vitesses de déformation : 10^{-3} s^{-1} (quasi-statique), 1 s^{-1} et 60 s^{-1}. Le détail des conditions

expérimentales de cette procédure est donné dans le tableau 4. Pour chacune des conditions d'essais de cette procédure (Amplitude, N/N_r, ε), les essais ont été réalisés quatre fois. La totalité des essais a été réalisée sur la géométrie d'échantillon optimisée au chapitre précédent afin d'assurer une bonne qualité des essais rapides.

Essai de fatigue (f=30 Hz, T° ambiante)			Essai de traction		
Contrainte appliquée	Nombres de cycles définis	N/N_r (%)	Vitesse de déformation		
0.38 $\sigma_{r(RO)}$	100 000 500 000 1 000 000	3 15 35	quasi-statique	1 s^{-1}	60 s^{-1}
0.45 $\sigma_{r(RO)}$	15 000 40 000 60 000	15 35 50	quasi-statique	1 s^{-1}	60 s^{-1}
0.55 $\sigma_{r(RO)}$	1 000 2 500	15 35	quasi-statique	1 s^{-1}	60 s^{-1}

Tableau 4 Paramètres de chargement lors d'essais pour l'étude du couplage fatigue-dynamique rapide pour le matériau RO-A-SMC.

4.2. Effets thermiques et effet de l'endommagement

Comme il a été indiqué ci-dessus et dans un souci de correspondance avec les conditions d'utilisation des structures automobiles, les essais de fatigue ont été réalisés à une fréquence de 30 Hz. Dans la figure 40, on a reporté les évolutions de l'augmentation de la température mesurées lors des essais de fatigue à 0.38 $\sigma_{r(RO)}$, 0.45 $\sigma_{r(RO)}$ et 0.55 $\sigma_{r(RO)}$. On note une température qui peut dépasser 50°C. Or, une analyse en DMA (figure 41) met en évidence pour ces matériaux des variations non négligeables dans cette gamme de température. Par conséquent, une part de la baisse de raideur mesurée et présentée sur les figures 38 et 39 est liée au phénomène d'auto-échauffement. Notre démarche étant fondée sur l'analyse des baisses de raideur liées à l'endommagement, on doit donc extraire l'évolution du module relatif dans la gamme de température allant de 25°C à 75°C qui correspond à la zone de la transition β connue dans les polymères amorphes comme étant la transition ductile-fragile. Celle-ci correspond à l'échelle des chaines macromoléculaires à une agitation thermique suffisante pour activer le mouvement des radicaux à la périphérie de la chaine carbonée. On peut alors considérer que cette zone soit centrée autour de 45°C. Il est à rappeler que les amplitudes de contraintes appliquées en DMA sont

extrêmement faibles et ne sont pas à même de produire de l'auto-échauffement quelle que soit la fréquence.

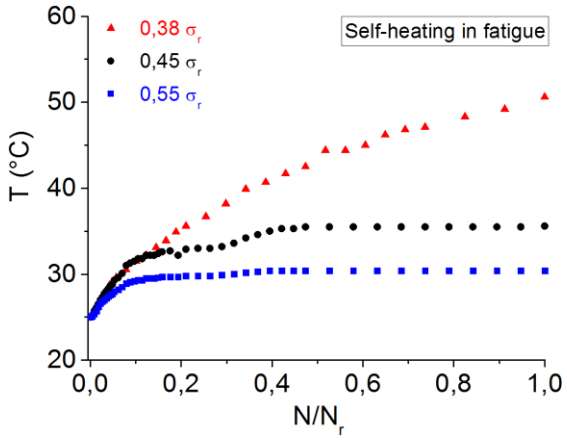

Figure 40 Exemples d'auto-échauffement lors d'essais de fatigue sur A-SMC (RO).

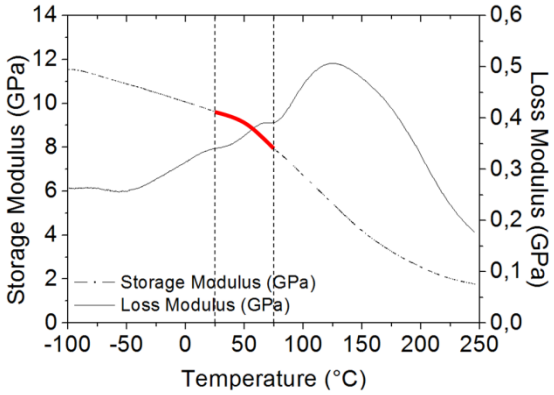

Figure 41 DMA réalisée sur un échantillon RO-A-SMC.

Notre méthodologie s'appuyant sur le suivi des baisses de raideur liées à l'endommagement, il faut s'affranchir de la part de la baisse de raideur relative qui est liée à l'augmentation de la température par auto-échauffement (adoucissement dû à la température). Il faut donc extraire cette contribution des courbes de la figure 39. Afin d'évaluer cette dernière, nous avons utilisé les courbes des figures 40 et 41 en discriminant la part thermique induite par l'auto-échauffement, $(E/E_0)_T$ en considérant que :

$$\frac{E}{E_0} = 1 - (\frac{E}{E_0})_T - (\frac{E}{E_0})_D \qquad \text{Equation 4}$$

Ou $(\frac{E}{E_0})_D$ correspond à la baisse de raideur induite par l'endommagement uniquement. Ce traitement est illustré dans le cas des amplitudes de 0.38 $\sigma_{r(RO)}$, 0.45 $\sigma_{r(RO)}$ et 0.55 $\sigma_{r(RO)}$ sur les courbes de la figure 42.

On note que pour cette fréquence, la part thermique reste relativement limitée sauf pour l'amplitude de 0.55 $\sigma_{r(RO)}$.

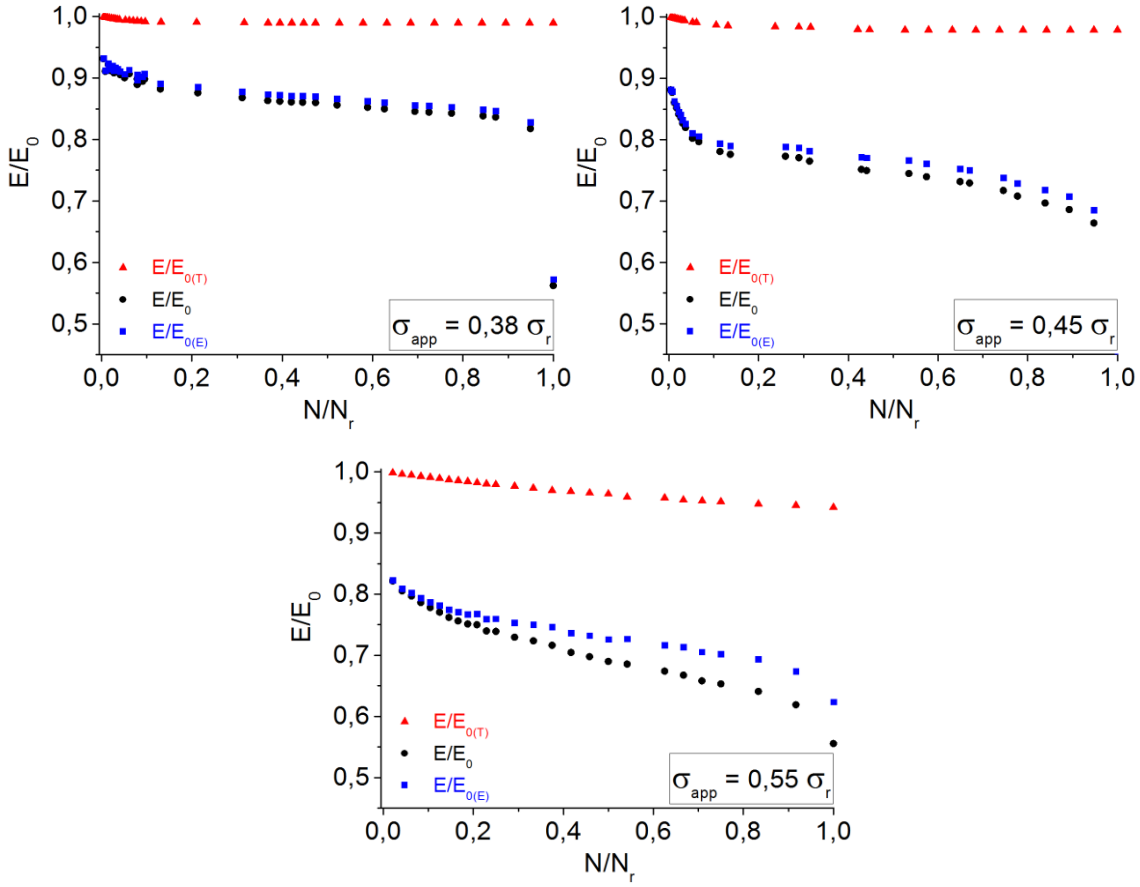

Figure 42 Décomposition de la baisse de raideur en une la part thermique et une la part induite par l'endommagement ; 0.38 $\sigma_{r(RO)}$ (a), 0.45 $\sigma_{r(RO)}$ (b), et 0.55 $\sigma_{r(RO)}$ (c).

4.3. Effet de la vitesse de déformation sur les caractéristiques du matériau pré-sollicité en fatigue

Les essais de traction à différentes vitesses (du QS à 60 s^{-1}) ont été réalisés sur les échantillons RO-A-SMC préalablement fatigués à trois niveaux d'amplitudes de contrainte : 0.38 $\sigma_{r(RO)}$, 0.45 $\sigma_{r(RO)}$ et 0.55 $\sigma_{r(RO)}$, selon le protocole présenté dans le tableau 4. A titre d'exemple, les courbes de contrainte-déformation (σ-ε) tracées pour différentes vitesses de déformation et différentes valeurs de fraction de durée de vie (N/N_r) sont montrées dans la figure 43 dans le cas d'amplitude de 0.38 $\sigma_{r(RO)}$. Il convient de noter que pour l'ensemble des courbes pour le matériau en configurations pré-endommagées, les

courbes des essais de traction monotone sont établies pour chaque vitesse de déformation. On voit bien clairement, après les essais couplage fatigue-dynamique, les échantillons préalablement fatigués présentent un module d'élasticité, une contrainte et une déformation à la rupture plus faible que les échantillons vierges.

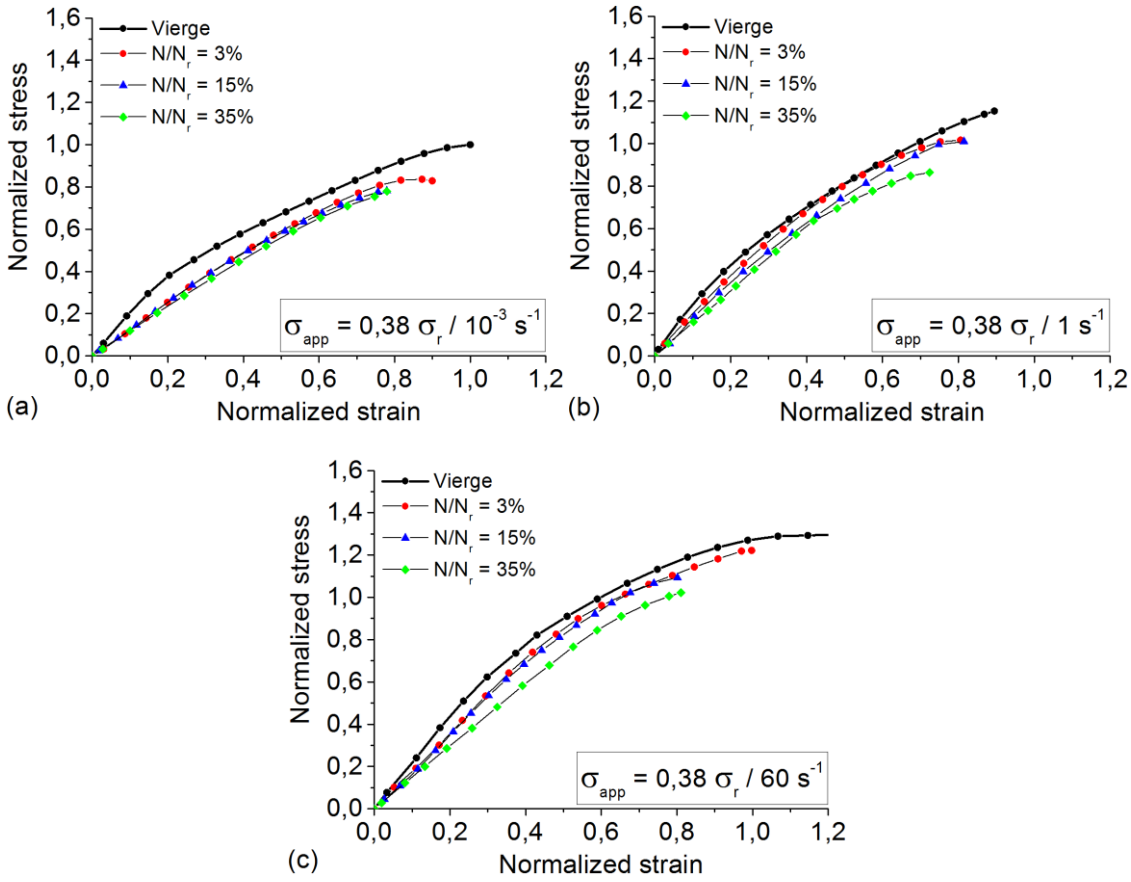

Figure 43 Courbe de traction post-fatigue réalisée à 0.38 $\sigma_{r(RO)}$. La traction est réalisée à des vitesses de déformation différentes quasi-statique (a), 1 s^{-1} (b), et 60 s^{-1} (c) sur des éprouvettes ayant subi une fatigue interrompue trois niveau de fraction de durée de vie (N/N$_r$) : 3, 15 et 35 %.

4.3.1. Effets de la sollicitation rapide (dynamique) post-fatigue sur la rigidité résiduelle

Pour les essais de traction à différentes vitesses (du QS à 60 s^{-1}) réalisés sur les échantillons ayant subi un chargement de fatigue dans les différentes conditions (d'amplitude et de nombres de cycle), nous avons tracé les courbes de l'évolution du module relatif (E/E$_0$) en fonction du nombre de cycle relatif (N/N$_r$), sur la figure 44.

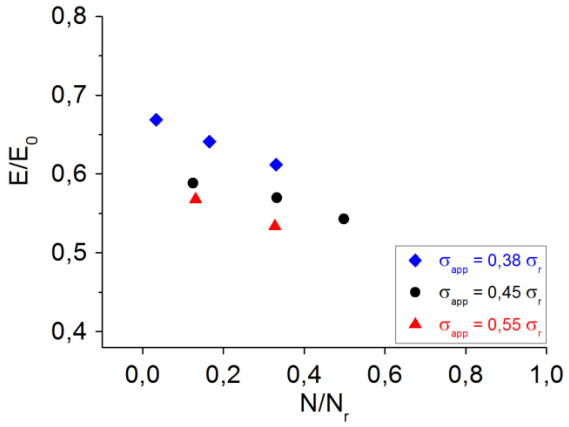

Figure 44 Evolution du module d'Young des échantillons fatigués dans les différentes conditions.

(Les essais de traction sont réalisés à la vitesse de 60 s^{-1}).

Les résultats montrent que l'amplitude de déformation joue un rôle important sur l'évolution du module d'Young. Pour une contrainte appliquée de 0.55 $\sigma_{r(RO)}$ et à une fraction de durée de vie (N/N_r) égale à 15%, la valeur du module d'élasticité diminue d'environ 43% ; alors que cette valeur est similaire à celle d'un échantillon fatigué avec une contrainte appliquée à 0.45 $\sigma_{r(RO)}$pour une fraction de durée de vie (N/N_r) de 35%. Sur la figure 44, on constate également qu'une pré-fatigue à 0.55 $\sigma_{r(RO)}$ et N/N_r = 35% génère le même niveau de perte de module ($E/E_0 \approx$ de 55%) qu'un chargement de fatigue à 0.45 $\sigma_{r(RO)}$ mené à N/N_r = 50%.

Les courbes montrent également que la diminution du module de Young de l'échantillon préalablement fatigué avec une amplitude de 0.38 $\sigma_{r(RO)}$ est moins importante par rapport à une éprouvette fatiguée à une amplitude de 0.55 $\sigma_{r(RO)}$. Ceci est vrai pour tous les échantillons fatigués par le nombre de cycles différents. Autrement dit la courbe d'évolution du module des échantillons fatigués avec une amplitude de contrainte de 0.38 $\sigma_{r(RO)}$ reste au-dessus de deux autres courbes obtenues avec des amplitudes de contrainte de 0.45 $\sigma_{r(RO)}$ et 0.55 $\sigma_{r(RO)}$.

4.3.2. Evolution des caractéristiques mécaniques dynamiques post-fatigue au seuil d'endommagement et à la rupture

Pour chaque amplitude de pré-fatigue (0.38 $\sigma_{r(RO)}$, 0.45 $\sigma_{r(RO)}$ et 0.55 $\sigma_{r(RO)}$), la déformation et la contrainte au seuil d'endommagement et à la rupture en fonction de la vitesse de déformation sont reportées en figures 45, 46 et 47.

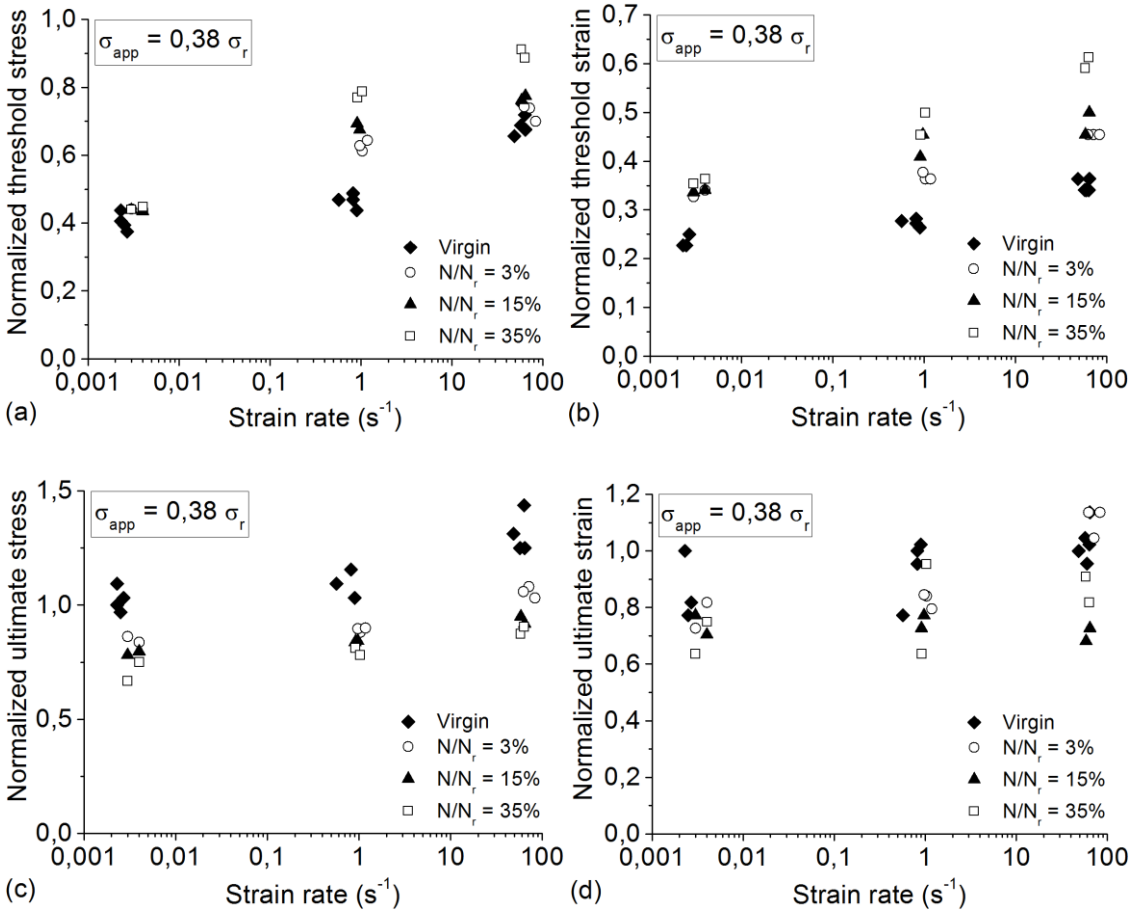

Figure 45 Influence de la vitesse de déformation sur ; la déformation de seuil (a), la contrainte de seuil (b), la déformation ultime (c) et la contrainte ultime (d). (σ_{app} = 0.38 $\sigma_{r(RO)}$).

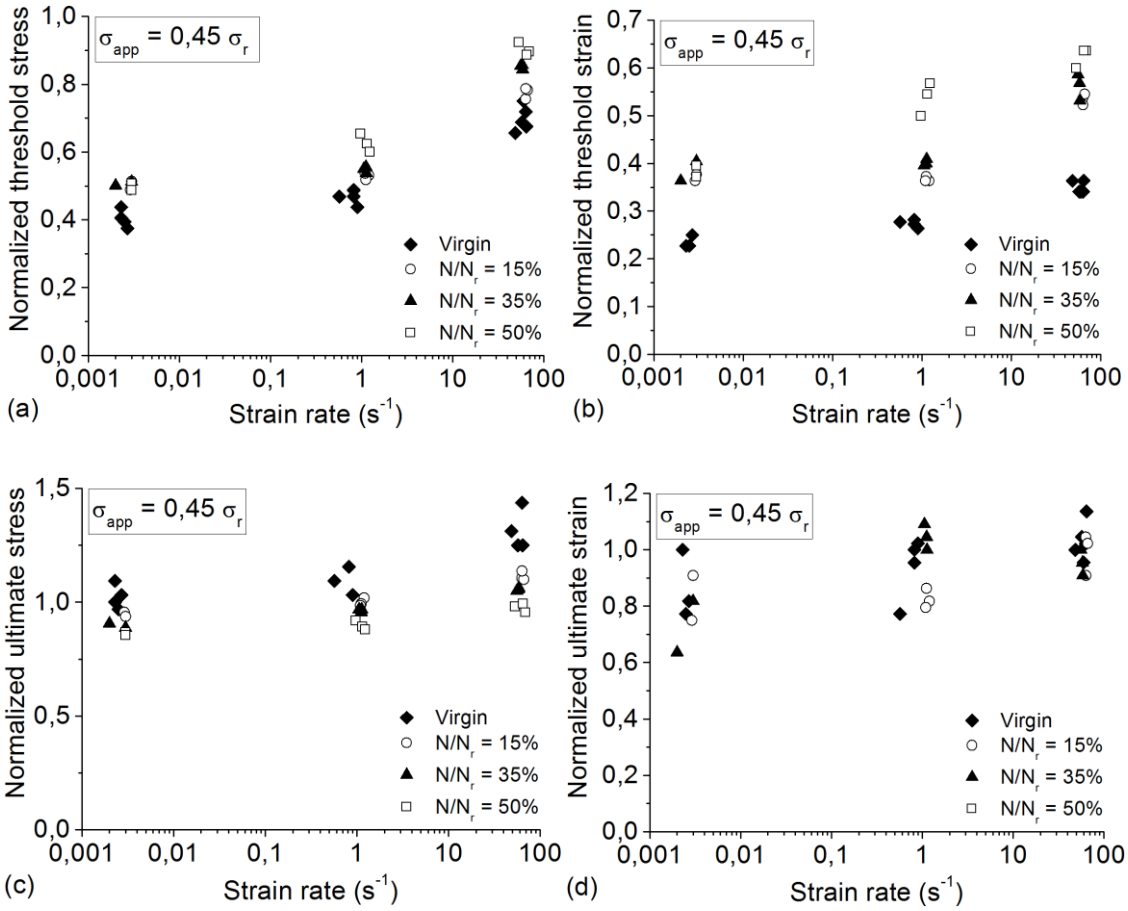

Figure 46 Influence de la vitesse de déformation sur ; la déformation de seuil (a), la contrainte de seuil (b), la déformation ultime (c) et la contrainte ultime (d). (σ_{app} = 0.45 $\sigma_{r(RO)}$).

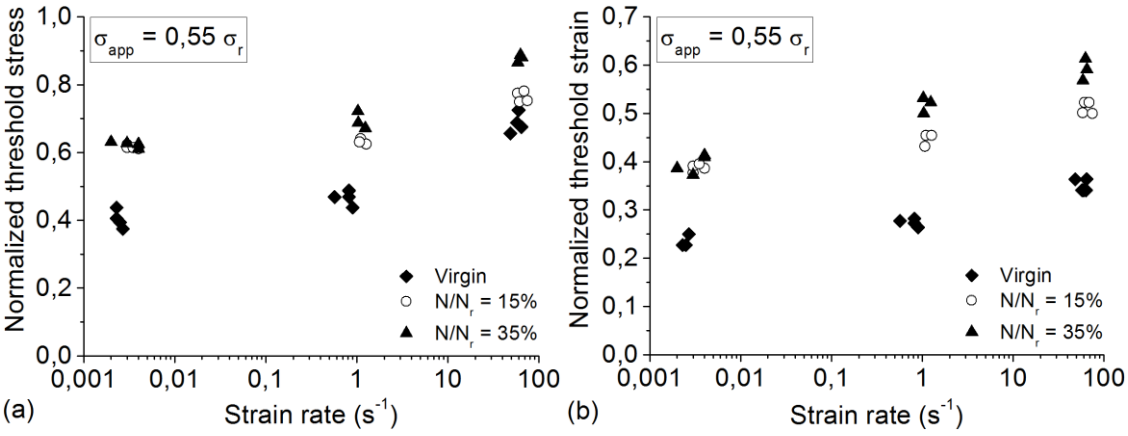

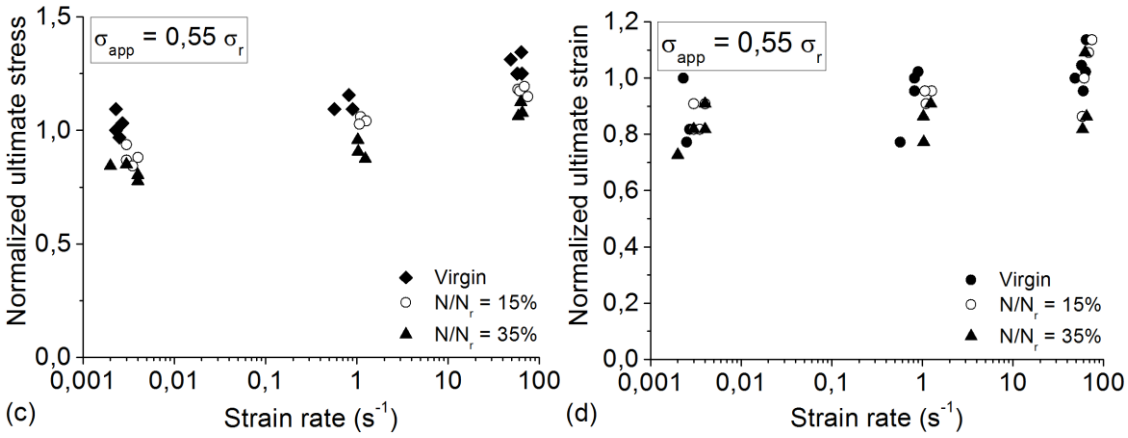

Figure 47 Influence de la vitesse de déformation sur ; la déformation de seuil (a), la contrainte de seuil (b), la déformation ultime (c) et la contrainte ultime (d). (σ_{app} = 0.55 $\sigma_{r(RO)}$).

L'analyse de ces courbes conduit à plusieurs remarques :

- ***Evolution des propriétés à la rupture***

Sur la base des courbes de la figure 43, on constate que les échantillons préalablement fatigués présentent un potentiel mécanique restant, plus faible que les échantillons vierges.

On peut constater également que les échantillons fatigués subissent l'effet de la vitesse avec la même intensité indépendamment du degré de fraction de durée de vie imposée. En effet, les courbes d'évolution de la contrainte à rupture en fonction de la vitesse restent quasi-parallèles quelle que soit la fraction de durée de vie considérée. Ceci est mis en évidence sur les courbes d'évolution de la valeur relative $\frac{\sigma^{r}(\dot{\varepsilon})}{\sigma^{r}_{QS}}$ (figure 48) qui tracent une courbe unique en fonction de la vitesse quelle que soit l'amplitude et la fraction de durée de vie imposées. Cela nous permet de conclure qu'il n'y a pas d'effet significatif de la fatigue sur la sensibilité à la vitesse au niveau des phénomènes locaux qui conduisent à la rupture.

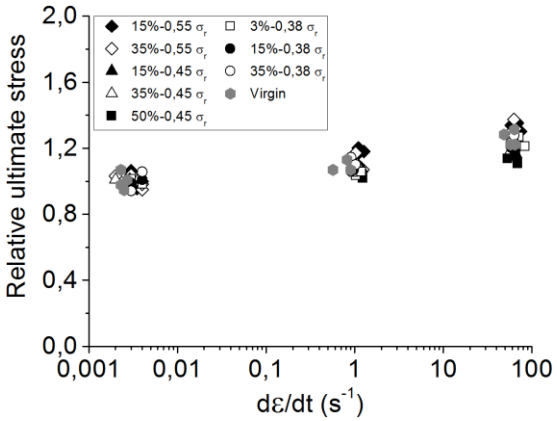

Figure 48 Evolution de la valeur relative de la contrainte à rupture pour différentes valeurs de la contrainte imposée et pour différentes valeurs de la fraction de durée de vie.

- ***Evolution du seuil d'endommagement***

L'effet de la vitesse de sollicitation sur les propriétés au seuil des échantillons pré-fatigués est par contre bien plus important. Il est de plus en plus marqué quand la fraction de durée de vie augmente. En reportant l'évolution du rapport $\frac{\sigma^{\text{seuil}}(\dot{\varepsilon})}{\sigma_{\text{QS}}^{\text{seuil}}}$ pour deux valeurs de la fraction de durée de vie (15% et 35%) (figure 49), on constate que quel que soit le degré d'endommagement atteint par fatigue, la sensibilité à la vitesse diminue lorsque la contrainte appliquée lors de la pré-fatigue augmente. En effet, lorsque la contrainte appliquée en pré-fatigue est importante, des modifications structurales liées aux microdéformations locales accumulées plus importantes peuvent contribuer à réduire l'effet retard du visco-endommagement mis en évidence au chapitre 3. Par contre, pour des amplitudes plus faibles, les modifications structurales de la matrice et des zones proches des interfaces fibre-matrice sont plus limitées.

Par ailleurs, on peut noter que plus le degré d'endommagement atteint par fatigue est important et plus la sensibilité à la vitesse de déformation augmente (figure 50). Ceci nous indique que l'effet visqueux de l'endommagement est fortement lié aux phénomènes de propagation de microfissures préexistantes par fatigue. Rappelons que nous avons démontré au chapitre 3 que le phénomène de propagation de fissures initiées aux interfaces fibre-matrice est le mécanisme de dégradation prédominant pour les A-SMC. Notons également que l'effet retard observé sur l'initiation de nouvelles fissures à l'interface fibre-matrice peut aussi participer à une plus grande sensibilité à la vitesse.

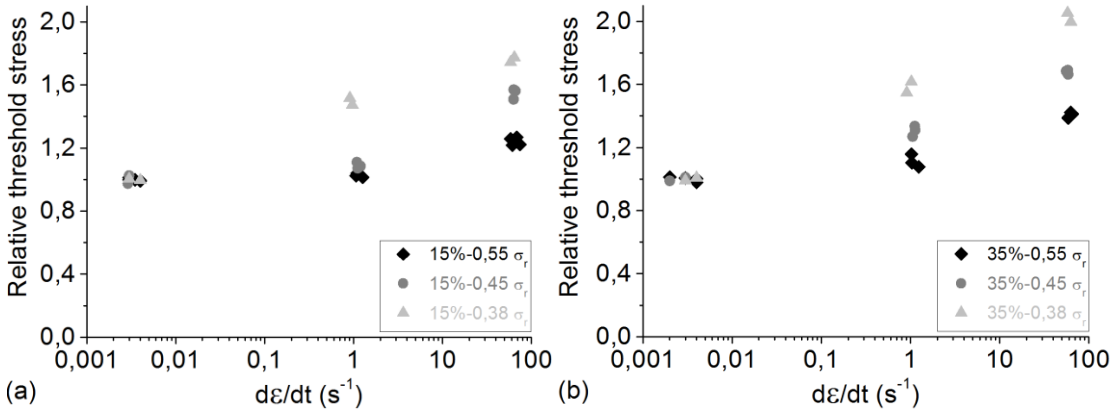

Figure 49 Evolution du seuil relatif post-fatigue en fonction de la vitesse de déformation pour différentes valeurs de la fraction de durée de vie ; 15% (a) et 35% (b).

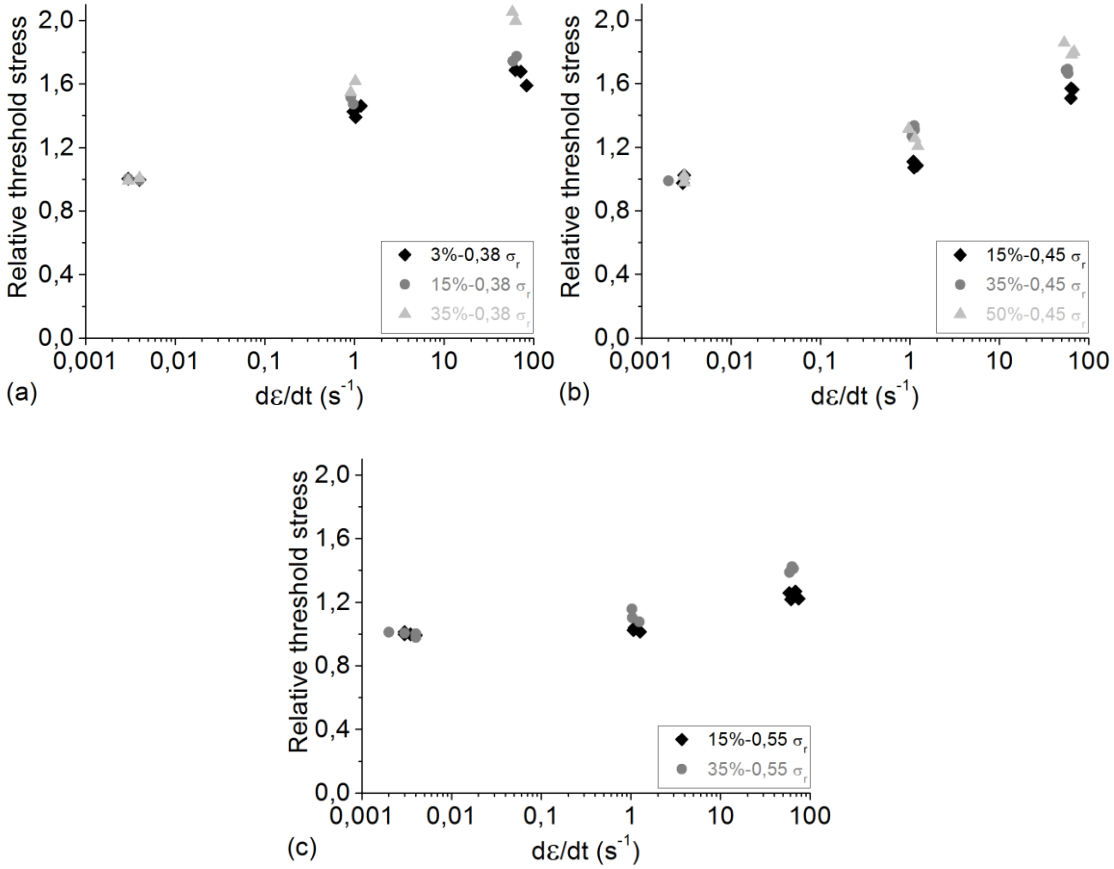

Figure 50 Sensibilité à la vitesse du seuil d'endommagement d'éprouvettes pré-fatiguées à différents degrés d'endommagement ; 0.38 $\sigma_{r(RO)}$ (a), 0.45 $\sigma_{r(RO)}$ (b) et 0.55 $\sigma_{r(RO)}$ (c).

- ***Etude de l'écart lié à la pré-sollicitation de fatigue***

Conformément à la méthodologie expérimentale présentée au paragraphe 4.1, une autre façon de quantifier l'effet spécifique d'une pré-sollicitation de type fatigue sur le comportement dynamique résiduel est de tracer l'évolution de l'écart entre les propriétés post-fatigue mesurées et celles de référence correspondant à un pré-endommagement équivalent effectué sous chargement de traction monotone (voir figure 51).

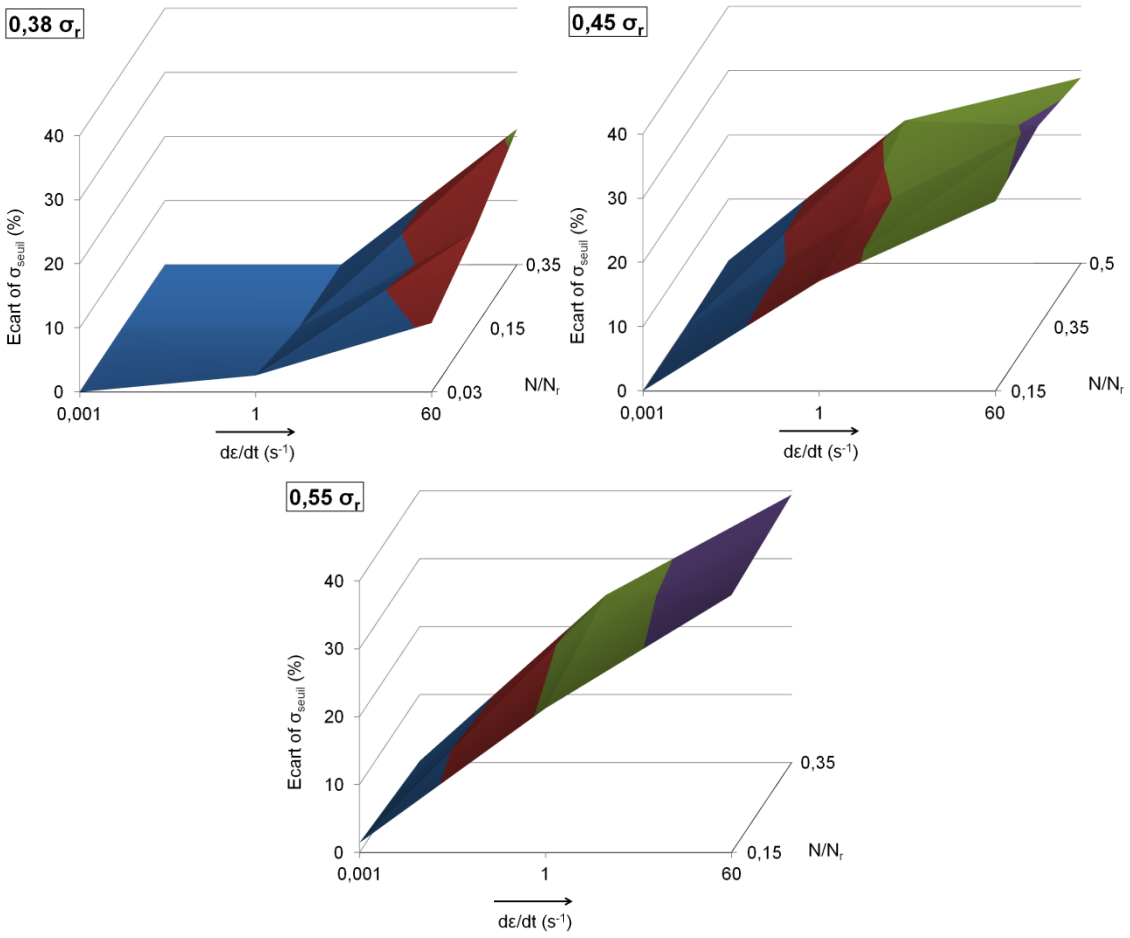

Figure 51 Evolution de l'écart entre les propriétés post-fatigue mesurées et celles de référence ; 0.38 $\sigma_{r(RO)}$ (a), 0.45 $\sigma_{r(RO)}$ (b) et 0.55 $\sigma_{r(RO)}$ (c).

Il a été indiqué que l'origine de l'écart observé entre les courbes de référence post-fatigue et celles en traction monotone est attribué aux phénomènes spécifiques développés en fatigue. Cet écart est présenté sur la figure 50 en termes de seuil d'endommagement. Globalement, on peut conclure que l'effet d'une sollicitation de type fatigue sur le seuil en traction est faible, voire négligeable, à faible vitesse et

devient important à grande vitesse. Cet effet est d'autant plus marqué que l'amplitude appliquée en fatigue est grande et que la fraction de durée de vie atteinte est importante. En effet, pour les plus grandes valeurs de fraction de durée de vie, on peut noter des écarts qui atteignent des valeurs de l'ordre de 20%, 30% et 40% pour des valeurs respectives d'amplitude de pré-fatigue de 0.38 $\sigma_{r(RO)}$, 0.45 $\sigma_{r(RO)}$ et 0.55 $\sigma_{r(RO)}$. Ces évolutions confirment l'analyse faite plus haut.

5. Conclusion

Une sécurité accrue de l'automobile est devenue un sujet préoccupant à la fois pour les fabricants et les utilisateurs. In fine, pour mieux protéger les occupants des automobiles lors d'un accident, une maîtrise optimale des effets de structure et des effets matériau ainsi qu'une connaissance du comportement en fatigue et sous sollicitation dynamique rapide est primordiale.

La ligne directrice de ce travail a été de procéder selon deux étapes essentielles et complémentaires. L'une est dédiée à l'analyse expérimentale sous des conditions de chargements rapides et de fatigue. Une attention particulière a été consacrée à l'étude de l'endommagement de deux types de composites (Advanced Sheet Molding Compound (A-SMC)) et Low Density SMC (LD-SMC)) en considérant les effets d'orientation des renforts à travers deux microstructures : La première présentant une distribution aléatoire d'orientation des fibres (RO), la seconde des fibres fortement orientées (HO). La deuxième étape du travail a été consacrée à l'analyse expérimentale comportement dynamique résiduel du composite A-SMC pré-endommagé par fatigue (dynamique post-fatigue).

Une investigation expérimentale du comportement en fatigue du A-SMC a été réalisée grâce à l'analyse approfondie de l'effet couplé de l'amplitude et de la fréquence. Celle-ci a permis de mettre en évidence l'effet de la fatigue thermique induite (auto-échauffement) et de la fréquence. Dans le même temps, l'amplitude de chargement est corrélée à la vitesse de baisse de raideur en fatigue pour l'ensemble des fréquences de chargement testées.

Par ailleurs, il a été démontré que la durée de vie est fortement influencée par la distribution d'orientation des fibres. En outre, pour les plus hautes fréquences et/ou les fortes amplitudes, la réponse globale en fatigue est caractérisée par une dissipation associée à l'auto-échauffement (fatigue thermique induite). Celle-ci affecte à la fois le taux de réduction de la rigidité ainsi que la durée de vie.

L'analyse du comportement mécanique avec endommagement de matériaux composites sous sollicitations rapides nécessite des outils théoriques et des approches expérimentales capables de cerner l'effet de la vitesse de déformation et la dépendance de l'endommagement à cet effet de vitesse. L'utilisation d'une machine d'essai servo-hydraulique a été adaptée pour examiner les effets de la vitesse de déformation sur l'ensemble des comportements des A-SMC et LD-SMC (RO et HO) jusqu'à 80 s^{-1}. La

vitesse de déformation est mesurée par une technique sans contact à l'aide d'une caméra à haute vitesse. Une approche numérique couplée à une stratégie expérimentale a été dédiée au développement et à l'optimisation d'essais de traction rapide. Ces derniers ont alors permis la caractérisation aux deux échelles micro et macroscopique du comportement dynamique des matériaux composites de l'étude. Suite à la validation de l'approche en dynamique, une méthode originale a été mise en œuvre afin d'étudier l'évolution de l'endommagement au cours de la déformation. Elle est basée sur des essais de traction rapide uni-axiale à effort maximal contrôlé (essais interrompus). L'apport de ce protocole expérimental réside dans le fait de produire des échantillons pré-endommagés à différents niveaux. Les essais mécaniques ainsi effectués ont été couplés à des observations microscopiques réalisées sous MEB pour procéder à une analyse qualitative et quantitative de l'évolution de l'endommagement à l'échelle macroscopique. D'autre part, à travers une analyse microscopique, cette approche expérimentale contribue à cerner les processus physiques régissant l'initiation et la cinétique d'endommagement. L'orientation privilégiée des renforts ainsi que la microstructure affectent inéluctablement le scénario d'endommagement (fissuration matricielle, décohésion d'interface, pseudo-délaminage) et sont à l'origine d'une dégradation progressive considérable des matériaux SMC. D'autant plus que cette dégradation évolue différemment lors des sollicitations rapides en termes de seuil et de cinétique.

Il a donc été montré dans cette étude que l'endommagement dans les composites SMC est le phénomène dissipatif majeur. Il constitue la principale source d'absorption d'énergie lors d'un choc ou d'un impact. Cependant, le développement de ce phénomène physique est conditionné à la fois par l'architecture, la morphologie des renforts, leur distribution d'orientation et la direction principale de la sollicitation qui engendre, dans la plupart des cas, un état de contrainte locale complexe. Ceci fait de l'étude de l'absorption d'énergie lors d'un essai dynamique rapide un des aspects importants à considérer lors de la conception et l'optimisation d'une structure. En outre, l'application des méthodologies expérimentales proposées dans cette étude a permis d'estimer, en fonction de la vitesse de déformation, l'évolution du comportement mécanique en termes de module d'élasticité, seuil d'endommagement et caractéristiques ultimes. Elle a permis également de constater que la vitesse de déformation affecte principalement l'initiation et la cinétique d'endommagement, d'où la notion de visco-endommagement qui

est une caractéristique spécifique au comportement dynamique de tous les SMC. Les conclusions générales suivantes peuvent être énoncées :

- La décohésion à l'interface fibre-matrice semble être le mécanisme prédominant au niveau de l'initiation pour le A-SMC et le SMC standard ;
- L'initiation de ce mécanisme est retardée lorsque la vitesse de déformation augmente, ce qui conduit à une phase élastique du comportement plus étendue à grande vitesse ;
- Alors que pour le SMC standard, l'endommagement interfacial se diffuse très largement jusqu'à la rupture finale, il reste limité dans le cas du A-SMC pour lequel la microfissuration transverse de la matrice devient rapidement le phénomène de propagation principal de l'endommagement ;
- Cette dernière semble être accentué à grande vitesse ;
- L'introduction des billes creuses de verre dans le LD-SMC influence fortement le scénario d'endommagement en fonction de la direction principale de la sollicitation. Pour des sollicitations transverses, la décohésion à l'interface fibre-matrice est remplacée par celle aux interfaces billes-matrice qui devient le phénomène prépondérant d'endommagement et de rupture des LD-SMC ;
- Un phénomène de pseudo-délaminage entre les mèches de fibres couplé à la microfissuration dans la matrice se produit toujours avant la rupture finale. Dans le cas du A-SMC, il a été montré que ce phénomène est extrêmement dissipatif (jusqu'à sept fois l'énergie d'endommagement) et est favorisée d'une part, par une vitesse de déformation élevée et d'autre part, par une orientation des fibres dans la direction de chargement.

Enfin, une méthodologie expérimentale originale a été développée afin d'étudier l'influence d'une pré-sollicitation en fatigue sur les propriétés résiduelles du A-SMC sollicité à grande vitesse. On montre tout d'abord que le module d'élasticité résiduel des échantillons de A-SMC pré-endommagé par fatigue reste insensible à la vitesse de déformation. Par contre, on met en évidence une forte influence d'un pré-endommagement en fatigue sur la sensibilité à la vitesse des matériaux A-SMC en terme de seuil d'endommagement. En effet, on peut noter que le seuil d'endommagement en termes de contrainte et de déformation augmente plus fortement avec la vitesse de déformation lorsque la fraction de durée de vie (ou le niveau d'endommagement) en fatigue augmente. Il convient toutefois d'indiquer que de par le développement de l'endommagement en fatigue la rigidité du A-SMC diminue de façon, plus ou moins

importante, en fonction de l'amplitude de la contrainte appliquée alors que le seuil d'endommagement en termes de contrainte et de déformation augmente. Par ailleurs, il a été montré qu'un pré-endommagement en fatigue produit une diminution du potentiel restant en terme de contrainte à rupture et ceci quelles que soient l'amplitude en fatigue et la vitesse de déformation post-fatigue. Par contre, on peut constater qu'un pré-endommagement en fatigue n'affecte pas la sensibilité à la vitesse de déformation de la contrainte à rupture.

Cette étude met donc en évidence une forte influence du type de chargement et de son histoire sur la sensibilité des matériaux SMC à la vitesse de sollicitation. L'ensemble des résultats de cette étude, de par son apport de compréhension des phénomènes mis en jeu, notamment l'endommagement, constitue une base expérimentale importante. Cette dernière est nécessaire à la construction de nouveaux outils de dimensionnement adaptés aux structures SMC sous sollicitations cycliques et dynamiques.

Références

[1] Castro J ,Griffith RM, Kia HG. Sheet molding compounds-science and technology. New York, USA: Hanser; 1993.

[2] Bogner BR, Kallaur M. Sheet molding compounds-science and technology. Munchen, Germany: Hanser; 1993.

[3] Dana D, YU J. Sheet molding compounds: science and technology. Hanser; 1993.

[4] Collister J, Allen A. Sheet molding compound rheology. vol. 14, Grenoble, France: 1993.

[5] Bonnet B. Comportement au choc de materiaux composites pour applications automobiles. Paris: 2005.

[6] Cara F. Etude des parametres du procede SMC influant sur la qualite des pieces [PhD thesis]. Institut National des Sciences Appliquees de Lyon, 2001.

[7] Feuillade V, Bergeret A, Quantin J, Crespy A. Characterisation of glass fibres used in automotive industry for SMC body panels. Composites Part A: Applied Science and Manufacturing 2006;37:1536–44.

[8] Glass S. Glass microspheres produce lower weight SMC. Reinforced Plastics 1997;41:34–7.

[9] Oldenbo M, Fernberg SP, Berglund LA. Mechanical behaviour of SMC composites with toughening and low density additives. Composites Part A: Applied Science and Manufacturing 2003;34:875–85.

[10] Kraemer A, Lin S, Brabandt D, Böhlke T, Lanza G. Quality control in the production process of SMC lightweight material. Procedia CIRP 2014;17:772–7.

[11] Jendli Z. Analyse et modelisation multi echelles du comportement mecanique sous sollicitations rapides de composites SMC. 2005.

[12] Le TH, Dumont PJJ, Orgéas L, Favier D, Salvo L, Boller E. X-ray phase contrast microtomography for the analysis of the fibrous microstructure of SMC composites. Composites Part A: Applied Science and Manufacturing 2008;39:91–103.

[13] Guiraud O, Dumont PJJ, Orgéas L, Favier D. Rheometry of compression moulded fibre-reinforced polymer composites: Rheology, compressibility, and friction forces with mould surfaces. Composites Part A: Applied Science and Manufacturing 2012;42:2107–19.

[14] Shokrieh MM, Mosalmani R. Modeling of sheet molding compound compression molding under non-isothermal conditions. Journal of Reinforced Plastics and Composites 2014;33:1183–98.

[15] Dumont P, Orgéas L, Favier D, Pizette P, Venet C. Compression moulding of SMC: In situ experiments, modelling and simulation. Composites Part A: Applied Science and Manufacturing 2007;38:353–68.

[16] Odenberger PT, Andersson HM, Lundström TS. Experimental flow-front visualisation in

compression moulding of SMC. Composites Part A: Applied Science and Manufacturing 2004;35:1125–34.

[17] Moo Sun K, Lee W, Han W, Vautrin A, Park C. Thickness optimization of composite plates by Box's complex method considering the process and material parameters in compression molding of SMC. Composites Part A: Applied Science and Manufacturing 2009;40:1192–8.

[18] Kim MS, Lee WI , Han WS, Vautrin A. Optimization of location and dimension of SMC pre-charge in compression molding process. Computers & Structures 2011;89:1523–34.

[19] Kim DK, Choi HY, Kim N. Experimental investigation and numerical simulation of SMC in compression molding. Journal of Materials Processing Tech 1995;49:333–44.

[20] Kim KT, Im YT. Experimental study on physical properties of compression molded SMC parts under plane strain condition. Composite Structures 1996;35:131–41.

[21] Kotsikos G, Gibson AG. Investigation of the squeeze flow behavior of sheet moulding compounds (SMC). Composites Part A: Applied Science and Manufacturing 1998;29:1569–77.

[22] Kluge NJ, Lundström TS, Westerberg LG, Olofsson K. Compression moulding of sheet moulding compound: Modelling with computational fluid dynamics and validation. Reinforced Plastics and Composites 2015.

[23] Abrams L, Castro J. Predicting molding forces during sheet molding compound (SMC) compression molding. Polymer Composites 2003;24.

[24] Barone MR, Caulk DA. A model for the flow of a chopped fiber reinforced polymer compound in compression molding. Journal of Applied Mechanics 1986;53:361–70.

[25] Advani S, Tucker C. A numerical simulation of short fiber orientation in compression molding. Polymer Composites 1990;11:164–73.

[26] Shirinbayan M, Fitoussi J, Meraghni F, Surowiec B, Bocquet M, Tcharkhtchi A. High strain rate visco-damageable behavior of Advanced Sheet Molding Compound (A-SMC) under tension. Composites Part B: Engineering 2015;82:30–41.

[27] Shirinbayan M, Fitoussi J, Bocquet M, Meraghni F, Surowiec B, Tcharkhtchi A. Multi-scale experimental investigation of the viscous nature of damage in Advanced Sheet Molding Compound (A-SMC) submitted to high strain rates. Composites Part B: Engineering 2016.

[28] Shirinbayan M, Fitoussi J, Abbasnezhad N, Meraghni F, Surowiec B, Tcharkhtchi A. Overall mechanical characterization of a Low Density Sheet Molding Compound (LD-SMC): Multi-scale damage analysis and strain rate effect. Composites Part B: Engineering 2017.

[29] Dumont P, Orgéas L, Le Corre S, Favier D. Anisotropic viscous behavior of sheet molding compounds (SMC) during compression molding. International Journal of Plasticity 2003;19:625–46.

[30] Esmaeillou B, Fitoussi J, Lucas A, Tcharkhtchi A. Multi-scale experimental analysis of the tension-tension fatigue behavior of a short glass fiber reinforced polyamide composite. Procedia Engineering 2011;10:2117–22.

[31] Fitoussi J, Guo G, Baptiste D. A statistical micromechanical model of anisotropic damage for SMC composites. Composites Science and Technology 1998;58:759–63.

[32] Jendli Z, Meraghni F, Fitoussi J, Baptiste D. Micromechanical analysis of strain rate effect on damage evolution in sheet molding compound composites. Composites Part A: Applied Science and Manufacturing 2004;35:779–85.

[33] Jendli Z, Meraghni F, Fitoussi J, Baptiste D. Multi-scales modeling of dynamic behaviour for discontinuous fibre SMC composites. Composites Science and Technology 2009;69:97–103.

[34] Jendli Z, Fitoussi J, Meraghni F, Baptiste D. Anisotropic strain rate effects on the fibre-matrix interface decohesion in sheet moulding compound composites. Composites Science and Technology 2005;65:387–93.

[35] Fitoussi J, Bocquet M, Meraghni F. Effect of the matrix behavior on the damage of ethylene-propylene glass fiber reinforced composite subjected to high strain rate tension. Composites Part B: Engineering 2013;45.

[36] Fitoussi J, Meraghni F, Jendli Z, Hug G, Baptiste D. Experimental methodology for high strain-rates tensile behaviour analysis of polymer matrix composites. Composites Science and Technology 2005;65:2174–88.

[37] Farley GL. Energy absorption in composite structures. Journal of Composite Materials 1983;17:267–79.

[38] Huang H, Talreja R. Numerical simulation of matrix micro-cracking in short fiber reinforced polymer composites: Initiation and propagation. Composites Science and Technology 2006;66:2743–57.

[39] Lee HK, Simunovic S. A damage mechanics model of crack-weakened, chopped fiber composites under impact loading. Composites Part B: Engineering 2002;33:25–34.

[40] Baste S, Gérard A. Evaluation of anisotropic damage in composite materials. Evaluation of Anisotropic Damage in Composite Materials 1994;3.

[41] Jacob GC, Fellers JF, Simunovic S, Starbuck JM. Energy absorption in polymer composites for automotive crashworthiness. Journal of Composite Materials 2002;36:813–50.

[42] Yang L, Wu Z, Gao D, Liu X. Microscopic damage mechanisms of fibre reinforced composite laminates subjected to low velocity impact. Computational Materials Science 2016;111:148–56.

[43] Dear JP, Brown SA. Impact damage processes in reinforced polymeric materials. Composites Part A: Applied Science and Manufacturing 2003;34:411–20.

[44] Hour KY, Sehitoglu H. Damage development in a short fiber reinforced composite. Journal of Composite Materials 1993;27:782–805.

[45] Krajcinovic D, Mastilovic S. Some fundamental issues of damage mechanics. Mechanics of Materials 1995;21:217–30.

[46] Krajcinovic D. Selection of damage parameter – Art or science. Mechanics of Materials 1998;28:165–79.

[47] Audoin B, Baste S. On internal variable in anisotropic damage. Journal of Mechanics-A/Solids 1991;10:587–606.

[48] Lemaitre J, Chaboche JL. Mécanique des matériaux solides. Paris: Donud; 1988.

[49] Talreja R. Fatigue of composite materials: damage mechanisms and fatigue-life diagrams. Proceedings of the Royal Sociey 1981:461–75.

[50] Degrieck J, Van Paepegem W. Fatigue damage modeling of fibre-reinforced composite materials. Review 2001:279–300.

[51] Avanzini A, Donzella G, Gallina D, Pandini S, Petrogalli C. Fatigue behavior and cyclic damage of peek short fiber reinforced composites. Compos Part B: Eng 2013;45:397–406.

[52] Bernasconi A, Davoli P, Basile A, Filippi A. Effect of fibre orientation on the fatigue behaviour of a short glass fibre reinforced polyamide-6. International Journal of Fatigue 2007;29:199–208.

[53] Launay A, Marco Y, Maitournam MH, Raoult I, Szmytka F. Cyclic behavior of short glass fiber reinforced polyamide for fatigue life prediction of automotive components. Procedia Engineering 2010;2:901–10.

[54] Wang SS, Suemasu H, Chim ESM. Analysis of fatigue damage evolution and associated anisotropic elastic property degradation in random short-fiber composite. Journal of Composite Materials 1987;21:1084–105.

[55] Tamboura S, Sidhom H, Baptiste H, Fitoussi J. Evaluation de la tenue en fatigue du composite SMC R42. Matériaux & Techniques 2001:3–4.

[56] Esmaeillou B, Ferreira P, Bellenger V, Tcharkhtchi A. Fatigue behavior of polyamide 66/glass fiber under various kinds of applied load. Polymer Composites 2012;33:540–7.

[57] Mortazavian S, Fatemi A, Mellott SR, Khosrovaneh A. Effect of cycling frequency and self-heating on fatigue behavior of reinforced and unreinforced thermoplastic polymers. Society of Plastics Engineers 2015:2005–8.

[58] Schladitz K, Büter A, Godehardt M, Wirjadi O, Fleckenstein J, Gerster T, et al. Non-destructive characterization of fiber orientation in reinforced SMC as input for simulation based design. Composite Structures 2017;160:195–203.

[59] Chaboche JL, Gallerneau F. An overview of the damage approach of durability modelling at elevated temperature. Fatigue and Fracture of Engineering 2001;24:405–18.

[60] Bussiba A, Kupiec M, Ifergane S, Piat R, Böhlke T. Damage evolution and fracture events sequence in various composites by acoustic emission technique. Composites Science and Technology 2008;68:1144–55.

[61] Askes H, Sluys LJ. Explicit and implicit gradient series in damage mechanics. European Journal of Mechanics and Solids 2002;21:379–90.

[62] Guerjouma RE, Baste S. Evaluation of anisotropic damage in ceramic-ceramic (Sic-Sic) composite by ultrasonic method. Ultrasonics International 1989;89:895–900.

[63] Meraghni F, Desrumaux F, Benzeggagh ML. Implementation of a constitutive micromechanical model for damage analysis in glass mat reinforced composite structures. Composites Science and Technology 2002;62:2087–97.

[64] Shao JF, Rudnicki JW. A microcrack-based continuous damage model for brittle geomaterials. Mechanics of Materials 2000;32:607–19.

[65] Krajcinovic D. Selection of damage parameter – Art or science. Mechanics of Materials 1998;28:165–79.

[66] Morozov E, Morozov K, Selvarajalu V. Progressive damage modelling of SMC composite materials. Composite Structures 2003;62:361–6.

[67] Derrien K, Fitoussi J, Guo G, Baptiste D. Prediction of the effective damage properties and failure properties of nonlinear anisotropic discontinuous reinforced composites. Computer Methods in Applied Mechanics and Engineering 2000;185:93–107.

[68] Chaturvedi SK, Sun CT, Sierakowski RL. Mechanical characterization of sheet molding compound composites. Polymer Composites 1983;4:167–71.

[69] Wang SS, Goetz DP, Corten HT. Shear fatigue degradation and fracture of random short-fiber SMC composite. Journal of Composite Materials 1984;18:2–20.

[70] Tanaka K, Kitano T, Egami N. Effect of fiber orientation on fatigue crack propagation in short-fiber reinforced plastics. Engineering Fracture Mechanics 2014:1–15.

[71] Fleckenstein J, Jaschek K, Büter A, Stoess N. Fatigue design optimization of safety components made of SMC. Procedia Engineering 2011;10:390–6.

[72] Mortazavian SV, Fatemi A. Fatigue behavior and modeling of short fiber reinforced polymer composites including anisotropy and temperature effects. International Journal of Fatigue 2015;77:12–27.

[73] Shirinbayan M, Fitoussi J, Meraghni F, Surowiec B, Laribi M, Tcharkhtchi A. Coupled effect of loading frequency and amplitude on the fatigue behavior of advanced sheet molding compound (A-SMC). Journal of Reinforced Plastics and Composites (JRP) 2016.

[74] Bellenger V, Tcharkhtchi A, Castaing P. Thermal and mechanical fatigue of a PA66/glass fibers composite material. International Journal of Fatigue 2006;28:1348–52.

[75] Handa K, Kato A, Narisawa I. Fatigue characteristics of a glass-fiber-reinforced polyamide. Journal of Applied Polymer Science 1999;72:1783–93.

[76] Dentsoras AJ, Kouvaritakis EP, Laboratory MD. Effects of vibration frequency on fatigue crack propagation of a polymer at resonance. Elsevier Science 1995;50:467–73.

[77] Atodrais DR, Putatundaa SK, Mallick PK. Fatigue crack growth model and mechanism of a random fiber SMC composite. Polymer Composites 2004;20:240–9.

[78] Zhang H, Yao Y, Zhua D, Mobasherb B, Huang L. Tensile mechanical properties of basalt fiber reinforced polymer composite under varying strain rates and temperatures. Polymer Testing

2016;51:29–39.

[79] Ramakrishna S. Microstructural design of composite materials for crashworthy structural applications. Materials & Design 1997;18:167–73.

[80] Pardo S, Baptiste D, Decobert F, Fitoussi J, Joannic R. Tensile dynamic behaviour of a quasi-unidirectional E-glass/polyester composite. Composites Science and Technology 2002;62:579–84.

[81] Arif M, Saintier N, Meraghni F, Fitoussi J, Chemisky Y, Robert G. Multiscale fatigue damage characterization in short glass fiber reinforced polyamide-66. Composites Part B: Engineering 2014;61:55–65.

Article N°1:

Shirinbayan M, Fitoussi J, Meraghni F, Surowiec B, Bocquet M, Tcharkhtchi A. High strain rate visco-damageable behavior of Advanced Sheet Molding Compound (A-SMC) under tension. Composites Part B: Engineering. 2015; 3670(82): 30-41.

Composites Part B 82 (2015) 30–41

Contents lists available at ScienceDirect

Composites Part B

journal homepage: www.elsevier.com/locate/compositesb

High strain rate visco-damageable behavior of Advanced Sheet Molding Compound (A-SMC) under tension

M. Shirinbayan [a, *], J. Fitoussi [a], F. Meraghni [b], B. Surowiec [c], M. Bocquet [a], A. Tcharkhtchi [a]

[a] Arts et Métiers ParisTech, PIMM, UMR CNRS 8006, 151 Boulevard de l'Hôpital, 75013 Paris, France
[b] Arts et Métiers ParisTech, LEM3, UMR CNRS 7239, 4 Rue Augustin Fresnel, 57078 Metz, France
[c] PLASTIC OMNIUM AUTO EXTERIOR SERVICES, Sigmatech, Sainte Julie, France

ARTICLE INFO

Article history:
Received 28 February 2015
Received in revised form
12 July 2015
Accepted 20 July 2015
Available online 29 July 2015

Keywords:
A. Glass fibres
B. Fibre/matrix bond
B. Delamination
High strain rate

ABSTRACT

Advanced Sheet Molding Compound (A-SMC) is a serious composite material candidate for structural automotive parts. It has a thermoset matrix and consists of high weight content of glass fibers (50% in mass) compared to standard SMC with less than 30% weight fiber content. During crash events, structural parts are heavily exposed to high rates of loading and straining. This work is concerned with the development of an advanced experimental approach devoted to the micro and macroscopic characterization of A-SMC mechanical behavior under high-speed tension. High speed tensile tests are achieved using servo-hydraulic test equipment in order to get required high strain rates up to 100 s^{-1}. Local deformation is measured through a contactless technique using a high speed camera. Numerical computations have led to an optimal design of the specimen geometry and the experimental damping systems have been optimized in terms of thickness and material properties. These simulations were achieved using ABAQUS explicit finite element code. The developed experimental methodology is applied for two types of A-SMC: Randomly Oriented (RO) and Highly Oriented (HO) plates. In the case of HO samples, two tensile directions were chosen: HO-0° (parallel to the Mold Flow Direction (MFD)) and HO-90° (perpendicular to the MFD). High speed tensile tests results show that A-SMC behavior is strongly strain-rate dependent although the Young's modulus remains constant with increasing strain rate. In the case of HO-0°, the stress damage threshold is shown an increase of 63%, when the strain rate varies from quasi-static (0.001 s^{-1}) to 100 s^{-1}. The experimental methodology was coupled to microscopic observations using SEM. Damage mechanisms investigation of HO and RO specimens showed a competition between two mechanisms: fiber-matrix interface debonding and pseudo-delamination between neighboring bundles of fibers. It is shown that pseudo-delamination cannot be neglected. In fact, this mechanism can greatly participate to energy absorption during crash. Moreover, the influence of fiber orientation and imposed velocity is studied. It is shown that high strain rate and oriented fiber in the tensile direction favor the pseudo-delamination.

1. Introduction

Sheet Molding Compounds (SMCs) are high strength glass reinforced thermoset moulding materials processed by thermo-compression [1,2]. SMC composites combine glass fiber and unsaturated polyester/phenolic/Vinyl and Acrylic modified resins to produce a high strength molding compound [3–5]. These materials are usually formulated to meet performance requirements of the part to be molded. Moreover, Vinyl-esters resins used for new Advanced SMCs (A-SMC) exhibit many desirable features, including mechanical properties comparable to those of epoxy, excellent chemical resistance and tensile strength, and cost competitiveness. Moreover, its low viscosity enables room-temperature infusion. SMC and A-SMC are ideal for large structural automotive components because of their high strength-to-weight ratio [6,7]. Due to significant tooling investment, overall component cost savings resulting from part consolidation, with the same coefficient of thermal expansion as steel and excellent corrosion resistance; A-

* Corresponding author. Tel.: +33 144246105.
E-mail addresses: mohammadali.shirinbayan@ensam.eu (M. Shirinbayan), joseph.fitoussi@ensam.eu (J. Fitoussi), fodil.meraghni@ensam.eu (F. Meraghni), benjamin.surowiec@plasticomnium.com (B. Surowiec), michel.bocquet@ensam.eu (M. Bocquet), abbas.tcharkhtchi@ensam.eu (A. Tcharkhtchi).

http://dx.doi.org/10.1016/j.compositesb.2015.07.010
1359-8368/

SMC is an ideal alternative to metals and can be used in the same fluctuating temperature environments [8,9].

Mechanical response of SMC composites is sensitive to the rate at which they are loaded [10–13]. Hence, for the effective use of these composites, their response under different strain rates should be clearly understood. During experimental high speed tests, the composite is generally subjected to rapid accelerations. So, at the beginning of the loading many complex processes occur due to rapid straining coupled to inertial disturbances and test system ringing [12]. Spatio-temporal variations of the strain and stress fields during a high speed test make the analysis more difficult [12,14]. Due to these complicated experimental conditions, not enough reliable material data has been determined at typical crash speeds. In order to increase safety, reliable material properties at typical crash speeds are essential for precise simulations of crash processes involving composite parts [15–17]. A first study on a standard SMC composite reinforced with 30% glass fiber [12] showed that the elastic modulus remains insensitive to the load rate for the explored velocity range; from quasi-static to up to 200 s^{-1}, a rough average value of 13 GPa is found. However, the microstructure variability of this class of materials can bring about a slight discrepancy [10–12] notably for dynamic loadings. Several studies [8–12] showed that the predominant damage mechanism for standard SMC composites is the debonding at the fiber-matrix interface. An experimental methodology [12] based on dynamic tensile tests has contributed to emphasize the strain rate effects on the overall behavior of SMCR26 composites. It has been demonstrated that as the strain rate increased, a delayed damage onset is followed by a slightly reduced damage accumulation kinetic. The notion of visco-damaged behavior due to the time-dependent fiber-matrix interface strength has been emphasized for this SMC composite. The results of this study have provided the experimental framework to identify and validate a multi-scale model integrating the material microstructure effects [8]. This model is currently implemented into a FE code [18].

In the present paper, an experimental study is carried-out to investigate the strain rate influence on the overall mechanical behavior of a new Advanced SMC. The organization of this work is as follow: after a presentation of the main physical characteristics and microstructure of A-SMC composite, an optimization of high speed tensile test until failure is proposed through finite element analysis using a commercial explicit code (ABAQUS explicit) in order to take into account the perturbations mentioned above. Two kinds of A-SMC microstructures are investigated: Randomly Oriented fibers (RO) and Highly Oriented fibers (HO). In the case of HO samples, two tensile directions were chosen in order to evaluate the anisotropic effect due to microstructure: HO-0° (parallel to the Mold Flow Direction (MFD)) and HO-90° (perpendicular to the MFD). Moreover, SEM fractography analysis emphasizes the effect of microstructure and strain rate on the main damage and failure micro-mechanisms. At the end of the paper, a special attention is given to the analysis of the pseudo-delamination occurring just before failure. The effect of microstructure and strain rate on the pseudo-delamination is studied.

2. Material description and methods

2.1. Advanced Sheet Molding Compound composite (A-SMC)

Advanced Sheet Molding Compound composite (A-SMC) consists of high content of glass fibers (50% in mass corresponding to 38.5% in volume) in contrast to standard SMC containing a maximum of only 30% in mass of glass fiber. Standard SMC is classically used in automotive industry for semi-structural part like rear floor or inner panel of a tailgate for instance. A-SMC as a thermoset material is a serious candidate for structural parts (security parts). Raw material (not consolidated) is flexible and stored on rolls. The sheets should be cut from these rolls with adapted size depending on the mold. Then it should be stacked several layers into the mold and close it [1]. The material consolidation is performed by thermo-compression process (~150 °C and 60–120 kg/cm^2). Under these conditions the viscosity of the materials decreases and allows it to fulfill the whole cavity of the mold; this is the first step of the process. Then the materials stay in position with no reticulation for a short duration; this is the second step of the process. The third step of the process consists of a reticulation time of the thermoset material that is the consolidation phase. The duration of whole process for one part is less than 2 min. This low process time is mandatory in automotive industry due to the high production rhythm.

A-SMC is a high mechanical performance SMC based on vinyl-ester resin and reinforced with high ratio of chopped bundles of glass fibers (25 mm length). The composition of A-SMC is shown in Table 1. For the need of this study, two types of A-SMC plates have been provided by PLASTIC OMNIUM AUTO EXTERIOR SERVICES: Randomly Oriented (RO) and Highly Oriented (HO) plates. HO plates have been obtained by an initial charge put only in the left part of a rectangular mold (30 × 40 cm) before compression leading to material flow. RO plates were obtained without material flow by completely filling the mold.

However, it would be interesting to have more comprehensive data for the other specimen orientations in order to get a more comprehensive analysis of the damage and induced behavior anisotropy of SMC behavior. However, only two directions have been tested and deeply analyzed for two reasons:

1) The present work aims at comparing the strain rate effect for two typical microstructures (randomly and oriented fibers) in order to define the sensitivity range as upper and lower bounds. In fact, damage behavior is mostly due to fiber matrix interface debonding. The three kinds of performed tests lead to three kinds of predominant local damage mechanisms. These degradation modes occurred for each kind of test are as follow:
   - FF-0° tests provide fiber breakage and pseudo-delamination,
   - FF-90° tests promote mainly fiber-matrix interface debonding at the 90° oriented fibers because of the high normal stress for this orientation,
   - RO damage initiate at the interface of the 90° oriented fibers and progressively propagates in the more oriented fiber interfaces.

   Furthermore, the rate sensitivity demonstrated in the paper is representative of the strain rate effect on the most commonly observed local damage mechanisms.

2) For this kind of oriented microstructure, performing off-axis tensile tests leads to an induced shear, non-homogeneous stress and strain fields and non-negligible edge effect. Therefore, it will be difficult to get optimized geometry for dynamic tests providing homogeneous fields and constant strain rate.

Table 1
A-SMC composition.

Product nature	Composition (content in mass percent)
Glass fibers	50%
Vinyl-ester resin	24%
Filler	24%
Other products	2%

2.2. Methods

2.2.1. Characterization methods

Microscopic observations and image analysis, using Scanning Electronic Microscope (HITACHI 4800 SEM), have been performed in the aim to investigate qualitatively the material microstructure and especially fibers orientation. In order to measure the main transitions temperatures, thermo-mechanical (DMTA) tests have been performed on RO samples using DMA Q800 instrument, from TA Company. The tests have been realized at following condition: alternating bending configuration; temperature range −100 °C to 250 °C; frequency 1 Hz; temperature rate 2 °C/min.

2.2.2. High-speed tensile tests

2.2.2.1. Testing devices. High-speed tensile tests have been performed upon a servo-hydraulic test machine. As specified by the manufacturer (Schenk Hydropuls VHS 5020), the test machine can reach a crosshead speed range from 10^{-4} m/s (quasi-static) to 20 m/s. Moreover, the load level is measured by a piezoelectric crystal load cell having a capacity of a 50 kN. High-strain rate tensile tests were conducted at different strain-rates until the composite specimen total failure. The test machine is equipped with a launching system. The A-SMC specimen is positioned between the load cell (upper extremity) and the moving device (lower extremity) as sketched in Fig. 1.

2.2.2.2. Optimization. Prior to the contact between the sliding bar and the hydraulic jack (see Fig. 1), the latter one is accelerated over a straight displacement of 135 mm (for maximum strain rate) in order to reach the nominal crosshead velocity before the load begins. Once the contact occurs, the specimen is then subjected to tension. The damping joint placed between the slide and the hydraulic jack has been experimentally optimized (material choice and geometry) in order to attenuate partially the perturbation due to mechanical waves caused by the dynamic shock and also to limit the system ringing [12] related to the hanging mass of the upper fixing system.

As pointed out above, the damping joint inserted between the sliding bar and the tube of the hydraulic jack enables a partial absorption of the generated stress wave. Nevertheless, the damping joint must be able to attenuate the shock wave during its compression. Moreover, in order to ensure the derivation of the Young's modulus, the joint compression must be completely finished before the end of the complete elastic deformation of the specimen. It is obvious that it affects the loading rate. An optimal design of the damping joint, in terms of constitutive material and geometry, may result in a constant strain-rate and in homogeneous strain and stress fields in the central zone of the composite specimen. We have chosen a damping joint consisting of a low impedance material: rubber nitrile (1.5 mm thickness).

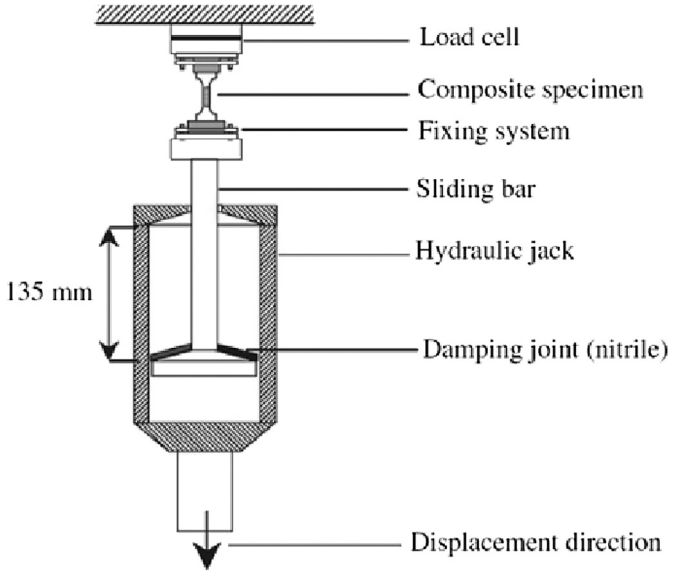

Fig. 1. Experimental device used for high-speed tensile tests.

2.2.2.3. Specimen geometry. Furthermore, specimen geometry has to be optimized in order to reduce the perturbation wave's effect. The idea is to produce a reduction of the stress wave propagation occurring for a high-speed tensile test by mean of brutal variation of the specimen mechanical impedance. This variation of mechanical impedance leads to the trapping of the mechanical waves in the lower part of the testing device far from the specimen.

Therefore, the composite specimen geometry has been optimized as a result of numerical computations using ABAQUS finite element (FE) code. The criterion used for the optimization consists in reaching a stabilized strain distribution and strain rate within the specimen gauge section at the beginning of the loading stage. The optimization procedure relies upon coupling FE numerical results and experimental data. It falls into four stages (Fig. 2):

i A tensile test is conducted at a fixed displacement rate. The displacement induced at specimen extremities is measured. The damping joint, positioned between the sliding and the hydraulic jack, may limit the shock effect until its maximal compression. Thus, at the beginning of the loading, a part of the total imposed displacement is consumed by the compression of the damping joint. It should be pointed out that the damping joint would be completely compressed before the end of the total elastic deformation of the specimen. Consequently, the specimen (which is placed in series with the damping joint) is submitted to a progressive acceleration until the total compression of the damping joint. Then, at the so called rise time (t_r), the displacement rate induced at specimen extremities becomes constant. Beyond this time, the composite specimen is therefore subjected to a dynamic tensile loading at constant strain rate. The first stage aims then at estimating experimentally the rise time (t_r) (see Fig. 2(a)). Its value lies in the range [10^{-4} to 10^{-5} s] and depends on the adopted joint thickness and the nominal test velocity.

ii Once the rise time is evaluated, boundary conditions are numerically applied on the specimen extremities in terms of imposed velocity, in order to compute the dynamic response of the specimen, according to Fig. 2(b): a linear increase of the velocity until the imposed value which is reached at the rise time.

iii On the basis of the FE simulations and assuming that the specimen behaves like an elastic anisotropic solid, a recursive optimization procedure results in the determination of optimal geometrical parameters: L_1, L_2, L_3 and R (Fig. 3). These parameters are those of a dumbbell-shaped specimen as sketched in Fig. 2(c) and are optimized in such a way of reducing the stress wave effects in the overall response through a rapid loss of mechanical impedance. Finally, the optimization aims at generating homogeneous stress/strain field and constant strain rate at the effective zone of the specimen. In order to keep a minimum volume of the sample (Representative Volume Element), width and length of the specimen have been fixed to 10 × 20 mm. Fig. 4(a) shows, for different values of radius and applied displacement velocity, the minimum stress at which the

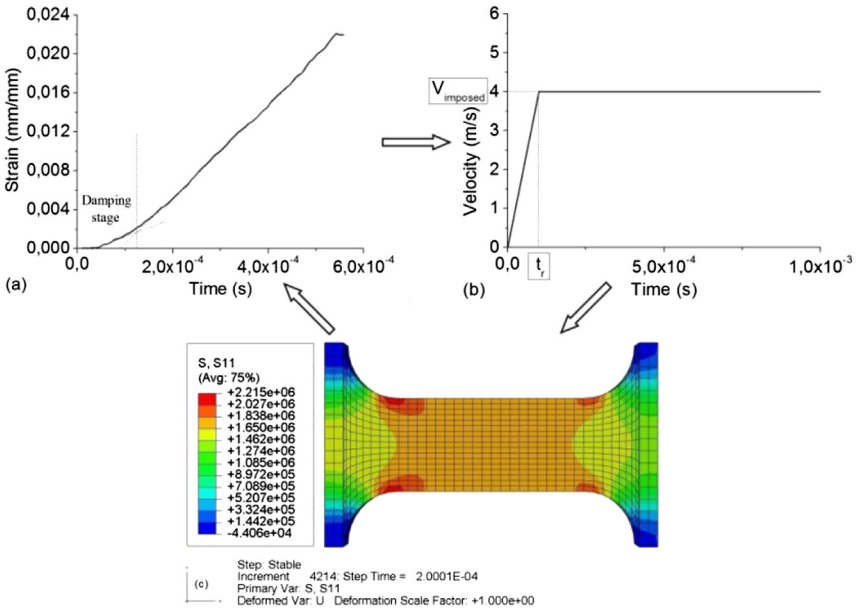

Fig. 2. Specimen optimization methodology coupling experimental tests and FE simulations. (a) Experimental data. (b) Boundary conditions. (c) FE computations optimizing the dumbbell-shaped specimen geometry parameters.

A-SMC		L_1 (mm)	L_2 (mm)	R (mm)	L_3 (mm)	L_4 (mm)
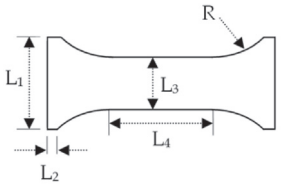	1	20	2	**5**	10	20
	2	22	2	**6**	10	20
	3	25	2	**7.5**	10	20
	4	25	2	**14**	10	20

Fig. 3. Used specimen dimensions for the optimization methodology.

stress field can be considered to be homogeneous together with a constant strain rate inside the gauge length (see an example of evolution in Fig. 5). One can see that, even for the higher imposed displacement velocity; optimal conditions are applied to the specimen for tensile stress less than 5 MPa. Moreover, Fig. 4(b) show the average value of the strain rate obtained inside the gauge length for different values of radius and imposed displacement velocity. One can see that strain rate for optimized specimens can be subjected to strain rates of more than 100 s^{-1}. The latter one can also be evaluated theoretically on the basis of the imposed velocity, such as: $\dot{\varepsilon} = V/L_4$. It should be noticed that, because of dynamic conditions, real strain rate should be 40% less than theoretical strain rate. For example, we get 60 s^{-1} instead of 100 s^{-1} for and velocity of 2 m/s imposed on a 6 mm radius specimen.

iv High-speed tensile tests are achieved on the composite specimen in order to validate its optimized geometry.

Finally, the 6 mm radius specimen corresponds to the optimized geometry. Fig. 5 shows the spatio–temporal profiles of the longitudinal stress (σ_{11}) calculated along the central line of the optimized A-SMC specimen. It can be observed that the shock wave

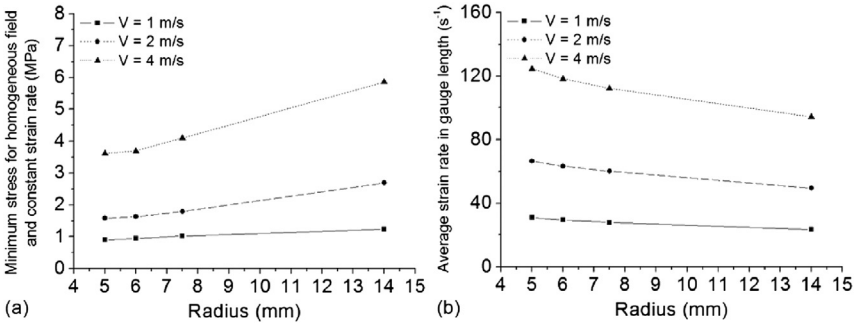

Fig. 4. Influence of the radius of the specimen; (a) Minimum stress for which homogeneous field and constant strain rate is obtained (b) Strain rate in the central zone.

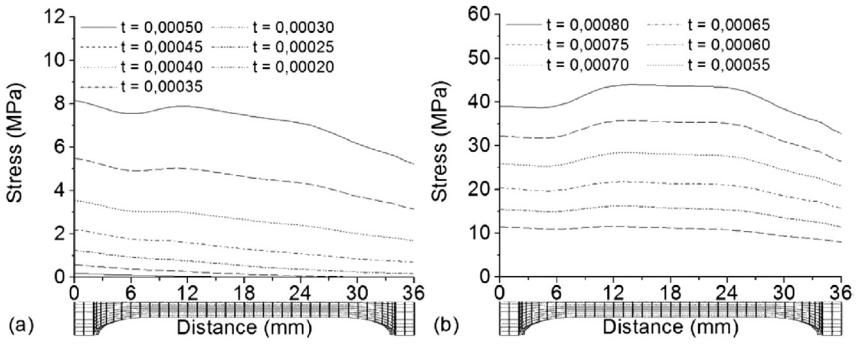

Fig. 5. Spatio-temporal profile of σ_{11} calculated along the central line of the A-SMC specimen. Loading conditions: imposed velocity V = 4 m/s. (a) First steps and (b) next steps.

vanishes very quickly. Actually, the stress distribution becomes relatively homogeneous (see Fig 2(c)).

2.2.2.4. Strain and strain rate measurements. Local deformation is measured through a contactless technique using a high speed camera: two points were marked on the surface of the specimens defining the initial gauge length which is about 20 mm. A high speed camera (FASTCAM-APX RS) with the capacity 250,000 frames per second was used to record pictures during high speed deformation. Image analysis is then used in order to follow the displacement of the centroid of each marked point to compute the evolution of the strain between the two points. After thresholding of the pictures, the evolution of the relative positions of the two points during deformation is computed. Then, strain measurement can be performed as shown in Fig. 6. One can note that after the damping stage characterized by a progressive increase of strain rate, the later becomes constant. Thus, strain rate can be easily determined from the slope of the linear part of the curve.

3. Experimental results and discussion

3.1. Characteristics of composite

3.1.1. Microstructure

Fig. 7 shows a comparison between a standard SMC microstructure and that of A-SMC. These SEM pictures obtained on polished surfaces show clearly the higher glass fibers content in A-SMC compared to standard SMC. Indeed, fibers are initially randomly oriented in the sheets plane before compression. The fibers are presented as bundles of constant length (L = 25 mm). Each bundle contains approximately 250 fibers of 15 μm diameter. Glass fibers weight content is of 50%.

Fig. 8 represents the distribution of the fiber content in the RO and HO plates as a function of the cutting orientation. It can be assumed that, due to the flowing during molding process, most of the fibers remain on the plane of the plate and tend to be oriented parallel to the Mold Flow Direction (MFD).

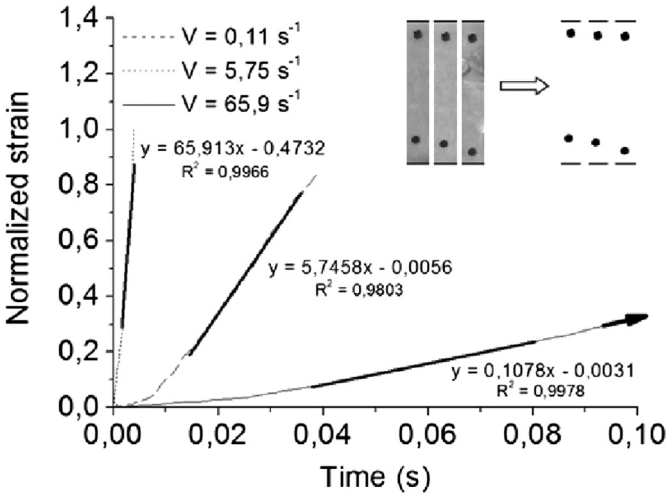

Fig. 6. Typical contactless strain measurements at various high strain rates.

3.1.2. Thermo-mechanical properties

DMTA test is preferentially performed to study the different transitions and change of physical state of polymers. It is achieved to measure T_α,T_β,T_γ etc. In the tension (traction) configuration, DMTA tests also provide a measure of the dynamic modulus.

In this work, DMTA tests have performed according to alternating bending configuration, to study the time–temperature superposition and to plot the relaxation spectrum. It is worth mentioning that the value of modulus obtained by bending DMTA is not far from that obtained by high strain rate tensile tests.

In this study, dynamic tests are performed at room temperature. In order to measure the main transitions temperatures due to molecular mobility as a function of temperature, DMTA tests have been performed on RO samples. Fig. 9 shows the evolution of the storage modulus and the loss modulus versus temperature obtained by DMTA test. A-SMCs present a vitreous transition temperature lying between 60 and 200 °C. It can be assumed that the glass transition temperature is about 130 °C. Although the storage modulus continues to slowly decrease until 50 °C due to the increase of macromolecular chain mobility, it can be assumed that at ambient temperature A-SMCs remain rigid.

3.2. Validation of the optimization procedure

Fig. 10 shows an example of strain evolution during a 2 m/s imposed velocity tensile test. Strain rate is stabilized after a measured rise time of about 1.3×10^{-4} s^{-1}. Moreover, it can be shown that at this time, the material still behaves elastically. Actually, the first non linearity is four time higher than the tensile stress at equilibrium. Thus, it can be assumed that the equilibrium of the specimen is reached before the end of the yield strength. Thus, the measurement of the Young's modulus is reliable. Moreover, a comparison between experimental and numerical evolution of the strain in the central zone of the specimen (obtained for the optimized geometry) is also shown in Fig. 10. A very good correlation is observed.

One can note that after 10^{-4} s, the strain rate is also stabilized and has a rough value of 60 s^{-1}. However, according to the finite elements calculations, the measured strain rate value is 40% less than the theoretical one (100 s^{-1}). As discussed above, this difference is due to inertial effects. On the basis of the very good agreement between the obtained experimental curves and

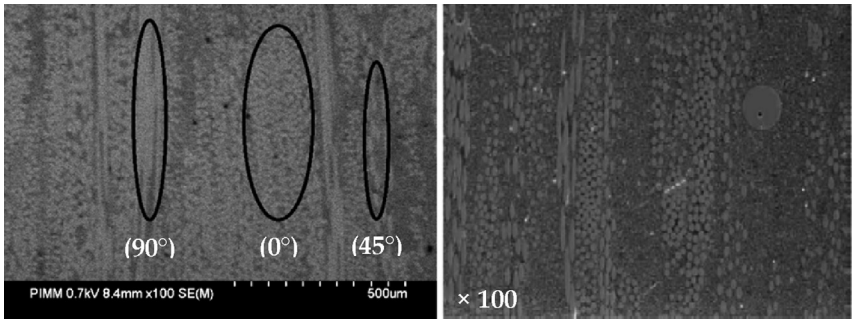

Fig. 7. Microstructure of A-SMC (left) and standard SMC (right): Randomly oriented bundle of fibers.

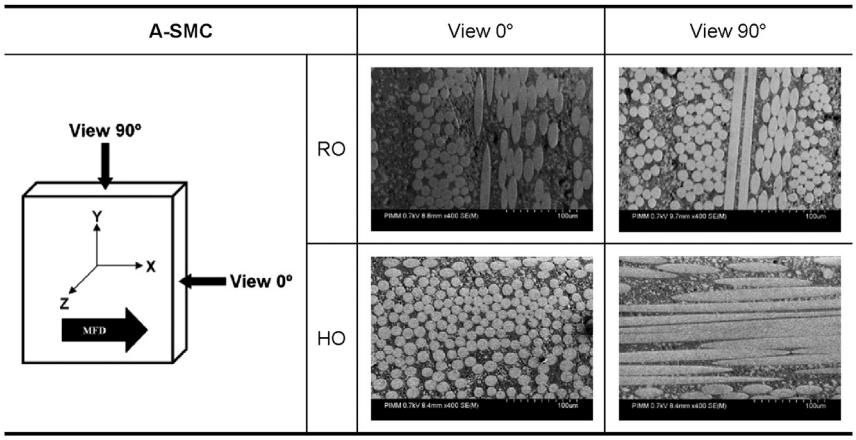

Fig. 8. Orientation of the fibers inside bundles in A-SMC.

numerical results, one can claim that our optimization procedure and the proposed geometry are validated.

3.3. High strain rate tensile curves

The stress–strain curves can be described by three stages:

(i) Linear elastic behavior,
(ii) Damage initiation corresponding to a knee point (apparition of a non-linear behavior),
(iii) Damage propagation corresponding to a second linear stage.

In Fig. 11, stress–strain (σ–ε) tensile curves are plotted for several strain rates. Tensile curves obtained for RO, HO-90°, and HO-0° show clearly that the overall behavior is highly load-rate dependent. Indeed, under rapid tensile load, A-SMC composites exhibit typically a non-linear response. It should be indicated that, in these curves, the part concerning delamination phenomena was eliminated for favorable comparison. Delamination effect will be discussed in section 3.4. Material mechanical characteristics have been estimated, as a function of strain rate. Fig. 11 show that initial slopes of the stress–strain curves are roughly identical for the range of tested strain rate values. Therefore, it means that the elastic modulus remains insensitive to strain rate. Young's moduli have a rough average value of 12, 14.5 and 18.5 GPa for HO-90°-, RO and HO-0°, A-SMCs respectively.

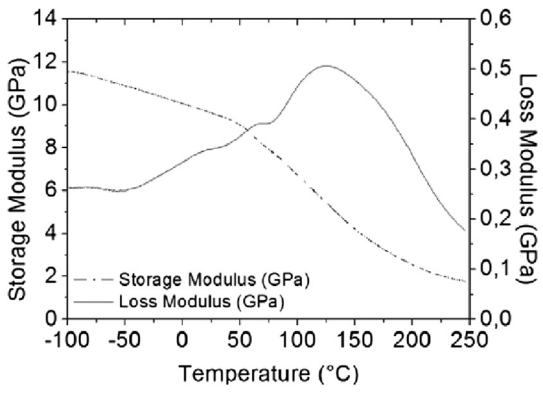

Fig. 9. DMTA test performed on RO sample.

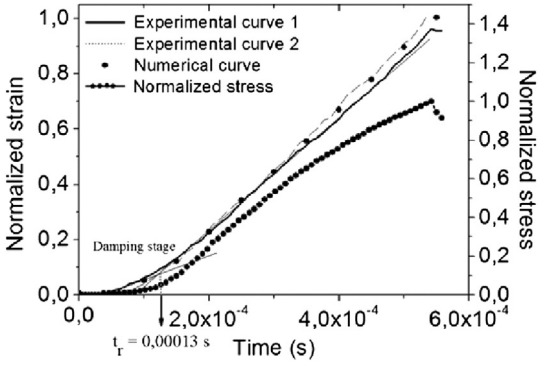

Fig. 10. Evolution of strain and stress in the central zone of the specimen. Comparison between experimental and numerical results obtained for the optimized geometry for A-SMC composites.

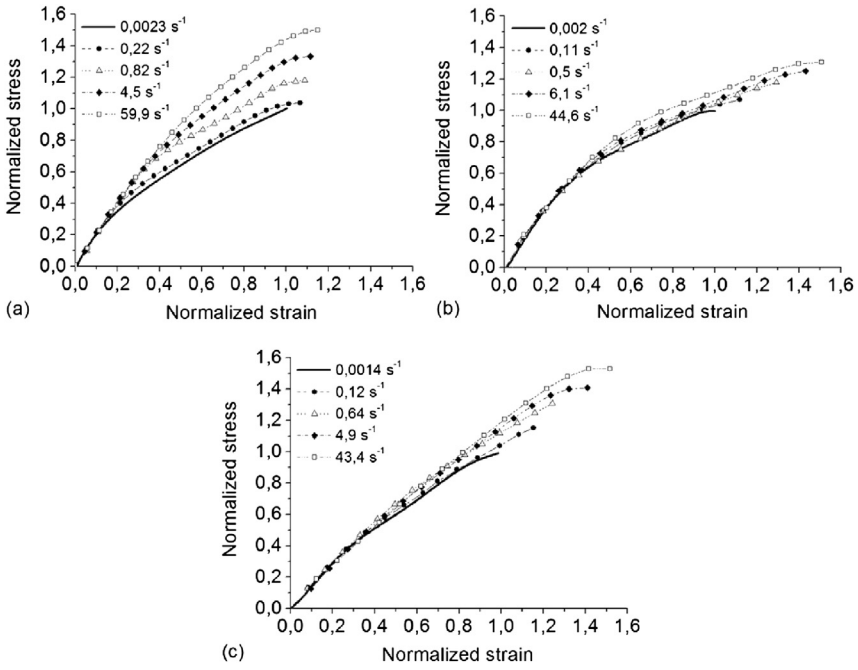

Fig. 11. Experimental high strain rate tensile curves (Normalized stress (resp. strain) = stress (resp. strain)/ultimate stress (resp. strain) obtained in quasi-static): (a) RO-A-SMC, (b) HO-90°-A-SMC and (c) HO-0°-A-SMC.

3.4. Effects of strain-rate on the overall tensile response

Material characteristics, namely Young's modulus (E); damage thresholds corresponding to the first non-linearity ($\sigma_{threshold}$; $\varepsilon_{threshold}$) and ultimate stress and strain ($\sigma_{ultimate}$; $\varepsilon_{ultimate}$) are shown in Figs. 12 and 13. Note that the ultimate characteristics correspond to the maximum stress level (before delamination when it occurs). Fig. 12 enables to emphasize that the material elastic modulus measured in the first stage of the stress–strain curve remain insensitive to the strain rate. However, the non-linear overall response of the A-SMC is drastically influenced by strain rate. Indeed, one can note that the damage threshold (Fig. 13), in terms of stress and strain, increases with strain rate. In fact, in the case of HO-0°, when varying the stain rate from the quasi-static to 100 s^{-1}, an increase of 63% of the stress damage threshold is shown. On the other hand, the ultimate stress shows an increase of 34%.

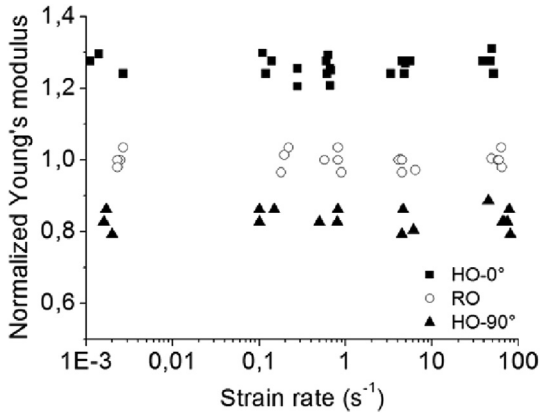

Fig. 12. Evolution of the normalized Young's modulus vs. strain rate (Normalized Young's modulus = Young's modulus/average Young's modulus obtained for quasi-static for RO-A-SMC).

In accordance to results obtained on a standard SMC [12], as the strain rate increases, noticeable effects consist of a delayed damage onset (delay of the knee-point) and ultimate stress. It can be established that the strain rate brings about a viscous nature of damage initiation and propagation. Like for standard SMC, A-SMCs also present a visco-damageable behavior. However, it must be noticed that, contrary to standard SMCs, the non-linear slope of the third stage of the A-SMCs curves (corresponding to the damage propagation stage) is also rate sensitive especially for RO A-SMC. Moreover, one can notice that for all microstructure orientation, no significant strain rate effect is noticed on the ultimate strain.

3.5. Damage mechanisms investigation

In order to understand the physical origin of the damage delay, it is necessary to perform experimental investigations at the microscopic scale in order to identify the corresponding damage mechanisms.

The first investigations concerns quasi-static (0.5 mm/min) bending behavior performed on HO-A-SMC composite. In order to identify the influence of the microstructure on damage mechanisms occurring at the local scale, four points bending tests have been performed inside a SEM on HO-0° and HO-90° rectangular specimens. For both orientations, debonding at the fiber-matrix interface appears clearly to be the predominant damage mechanism. Interface debonding mostly appears on the fibers oriented orthogonally to the principal stress direction (90° oriented fibers) due to high local normal stresses at the interface. Coalescence of interface failure between adjacent fibers leads to localized transverse cracks appearing on several locations in the 90° oriented bundles. Propagation of these cracks into the matrix can also occur but the high content of fibers leads, in general, to the bifurcation of these cracks around surrounding more disoriented bundles of fibers. Then, pseudo-delamination between bundles is initiated. Fiber breakage can also appear at the end of the test just before failure. Interface debonding coupled to pseudo-delamination finally leads to failure by coalescence of the microcracks.

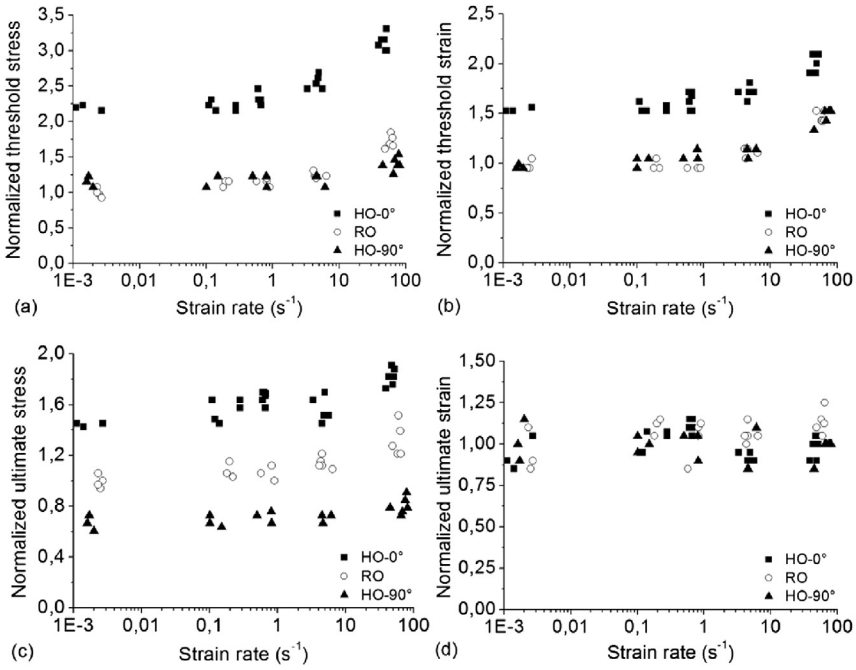

Fig. 13. Influence of strain rate: (a) Normalized threshold strain, (b) Normalized threshold stress, (c) Normalized ultimate strain and (d) Normalized ultimate stress (Normalized value = current value/average value obtained for quasi-static tests performed on RO-A-SMC).

However, the thresholds of fiber-matrix interface damage and delamination are very dependant of the orientation of the sample. Fig. 14 shows for each orientation a first picture obtained at the initiation of the fiber-matrix interface debonding and a second one for the ultimate stress corresponding to pseudo-delamination just before failure. It has been shown that, for HO-0°, interface failure remains limited while pseudo-delamination is favored. On the other hand, when the fibers are oriented perpendicularly to the principal stress direction, pseudo-delamination is limited when fiber-matrix interface becomes predominant. Thus, it can be conclude that two principal mechanisms are in competition: fiber-matrix interface debonding and pseudo-delamination. Moreover, the relative participation of each mechanism strongly depends on the orientation of the fibers.

On the other hand, SEM observations have been performed on the fracture surfaces for tensile specimens for quasi-static and high strain rate (around 100 s^{-1}) loadings. Note that, in all micrographs shown after, the tensile direction corresponds to the horizontal direction.

SEM analysis performed on tensile specimens highlight the same damage mechanisms as shown in quasi-static bending test: fiber-matrix interface debonding and pseudo-delamination (see Fig. 15). These two mechanisms are observed for both quasi-static and dynamic tests regardless of the orientation of the bundles of fibers.

Fig. 16(a)–(c) shows fiber-matrix interface debonding for 0°, 45°, and 90° oriented fibers relative to the tensile direction. One can notice that broken interfaces are always surrounded by pieces of matrix. This indicates high strength properties of the fiber-matrix interface for both quasi-static and dynamic loading.

In Fig. 17, it is noticeable to see that during pseudo-delamination, bundles of fibers are pulled out from each other

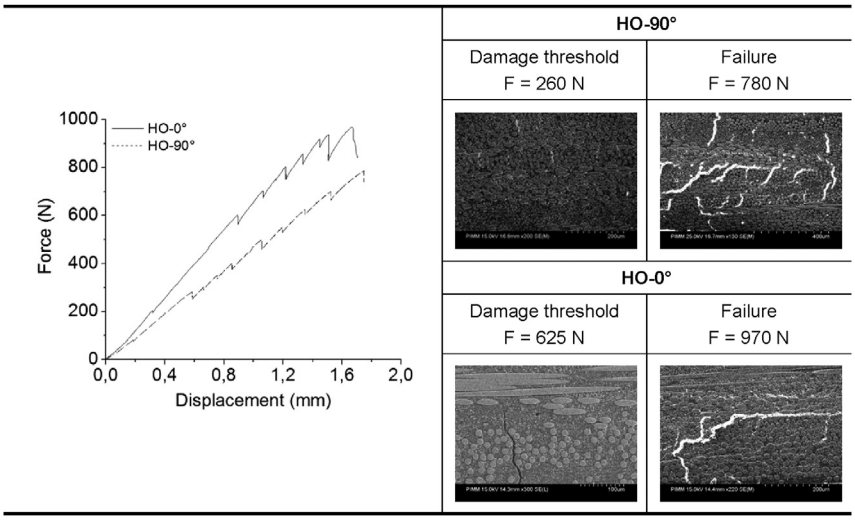

Fig. 14. Damage mechanisms under bending loading for HO-A-SMC composites.

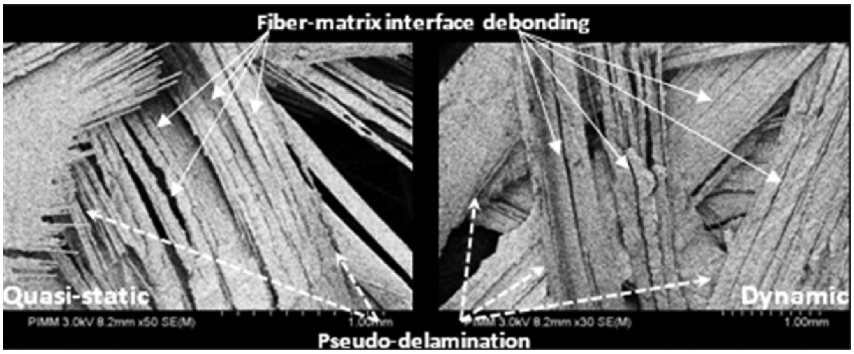

Fig. 15. Damage mechanisms for quasi-static and dynamic tensile tests.

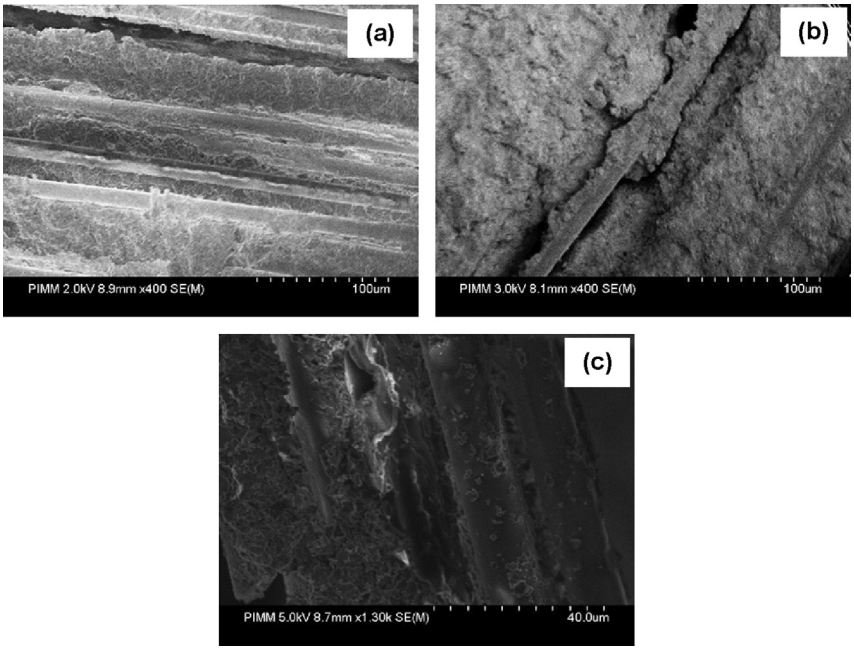

Fig. 16. Fiber-matrix interface debonding for several fiber orientation (a) 0° (around 100 s^{-1}), (b) 45° (around 100 s^{-1}), (c) around 90° (quasi-static).

simultaneously with breakage of the surrounding matrix. See also Fig.16(b) for higher magnification.

In a further paper, we will show how interrupted tensile tests [12,19] enable to quantify the strain rate effect at the local scale through the analysis of the evolution of the fiber-matrix interface failure density.

3.6. Pseudo-delamination mechanism

In this section, the influence of the loading rate and orientation of fibers on pseudo-delamination is investigated. Tensile tests have been performed until specimen total failure under variable strain rates from quasi-static (0.001 s^{-1}) to 100 s^{-1}. All the results shown above have been analyzed only until the ultimate stress. However, because of the pseudo-stratificated microstructure, local delamination between the bundles of fibers can occur before the total separation into two parts. This phenomenon can greatly participate to energy absorption during crash. In this section, we focus on the influence of the microstructure and imposed velocity on the magnitude of the pseudo-delamination.

Fig.18(a) shows a typical evolution of the tensile strain until total separation into two parts including the deformation provided by

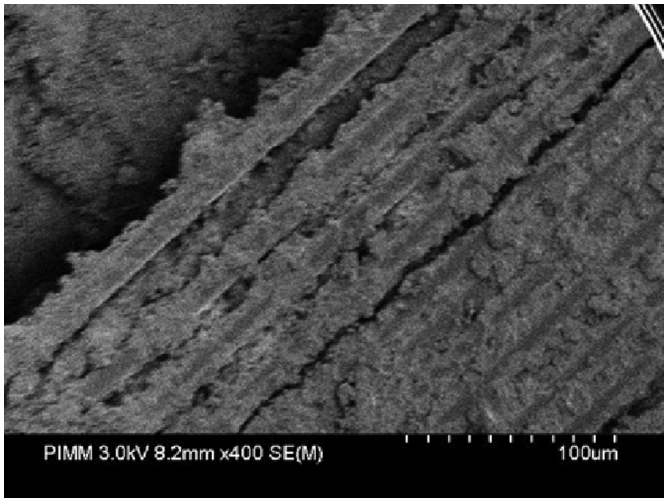

Fig. 17. Pseudo-delamination through surrounding matrix breakage.

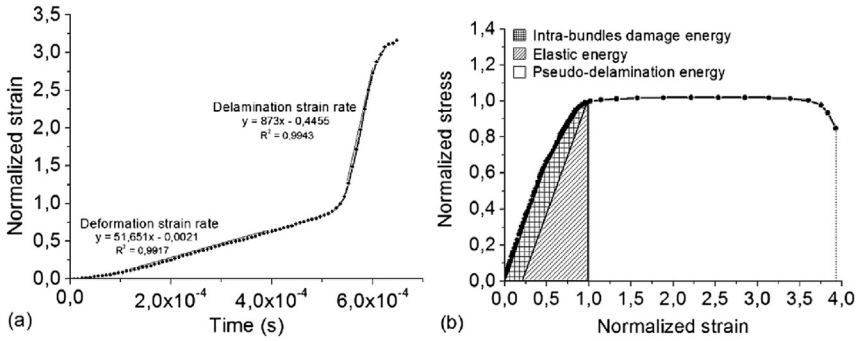

Fig. 18. (a) Normalized strain vs. time and (b) Normalized tensile strain curve for HO-0°-A-SMC obtained for test carried out at strain rate of 52 s^{-1} (All values are normalized by dividing to the value corresponding to the ultimate stress and before delamination).

local delaminations between bundles of fibers. For high speed tensile tests, pseudo-delamination stage duration appears to be very short (about 10^{-4} s) compared to that of the elastic and damage stages (about 5.5×10^{-4} s). Tensile strain rate during delamination is more than 15 time higher. Stress–strain curves in tension can also be plotted as shown in Fig. 18(b). The area under the stress–strain curve corresponds to the total strain energy per unit volume absorbed by the composite until complete separation into two parts: E^T. The area under the curve until the ultimate stress corresponds to the elastic and damage energy: E^e and E^d respectively. As discussed before, damage energy is mostly due to the debonding at the fiber-matrix interface inside the bundles (intra-bundles damage). Then, from the ultimate stress until the total separation into two parts, the area under the curve corresponds to absorbed energy by delamination between the bundles: E^D. It is very obvious that the pseudo-delamination can highly participate to energy dissipation during a crash test. In fact, in the case of HO-0° tensile tests performed under high strain rates, absorbed energy by pseudo-delamination can be 6 time higher than the absorbed energy during elastic and damage stages.

Fig. 19 presents typical whole curves for different microstructure and different imposed velocity together with macroscopic failure photography. Qualitatively, one can see that increasing loading speed leads to more intensive pseudo-delamination regardless of orientation of fibers. Relative elastic, damage and pseudo-delamination energy values; E^e/E^T, E^d/E^T, E^D/E^T respectively have been measured (area under the curves (see Fig. 18(b)). Relative damage and pseudo-delamination evolution are plotted in Fig. 20

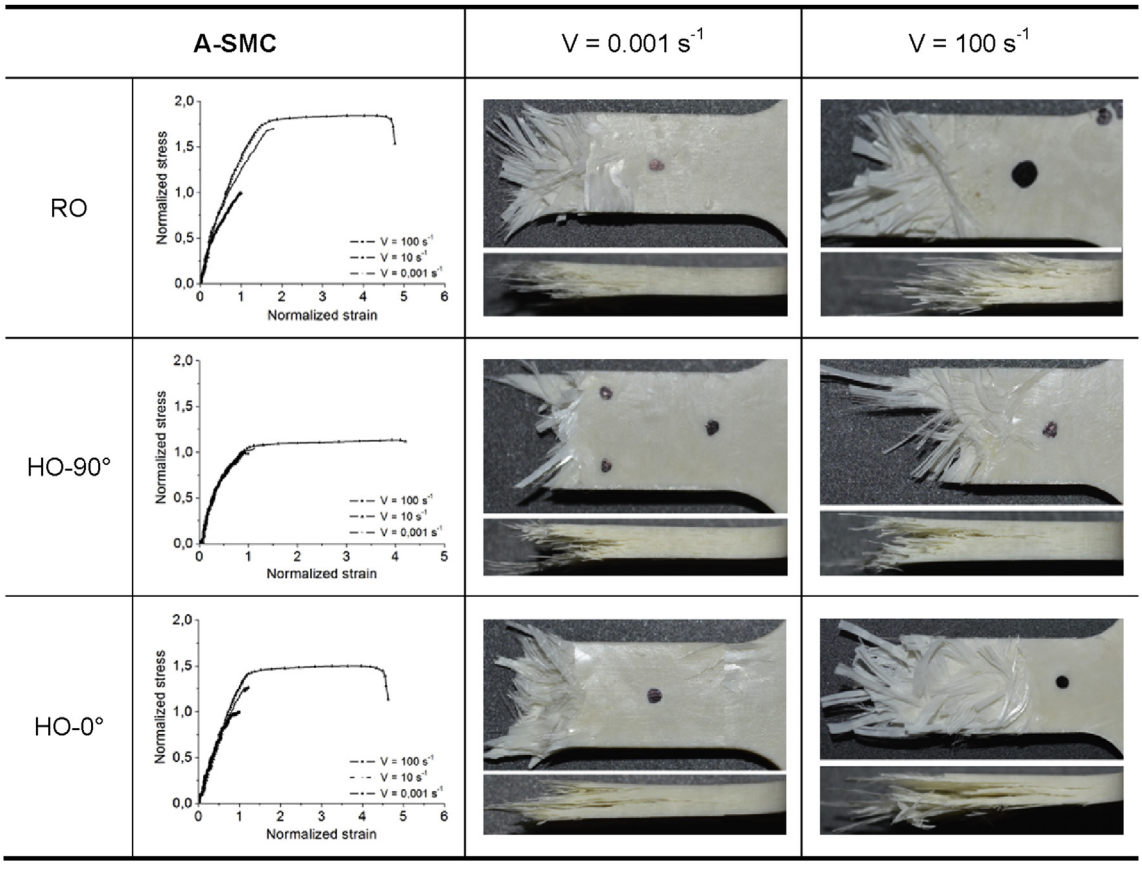

Fig. 19. Typical whole curves for different microstructure and different imposed velocity together with macroscopic failure appearance.

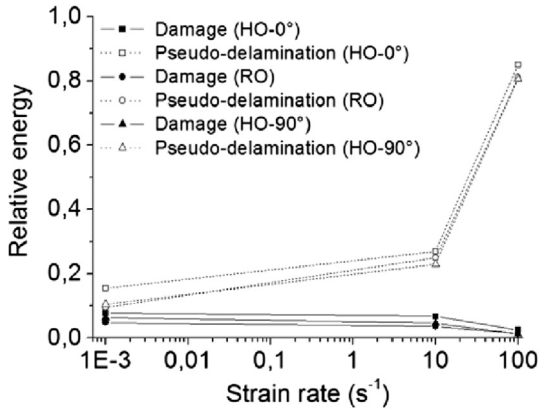

Fig. 20. Evolution of the relative damage and pseudo-delamination energy versus strain rate.

as a function of strain rate. One can clearly conclude that high loading speed favor the increase of the pseudo-delamination intensity. Moreover, Fig. 21 shows the evolution of the ratio E^D/E^D_{RO} where E^D_{RO} is the pseudo-delamination energy measured for RO-A-SMC for a 10 s^{-1} applied strain rate. It is obvious to note that oriented fibers in the tensile direction also favor delamination.

It is important to notice that the end of experimental curves (Fig. 19) represents the last stage of the damage mechanisms propagation and accumulation prior to the macroscopic failure of the specimen. Two kinds of failure mechanisms have been observed.

- The first one appears for the lower strain rate values independently of the microstructure: it corresponds to the coalescence and the accumulation of the fiber-matrix interface cracks through the matrix between bundles of fibers [12].
- The second one appears for higher strain rate values independently of the microstructure: in this case, the pseudo-delamination becomes the predominant failure mechanism. Fiber-matrix interface cracks coalescence in the matrix is limited by the pseudo-delamination which becomes the predominant failure mechanism at high strain rate. A plateau is observed before the failure corresponding to the propagation of the cracks around the bundles of fiber prior to the coalescence leading to the final failure (Fig. 19). This mechanism is more intense for oriented microstructure (Fig. 21).

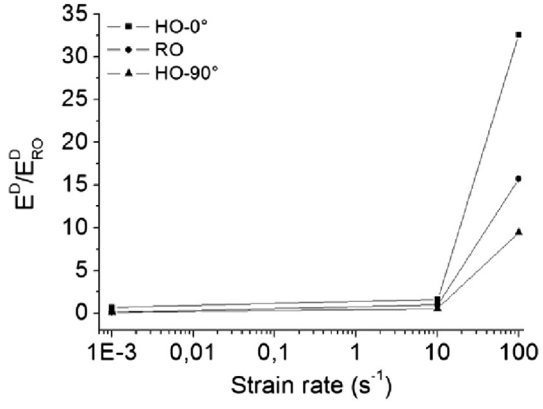

Fig. 21. Evolution of the pseudo-delamination energy for various fiber orientations and strain rates.

In conclusion, pseudo-delamination strongly participates to energy dissipation. Thus, this mechanism can't be neglected for crash simulations.

4. Conclusion

A-SMC is a high mechanical performance SMC based on vinylester resin and reinforced with high content of glass fibers (>50% weight content) compare to standard SMC (30% weight content). An original method for high strain rate testing optimization has been validated for moderate rates up to 100 s^{-1}. A damping joint have been optimized in terms of thickness and material properties. Then, the resulting experimental conditions (rise time and imposed velocity) were input into a numerical computations using ABAQUS FE explicit code. Iterative calculations led to determine the optimal specimen geometry through the analysis of the stress wave propagation occurring during a high-speed tensile test. It has been demonstrated that the resulting specimen design generates uniform strain and stress fields and constant strain-rate into the tested specimen.

The developed experimental methodology based on dynamic tensile tests has contributed to emphasize the strain rate effects on the overall behavior of A-SMC composites. The use of a servo-hydraulic testing machine has been suitable to examine strain-rate effects on overall A-SMC (RO and HO) behavior for moderate rates up to 100 s^{-1}. The strain rate is measured through a contactless technique using a high speed camera. Moreover, SEM micrographs show that most of the fibers are more or less oriented according to the disposition of the A-SMC prepreg and process parameters. In order to represent as well the structural response during an automotive crash, the strain rate effects on the mechanical behavior of two type of microstructure have been studied: Randomly Oriented fibers (RO) and Highly Oriented fibers (HO). Experimental results of high strain rate tensile tests show that the composite behavior is strongly strain-rate dependent although the Young's modulus remains constant for RO and HO samples when strain rate increases. On the contrary, as the strain rate increased, noticeable effects consist of a delayed damage onset: for example, the stress damage threshold of HO-0°-A-SMC showed an increase of 63% when increasing the strain rate from quasi-static (0.001 s^{-1}) to 100 s^{-1}. In the same time, a 40% increase of the ultimate stress can be observed when the ultimate strain does not seem to be significantly affected.

Moreover, SEM analysis performed on broken tensile specimens highlight the same damage mechanisms as shown in quasi-static bending tests: fiber-matrix interface debonding and pseudo-delamination between bundles of fibers. Until the ultimate stress, damage energy is mostly due to the debonding at the fiber-matrix interface inside the bundles (intra-bundles damage). However, it has been shown that the pseudo-delamination also greatly participates to the energy absorption. Then, the second part of the curve appearing as a plateau from the ultimate stress until the total separation into two parts cannot be neglected. Indeed, the area under the curve corresponding to the absorbed energy by pseudo-delamination between bundles can be ten times higher than the energy absorbed through fiber-matrix interface debonding (intra-bundles damage). It is important to note that increasing loading speed and oriented fibers in the tensile direction favor a more intensive pseudo-delamination. These two effects have been also quantified. This study clearly establishes that the strain rate effect is related to a certain viscous nature of both intra-bundles and pseudo-delamination damage evolution. One can speak about a time dependent visco-damage behavior leading to the increase of the fiber-matrix and inter-bundles interfaces strengths.

Consequently, it is very obvious that intra-bundle damage and pseudo-delamination highly participate to energy dissipation during a crash test and that stain rate effect on these two damage mechanisms cannot be neglected for automotive structural crashworthiness simulations. The optimized experimental methodology will provide the experimental framework to develop, identify and validate a multi-scale model integrating the material microstructure influence. This model will be used as a simulation tool for the optimization of A-SMC composite structure crashworthiness in accordance with design requirements and material microstructure distribution.

References

[1] Le TH, Dumont PJJ, Orgéas L, Favier D, Salvo L, Boller E. X-ray phase contrast microtomography for the analysis of the fibrous microstructure of SMC composites. Compos Part A Appl Sci Manuf 2008;39(1):91–103.

[2] Palmer J, Savage L, Ghita OR, Evans KE. Sheet moulding compound (SMC) from carbon fibre recyclate. Compos Part A Appl Sci Manuf 2010;41(9):1232–7.

[3] Fitoussi J, Guo G, Baptiste D. A statistical micromechanical model of anisotropic damage for S.M.C. composites. Compos Sci Technol 1998;58(5):759–63.

[4] Wulfsberg J, Herrmann A, Ziegmann G, Lonsdorfer G, Stöβ N, Fette M. Combination of carbon fiber sheet moulding compound and prepreg compression moulding in aerospace industry. Procedia Eng 2014;81:1601–7.

[5] Feuillade V, Bergeret A, Quantin J, Crespy A. Characterisation of glass fibres used in automotive industry for SMC body panels. Compos Part A Appl Sci Manuf 2006;37(10):1536–44.

[6] Lu J, Khot S, Wool RP. New sheet molding compound resins from soybean oil. I. Synthesis and characterization. Polymer 2005;46(1):71–80.

[7] Guiraud O, Dumont PJJ, Orgéas L, Favier D. Rheometry of compression moulded fibre-reinforced polymer composites: rheology, compressibility, and friction forces with mould surfaces. Compos Part A Appl Sci Manuf 2012;43(11):2107–19.

[8] Jendli Z, Meraghni F, Fitoussi J, Baptiste D. Multi-scales modeling of dynamic behaviour for discontinuous fibre SMC composites. Compos Sci Technol 2009;69(1):97–103.

[9] Dear JP, Brown SA. Impact damage processes in reinforced polymeric materials. Compos Part A Appl Sci Manuf 2003;34(5):411–20.

[10] Jendli Z, Meraghni F, Fitoussi J, Baptiste D. Micromechanical analysis of strain rate effect on damage evolution in sheet molding compound composites. Compos Part A Appl Sci Manuf 2004;35(7–8):779–85.

[11] Jendli Z, Fitoussi J, Meraghni F, Baptiste D. Anisotropic strain rate effects on the fibre-matrix interface decohesion in sheet moulding compound composites. Compos Sci Technol 2005;65(3–4):387–93.

[12] Fitoussi J, Meraghni F, Jendli Z, Hug G, Baptiste D. Experimental methodology for high strain-rates tensile behaviour analysis of polymer matrix composites. Compos Sci Technol 2005;65(14):2174–88.

[13] Le Corre S, Orgéas L, Favier D, Tourabi A, Maazouz A, Venet CC. Shear and compression behaviour of sheet moulding compounds. Compos Sci Technol 2002;62(4):571–7.

[14] Naik NK, Yernamma P, Thoram NM, Gadipatri R, Kavala VR. High strain rate tensile behavior of woven fabric E-glass/epoxy composite. Polym Test 2009;29(1):14–22.

[15] Brown KA, Brooks R, Warrior NA. The static and high strain rate behaviour of a commingled E-glass/polypropylene woven fabric composite. Compos Sci Technol 2009;70(2):272–83.

[16] Jacob GC, Starbuck JM, Fellers JF, Simunovic S, Boeman RG. Strain rate effects on the mechanical properties of polymer composite materials. J Appl Polym Sci 2004;94(1):296–301.

[17] Hsiao HM, Daniel IM. Strain rate behavior of composite materials. Compos Part B Eng 1998;29(5):521–33.

[18] Meraghni F, Desrumaux F, Benzeggagh ML. Implementation of a constitutive micromechanical model for damage analysis in glass mat reinforced composite structures. Compos Sci Technol 2002;62(16):2087–97.

[19] Fitoussi J, Bocquet M, Meraghni F. Effect of the matrix behavior on the damage of ethylene-propylene glass fiber reinforced composite subjected to high strain rate tension. Compos Part B Eng 2013;45(1):1181–91.

Article N°2:

Shirinbayan M, Fitoussi J, Bocquet M, Meraghni F, Surowiec B, Tcharkhtchi A. Multi-scale experimental investigation of the viscous nature of damage in Advanced Sheet Molding Compound (A-SMC) submitted to high strain rates. Composites Part B: Engineering. 2016.

Composites Part B 115 (2017) 3–13

Contents lists available at ScienceDirect

Composites Part B

journal homepage: www.elsevier.com/locate/compositesb

Multi-scale experimental investigation of the viscous nature of damage in Advanced Sheet Molding Compound (A-SMC) submitted to high strain rates

M. Shirinbayan [a, *], J. Fitoussi [a], M. Bocquet [a], F. Meraghni [b], B. Surowiec [c], A. Tcharkhtchi [a]

[a] Arts et Métiers ParisTech, PIMM – UMR CNRS 8006, 151 Boulevard de l'Hôpital, 75013 Paris, France
[b] Arts et Métiers ParisTech, LEM3 – UMR CNRS 7239, 4 Rue Augustin Fresnel, 57078 Metz, France
[c] Plastic Omnium Auto Exterior, Sigmatech, Sainte Julie, France

ARTICLE INFO

Article history:
Received 7 June 2016
Received in revised form
19 October 2016
Accepted 22 October 2016
Available online 24 October 2016

Keywords:
Microstructure
Damage
Multi-scale analysis

ABSTRACT

This paper aims to present an experimental multi-scale analysis of quasi-static and high strain rate damage behavior of a new formulation of SMC composite (Advanced SMC). In order to study its capability to absorb energy through damage accumulation, Randomly Oriented (RO) and High oriented (HO) A-SMC composites damage has been investigated at both microscopic and macroscopic scales. A specific device has been developed in order to perform Interrupted Dynamic Tensile Tests (IDTT) which allows analyzing the evolution of the microscopic damage mechanisms occurring during rapid tensile tests. Several damage micro-mechanisms have been pointed out. The relative influences of these micro-damage events and their interactions have been related to the macroscopic damage behavior through the definition of microscopic and macroscopic damage indicators. Damage threshold and kinetic have been quantified at various strain rate for different microstructures and loading cases (RO, HO-0° and HO-90°). It has been shown at both scales that increasing strain rate leads to an onset of damage initiation together with a reduction of the damage accumulation kinetic. Moreover, the influence of the fiber orientation has been studied in order to emphasize the anisotropic strain rate effect at the fiber-matrix interface scale. The latter was related to the influence of the microstructure of A-SMC composites. Finally, on the basis of the whole experimental results, the microscopic origin of the viscous nature of the damage behavior of A-SMCs composites have been discussed and related to the influence of the strain rate and microstructure.

1. Introduction

Because of their high energy absorption capacity, short fiber reinforced composite materials are often used for automotive structures submitted to crash events. In contrast to metallic materials for which energy absorption is provided by plastic deformation [1], composites material structures crashworthiness mostly consists of several diffuse and progressive damage mechanisms occurring at the local scale such as matrix micro-cracking [2], fiber failure [3], debonding at the fiber-matrix interface [4–6], delamination or pseudo-delamination [7]. This is an extremely important issue for automotive industry. Indeed, local damage development allows composite structures to absorb significant impact energy in such a way that the progressive degradation enables to minimize the transmitted energy to passenger and to assure his safety. On the other hand, several earlier studies [8,9] have shown that the energy absorption capacity of polymers and composites materials is highly dependent on the microstructure parameters such as fiber content, type of fiber and matrix or fiber orientation and length. Furthermore, a good crashworthiness requires avoiding damage localization leading to a brittle failure and limited absorbed energy. So, in order to favor a diffuse damage development, a better understanding of the damage mechanisms which can occur during high strain rate loading is required.

Composite design capable of good crash resistance requires acquiring a thorough knowledge of its capacity to develop damage phenomenon [10,11]. However, short fiber reinforced composite structure design is in general a difficult challenge because of several specificities such as the variability of the microstructure [7], the anisotropic behavior [12], multiple coupled damage mechanisms

* Corresponding author.
E-mail addresses: mohammadali.shirinbayan@ensam.eu (M. Shirinbayan), joseph.fitoussi@ensam.eu (J. Fitoussi), michel.bocquet@ensam.eu (M. Bocquet), fodil.meraghni@ensam.eu (F. Meraghni), benjamin.surowiec@plasticomnium.com (B. Surowiec), abbas.tcharkhtchi@ensam.eu (A. Tcharkhtchi).

http://dx.doi.org/10.1016/j.compositesb.2016.10.061
1359-8368/

which produce an evolution of the anisotropy during loading [13] etc. A lack of unawareness regarding the influence of high loading rate on the local damage mechanisms could lead to a less effective composite structure design. In particular with regard to the choice of damage behavior laws used in finite element calculations for crashworthiness design, the influence of microstructure parameters and strain rate on the threshold and kinetic of damage is of prime importance. Indeed, when damage behavior of composite materials is analyzed especially at different strain rate, the architecture (Orientation of reinforcements, laminate) and the matrix behavior (Elastic, visco-elastic, visco-plastic) should be considered. Thermoplastic [14] and thermoset materials [7] have different damage behavior subjected to loading at different strain rate.

Several studies have proposed models to account for the damage behavior of composite and specific implementation techniques for numerical simulations have been developed [15–17]. One may distinguish two kind of predictive modeling of composite material behavior: phenomenological and micro-mechanical approach. For both approach, damage variables are described. For the micro-mechanical approach theses variables describe the evolution of the micro-cracks content during loading [18–21]. The phenomenological approach aims to describe the consequence of the local damage at the macroscopic scale such as loss of stiffness. In this approach, the macroscopic scale corresponds to the Representative Volume Element (RVE) of composite material. However, to make easy the micro-mechanical calculations, the damage variable is sometimes non-local [22]. In this case, the crack data are usually homogenized. This approach is often adopted in mixed models of damage, combining micro-mechanical and phenomenological aspects [23]. Conversely, in energy approaches, the damage variable is mostly unrelated to the physical reality [24]. Most damage models can represent a softening deformation [25]. Mixed models are most often associated with a fracture criterion [26]. In phenomenological models, mechanical behavior laws are derived from thermodynamic potentials and the representation of the mechanical degradation is more finite [18]. Damage phenomenological models can be used more easily that the micro-mechanical damage models in numerical simulation, because energy formulations do not need the microscopic data [18,19]. On the other hand, in micro-mechanical models, the damage variable has a physical sense related to the volume fraction occupied by cracks in the damaged composite, the rate of energy dissipated by fracture or cracks parameters [20,21].

Moreover, especially with regard to the anisotropy evolution due to damage observed in the short fiber reinforced composite [13], the micromechanical modeling seems to be a more suitable approach for the prediction of the behavior and damage of this class of materials. In these models, damage can be taken into account through several local damage criterions which are in competition and determine the introduction of micro-cracks at the local scale [27–29].

One can conclude that, whatever the numerical approach used, a thorough knowledge of the type of local damage mechanisms, their threshold and kinetic is always needed on one hand for the choice of a suitable damage behavior law and for the identification of its variables on the other hand [28–30].

The purpose of this study concerns a new formulation of SMC composite which have recently be developed: A-SMC. Advanced Sheet Molding Compound (A-SMC) is a high performance SMC composite based on vinylester resin and reinforced with 50% (in mass) of chopped bundles of glass fibers [7]. A-SMCs are provided by Plastic Omnium Auto Exterior and are processed by thermo-compression [7]. These composites are commonly used as a substitute for steels in structural automotive components because of their high strength-to-weight ratio [31,32]. A recent study [7] have demonstrated their high stiffness and strength together with low density compared to metals which make them suitable materials for crashworthy small weight automotive structures. This paper aims to the determination of the damage mechanisms and their influence on the macroscopic response of A-SMC composites when they are submitted to high strain rates.

Different experimental techniques characterize the damage at macroscopic and microscopic scales: Loading unloading at different loading directions, acoustic emission technique [33], in-situ SEM microscopy testing [5] and also micro-tomography X method [29], anisotropic stiffness reduction measurement by ultrasonic technique and etc [13]. In the case of dynamic loading, it is not possible, because of uncontrolled inertial effect, to measure the stiffness reduction by loading-unloading tests. Likewise, the micro-scale monitoring of the damage phenomenon is difficult. In this study, the methodology of interrupted tests already used in the case of standard SMC and PP composite [4,5] will be illustrated in the case of A-SMC. In these previous studies, the experimental results showed that the predominant damage mechanism is the fiber-matrix interface debonding. However, micro-cracking of the matrix can also play a significant role in particular during the last stages before failure through the coalescence of the fiber-matrix interface micro-cracks across the matrix. It has been shown that, for a standard SMC, when the strain rate increases, a delayed damage onset is followed by of a reduction damage accumulation kinetic.

Several studies show that the mechanical response of A-SMC and also SMC composites is strongly dependent on the microstructure variability and strain rate [4–7]. A micro-mechanical model based on a statistical local interface failure criterion introduced in the Mori and Tanaka model was earlier proposed by Fitoussi [6], in order to predict the tensile curves and the stiffness reduction due to damage for SMC composite. This kind of micro-mechanical model was introduced in a finite element analysis for composites structure damage analysis by Derrien et al. [34] and Meraghni et al. [35]. This approach was validated in the case of bending-torsion test. Jendli et al. [12] have generalized this approach to high strain rate loading. They used the multi-scale experimental analysis of high strain rate interrupted tensile tests [5] to identify and validate a multi-scale visco-damageable model [27].

In the present paper, we apply the method of interrupted tensile test to identify damage mechanisms (Damage thresholds and kinetic) depending on the orientation of reinforcements and strain rate in order to make the database needed to built a predictive model of the micro-mechanical behavior of A-SMC under crash loading.

The organization of this paper is as follow: A-SMC composite composition and two kind of this composite (Randomly Oriented (RO) and Highly Oriented (HO) plates) provided by Plastic Omnium Auto Exterior are introduced in material specification section. In the case of HO samples, two tensile directions were selected in order to evaluate the anisotropic effect due to microstructure: HO-0° (parallel to the Mold Flow Direction (MFD)) and HO-90° (perpendicular to the MFD). Quasi-static tensile tests with damage evolution at macroscopic scales are investigated for HO samples. Subsequently, the results of low and high strain rate tensile test until failure and damage evolution at macroscopic and microscopic scales for RO samples are presented. The visco-damageable behavior of A-SMC composites is correlated to observations performed at the local scale. The effect of high strain rate on elastic properties, damage threshold and kinetic are analyzed at both microscopic and macroscopic scale. A previous work [5] showed that, depending on microstructure and strain rate, the development of a pseudo-delamination stage between bundles of fibers which can occur before failure. At the end of this paper, SEM analysis emphasizes the effect of strain rate on the pseudo-delamination.

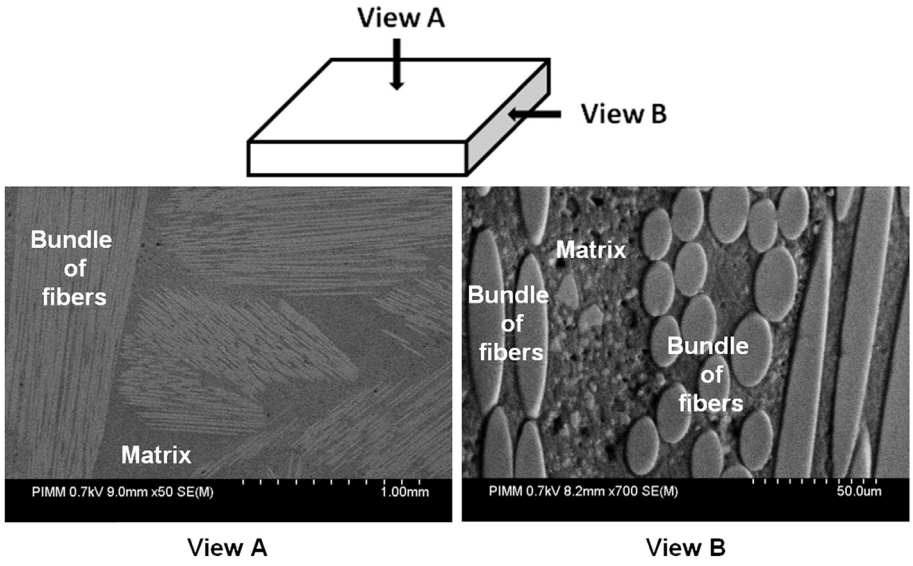

Fig. 1. Microstructure of RO-A-SMC composite.

2. Material specification and methods

2.1. Advanced Sheet Molding Compound (A-SMC) composite

Advanced Sheet Molding Compound (A-SMC) composite is typically used in automotive industry. A-SMC is a high mechanical performance SMCs consisting of a vinyl-ester resin reinforced by a high content of chopped bundles of glass fibers (50% in mass corresponding to 38.5% in volume). Two types of A-SMC plates have been provided by Plastic Omnium Auto Exterior: Randomly Oriented (RO) and Highly Oriented (HO) plates. HO plates have been obtained by placing the initial charge of SMC prepreg sheets only in the left part of a rectangular mold (30×40 cm^2). Thus, compression molding leads to material flow and fiber orientation. RO plates were obtained without material flow by completely filling the mold. Fig. 1 shows microstructure of A-SMC observed by SEM microscope on polished surfaces. Indeed, fibers are initially randomly oriented in the SMC prepreg sheets before compression. The fibers are presented as bundles of constant length ($L = 25$ mm). Each bundle contains approximately 250 fibers of 15 μm diameter.

2.2. Methods

In order to study the damage behavior of A-SMC composite, interrupted high speed tensile test at different strain rate have been performed and deeply analyzed at both microscopic and macroscopic scales on Randomly Oriented (RO) plates. Moreover, in the case of HO plates, two tensile directions; HO-0° (parallel to the Mold Flow Direction (MFD)) and HO-90° (perpendicular to the MFD) were used to investigate the damage behavior in quasi-static tensile test.

2.2.1. Low and high speed tensile tests

Low-speed tensile tests and also quasi-static loading-unloading tensile tests have been performed at different defined maximum stress using a MTS 830 hydraulic machine. The analysis of the reloading slope leads to the determination of the loss of stiffness (see equation (1) in section 3.3).

At the other hand, a servo-hydraulic machine as specified by the manufacturer (Schenk Hydropuls VHS 5020) was used to perform tensile tests at different strain rates from quasi-static to 60 s^{-1}. The A-SMC sample is positioned between the load cell (upper extremity) and the moving device (lower extremity) as shown in Fig. 3(a). In order to get a constant strain rate from the beginning of the high speed tensile test, a tube-piston device allows applying a displacement of the moving device without loading during the acceleration stage.

2.2.2. Interrupted high-velocity tensile test

In order to identify the damage mechanisms occurring during dynamic loading, it is necessary to perform experimental investigations at both macroscopic and microscopic scale. To that end, rectangular specimens with polished surfaces which enable microscopic SEM observations were used as drawn in Fig. 2.

Interrupted high-strain rate tensile test have been originally proposed by Lataillade et al. [36] in the case of glass fiber epoxy laminates. Fitoussi et al. used it for standard SMC composites, carbon Epoxy laminate [5] and short glass fiber reinforced polypropylene [4]. On one hand, this test aims to identify damage mechanisms occurring progressively at the microscopic scale. On the other hand it allows determining the progressive loss of stiffness due to damage. The threshold and kinetic of damage are determined and correlated at both microscopic and macroscopic scale. In this paper, the interrupted dynamic tensile test was developed for A-SMC composite. IDTT is a dynamic loading-unloading test which allows producing successive damaged samples states obtained at different force levels during high-speed loading. The same sample is used several times for increasing levels of applied force. Moreover, before each reloading stage, Scanning Electronic Microscope observations (HITACHI 4800 SEM) have been performed on the polished surface in order to quantify the strain rate effects on the microscopic damage mechanisms (see equations (2) and (3)) in section 3.3 related to the mechanical loss of stiffness of the composite. Thus, A-SMC composites damage was pointed out at two scales (micro and macro).

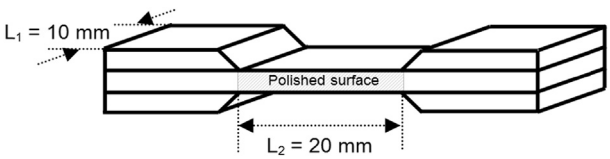

Fig. 2. Rectangular specimen dimension.

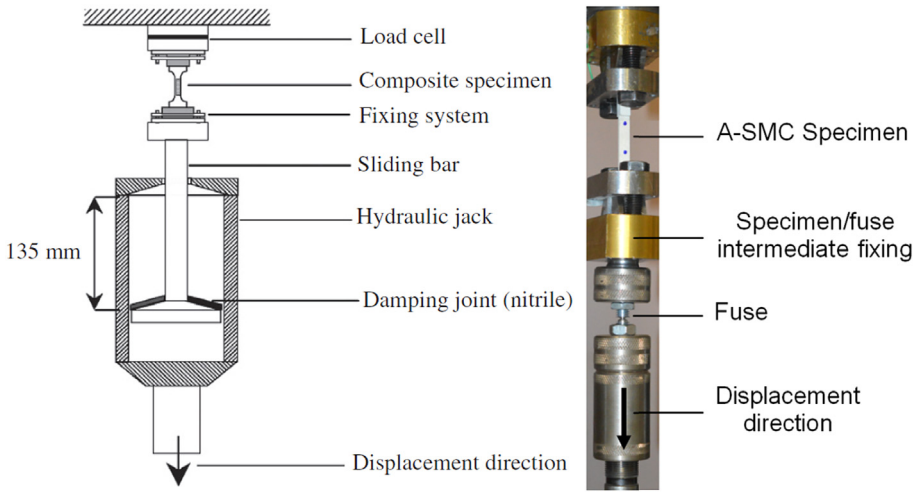

Fig. 3. Interrupted dynamic tensile test: (a) High-strain rate tensile device; b) Specimen-fuse device for interrupted high-speed tensile test.

The IDTT device is illustrated in Fig. 3(b). During dynamic loading of the sample, the inertia of the hydraulic cylinder, when it is launched, does not allow interrupted test at chosen stress level such as in quasi-static loading-unloading tests. Therefore, the loading of specimen will continue until macroscopic failure. To solve this problem, the basic idea is to place an elastic brittle fuse in series with the composite sample. In this study, a special device was developed and adapted for cylindrical notched steel fuse. The ligament length is related to the maximum value of the required force (see Fig. 7 in section 3.2.2).

2.2.2.1. Fuse characterization. Tensile tests have been performed of the steel fuse for different ligament lengths in order to determine the order of magnitude of the maximum stress. Fig. 4 shows the ultimate force as a function of the fuse ligament length. In fact, the defined force during interrupted high strain rate can be achieved by varying of ligament length. One can note that the ultimate stress can vary for high strain rates. However, no significant variation has been observed during IDTT.

2.2.3. Strain and strain rate measurements

A contactless technique is used to measure the local deformation using a high speed camera (FASTCAM-APX RS). The strain rate measurements procedure has been presented in a previous paper [7] and consists in analyzing the images of the filmed surface during deformation.

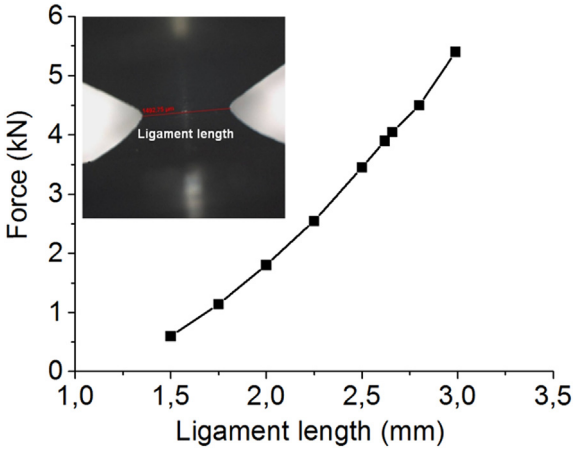

Fig. 4. Required ultimate force as a function of fuse diameter.

3. Experimental results and discussion

3.1. Low and high strain-rate tensile test until rupture

In this section, some of the results described in a previous paper [7] are reported in order to justify the choice of the damage experimental analysis presented in this paper.

Quasi-static tensile curves for different fiber direction (HO-90°, RO and HO-0° samples) and the tensile behavior of RO samples at different strain rate of quasi-static, 1 s^{-1} and 60 s^{-1} are presented in Fig. 5(a) and (b), respectively. The material elastic moduli measured in the first stage of the stress-strain curve show a rough average value of 12, 14.5 and 18.5 GPa for HO-90°, RO and HO-0° A-SMCs respectively. However, the non-linear overall response of the A-SMC is obviously clear. These curves are suitable to damage study of different fiber direction.

Previous paper [7] indicated that a variation of the strain rate from quasi-static to 60 s^{-1}, lead to an increase of the damage threshold starting from a strain rate of about 1 s^{-1} (Fig. 6). One can note, for RO samples, an increase of 50% of the stress damage threshold and 40% of the ultimate stress when varying the stain rate from the quasi-static to 60 s^{-1}. Therefore, three strain rate ranges were selected for qualitative analysis and quantitative evolution of the damage mechanism of RO samples: quasi-static, 4 s^{-1} and 40 s^{-1}.

3.2. Multi-scale qualitative damage investigation

3.2.1. Quasi-static loading-unloading tensile tests

Experimental stress-strain curves for quasi-static loading-unloading tensile test coupled to microstructure observations performed before each reloading stage is shown in Fig. 7.

The same representative observation zone was microscopically analyzed at consecutive increasing value of applied stress level (about 3 × 5 mm^2). This means that the investigation zone is large enough to contain all the heterogeneities of the material microstructure. The local investigation can be assumed as statistically representative of the damage accumulation in the studied material composite. As mentioned, one must bear in mind that the investigation zone is considered as representative of the material microstructure. In addition, microscopic observations have confirmed the

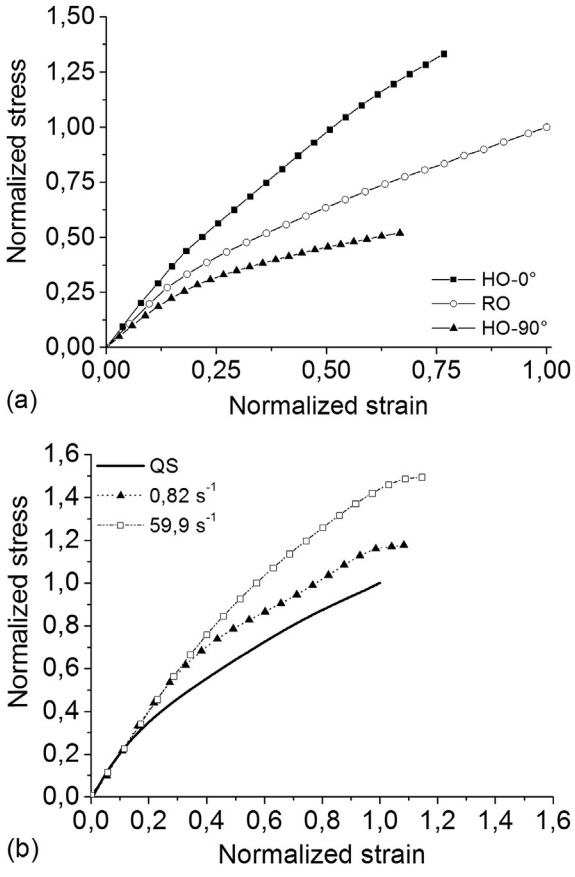

Fig. 5. (a) Normalized quasi-static tensile behavior of A-SMC composites, (b) Normalized tensile curves at different strain rate for RO-A-SMC samples (One can mention that normalized stress (respectively strain) = stress (respectively strain)/ average ultimate stress (respectively strain) obtained for quasi-static tests performed on RO-A-SMC samples used as a reference).

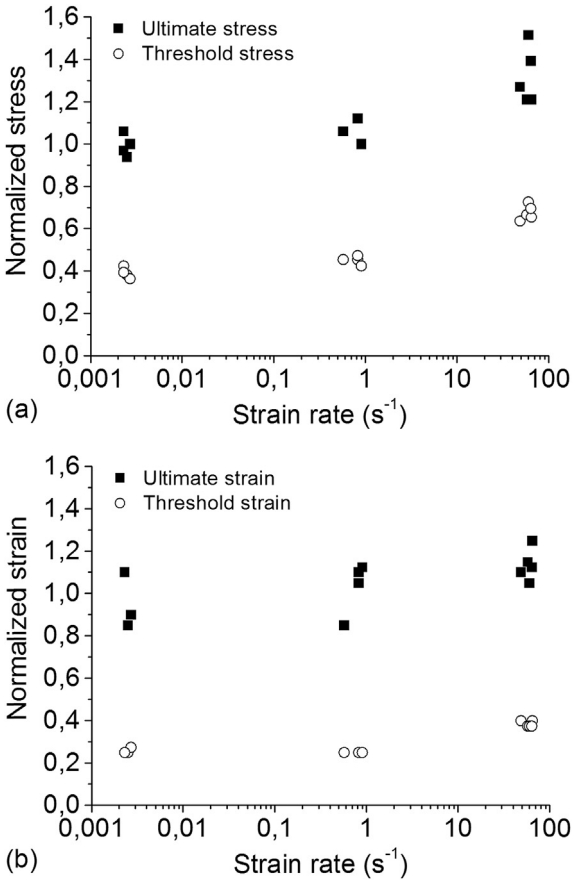

Fig. 6. Influence of strain rate on: (a) Threshold and ultimate stress, (b) Threshold and ultimate strain (Normalized value = current value/average ultimate value obtained for quasi-static tests performed on RO-A-SMC).

fact that this zone is statistically representative for the damage accumulation.

The first observed damage phenomenon corresponds to the debonding of the fiber-matrix interface. For quasi-static loading, this phenomenon is the predominant damage mechanism. It appears very soon (for 0.35% of σ_r) and propagates through the overall volume of the material as a diffuse manner from the more miss-oriented fibers (90°) to the more oriented fibers (30°). It should be noted that interface debonding is largely favored on the fibers bundles oriented perpendicularly to the principal stress direction. Indeed, these fibers are submitted to a high local normal stress at the interface. Inside each bundle of fibers, fiber-matrix interface failure propagates from one fiber to its neighbor. This phenomenon appears several times on each bundle (from 3 to 5 times) and leads to localized transverse cracks which can be observed in the micrograph performed at an applied stress equal to 0.70 σ_r. Finally, when approaching the ultimate stress, the localized propagate through the matrix located between the bundles and induce pseudo-delamination of the bundles just before final failure. One can conclude that for quasi-static loading, the predominant damage mechanism brings about the diffusion of debonding at the fiber-matrix interface beginning at the more miss-oriented fibers (90°) and progressively diffusing on the less miss-oriented fibers (until 30°). Matrix micro-cracking and pseudo-delamination are secondary damage diffusion mechanisms appearing just before failure. However, they cannot be neglected in the description of the failure process.

3.2.2. *Interrupted high velocity tensile test*

Fig. 8 and Fig. 9 show the experimental results of interrupted high strain rate tensile tests performed at 4 s^{-1} and 40 s^{-1}.

The Young's modulus reduction resulting of an increasing applied stress appears clearly and indicates a progressive damage process. At the microscopic scale, one can note debonding at the fiber-matrix interface appearing later than for the quasi-static loading case. This onset of fiber-matrix interface damage increases when increasing strain rate (at 0.45 σ_r and 0.60 σ_r for strain rates of 4 s^{-1} and 40 s^{-1}, respectively). On the other hand, one can observe that when increasing the strain rate, the interface damage appears to be less diffuse. Moreover, one can observe that increasing the strain rate favors the propagation of the transverse micro-cracks into the matrix and pseudo-delamination.

3.2.3. *Pseudo-delamination mechanism*

This phenomenon is called hereafter pseudo-delamination. A previous study [7] showed that, prior to the final failure, local delamination between bundles of fibers always occur independently of the microstructure and strain rate. However, it has been shown that increasing strain rate and orientated fibers favor the pseudo-delamination. Fig. 10 shows a comparison between SEM micrographs performed on RO samples submitted to QS, 4 s^{-1} and 40 s^{-1}. It is obvious to note that in the case of quasi-static loading, pseudo-delamination remains limited while a wide diffuse damage is observed. For higher strain rates, a less diffuse damage and more localized pseudo-delamination is highlighted.

From the overall obtained results of interrupted dynamic tensile tests performed on RO samples, the following conclusions can be

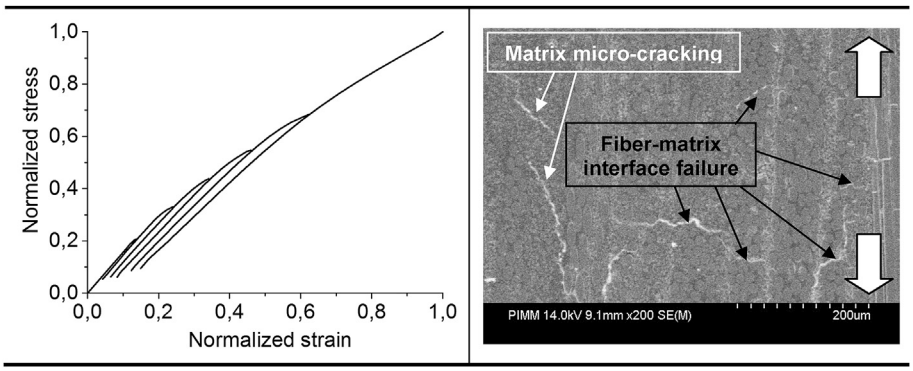

Fig. 7. Damage mechanisms under quasi-static loading unloading tensile test for RO sample (Normalized value = current value/average ultimate stress (σ_r) value obtained for quasi-static tests performed on RO-A-SMC).

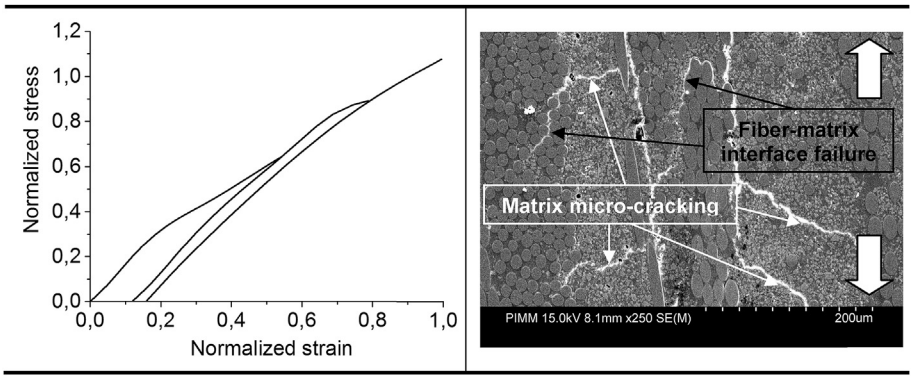

Fig. 8. Damage mechanisms under high strain rate (4 s^{-1}) tensile test for RO sample (Normalized value = current value/average ultimate stress (σ_r) value obtained for quasi-static tests performed on RO-A-SMC).

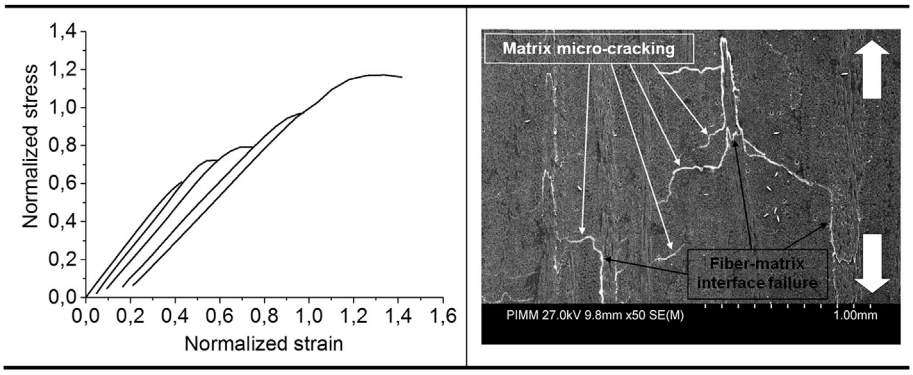

Fig. 9. Damage mechanisms under high strain rate (40 s^{-1}) tensile test for RO sample (Normalized value = current value/average ultimate stress (σ_r) value obtained for quasi-static tests performed on RO-A-SMC).

drawn:

- For both quasi-static and dynamic tests, debonding at the fiber-matrix interface seems to be the predominant diffuse local damage mechanism. Matrix breakage and pseudo-delamination can also appear for higher stress levels.
- When the strain rate increases from quasi-static to 40 s^{-1}, noticeable effect consists of a delayed fiber-matrix damage onset and favored matrix micro-cracking and pseudo-delamination.

3.3. Multi-scale quantitative damage investigation

In this section, a quantitative multi-scale analysis of the damage effect is performed. At the macroscopic scale, the evolution of stiffness reduction is determined for RO, HO-90° and HO-0° samples under quasi-static loading in order to emphasize the influence of fiber orientation. On the other hand, for RO samples, the microscopic damage propagation has been quantitatively related to its consequence on the macroscopic stiffness reduction. This quantitative analysis has been especially focused on the fiber-matrix interface mechanism which has been demonstrated in the previous section to be the predominant damage mechanism for A-SMC. The anisotropic strain rate effect on the fiber-matrix interface decohesion have been also studied through the comparison between damage threshold and kinetic measured for several fiber orientations chosen in RO samples.

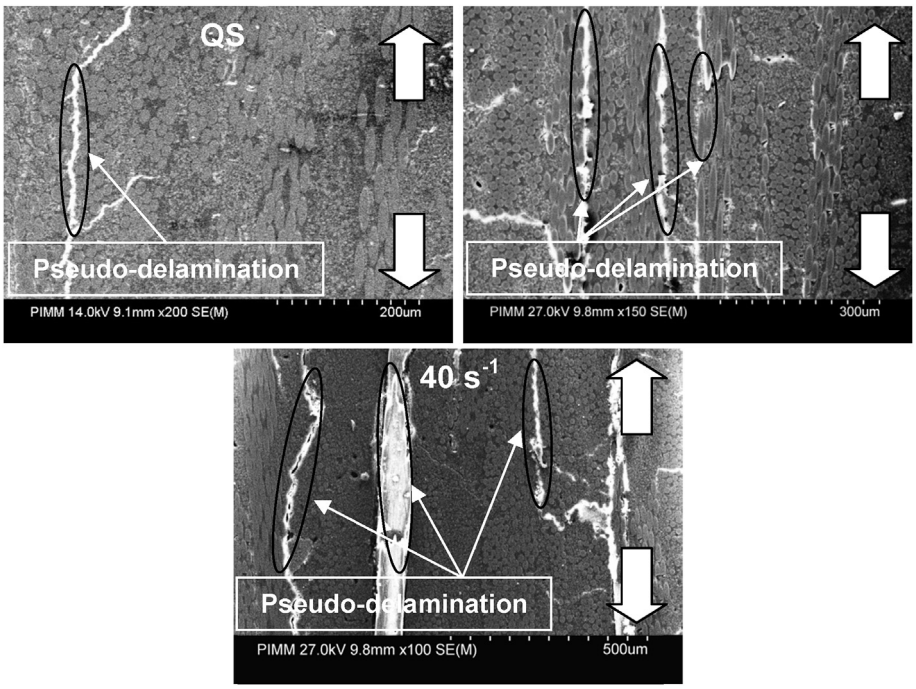

Fig. 10. Pseudo-delamination phenomenon at microscopic scale.

3.3.1. Damage indicators

Stiffness reduction is an appropriate macroscopic damage indicator to define damage development in short fiber reinforced composite materials [4–6]. In the case of tensile loading, one can define a macroscopic damage variable as [37]:

$$D_{macro} = 1 - \frac{E^D}{E^0} \quad (1)$$

E_0 and E_D are the Young's modulus of virgin and damaged material, respectively.

On the other hand, damage accumulation can be characterized in SMC composites by several elementary failure mechanisms such as matrix cracking, fiber breakage, debonding at the fiber-matrix interface and pseudo-delamination [4–6]. At microscopic scale, the stiffness reduction related to evolution of the micro-cracks density, the threshold and the kinetics of the cracks growth were demonstrated [12]. The damage mechanisms at the microscopic scale have been identified by means of SEM micrographs observations achieved upon polished specimen surfaces in the previous section. The evolution of the fiber-matrix damage mechanism can be quantitatively described by a local variable as [4–6]:

$$d_{micro} = \frac{f_d}{f_v} \quad (2)$$

Where f_d is the volume fraction of debonded fibers and f_v is the fiber volume content in the Representative Elementary Volume (REV). d_{micro} can also be defined as the debonded fibers proportion which is measured directly on the SEM micrographs by counting the number of fiber presenting an interface failure inside a bundle. Moreover, in order to study the influence of the fiber orientation on the damage strain rate effect, one can define the parameter $d(\theta)$ as follows [12]:

$$d_\theta = \frac{f_d^\theta}{f_\theta} \quad (3)$$

Where f_d^θ and f_θ are the volume fraction (or number) of the $\theta°$ oriented debonded fibers and the fibers volume content (or total number of fiber contained inside the bundle which is about 250) oriented at $\theta°$, respectively.

3.3.2. Macroscopic scale

3.3.2.1. Quasi-static loading: effect of fiber orientation distribution. Fig. 11 shows the evolution of the macroscopic damage parameter, D, under quasi-static loading-unloading tensile test as a function of applied stress. It should be indicated that, for each microstructure, several tests (at least 3) were performed and the results have been reported in this figure in such a way that at least 15 points have been measured until the very last stages just before failure. One can note that in the case of HO-0° sample, the values of macroscopic damage parameter remains very low. This confirms that interface failure remains limited leading to a relative linear behavior as seen in Fig. 5(a) while pseudo-delamination is favored.

It should be noticed that HO-90° damage kinetic is higher than that of RO. This is essentially due to the fact that more fiber-matrix

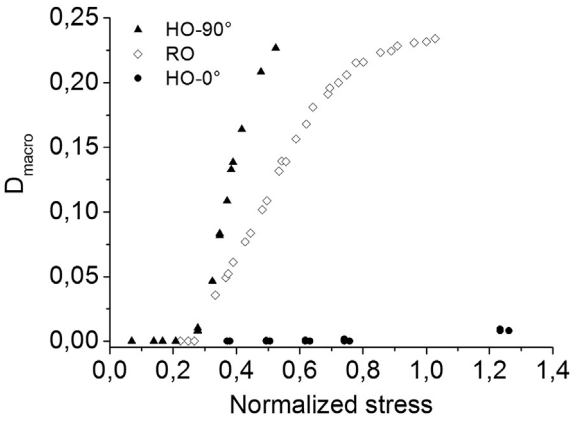

Fig. 11. Macroscopic damage evolution vs. applied stress for RO, HO-0° and HO-90° samples (Normalized value = current value/average ultimate stress (σ_r) value obtained for quasi-static tests performed on RO-A-SMC).

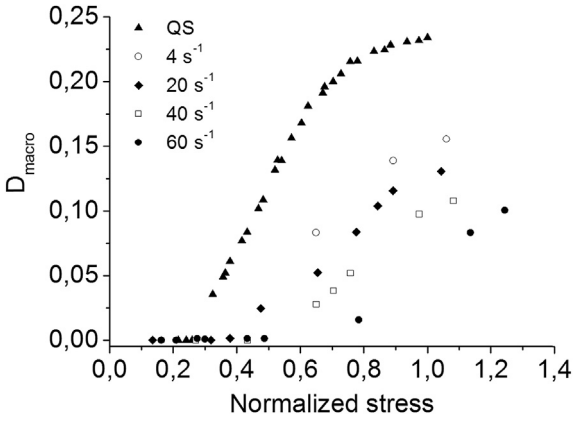

Fig. 12. Macroscopic damage evolution versus applied stress for different strain rates (Normalized value = current value/average ultimate stress (σ_r) value obtained for quasi-static tests performed on RO-A-SMC).

decohesions are involved in the case of HO-90° samples. On the other hand, one can also observe for RO samples an altered slope of the curve (from D = 0.18) indicating the saturation of the fiber-matrix interface failure occurring together with the beginning of the propagation of transverse cracks into the matrix. Finally, the critical value of D at failure for these two microstructures appears to be of the same order of magnitude which indicates a similar state of damage.

3.3.2.2. Effect of strain rate for RO samples. Experimental findings from Interrupted tensile tests (Fig. 12) performed at five different strain rates values varying from quasi-static (QS) to 60 s^{-1} confirm that strain rate increase leads to a delayed macroscopic damage initiation. Indeed, macroscopic loss of stiffness begins at a stress level of 0.30 σ_r in the case quasi-static tensile test whereas for a strain rate of 60 s^{-1}, the first stiffness reduction appears around a stress of about 0.60 σ_r which corresponds to a 100% augmentation of the damage threshold. Moreover, it should be indicated that the damage kinetic is more than three times reduced as the strain rate increases from quasi-static to 60 s^{-1}.

3.3.3. Microscopic scale

In order to understand the physical origin of the damage delay described in the previous sections, experimental investigations at the microscopic scale have been performed in order to identifying the corresponding damage mechanisms, their threshold and kinetic. Fig. 13 illustrates the global microscopic damage parameter (d_{micro}) evolution as a function of the applied stress, previously defined in equation (2), for Randomly Oriented (RO) samples at different strain rates ranging from quasi-static to 40 s^{-1}.

In accordance with the macroscopic damage indicator evolution, the damage threshold analyzed at the microscopic scale is shifted to higher values and the damage growth is reduced when increasing strain rate. These aspects account on the well known visco-damage effect described in previous papers [4–7].

3.3.3.1. Anisotropic strain rate effects on the fiber-matrix interface decohesion. In the following, the influence of fiber orientation on interfacial micro-cracks density evolution is discussed. Different families of fiber orientation bundles were selected at microscopic scale and their damage evolution were investigated at each defined applied stress and strain rates. Note that the 30° family (respectively 45° and 90°) results presented in Fig. 14 correspond to the

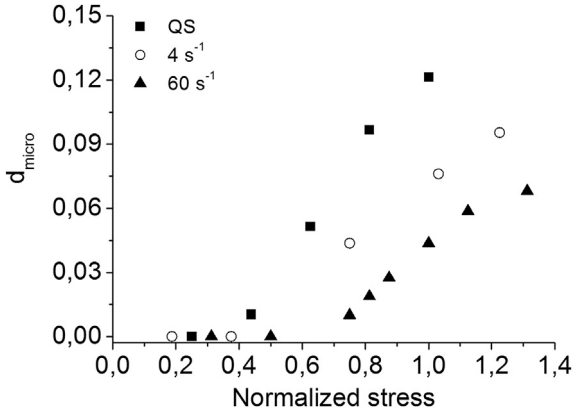

Fig. 13. Global microscopic damage evolution versus strain rate (Normalized value = current value/average ultimate stress (σ_r) value obtained for quasi-static tests performed on RO-A-SMC).

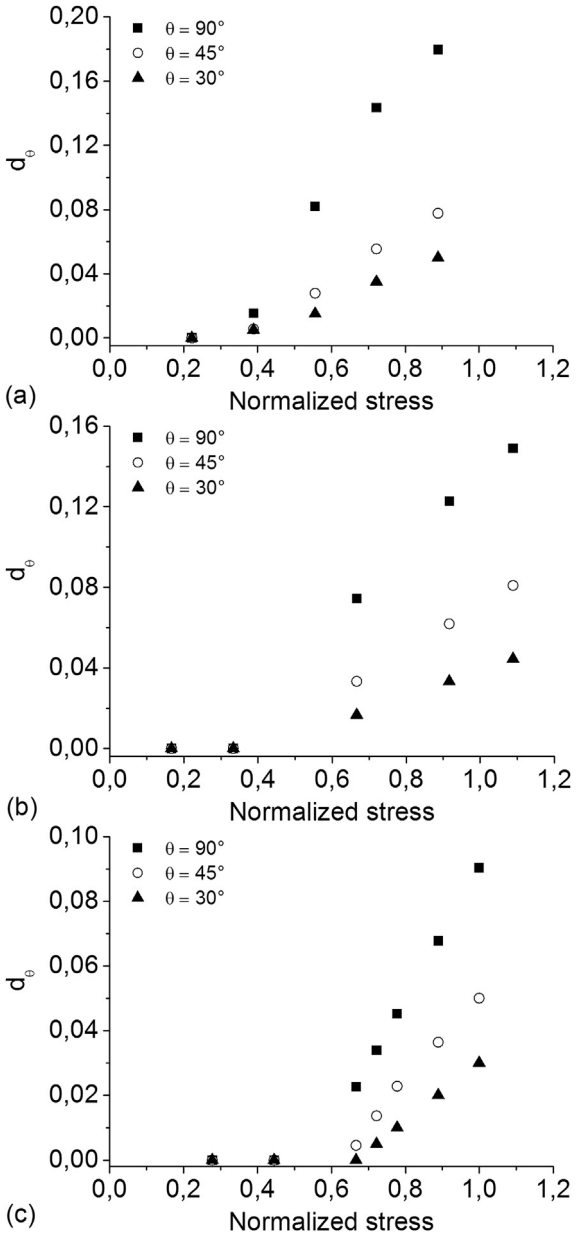

Fig. 14. Evolution of d_θ as a function of applied stress; (a) Quasi-static, (b) Strain rate of 4 s^{-1} and (c) Strain rate of 40 s^{-1} (Normalized value = current value/average ultimate stress (σ_r) value obtained for quasi-static tests performed on RO-A-SMC).

averaged crack density evolution obtained for fiber orientation ranging from 20° to 30° (respectively from 35° to 55° and from 80° to 90°).

Fig. 14 shows the evolution of the fiber-matrix interface local damage indicator for each specified orientation family (d_θ), at strain rates varying from quasi-static to 40 s^{-1}. One can note that independently of applied strain rate, when increasing fiber orientation, damage threshold stress decreases while the damage kinetic increases.

Fiber-matrix decohesion can occur when a combination of a local ultimate normal and shear stress are reached on the interface [4]. 45° oriented fibers are submitted to higher interfacial shear stresses while fiber-matrix interface of 90° oriented fibers fails under a pure normal stress.

In Fig. 15, the evolution of the relative damage threshold and kinetic (determined by the slope of between the density evolution curve) have been plotted as a function of the strain rate for the three defined fiber orientations. A noticeable local anisotropic strain rate effect can be pointed out. Indeed, this figure shows that when the fibers are oriented in the tensile direction, the damage onset due to increasing strain rate is favored while the damage kinetic is altered. These coupled effect of strain rate and orientation on the fiber-matrix interface failure will be discussed in the next section.

4. Viscous nature of the microscopic damage

In this section, the whole experimental results described above are use to propose an interpretation of the origin of the strain rate effect on damage of A-SMC composites. Obviously, interactions between microscopic and macroscopic scale are considered. Moreover, it is shown that to get a thorough understanding of the strain rate dependent damage behavior of A-SMC, it is also necessary to analyze the influence of the deformation mechanisms occurring at the polymer chains scale. Note that the multi-scale analysis proposed hereafter is also suitable for many short fiber reinforced composites.

4.1. Characteristic times and relaxation times

In order to understand the origin of the viscous nature of damage accumulation, one can define a specific characteristic time which is required for a local damage or deformation mechanism to occur. Indeed, this characteristic time is related to the viscoelastic behavior of the matrix or fiber/matrix interface-interphase or, more precisely, to the relaxation time of the constitutive polymers of the latter. These relaxation times are related to the mobility of the molecular chains constituting the matrix and the fiber-matrix interface (on which depend adhesion properties). The relaxation time of a polymer is defined as $\tau = \eta/E$ where η and E are viscosity and modulus, respectively. It is important to remember that these two parameters are intrinsic properties of polymers and are directly related to the adhesion force between molecular chains and their mobility. Then, the relative values of the different relaxation times (matrix and fiber-matrix interface) versus the loading rate determine how the damage will develop over time. Indeed, the value of the imposed strain rate determine a characteristic time of the loading.

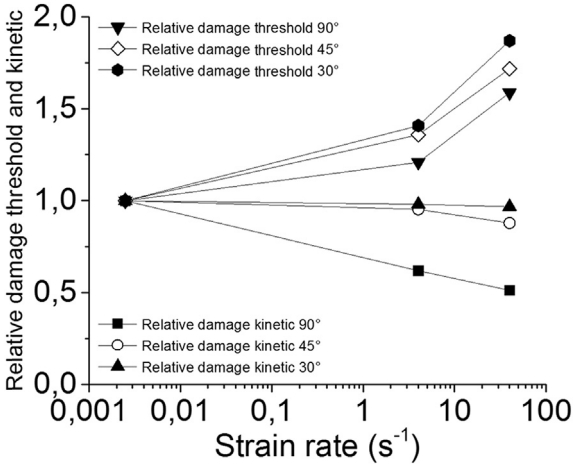

Fig. 15. Evolution of the relative damage threshold and kinetic as a function of the strain rate.

4.2. Origin of the strain rate effect on damage threshold, kinetic and diffusion

Under quasi-static loading, the local damage characteristic times related to the relaxation times of each constitutive polymer (matrix and fiber-matrix interface) are far below that of the imposed loading characteristic time. Under such conditions, damage can easily occur in a diffuse manner. In fact, when damage occurs on one location, sufficient time remains for the material to generate other damage events on other locations. Consequently, damage is systematically delocalized to other sites. This leads to foster diffuse damage. As a result, low threshold and high kinetic of local degradation are observed. When one type of mechanism get saturated, another one can take place as it can be seen on Fig. 12 for quasi-static curve (see the altered slope from D = 0.18 highlighting a saturation of the fiber-matrix decohesion together with the beginning of the micro-cracks propagation from the interfaces to the matrix).

On the other hand, when increasing strain rate, the characteristic loading time can reach the same order of magnitude than the required time for local damage mechanisms to occur (which is related to matrix and/or fiber-matrix interface relaxation times). At these speeds, polymer chains mobility is not sufficient to allow easy local deformation. Thus, local deformation and damage initiation require more energy. On one hand, this leads to shift damage threshold to higher values of applied stress and to reduce the local degradation kinetic on the other hand. Moreover, under rapid loading, relatively high value of local relaxation times (matrix and/or fiber-matrix interface) versus strain rate do not allow the accommodation of the deformation through systematic damage delocalization. Consequently, one can observe an easier concentrate accumulation of micro-cracks which can rapidly lead to more localized failure when increasing strain rate.

4.3. Influence of the deformation mechanisms at the polymer chains scale on fiber-matrix interface damage rate

In the case of A-SMC composites, it is of first importance to understand the origin of the strain rate effect on the fiber-matrix interface failure which appears to be the predominant damage mechanism and the more sensitive to strain rate effect. Indeed, the mobility of the macromolecules near to the surface of the fibers (interface or interphase) may be affected by the rigidity of the fibers. So, one may suppose that the relative values of τ and τ', corresponding to the relaxation times relative to the molecular mobility respectively far and near to the fibers can play an important role in the fiber-matrix interface damage delay and altered damage kinetic observed when increasing strain rate. Actually, because of lower crosslinking density of the matrix around the fibers, because of chemical bonds between matrix and coupling

agent and finally because of the high rigidity of this later (Fig. 16), τ' is generally higher than τ. Thus, when loading rate increases, the mobility of the macromolecules near to the interface is not sufficient to accommodate the deformation. Therefore, the high sensitivity to strain rate observed especially for fiber-matrix interface damage can be interpreted as a consequence of the higher value of τ'.

Moreover, by increasing the temperature, the relaxation time of polymers generally increases. Moreover, under high strain rate loading, self-heating probably occurs at local scale (matrix and fiber-matrix interface). Thus, because of lower crosslinking and higher local self-heating due to strain localization at interface, this effect is more significant for the macromolecules near to the fibers.

4.4. Microstructure and local anisotropic strain rate effect on fiber-matrix interface damage

Moreover, in the previous section (Figs. 14 and 15), it has been shown that, at the fiber-matrix interface scale, the ultimate normal stress is more sensitive to strain rate than the ultimate interface shear stress. Indeed, under high strain rate, normal interface failure requires more energy. In fact, when the stress is normal, at local scale, mostly the bonds between matrix and coupling agent (at the surface of fibers) will be under loading; while for shear stress, both matrix and bonds at interface will be submitted to the local load. It is important to precise that generally the chemical cross-linking bonds are more important than the bonds between matrix and fibers. Consequently, at a given strain rate, normal failure at the fiber-matrix interface is always favored compared to shear mode failure (See damage threshold evolution on Fig. 15). Thus, transversely oriented fibers and high strain rate will contribute to lower kinetic of damage accumulation. This leads to a prompt loss of stiffness in the case of HO-90° samples, a moderate one for RO samples and to a very limited one for HO-0° samples (see Fig. 11).

4.5. Strain rate and fiber orientation effects on pseudo-delamination

On the other hand, it has been shown that high strain rate and oriented fibers favor pseudo-delamination. This mechanism occurring prior to the final failure is always preceded by the propagation of localized micro-cracks coming from neighbor's interfaces decohesion inside the bundles into the matrix until another bundle.

The multi-scale damage analysis showed that the fiber-matrix interface damage is limited for a high oriented microstructure. On the other hand, the strain rate effect appears to be predominantly due to the local damage at the most miss-oriented fiber interface. Thus, in the case of highly oriented microstructure, interfacial damage and strain rate effect on its accumulation remain limited.

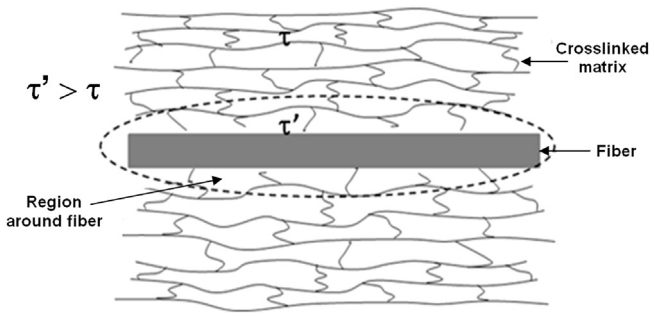

Fig. 16. Polymer structure near and far from the interface and related relaxation times.

Consequently, high strain rate and orientation together contribute to a rapid saturation of the fiber-matrix interface damage accumulation and a prompt propagation of the micro-cracks from the interface into the matrix between the bundles of fibers. Consequently, especially for HO-0° samples submitted to high applied strain rate, fiber-matrix interface damage accumulation is altered while damage onset increases and pseudo-delamination is favored.

5. Conclusion

In automotive industry, a new formulation of high glass fiber content SMC is used for structural parts submitted to crash events. These Advanced Sheet Molding Compound composites must be able to absorb sufficient energy during a crash event in order to assure safety of the passengers. To this aim, the capability of the constitutive material to develop a non linear behavior through damage accumulation is a central purpose of study.

In this paper, a multi-scale experimental analysis of the damage behavior of an A-SMC composite has been performed. A specific device has been developed in order to be able to characterize at both microscopic and macroscopic scales, the evolution of the damage accumulation at quasi-static and high applied strain rates. Interrupted tensile test technique has been used in order to determine, for several microstructure configurations (RO, HO-90° and HO-0°), qualitatively and quantitatively the damage effect during high speed tensile loading ranging from quasi-static to 60 s^{-1}. Quantitatively, the SEM analysis coupled to IDTT led to the following conclusions:

- Fiber-matrix interface failure appears to be the predominant mechanism,
- Matrix micro-cracking coming from the propagation of the interface micro-cracks into the matrix located between the bundles of fibers is favored at high strain rates,
- Pseudo-delamination between the bundles of fibers coupled with the matrix micro-cracking described above always occurs prior to the final failure and is favored by high strain rate and orientation of the fibers in the loading direction.

Microscopic and macroscopic damage indicators have been proposed and well correlated each other for various microstructures and strain rates. The evolution of the fiber-matrix interface cracks density has been measured as a function of applied strain rate ranging from quasi-static to 40 s^{-1} for Randomly Oriented samples. An increase of the strain rate leads to an augmentation of the damage threshold together with a diminution of the damage accumulation kinetic and a less diffuse spatial distribution of the micro-cracks. Moreover, in order to emphasize the effect of the fiber orientation, an analysis of the interface damage accumulation have been performed on 30°, 45° and 90° oriented bundles of fibers statistically chosen on RO samples micrographs. It has been shown that the strain rate effect on microscopic damage accumulation is mostly due to the specific sensitivity of the ultimate normal stress at the interface. The latter leads to a more sensitive strain rate effect for RO and HO-90° A-SMC samples observed at the macroscopic scale.

Finally, the origin of the viscous nature of the microscopic damage has been discussed and correlated to the macroscopic damage thresholds delays and damage kinetics as a function of the microstructure and the strain rate. Specific considerations at the polymer chains scale allow proposing a consistent interpretation of the origin and the nature of strain rate effect described in this study.

The multi-scale experimental analysis performed in this study led also to a deep understanding of the origin of the anisotropic elastic visco-damageable behavior of A-SMC composites and

constitutes a rich database for the development of further micro-mechanical modeling for A-SMC automotive structures submitted to crash events [27].

References

[1] Sun L, Gibson RF, Gordaninejad F, Suhr J. Energy absorption capability of nanocomposites: a review. Compos Sci Technol 2009;69(14):2392–409.
[2] Huang H, Talreja R. Numerical simulation of matrix micro-cracking in short fiber reinforced polymer composites: initiation and propagation. Compos Sci Technol 2006;66(15):2743–57.
[3] Kun F, Zapperi S, Herrmann HJ. Damage in fiber bundle models. Eur Phys J B - Condens Matter Complex Syst 2000;17(2):269–79.
[4] Fitoussi J, Bocquet M, Meraghni F. Effect of the matrix behavior on the damage of ethylene-propylene glass fiber reinforced composite subjected to high strain rate tension. Compos Part B Eng 2013;45(1):1181–91.
[5] Fitoussi J, Meraghni F, Jendli Z, Hug G, Baptiste D. Experimental methodology for high strain-rates tensile behaviour analysis of polymer matrix composites. Compos Sci Technol 2005;65(14):2174–88.
[6] Fitoussi J, Guo G, Baptiste D. A statistical micromechanical model of anisotropic damage for S.M.C. composites. Compos Sci Technol 1998;58(5):759–63.
[7] Shirinbayan M, Fitoussi J, Meraghni F, Surowiec B, Bocquet M, Tcharkhtchi A. High strain rate visco-damageable behavior of Advanced Sheet Molding Compound (A-SMC) under tension. Compos Part B Eng 2015;3670(82):30–41.
[8] Farley GL. Energy absorption in composite structures. J Compos Mater 1983;17:267–79.
[9] Jacob GC, Fellers JF, Simunovic S, Starbuck JM. Energy absorption in polymer composites for automotive crashworthiness. J Compos Mater 2002;36(7):813–50.
[10] Lee HK, Simunovic S. A damage mechanics model of crack-weakened, chopped fiber composites under impact loading. Compos Part B Eng 2002;33(1):25–34.
[11] Okoli OI. The effects of strain rate and failure modes on the failure energy of fibre reinforced composites. Compos Struct 2001;54(2):299–303.
[12] Jendli Z, Fitoussi J, Meraghni F, Baptiste D. Anisotropic strain rate effects on the fibre-matrix interface decohesion in sheet moulding compound composites. Compos Sci Technol 2005;65(3–4):387–93.
[13] Baste S, Gérard A. Evaluation of anisotropic damage in composite materials. Eval anisotropic damage Compos Mater 1994;3:2025–32.
[14] Achour N, Chatzigeorgiou G, Meraghni F, Chemisky Y, Fitoussi J. Implicit implementation and consistent tangent modulus of a viscoplastic model for polymers. Int J Mech Sci 2015;103:297–305.
[15] Kästner M, Obst M, Brummund J, Thielsch K, Ulbricht V. Inelastic material behavior of polymers-experimental characterization, formulation and implementation of a material model. Mech Mater 2012;52:40–57.
[16] Kim J, Muliana A. A time-integration method for the viscoelastic-viscoplastic analyses of polymers and finite element implementation. Int J Numer Methods Eng 2009;79(5):550–75.
[17] Kweon S, Benzerga A. Finite element implementation of a macromolecular viscoplastic polymer model. Int J Numer Methods Eng 2013;94(10):895–919.
[18] Patel BP, Gupta AK. An investigation on nonlocal continuum damage models for composite laminated panels. Compos Part B Eng 2014;60:485–94.
[19] Bere P, Berce P, Nemes O. Phenomenological fracture model for biaxial fibre reinforced composites. Compos Part B Eng 2012;43(5):2237–43.
[20] Tanaka K, Mori T. The hardening of crystals by non-deforming particles and fibres. Acta Metall 1970;18(8):931–41.
[21] Morozov EV, Morozov KE, Selvarajalu V. Damage model development for SMC composites. Compos Struct 2003;62:373–8.
[22] Lacy TE, MacDowell DL, Talreja R. Gradient concepts for evolution of damage. Mech Mater 1999;31(12):831–60.
[23] Shao JF, Rudnicki JW. A microcrack-based continuous damage model for brittle geomaterials. Mech Mater 2000;32:607–19.
[24] Nedjar B. Elastoplastic-damage modelling including the gradient of damage: formulation and computational aspects. Int J Solids Struct 2001;38(30–31):5421–51.
[25] Askes H, Sluys LJ. Explicit and implicit gradient series in damage mechanics. Eur J Mech Solids 2002;21(3):379–90.
[26] Shao JF, Rudnicki JW. A microcrack-based continuous damage model for brittle geomaterials. Mech Mater 2000;32:607–19.
[27] Jendli Z, Meraghni F, Fitoussi J, Baptiste D. Multi-scales modeling of dynamic behaviour for discontinuous fibre SMC composites. Compos Sci Technol 2009;69(1):97–103.
[28] Jendli Z, Meraghni F, Fitoussi J, Baptiste D. Micromechanical analysis of strain rate effect on damage evolution in sheet molding compound composites. Compos Part A Appl Sci Manuf 2004;35(7–8):779–85.
[29] Arif MF, Saintier N, Meraghni F, Fitoussi J, Chemisky Y, Robert G. Multiscale fatigue damage characterization in short glass fiber reinforced polyamide-6. Compos Part B Eng 2014;61:55–65.
[30] Aymerich F, Meili S. Damage assessment in an SMC composite by means of ultrasonic techniques. NDT.NET 1999;4(3).
[31] Le TH, Dumont PJJ, Orgéas L, Favier D, Salvo L, Boller E. X-ray phase contrast microtomography for the analysis of the fibrous microstructure of SMC composites. Compos Part A Appl Sci Manuf 2008;39(1):91–103.
[32] Feuillade V, Bergeret A, Quantin J, Crespy A. Characterisation of glass fibres used in automotive industry for SMC body panels. Compos Part A Appl Sci Manuf 2006;37(10):1536–44.
[33] Bussiba A, Kupiec M, Ifergane S, Piat R, Böhlke T. Damage evolution and fracture events sequence in various composites by acoustic emission technique. Compos Sci Technol 2008;68(5):1144–55.
[34] Derrien K, Baptiste D, Guedra-Degeorges D, Foulquier J. Multiscale modeling of the damaged plastic behavior and failure of Al/SiCp composites. Int J Plasticity 1999;15(6):667–85.
[35] Meraghni F, Benzeggagh ML. Micromechanical modelling of matrix degradation in randomly oriented discontinuous-fibre composites. Compos Sci Technol 1995;55(2):171–86.
[36] Lataillade JL, Delaet M, Collombet F, Wolff C. Effects of the intralaminar shear loading rate on the damage of multi-ply composites. Int J Impact Eng 1996;18(6):679–99.
[37] Krajcinovic D, Mastilovic S. Some fundamental issues of damage mechanics. Mech Mater 1995;21(3):217–30.

Article N°3:

Shirinbayan M, Fitoussi J, Meraghni F, Surowiec B, Laribi M, Tcharkhtchi A. Coupled effect of loading frequency and amplitude on the fatigue behavior of advanced sheet molding compound (A-SMC). Journal of Reinforced Plastics and Composites. 2017; 36(4): 271-82.

Original Article

JOURNAL OF REINFORCED PLASTICS & COMPOSITES

Journal of Reinforced Plastics and Composites
2017, Vol. 36(4) 271–282

DOI: 10.1177/0731684416682853
jrp.sagepub.com

SAGE

Coupled effect of loading frequency and amplitude on the fatigue behavior of advanced sheet molding compound (A-SMC)

M Shirinbayan[1], J Fitoussi[1], F Meraghni[2], B Surowiec[3], M Laribi[1] and A Tcharkhtchi[1]

Abstract

This paper presents the experimental results of tension-tension stress-controlled fatigue tests performed on advanced sheet molding compound (A-SMC). It aims at analyzing the effect of fiber orientation, loading amplitude, and frequency on the fatigue response and the related temperature evolution due to the self-heating phenomenon. Two types of A-SMC have been analyzed: randomly oriented (RO) and highly oriented (HO). The coupled effect of the loading amplitude and the frequency has been studied. It has been shown that the couple frequency-amplitude affects the nature of the fatigue overall response which can be governed by the damage mechanisms accumulation (mechanical fatigue) and/or by the self-heating (induced thermal fatigue). For fatigue loading at 100 Hz, self-heating has been observed and yielded to a temperature rise up to 70°C. The latter causes a decrease of the storage modulus related to the β-transition of the vinylester. It has been demonstrated that the self-heating produced a material softening and decreased the fatigue life. SEM observations revealed that the samples tested at 100 Hz, exhibit smooth debonding surfaces due to the induced thermal softening of the matrix whereas more brittle fracture of the matrix surrounding fibers is observed during the fatigue tests achieved at 10 Hz.

Keywords

Advanced SMC composite, fatigue strength, damage, self-heating, induced thermal fatigue, experimental analysis

Introduction

Sheet molding compounds (SMCs) are commonly used in automotive industry for light-weight structural component with an improvement of the thermomechanical performance to cost ratio. These composites are ideal for large structural automotive components owing to their high strength-to-weight ratio.[1–3] Recently, a new advanced SMC (A-SMC) composite has been developed by Plastic-Omnium as innovative solution for automotive components such as the new generation of tailgate or the new automotive front floor module. A-SMC combines short glass fiber/bundles and vinylester thermoset which exhibit many desirable features, including mechanical properties, excellent chemical resistance and tensile strength, and cost competitiveness. A-SMCs are high strength glass reinforced thermoset molding materials processed by thermo-compression.[4–6]

Composite design in the case of fatigue loading is usually characterized by a S–N curve, by which one may obtain the Wöhler curve.[7] This later can be presented as a curve giving the value of a cyclic stress amplitude, σ_{max} versus the number of cycles to failure N_r. Fiber orientations and the related process induced microstructure,[8] nature of matrix, applied stresses, temperature, frequency, and induced self-heating

[1]Arts et Métiers ParisTech, PIMM—UMR CNRS 8006, Paris, France
[2]Arts et Métiers ParisTech, LEM3—UMR CNRS 7239, Metz, France
[3]PLASTIC Omnium Auto Exterior, Sigmatech, Sainte Julie, France

Corresponding author:
M Shirinbayan, Arts et Métiers ParisTech, PIMM—UMR CNRS 8006, 151 Boulevard de l'Hôpital, 75013 Paris, France.
Email: mohammadali.shirinbayan@ensam.eu

phenomenon or environmental effects are appropriated aspects that have to be taken into account to reliably estimate the fatigue life of short fiber reinforced polymer composites.[7–9]

Fleckenstein et al.[10] performed experimental investigation on SMC samples with different preferred fiber orientations. As expected, experimental results showed that the specimens with predominantly 0° fiber alignment have the highest fatigue strength.

Wang et al.[11] have shown that increasing the applied fatigue stress σ_{max} leads to a higher stiffness reduction rate and shorter fatigue life.

To study the cyclic loading frequency (f) effect, Handa et al.[12] performed a study of fatigue behavior on glass fiber-reinforced polyamide at different frequencies ranging from 5 to 50 Hz and showed that increasing the frequency decreases the fatigue life and strength. Different authors[13–14] studied the effect of frequency during the fatigue test of nylon 66 reinforced with 30% short glass fibers and concluded that, for the frequency higher than 2 Hz, the rate of crack initiation and growth increase, leading to the decrease of life time. The self-heating is related directly to the viscoelastic nature of matrix and to the dissipated energy during fatigue tests. Indeed because of self-heating the matrix may passes from glassy state (high modulus) to rubbery state (low modulus).

Especially at high frequencies, when temperature rise due to self-heating is significant. This aspect has been noticed notably for short fiber-reinforced thermoplastic composites.[13–15] For instance, for polyamide 66 reinforced with short glass fiber, several works have shown that for low frequencies, there was only an effect of the mechanical loading, whereas for high frequencies a coupling between mechanical and thermal effects were observed and evidenced.[15] SEM micrographs showed that the matrix remained ductile locally around fibers before debonding.[13–15] From a macroscopic point of view, evolution of the slope of the hysteresis loop is a common indicator of damage that occurs in reinforced thermoplastic composites.[15,16]

One can notice that the coupled effect of loading frequency and amplitude on the fatigue has never been addressed for SMC composites.

For random short glass fiber-reinforced polymer composite subjected to cyclic loading, it has been shown that dynamic fatigue behavior brings about a diffuse crack initiation and growth which leads consequently to a stiffness reduction.[17] Based on experimental results, a damage parameter[17,18] was introduced to quantify the fatigue damage as

$$D = 1 - E/E_0$$

where E_0 is the initial Young's modulus and E is the residual Young's modulus of the damage material. Normalized stiffness reduction as a function of inelastic density of energy was proposed and described by Launay et al.[19] for short glass fiber-reinforced polyamide under cyclic loading. This energy was defined as the difference between the total mechanical energy and the elastic strain energy. Cyclic stiffness softening has been successfully correlated to the inelastic energy density, and may stand for material progressive degradation. Damage development can be characterized by a more or less stabilized temperature and Young's modulus. Moreover, fatigue life prediction requires thorough understanding of the damage mechanisms.[20–24]

In the present paper, an experimental study is carried-out to investigate the influence of fiber orientation as well as the coupled effect of the cyclic loading amplitude and frequency on the fatigue behavior and the induced self-heating of A-SMC.

The organization of this work is as follows: Material description and methods section is devoted to a description of the main physical characteristics and the process-induced microstructure of A-SMC composite as well as the developed experimental procedure for fatigue testing at several frequencies. In Experimental results and discussion section, experimental results obtained under quasi-static and fatigue loading are presented and discussed in terms of coupled effect of the fatigue loading amplitude and the frequency. The nature of the fatigue overall response that can be mechanical fatigue (MF) and/or induced thermal fatigue (ITF) and analyzed in terms of SEM observations and are related to the loading conditions governing the self-heating phenomenon. Concluding remarks are given in Conclusion section to summarize the main experimental findings to highlight the coupled effect of loading frequency and amplitude on the fatigue and its relation with the induced self-heating occurring.

Material description and methods

Advanced sheet molding compound composite (A-SMC)

A-SMC consists of a vinylester matrix with a high content of glass fibers (50% in mass corresponding to 38.5% in volume) as given in Table 1.

Raw material is nonconsolidated, flexible, and stored on rolls. The sheets are cut from these rolls with adapted size depending on the mold. Then, several layers should be stacked into the mold. The material consolidation is performed by thermo-compression process (150°C at 60–120 kg/cm^2). Under these conditions the viscosity of the vinylester decreases and allows fulfill the whole cavity of the mold; this is the first step

Table 1. A-SMC composition and the constituents weight content.

Product nature	Composition (content in mass percent)
Glass fibers	50%
Vinyl-ester resin	24%
Filler	24%
Other products	2%

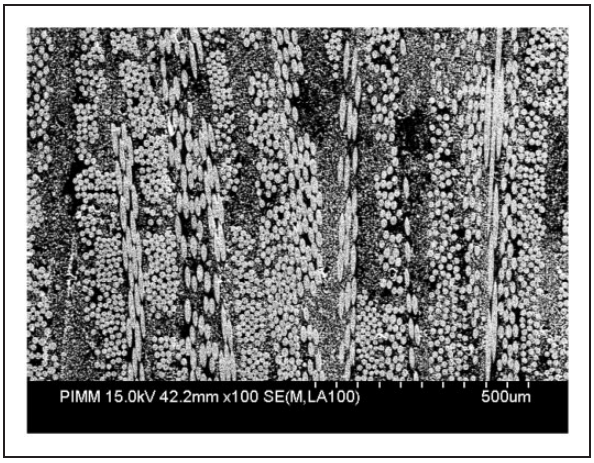

Figure 1. Typical microstructure of A-SMC observed by mean of a SEM: randomly oriented bundle of fibers.

of the manufacturing process. Then, the material stays in position without reticulation for a short duration; this is the second step. The third step of the process consists of a reticulation time of the thermoset polymer during the consolidation phase. The duration of the whole process for one part is less than 2 min which is mandatory for automotive applications due to the required high production rate.

Figure 1 shows the typical A-SMC microstructure observed on a polished surface. The bundle of fibers can be oriented due to the polymer flow during compression. The fibers are presented as bundles of constant length ($L = 25$ mm). Each bundle contains approximately 250 glass fibers of about 15 μm diameter. Microscopic observations, using scanning electronic microscope (HITACHI 4800 SEM), have been performed in order to investigate qualitatively the material microstructure and especially the fibers orientation.

Two types of A-SMC plates have been provided by Plastic-Omnium Auto Exterior: randomly oriented (RO) and highly oriented (HO) plates. HO plates have been obtained by an initial charge putting only in the left part of a rectangular mold ($30 \times 40\,cm^2$) before compression leading to an oriented material flow. RO plates were obtained without significant material flow by completely filling the mold. The fiber distribution in the RO and HO plates as a function of the cutting orientation has been characterized and presented in a previous work.[6] It is worth noting that for both studied configurations (RO and HO), it can be assumed that, most of the fibers remain on the plane of the plate. Nevertheless, for the highly oriented (HO) plates, due to the polymer flow, fibers tend to be oriented parallel to the mold flow direction (MFD) before compression.

Methods and experimental procedure

DMTA characterization. Besides the SEM microscopic observations thermo-mechanical (DMTA) flexural tests have been achieved to measure the main transitions temperatures on RO samples using DMA Q800 instrument from TA Company. The flexural test has been realized at following condition: temperature range varying from 0°C to 250°C, temperature rate of 2°C/min, and a frequency of 1 Hz.

Fatigue tests. Tension-tension stress-controlled fatigue tests have been performed at different applied maximum stress (σ_{max}) on a MTS 830 hydraulic fatigue machine. The minimum applied stress (σ_{min}) is always chosen to be equal to 10% of the maximum applied stress. The chosen stress-ratio is thus ($R_\sigma = 0.1$) and the mean stress-level is equal to 0.55 σ_{max}.

In this paper, the results of experiments performed at different frequencies, namely 10, 30, 50, and 100 Hz are presented. In order to measure precisely the stiffness reduction due to the first loading stage (initial damage), each fatigue test is preceded by a quasi-static tensile loading-unloading-elastic reloading stage. During cyclic loading, the temperature rise, due to the material self-heating, has been measured on the surface of the specimen using an infrared camera (Rayngers-MX4). The damage evolution has been estimated through the measurement of the Young's modulus evolution.

In a previous study,[6] a recursive optimization procedure results in the determination of the specimen's optimal geometrical parameters adopted for high speed tensile tests. To this aim, a FE simulation assuming that the specimen behaves like an anisotropic solid, is performed and leads to the optimized geometry showed in Figure 2 which allows reducing the perturbations due to stress waves effect, in order to generate homogeneous stress and strain field and a constant high strain rate.

In this work, the experimental fatigue tests have been performed at room temperature on the same sample geometry. Fatigue experiments have been

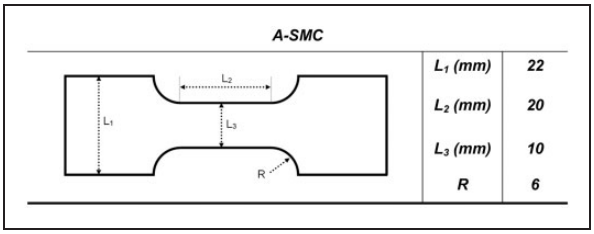

Figure 2. Optimized specimen geometry and its related dimensions.

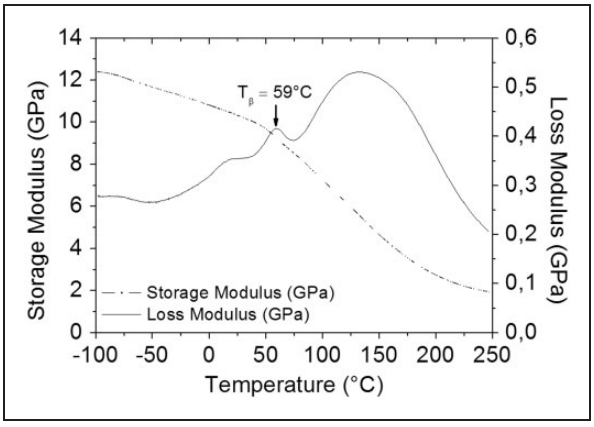

Figure 3. DMTA scan showing the types of transitions for RO-A-SMC sample.

achieved at different load directions, applied maximum stress (ranging from 35% to 80% of the material UTS noted hereafter as σ_r) and frequencies (ranging from 10 to 100 Hz).

Experimental results and discussion

Thermo-mechanical properties

To measure the main transition temperatures due to molecular mobility as a function of the temperature, DMTA tests have been performed on RO samples. Figure 3 shows the evolution of the storage and loss moduli versus temperature.

As it can be noticed, A-SMCs present at least three distinct transition zones in the temperature range of 0°C–250°C. The first zone, extended between 70°C and 200°C, is indeed the α-transition, related to the glass transition of A-SMC. The value of T_α is nearly 130°C. This extent of the glass transition region can be explained by the effect of

- The chemical modification of the matrix during DMTA test. In fact, when the cross-linking of the polymer matrix, namely vinylester resin is not completed, the post cross-linking during DMTA test prevents sudden decrease of the modulus in the glass transition region.
- The presence of glass fibers which may prevent the sudden drop of the elastic modulus in the glass transition region.

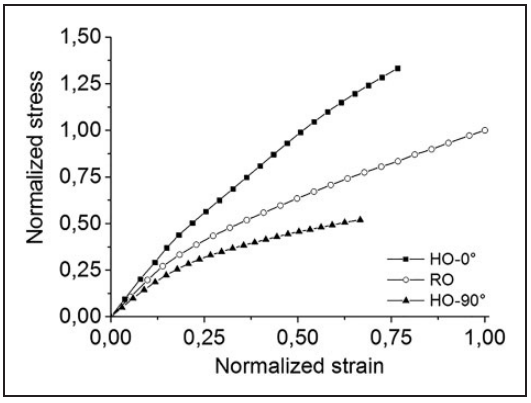

Figure 4. Normalized quasi-static tensile behavior of A-SMC composite at room temperature. One can mention that normalized stress (respectively strain) = stress (respectively strain)/ultimate stress (respectively strain) obtained for tests performed on RO-A-SMC serving as a reference.

The second transition corresponds to the β-transition with a T_β almost 59°C. T_β is known as a brittle-ductile transition for amorphous polymers and it is generally related to the mobility of the small segments of molecular chains.

The third transition corresponds to γ-transition with a T_γ equal to 18°C. The origin of this transition has not been clearly identified. DMTA results will be very helpful to analyze the induced self-heating phenomenon and to relate it to the measured temperature rise during fatigue test at different amplitude and frequencies.

Quasi-static tensile behavior

Effect of fiber orientation. Figure 4 shows the results of quasi static tensile tests on HO-0°, RO, and HO-90° samples at room temperature. As it can be seen, the value of Young's modulus of HO-0° is about 18.5 GPa which is higher than those of RO (14.5 GPa) and HO-90° (12.5 GPa) samples. The failure stress also highly depends on the fibers orientation. Failure stress of HO-0° is about three times higher than that of HO-90° samples.

Effect of temperature. In order to show the effect of temperature on the mechanical properties of randomly oriented and highly oriented samples, tensile tests have

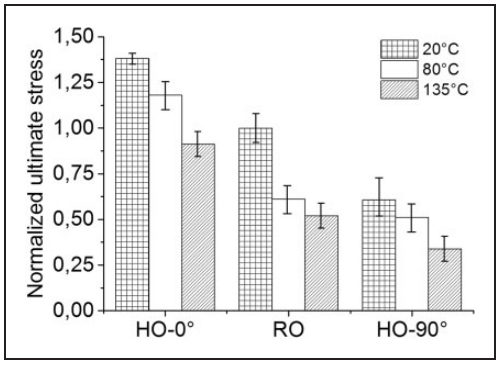

Figure 5. Normalized ultimate stress of oriented and nonoriented samples at 20°C, 80°C, and 135°C; (normalized value = current value/average ultimate stress (σ_r) value obtained for tests performed at 20°C on RO-A-SMC).

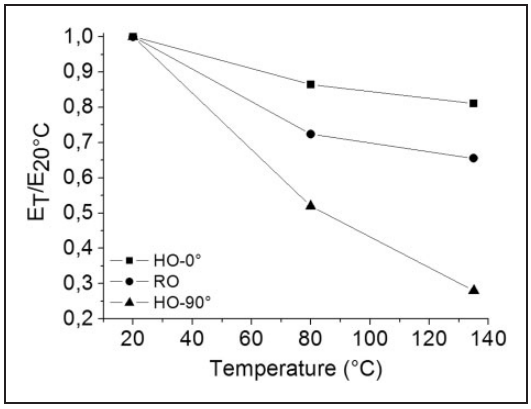

Figure 6. Evolutions of the relative Young's modulus of HO-0°, RO, and HO-90° samples at different temperatures.

been realized at different temperatures ranging from 20°C to 135°C.

The analysis of the results shown in Figures 5 and 6 leads to the following remarks:

- For HO-0° oriented samples, the effect of temperature on Young's modulus is relatively limited due to the presence of oriented fibers parallel to the loading direction. Young's modulus decreases from 18.7 to 15 GPa as the temperature increases from 20°C to 135°C (Figure 6). Concerning the failure stress, this effect has not been clearly established because of slipping of the sample during the tensile tests performed at 135°C (Figure 5).
- For HO-90° oriented samples, the effect of temperature on Young's modulus as well as on failure stress and failure strain is significant. A variation of the temperature from 20°C to 135°C, leads to an abrupt decrease of the Young's modulus from 12.5 to 3.33 GPa while failure stress decreases by 40% and failure strain increases by 60%. It is important to notice that when the sample is loaded at 135°C, the matrix is at rubbery state. This variation indicates also that the role of vinylester matrix in HO-90° specimens is very important. At macroscopic failure appearance (Figure 7) a pseudo-delamination between the bundles of fibers seems to be favored.

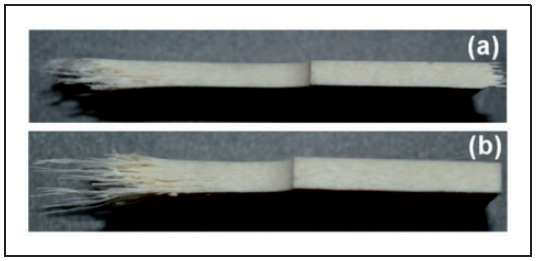

Figure 7. Macroscopic failure appearance of HO-90° sample loaded at (a) 20°C and (b) 135°C.

As expected for RO samples, the influence of temperature on stiffness and failure properties is midway between the two other orientations (HO-0° and HO-90°). Young's modulus decreases from 14.5 to 9.5 GPa when the temperature increases from 20°C to 135°C.

Figure 6 shows the relative Young's modulus defined by the ratio Young's modulus/Young's modulus at room temperature for HO-0°, RO, and HO-90°. As expected, it decreases when the temperature is increased. However, this decrease for HO-0° sample is less important than those of RO and HO-90° samples. One can see that, in the case of HO-90° samples, the damage indicator (D) is hence strongly related to the effect of temperature.

Fatigue behavior analysis

Effect of the fiber orientation distribution. Figure 8 shows the normalized Wöhler curves obtained in tension-tension stress-controlled fatigue tests at a frequency of 10 Hz for HO-0°, RO, and HO-90° A-SMC samples. It can be noticed that in the case of RO samples for an applied stress equal to 0.44 $\sigma_{r(RO)}$, the fatigue life is about 50,000 cycles whereas the fatigue life is about 10^6 cycles for an applied stress of 0.39 $\sigma_{r(RO)}$. So, a variation of 12% leads to a fatigue life about 20 times higher.

For RO-A-SMC samples, fatigue test performed at 34% of its ultimate stress, no failure is observed until 10^7 cycles. For lower values, the specimen does not fail until 10^7 cycles. It is obvious to note that for an applied stress corresponding to the endurance limit value for HO-0° sample, RO, and HO-90° composites fail after less than 500 cycles. Thus, it can be establish that the

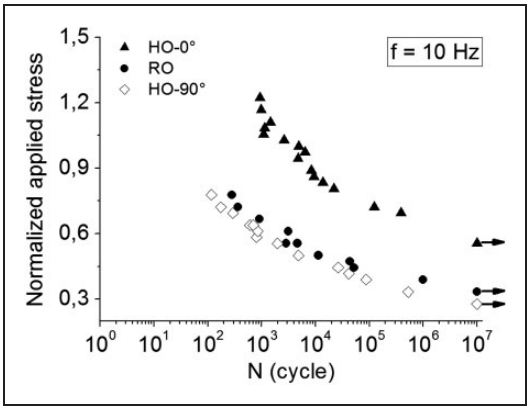

Figure 8. Normalized Wöhler curves for HO-0°, RO, and HO-90° samples at 10 Hz.
Normalized value = current value/average ultimate stress value (σ_r) obtained for tests performed on RO-A-SMC.

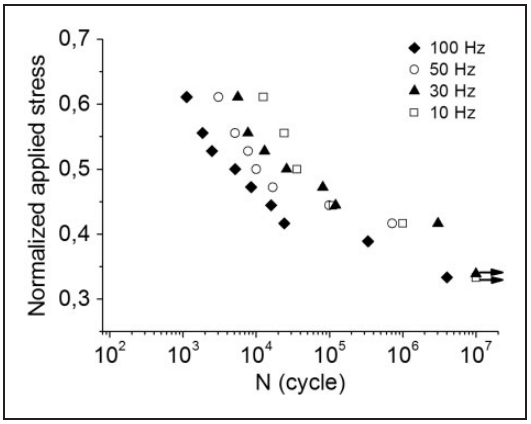

Figure 9. Normalized Wöhler curves at different frequencies for RO samples.
Normalized value = current value/average ultimate stress value (σ_r) obtained for tests performed on RO-A-SMC.

fatigue life is strongly influenced by the distribution of fiber orientation. However, Figure 8 also shows that the fatigue life for HO-90° samples is not significantly affected, compared to that of the RO samples. It can be established thus that for A-SMC composite, the fatigue design can be efficiently optimized through fiber orientation without critical reduction of material properties in the transverse direction.

Regarding to RO and HO samples at 10 Hz, it can be noted that Wöhler curves show a bilinear form defining two different zones related to the high and low loading amplitude fatigue behavior. For RO and HO-90° orientations high loading amplitude zone corresponds to fatigue life less than 10^4 cycles for loading amplitude up to 0.47 $\sigma_{r(RO)}$, while for HO-0° samples, this upper zone corresponds to fatigue life less than 30,000 cycles for stress values up to 0.75 $\sigma_{r(RO)}$. Under these values, the curves start deviating and tend to an asymptotic evolution defining a limit for which no failure is observed until 10^7 cycles as described above.

Effect of frequency. Normalized Wöhler curves obtained from fatigue tests for the frequencies of 10, 30, 50, and 100 Hz in the case of RO samples are shown in Figure 9. As it can be seen, there is small difference between the curves of 10, 30, and 50 Hz at low amplitude while at high loading amplitude, increasing frequency leads to Wöhler curves shifted to lower fatigue life.

For example, for an applied stress equal to 0.55 $\sigma_{r(RO)}$, a variation of the frequency from 50 to 10 Hz leads to a fatigue life six times higher (3×10^3 and 1.8×10^4, respectively). On the other hand, it can be noted that even at a low value of the applied stress (applied stress equal to 0.40 $\sigma_{r(RO)}$) the fatigue life of the sample loaded at 100 Hz is about 40 times lower than the samples tested at 10, 30, and 50 Hz (2×10^4 and around 10^6 cycles, respectively). This ratio becomes more significant when the fatigue stress increases. It can be concluded that independently of the loading amplitudes, for values up to 50 Hz, frequency has a determinant influence on the fatigue life. This phenomenon, in fact, is owing to the self-heating during fatigue test studied in the next paragraph.

ITF and MF

Depending on the loading conditions in terms of frequency and amplitude, the fatigue behavior induces self-heating. The latter influences the viscous behavior of the vinylester as a function of the level of the temperature rise with respect to material transition temperatures.

High frequency and applied stress lead to an increase of the self-heating phenomenon and cause an "induced thermal fatigue" (ITF). For low frequency, the fatigue behavior is mainly driven by the damage mechanisms occurring at the microscopic scale such as fiber–matrix interface debonding, micro-cracking of the matrix and pseudo-delamination between the bundles of fibers. This kind of phenomenon is introduced as "mechanical fatigue" (MF).

These two natures of fatigue behavior are analyzed and discussed in the following section on the basis of the temperature measurements for four loading conditions. Indeed, coupled effect between loading amplitude and frequency leads to a competition between induced self-heating and damage phenomenon. In order to illustrate the coupled effect of loading amplitude and

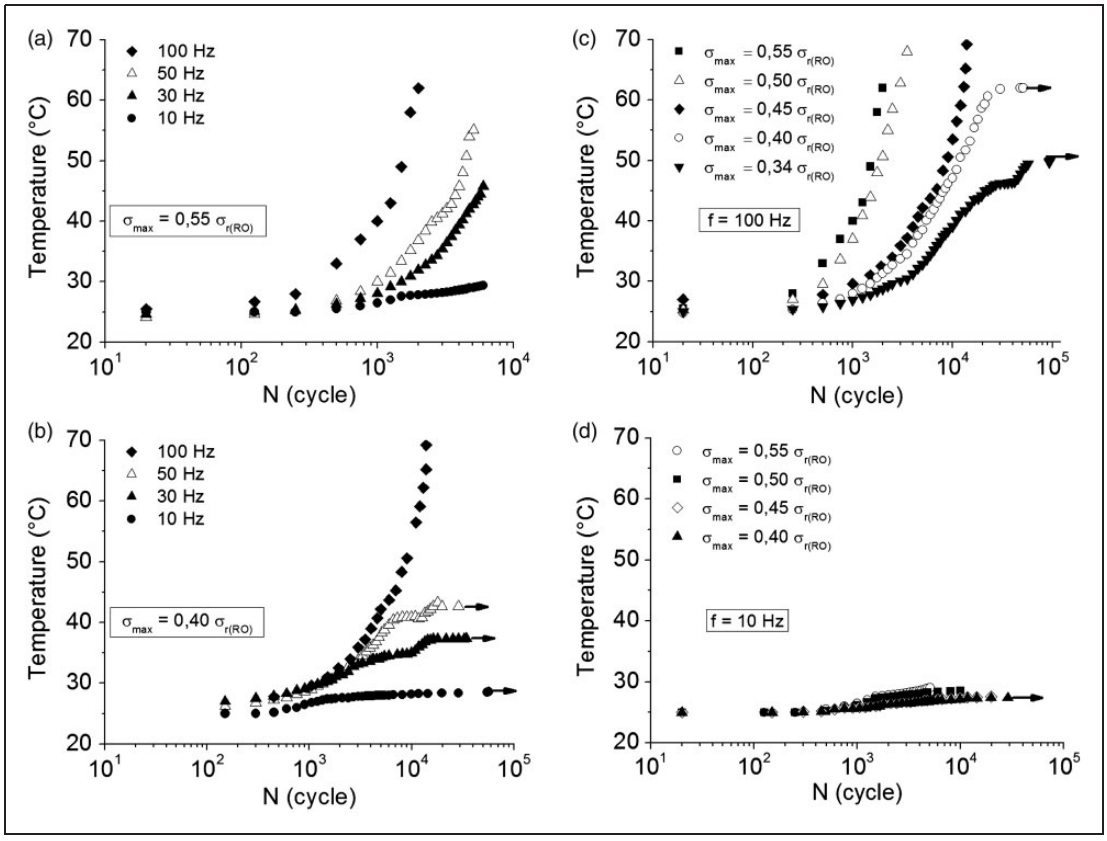

Figure 10. Temperature variation at different frequencies and amplitudes for RO samples: (a) $\sigma_{max} = 0.55\ \sigma_{r(RO)}$ and different frequencies, (b) $\sigma_{max} = 0.40\ \sigma_{r(RO)}$ ultimate stress and different frequencies, (c) f = 100 Hz and different amplitudes and (d) f = 10 Hz and different amplitudes.

frequency, one can define two limit cases (a) and (d) and two intermediate cases (b) and (c):

a. High frequency and high loading amplitude
b. High frequency and low loading amplitude
c. Low frequency and high loading amplitude
d. Low frequency and low loading amplitude

Induced self-heating

Figure 10 illustrates the variation of temperature during fatigue tests in the case of RO samples at different frequencies and loading amplitudes. As it can be shown, no significant temperature changes are noticed until 200 cycles. For an applied stress equal to 0.55 $\sigma_{r(RO)}$ (Figure 10(a)) at frequency of 100 Hz, the temperature increases rapidly from room temperature to 62°C up to 2000 cycles while it remains almost constant for 10 Hz fatigue tests.

The same tendencies are observed concerning the applied stress: as shown in Figure 10(c) and (d) for both frequencies, the temperature increases more rapidly until fracture for high applied stresses. Moreover, at low applied stresses, a stabilization of the temperature can be observed until specific number of cycles which highlights the effect of heat exchange made possible by a lower rate of self-heating.

Moreover, in the range of temperature between 30°C and 45°C, the curves (in Figure 10(a) to (c)) show an acceleration of the induced self-heating phenomenon. Indeed, this range of temperature corresponds to the beginning of the modification of the physical state of the polyester matrix as it can be seen in Figure 3. This transition, as it was shown before, may correspond to the beta transition of vinylester under study.

Influence of fatigue conditions on ITF and MF

The study of the self-heating phenomenon together with the evolution of the relative Young's modulus is identified to be a good way to separate ITF and MF phenomena. Figure 11 shows the evolution of the relative Young's modulus together with the self-heating temperature evolution during tension-tension fatigue tests for the four limit fatigue test conditions described above: two applied maximum stresses equal to 0.55

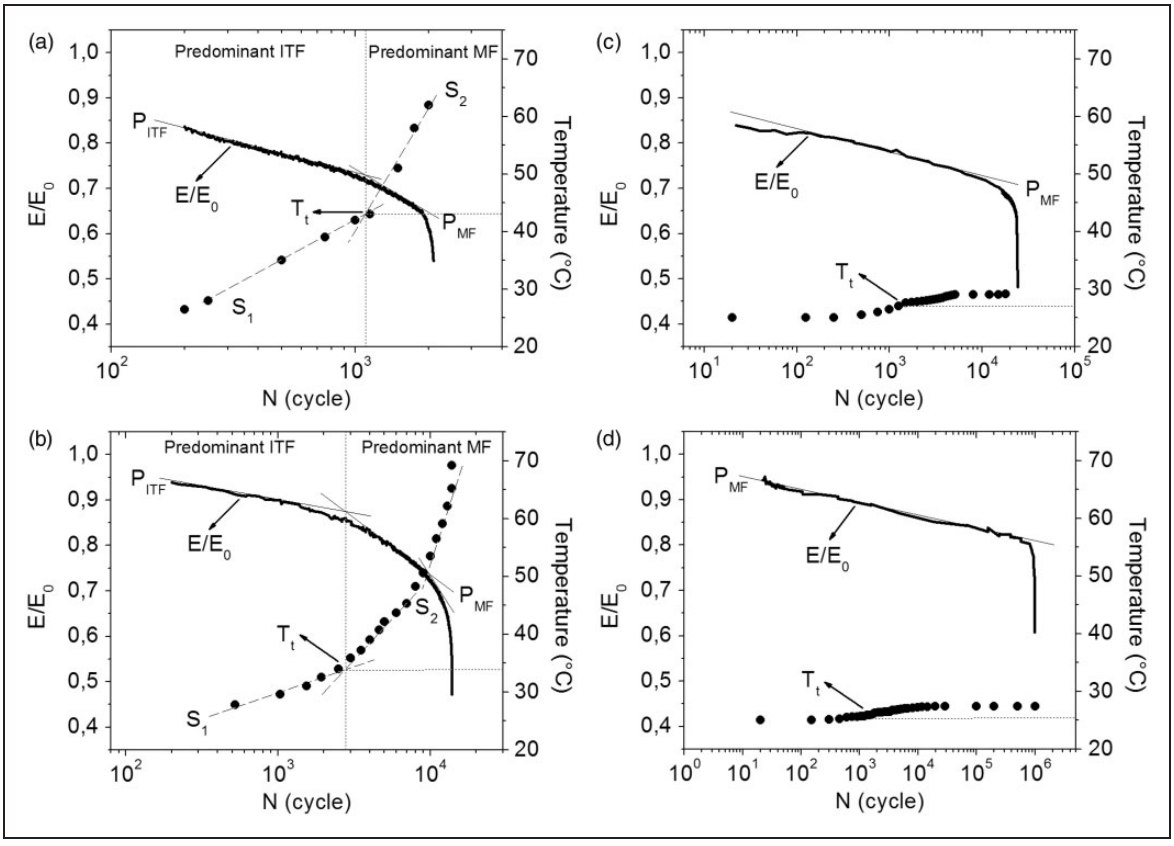

Figure 11. Evolutions of the relative Young's modulus (E/E_0) and the self-heating phenomenon during fatigue tests: (a) f = 100 Hz and $\sigma_{max} = 0.55\ \sigma_{r(RO)}$, (b) f = 100 Hz and $\sigma_{max} = 0.40\ \sigma_{r(RO)}$, (c) f = 10 Hz and $\sigma_{max} = 0.55\ \sigma_{r(RO)}$ and (d) f = 10 Hz and $\sigma_{max} = 0.40\ \sigma_{r(RO)}$.

$\sigma_{r(RO)}$ and 0.40 $\sigma_{r(RO)}$ at different frequencies: 10 Hz and 100 Hz.

In what follows, one introduces two quantities, noted: P_{ITF} and P_{MF} defined respectively as the rate of stiffness reduction during the predominant ITF and the predominant MF stages (Figure 11). The rates represent the slope of the stiffness reduction curves.

On the other hand, one introduces two other terms: S_1 and S_2, which are defined respectively as the first and second rate of temperature increase during fatigue test as illustrated in Figure 11(a) and (b). Finally, a term T_t is introduced as the specific temperature associated with a regime change of the temperature evolution between two stages as illustrated in Figure 11. For instance, in Figure 11(a), T_t is about 43°C.

For low amplitude and low frequency (case (d)) the RO-A-SMC exhibits a fatigue behavior mostly governed by the MF nature due to damage phenomenon, whereas for high amplitude and high frequency (case (a)), the ITF is the predominant nature of the RO-A-SMC fatigue behavior at low cycles. In this case, combined effect of high loading amplitude and high frequencies generates more intensive self-heating and damage phenomena. Indeed, for the test performed at 100 Hz and applied stresses equal to 0.55 $\sigma_{r(RO)}$, the temperature increases up to 62°C (Figure 11(a)). This temperature corresponds to the end of the β-transition zone associated with the brittle-ductile transition for amorphous polymers. At this stage, the vinylester resin stiffness strongly decreases as shown in Figure 3. For these loading conditions (cases (a) and (b)), the polymer matrix is subjected to important thermally activated modifications of its physical state.[6,15]

Thus, the fatigue behavior and failure are not only due to the devolvement of a diffuse damage at the microscopic scale but also to the evolution of the viscous behavior of the matrix and the inherent brittle-ductile transition. So, for high frequency and amplitude tests (Figure 11(a)), the fatigue behavior is driven by both ITF and MF. Two different rates of stiffness reduction can be observed. During the first stage, the effect of damage is less important compared to the ITF. After a transition zone around 2000 cycles, damage becomes predominant (MF) and leads to the final failure.

On the other hand, for the lower fatigue test conditions (10 Hz and applied stresses equal to 0.40 $\sigma_{r(RO)}$, see Figure 11(d)), self-heating remains very limited: only a temperature increases of 2.5°C is noticed (from 25°C up to 27.5°C). The relative Young's modulus is not significantly affected by the self-heating. One observes a linear stiffness reduction prior to the failure. This sharp decrease is essentially due to the damage evolution and the fatigue behavior is mainly driven by the MF nature.

Analysis of the ITF and MF kinetics

One can notice that simultaneously with the temperature evolution, a stiffness reduction occurs according to two regimes characterized by two different slopes. The transition between the two regimes is clearly illustrated in Figure 11(a) and (b). The stiffness reduction is caused by the self-heating (softening) of the matrix and by the damage accumulation. It should be pointed that, at the end of some fatigue tests, a third stage can be observed which is accompanied by a very high temperature rise rate due to the rapid accumulation of the damage prior to the total failure, as shown in Figure 11(b).

In Figure 12, the relative values of P_{ITF}, P_{MF}, S_1, and S_2 evolutions have been reported and plotted as a function of the applied stress and frequency. The relative values are defined as the ratio between the measured slope and the maximum value reached during fatigue test. As it can be observed in P_{ITF} and S_1 evolutions curves (Figure 12(a) and (c)) the self-heating phenomenon is highly favored by increasing of applied stress for both frequencies which confirms the effect of high applied stress on the self-heating kinetic. Obviously, this effect is more intensive for a high frequency. Indeed, for an applied stress equal to 0.34 $\sigma_{r(RO)}$, the stiffness reduction rate increases by less than 10% while it increases by 100% for an applied stress equal to 0.60 $\sigma_{r(RO)}$. The evolution of P_{MF} and S_2 also confirms the effect of high applied stress and frequency on the stiffness reduction kinetic during the predominant MF stage ((Figure 12(b) and (d)).

On one hand, it can be noticed that, in the case of low frequency fatigue, there is no influence of the applied stress on the stiffness reduction kinetic during the first stage of fatigue life (low cycles). On the other hand, one can observe a rate augmentation of the stiffness reduction due to damage (MF during the second stage) of about 18% when increasing the applied stress from 0.34 $\sigma_{r(RO)}$ to 0.60 $\sigma_{r(RO)}$. At the same time, the temperature rise kinetic increases by about 7%, which confirm the participation of the damage to the increase of the temperature.

Furthermore, Figure 12 allows getting more comprehensive data for the other loading amplitudes and

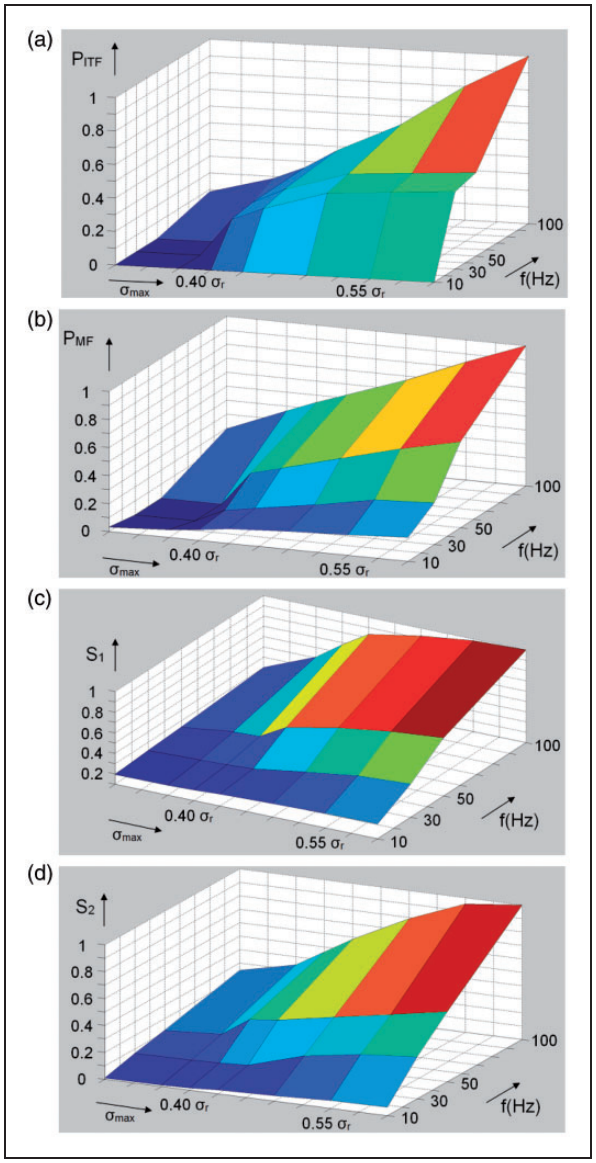

Figure 12. (a) P_{ITF}, (b) P_{MF}, (c) S_1, and (d) S_2 evolutions versus applied stress and frequency.

frequencies in order to get a more suitable quantitative and complete analysis of the self-heating effect coupled to damage. It also provides a cross-analysis of the coupled effect of amplitude and frequency which can be very suitable for automotive structure design.

In addition, the experimental data can enable the identification of a thermo-mechanical behavior law describing fatigue damage kinetic of A-SMC composites under various amplitudes and frequencies.

Finally, it can be concluded that both fatigue behavior and fatigue life of A-SMC composites are strongly influenced by a coupled effect between loading amplitude and frequency which induced thermal effect and progressive damage occurring at the microscopic scale.

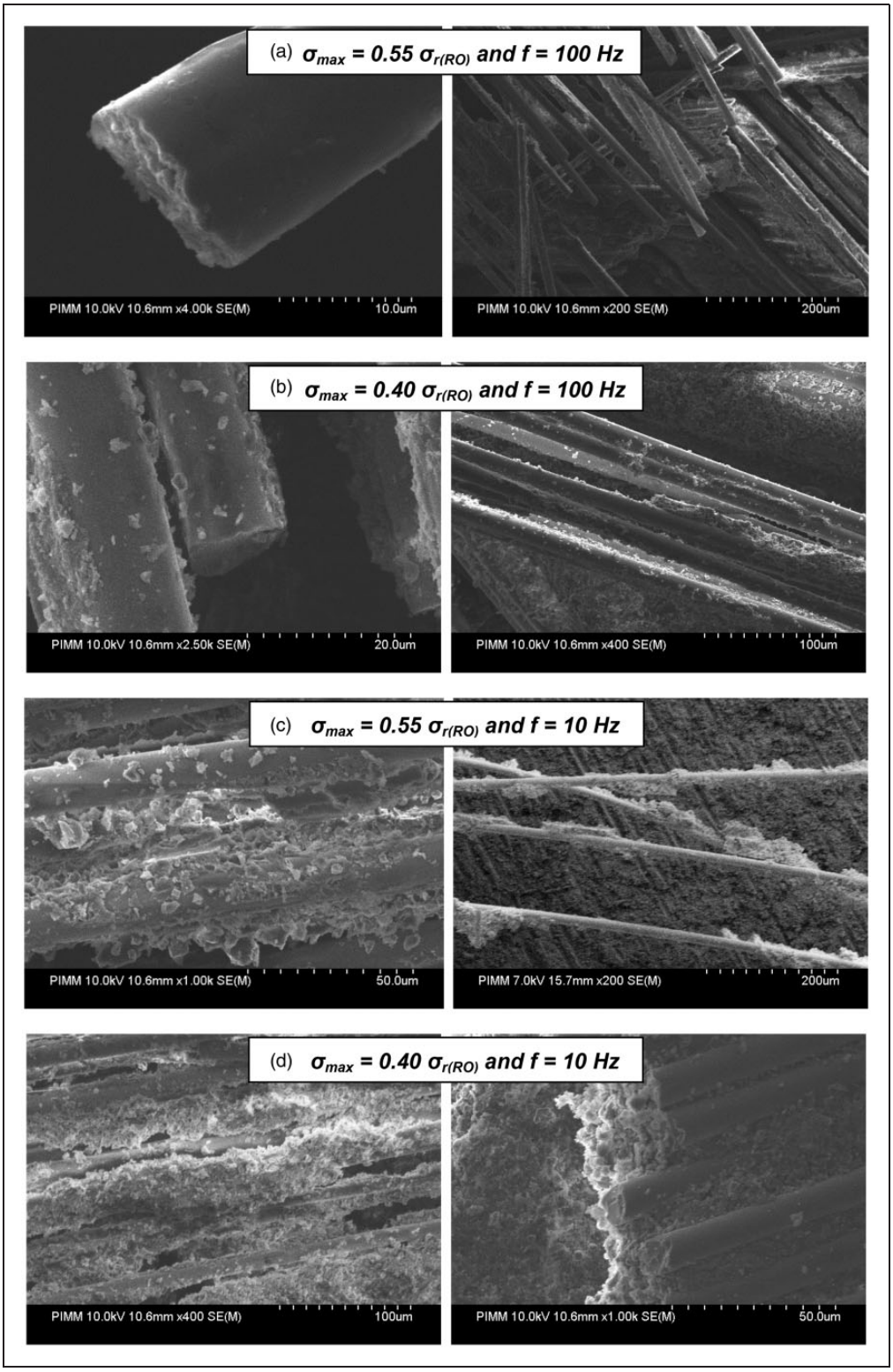

Figure 13. Fracture surface observation performed at different loading conditions: (a) $\sigma_{max} = 0.55\ \sigma_{r(RO)}$ and f = 100 Hz, (b) $\sigma_{max} = 0.40\ \sigma_{r(RO)}$ and f = 100 Hz, (c) $\sigma_{max} = 0.55\ \sigma_{r(RO)}$ and f = 10 Hz and (d) $\sigma_{max} = 0.40\ \sigma_{r(RO)}$ and f = 10 Hz.

Fracture surface observation

Fracture surface observations have been performed in order to emphasize the coupled effect of loading amplitude and frequency at microscopic scale. Figure 13 compares the fracture surfaces obtained for the four fatigue conditions described in ITF and MF section. SEM analysis highlights that, compared to lower frequency or applied stress, the fracture surface observed in the case of low applied stress and frequency (0.40 $\sigma_{r(RO)}$, 10 Hz), bundles of fibers are pulled out from each other simultaneously with breakage of more surrounding matrix.

SEM observations and analysis on the samples tested at 100 Hz, highlight more smooth debonded interfaces. Predominantly for the samples tested at $\sigma_{max} = 0.55\ \sigma_{r(RO)}$ and 100 Hz, no surrounding matrix is observed on the debonded fiber/matrix interfaces. In fact, self-heating contributes to the matrix softening and brings it in beyond the brittle/ductile transition. Favored by high applied stress and frequency, a more ductile behavior during fatigue loading leads finally to a smoother debonding of the fiber–matrix interface as it can be observed in Figure 13(a) and (b). Furthermore, during fatigue tests performed at 10 Hz, the self-heating remains limited leading to a more brittle fracture of the surrounding matrix and the related interfaces (Figure 13(c) and (d)).

Conclusion

An overall analysis of the fatigue behavior of A-SMC composite has been performed through the analysis of the coupled effect of loading amplitude and frequency. In order to highlight the ITF, the effect of frequency has been studied. At the same time, the effect of the loading amplitude allowed emphasizing the effect of damage kinetic on the nature of fatigue behavior of the A-SMC. Based on the results, the following concluding remarks are drawn to summarize the experimental findings:

- Whöler curves have been established for three loading directions and four frequencies. It has been shown that the fatigue life is strongly influenced by the distribution of fiber orientation. However, for transverse highly oriented material configuration (HO-90°), the fatigue life is not significantly affected compared to that of the randomly oriented material configuration (RO).
- It has been shown that the β-transition characterizing the brittle-ductile transition for amorphous polymers and which is generally related to the mobility of the small segments of molecular chains plays an important role on the overall fatigue response of A-SMC composite notably for high frequency cyclic loading. In fact, the self-heating brings up the material close to the β-transition zone ranging from 35°C to 60°C. The matrix behaves as a viscous media. The overall fatigue response exhibits an ITF nature which affects both stiffness reduction rate and fatigue life. This phenomenon is amplified by an increasing of the cyclic loading amplitude and frequency.
- It has been shown that for the high values of applied stress and frequency, the A-SMC exhibits an overall fatigue response mainly governed by the ITF nature during the first stage corresponding to low cycles. The MF nature becomes predominant during the second stage prior to the failure.
- For low applied amplitude and frequency loading conditions, no significant self-heating phenomenon has been observed and the overall fatigue response and fatigue life are mostly due to damage accumulation and the A-SMC exhibits predominantly a MF nature.
- Fracture surfaces observations evidenced the influence of the ITF on the fatigue overall response. Indeed, in the case of high values of frequency and applied stress, the surrounding matrix close to the fiber–matrix interface becomes ductile leading to a smooth interface debonding. On the other hand, low values of the frequency and applied stress lead to a brittle behavior of the surrounding matrix close to the interface showing a lot of matrix fragments around the debonded fibers.
- Evolution of the stiffness reduction and temperature increase and their related rates with respect to the number of cycle has been plotted as a function of frequency and loading amplitude. These evolution constitute an experimental database that can help formulating thermo-mechanical predictive models of the fatigue overall response.

Declaration of Conflicting Interests

The author(s) declared no potential conflicts of interest with respect to the research, authorship, and/or publication of this article.

Funding

The author(s) received no financial support for the research, authorship, and/or publication of this article.

References

1. Jendli Z, Meraghni F, Fitoussi J, et al. Multi-scales modeling of dynamic behaviour for discontinuous fibre SMC composites. *Compos Sci Technol* 2009; 69: 97–103.
2. Oldenbo M, Fernberg SP and Berglund LA. Mechanical behaviour of SMC composites with toughening and low

density additives. *Compos Part A Appl Sci Manuf* 2003; 34: 875–885.
3. Le TH, Dumont PJJ, Orgéas L, et al. X-ray phase contrast microtomography for the analysis of the fibrous microstructure of SMC composites. *Compos Part A Appl Sci Manuf* 2008; 39: 91–103.
4. Palmer J, Savage L, Ghita OR, et al. Sheet moulding compound (SMC) from carbon fibre recyclate. *Compos Part A Appl Sci Manuf* 2010; 41: 1232–1237.
5. Shokrieh MM and Mosalmani R. Modeling of sheet molding compound compression molding under non-isothermal conditions. *J Reinf Plast Compos* 2014; 33: 1183–1198.
6. Shirinbayan M, Fitoussi J, Meraghni F, et al. High strain rate visco-damageable behavior of Advanced Sheet Molding Compound (A-SMC) under tension. *Compos Part B-Eng* 2015; 82: 30–41.
7. Guster C, Pinter G, Mosenbacher A and Eichlseder W. Evaluation of a simulation process for fatigue life calculation of short fibre reinforced plastic components. *Procedia Eng* 2011; 1: 2104–2109.
8. Quaresimin M and Guglielmino E. Influence of quick ageing on the fatigue behaviour of SMC composite materials. *J Reinf Plast Compos* 2001; 20: 147–165.
9. Bernasconi A, Davoli P, Basile A, et al. Effect of fibre orientation on the fatigue behaviour of a short glass fibre reinforced polyamide-6. *Int J Fatigue* 2007; 29: 199–208.
10. Fleckenstein J, Jaschek K, Büter A, et al. Fatigue design optimization of safety components made of SMC. *Procedia Eng* 2011; 10: 390–396.
11. Wang SS, Suemasu H and Chim ESM. Analysis of fatigue damage evolution and associated anisotropic elastic property degradation in random short-fiber composite. *J Compos Mater* 1987; 21: 1084–1105.
12. Handa K, Kato A and Narisawa I. Fatigue characteristics of a glass-fiber-reinforced polyamide. *J Appl Polym Sci* 1999; 72: 1783–1793.
13. Bellenger V, Tcharkhtchi A and Castaing P. Thermal and mechanical fatigue of a PA66/glass fibers composite material. *Int J Fatigue* 2006; 28: 1348–1352.
14. Zhou Y and Mallick PK. Fatigue performance of injection-molded short E-glass fiber reinforced polyamide-6,6. II. Effects of melt temperature and hold pressure. *Polym Compos* 2011; 32: 268–276.
15. Esmaeillou B, Ferreira P, Bellenger V, et al. Fatigue behavior of polyamide 66/glass fiber under various kinds of applied load. *Polym Compos* 2012; 33: 540–547.
16. Arif M, Saintier N, Meraghni F, et al. Multiscale fatigue damage characterization in short glass fiber reinforced polyamide-66. *Compos Part B-Eng* 2014; 61: 55–65.
17. Mortazavian S and Fatemi A. Fatigue behavior and modeling of short fiber reinforced polymer composites including anisotropy and temperature effects. *Int J Fatigue* 2015; 77: 12–27.
18. Atodrais DR, Putatundaa SK and Mallick PK. Fatigue crack growth model and mechanism of a random fiber SMC composite. *Polym Compos* 2004; 20: 240–249.
19. Launay A, Marco Y, Maitournam MH, et al. Cyclic behavior of short glass fiber reinforced polyamide for fatigue life prediction of automotive components. *Procedia Eng* 2010; 2: 901–910.
20. Renz R, Alstadt V and Ehrenstein GW. Hysteresis measurements for characterizing the dynamic fatigue of R-SMC. *J Reinf Plast Compos* 1988; 7: 413–434.
21. Jendli Z, Fitoussi J, Meraghni F, et al. Anisotropic strain rate effects on the fibre–matrix interface decohesion in sheet moulding compound composites. *Compos Sci Technol* 2005; 65: 387–393.
22. Jendli Z, Meraghni F, Fitoussi J, et al. Micromechanical analysis of strain rate effect on damage evolution in sheet molding compound composites. *Compos Part A Appl Sci Manuf* 2004; 35: 779–785.
23. Hour KY and Sehitoglu H. Damage development in a short fiber reinforced composite. *J Compos Mater* 1993; 27: 782–805.
24. Houston DQ, Hunt J and Jiang C. Fatigue performance of SMC composite material under different environmental damage and temperature conditions. In: *Society of Plastics Engineers – 11th annual automotive composites conference and exhibition, ACCE 2011*, MSU Management Education Center 811 W. Square Lake Road, Troy, MI 48084, USA, 13–15 September 2011.

Article N°4:

Shirinbayan M, Fitoussi J, Abbasnezhad N, Meraghni F, Surowiec B, Tcharkhtchi A. Mechanical characterization of a Low Density Sheet Molding Compound (LD-SMC): Multi-scale damage analysis and strain rate effect. Composites Part B: Engineering. 2017.

Mechanical characterization of a Low Density Sheet Molding Compound (LD-SMC): Multi-scale damage analysis and strain rate effect

M. Shirinbayan[1,*], J. Fitoussi[1], N. Abbasnezhad[1], F. Meraghni[2], B. Surowiec[3], A. Tcharkhtchi[1]

[1] Arts et Métiers Paris Tech, PIMM – UMR CNRS 8006, 151 Boulevard de l'Hôpital, 75013 Paris, France:

E-mails: joseph.fitoussi@ensam.eu, navideh.abbasnezhad@ensam.eu, abbas.tcharkhtchi@ensam.eu;

[2] Arts et Métiers Paris Tech, LEM3 – UMR CNRS 7239, 4 Rue Augustin Fresnel, 57078 Metz, France:

E-mail: fodil.meraghni@ensam.eu;

[3] Plastic Omnium Auto Exterior, Sigmatech, Sainte Julie, France:

E-mail: benjamin.surowiec@plasticomnium.com.

Abstract

This paper presents the results of an overall experimental characterization of the mechanical behavior of a Low Density Sheet Molding Compound (LD-SMC). LD-SMC is a polyester matrix containing mineral charge ($CaCO_3$) reinforced by discontinuous bundles of glass fibers and Hollow Glass Microspheres (HGM). After a description of its specific microstructure using several experimental methods (notably a new ultrasonic method), the overall mechanical response of two microstructure configurations (Randomly Oriented (RO) and Highly oriented (HO)) is analyzed at both macroscopic and microscopic scales in the case of tensile and compression tests. HGMs are homogeneously distributed into the overall volume of the material. At the microscopic scale, in-situ tensile tests inside a SEM and fracture surfaces observations allows analyzing the specific damage mechanisms occurring during tensile and compression loading performed in the mold flow direction (HO-0°) and perpendicularly to it (HO-90°). A strong coupled influence of the presence of the HGM and fibers orientation has been emphasized. The results show that for HO-0° configuration fiber-matrix debonding appears to be the predominant damage mechanism, whereas for HO-90° configuration HGM-matrix debonding appears to be the predominant damage mechanism. High speed tensile tests are achieved using servo-hydraulic test equipment in order to study the strain rate effects (until 80 s^{-1}) on mechanical macroscopic responses of HO-0°, RO and HO-90° samples. Strain rate has an obvious influence on the inelastic properties of LD-SMCs samples for all microstructures particularly on the damage threshold.

Keywords: Hollow Glass Microspheres, Low Density SMC, damage, strain rate effect

[*] Corresponding author, mohammadali.shirinbayan@ensam.eu, Tel: +33-144246105

1. Introduction

.

According to the E. Commission [1], there is a trend to reduce weight in the transportation market. For example, by 2020, automakers should reduce carbon dioxide emission of their new cars by 30% compared to the admissible emission in 2011. On the other hand, several industrial reports [2] claim that using hollow glass microspheres can highly participate to the weight reduction. Moreover, the use of low weight materials can also provide more precise molding, greater dimensional stability and improved resistance to heat distortion. From these points of view, weight reduction has become a major issue for automotive industry [1, 3-4].

Due to their high strength-to-weight ratio, SMC composites became a classical ideal choice for large structural automotive components [5-6]. Sheet molding compounds (SMCs) are fiber-reinforced thermosetting semi-finished products processed by thermo-compression. Since the last two decades, SMC composite materials are successfully and widely used in automotive industry [2, 7]. Consequently, a wide range of research was focused on the processing of SMC composites (material preparation, mold filling, curing, ejection and cooling) [2, 5, and 8-9]. The first known SMC material development date back to the 1950s, but SMC compression molding analysis has been widely discussed only from the past decade [7, 10-13]. Standard SMC products are manufactured in thin uncured and thickened sheets ranging from 1 to 4 mm thickness and usually consist of discontinuous fiber bundles, a mixture of thermosetting resin (polyester or vinylester and sometimes epoxy), fillers (calcium carbonate, alumina, etc.), and also additives (such as initiators, inhibitors, thickeners, etc.) [10-14]. Glass fiber has been mostly used for SMC materials reinforcement but carbon fiber SMC are recently developed especially for fatigue applications [2].

Classically, standard SMC materials have a wide range of advantages when compared to steel and other metal materials. For example, structural parts made from SMC can provide up to 30% lower weight compared to the corresponding steel parts. Moreover, standard SMCs are less expensive than metal sheets for low or middle volume productions since they need lower tool costs. Another important advantage for these non-corroding polymer composites concerns

the more freedom design since smaller press radii can be used unlike steel and other metals. Furthermore, SMC composites are versatile materials and their formulation can be adjusted and tailored to meet the requirements of a diverse range of application [3-4, 6].

It is also meaningful to research Low Density SMC because of weight and cost reduction for industrial production. Oldenbo et al [15] investigated a low density type of SMC (Flex-SMC) for automotive exterior body panels. This flex-SMC has a density almost 20% lower than standard SMC and provides higher impact resistance. Indeed, standard SMC and low density SMC develop different damage mechanisms. In standard SMC, Oldenbo et al. [15] show that damage initiation is due to debonding at the $CaCO_3$ filler particle/matrix interface and leads to large matrix transverse cracks crossing the more miss-oriented fiber bundles. On the other hand, Jendli et al. show that fiber-matrix interface debonding is the predominant damage mechanism in standard SMC composites [16-17]. Comparatively, for low density SMC, damage initiates in transverse fiber bundles and extends to macro-scale transverse cracks [15].

On the other hand, the mechanical response of fiber reinforced polymeric composite materials varies significantly under different strain rates [18-19]. In the case of standard SMC, Jendli et al [16] analyzed the damaged behavior of a standard SMC composite under dynamic loading. They showed that strain rate mainly governs the damage threshold and accumulation. They also introduced the notion of visco-damageable behavior leading to an increase of the ultimate strain and stress and owing to local effect of the strain rate at the fiber-matrix interface [16], [17]. More recently, the visco-damage effect has been also demonstrated in the case of new vinylester based Advanced SMC composite presenting high fiber volume content [20-21]. It has been shown that increasing strain rate leads to a fiber-matrix damage threshold delay and lower damage accumulation kinetic. Moreover, these studies highlight that higher fiber content is causing a more intensive pseudo-delamination phenomenon between bundles which appears to be enhanced by more oriented fibers in the tensile direction and by higher strain rate.

On the other hand, despite the great interest of using LD-SMCs to develop lighter vehicles, only few authors have studied the relations between microstructure and mechanical and damage behavior for this class of material. In particular, an investigation of the strain rate effect until 80 s^{-1} on the mechanical response and damage of these materials is missing in the

literature (as well as it is known by the authors). This result is of first importance for crashworthiness optimization in the automotive industry.

In the present work, an experimental study is carried-out in order to widely investigate the mechanical behavior of a Low Density SMC provided by Plastic Omnium Auto Exterior. Special issues of this work concern strain rate and multi-scale damage effects on the overall behaviors of this material. Two kinds of LD-SMC specimen microstructures were prepared for physical, damage and mechanical characterizations: Randomly Oriented fibers (RO) and Highly Oriented fibers (HO). In the case of HO samples, two tensile directions were chosen in order to evaluate the anisotropic effect due to microstructure: HO-0° (parallel to the Mold Flow Direction (MFD)) and HO-90° (perpendicular to the MFD). After physical and microstructure characterization, quasi-static tensile and compression tests have been performed for RO, HO-90° and HO-0° specimens. Moreover, a multi-scale damage analysis has been performed in order to emphasize the effect of the presence of hollow glass microspheres. Strain rate effect has been investigated by performing high-speed tensile tests up to 80 s^{-1}.

The main structure of this paper is as follows: firstly, density and microstructure of LD-SMC was pointed out. Special attention was given to the comparing analysis of quasi-static compression and tensile tests. Besides, in-situ tensile tests performed inside a Scanning Electron Microscope and fracture surface analysis have been performed in order to emphasize the effect of microstructure and loading direction on the main damage and failure micro-mechanisms. An experimental study of the strain rate effect (from quasi-static to 80 s^{-1}) on the overall tensile response of LD-SMC is presented at the end of the paper. Finally, a multi-scale analysis of the damage effect for various microstructures, loading types and loading speeds is proposed in order to highlight the influence of the local damage mechanisms on the overall response of LD-SMCs.

2. Material description and methods

2.1. Low Density Sheet Molding Compound (LD-SMC) composite

Low Density Sheet Molding Compound (LD-SMC) composite is a type of SMC reinforced with chopped glass fibers bundles (25 mm length) and hollow glass spheres. This pigmented SMC composite presents high mechanical properties and a good surface aspect. LD-SMC compression molding is a complicated process. In the manufacturing process, raw materials on rolls should be cut to certain size and put into the mold under high temperature between 145°C and 155°C and pressure between 80 and 120 bars. These conditions lead to decreasing of the viscosity of the materials and allow fulfilling the whole cavity of the mold. Then the materials stay in position with no reticulation for a short duration. The next step of the process consists of a reticulation time of the thermoset material that is the consolidation phase.

The composition of the studied LD-SMC is presented in Table 1. Two types of LD-SMC plates have been provided by Plastic Omnium Auto Exterior: Randomly Oriented (RO) and Highly Oriented (HO) plates. HO plates have been obtained by an initial charge put only in the left part of a rectangular mold (30 × 40 cm^2) before compression leading to material flow. RO plates were obtained without material flow by completely filling the mold.

Product nature	Composition (content in mass percent)
Glass fibers	30 %
Hollow glass spheres	22 %
Polyester resin	12 %
Filler	32 %
Other products	4 %

Table 1. LD-SMC composition

2.2. Microstructure characterization methods

2.2.1. Microscopic observations

Microscopic observations and image analysis, using Scanning Electronic Microscope (HITACHI 4800 SEM), have been performed in order to qualitatively investigate the material microstructure and especially fibers orientation.

2.2.2. X-ray micro-tomography

X-ray tomography allowed a three-dimensional visualization of LD-SMC. EasyTom nano setup, which comprises an X-Ray source, a rotating table and an X-ray detector, was used. The studied sample ($1 \times 1 \times 3$ cm^3) was placed between the X-ray beam and the camera detector.

The principle of operation of the microstructure analysis by X-ray micro-tomography is widely described in [22].

Fig. 1. Experimental setup of X-Ray micro-tomography (EasyTom nano)

2.2.3. Ultrasonic measurement

Ultrasonic waves have been recently used to characterize the orientation distribution of the fibers in an SMC composite [23]. In this paper, an original and simple ultrasonic measurement procedure is proposed in order to highlight the orientation distribution of the fiber bundles. The ultrasonic measurements were performed in immersion. The ultrasonic apparatus is composed of two probes, one transmitting (E) and other one receiving (R), separated by a known and constant distance d. The diameter of the probe is of 10mm. The sample is placed between the two probes with an angle of about 45° versus the incident ultrasonic wave in order to create a shear wave which propagates inside the material in a direction determined by the

Snell-Descarte law [24]. Consequently, the material is submitted to an ultrasonic shear stress in the plane defined by the incident wave (OL in Fig. 2) and the vector normal to the plane of the specimen ($\vec{n}$ in figure 2). In Figure 2, one can consider two limit cases:

a) Longitudinal orientation of the fibers,

b) Transverse orientation of the fibers.

In the case (a), the fibers are contained in the ultrasonic shear stress plane. This configuration corresponds to the maximum section of fiber submitted to the shear stress. Consequently, for longitudinally oriented fiber, the measured value of shear wave velocity, V_T, will be maximal. On the other hand, in the case of transversely oriented fibers (case (b)), fiber sheared section is reduced and leads to a minimal value of the shear wave velocity.

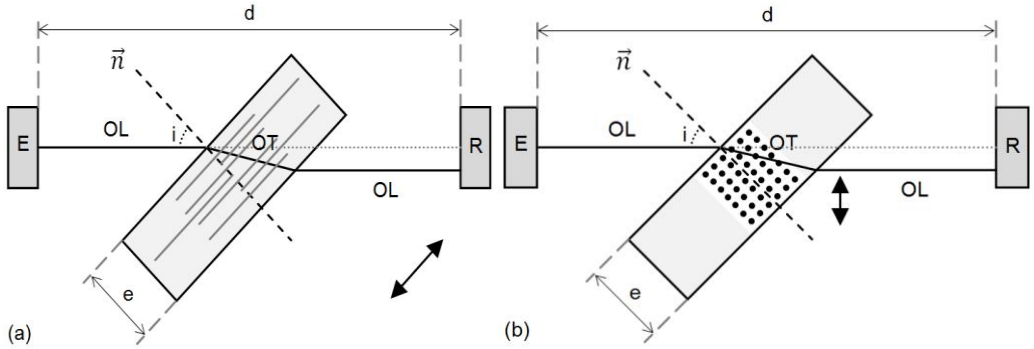

Fig. 2. Two limit cases fiber direction: (a) High V_{OT} and (b) Low V_{OT}

Thus, by rotating the sample around the axis $\vec{n}$ from 0° to 360°, the value of V_T varies as a function of the orientation distribution of the fibers. Fig. 3 shows an example of variation for a SMC specimen with strongly oriented in the 0° direction. Thus, maximum V_{OT} values are found to be 0°, 180° and 360°.

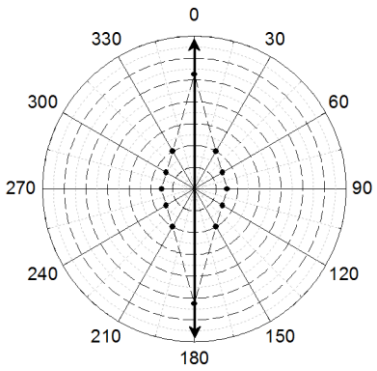

Fig. 3. Evolution of the shear wave velocity for a SMC composite with oriented fibers

For this sample, all the bundles of fibers are globally parallel to the plane of the SMC plate. Consequently, the V_T curve appears to be symmetric. On the contrary, in the case of an out of plane fiber orientation, the evolution of V_{OT} will be non symmetric. Indeed, out of plane oriented fibers are not in the same relative orientation versus the shear stress plane after a rotation of 180° for example as illustrated in Fig. 4.

Ultrasonic measurements are a good and easy way to obtain a direct image of the distribution of orientation through the evolution of the shear wave velocity. This ultrasonic analysis was performed upon a volume that the surface was 60 × 60 mm^2 with thickness of 2.9 mm for both RO and HO samples.

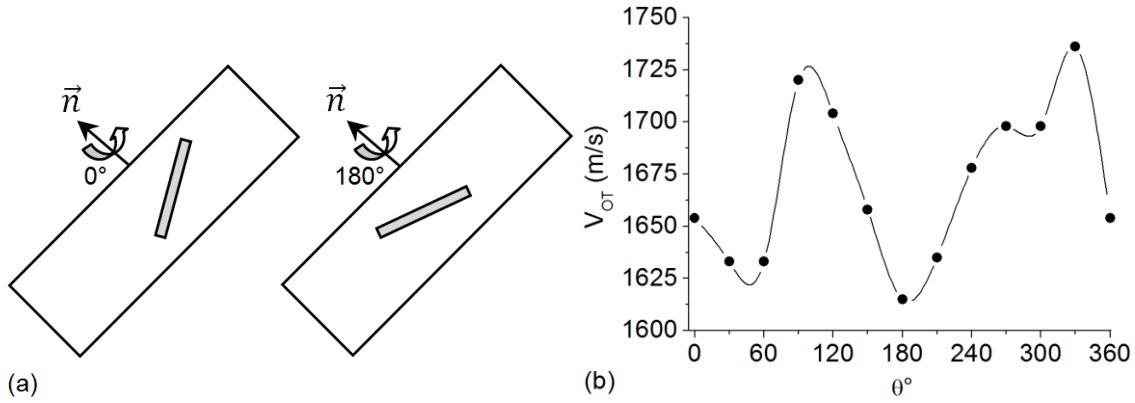

Fig. 4. (a) Effect of the sample rotation around $\vec{n}$ on the relative orientation on out of plane fibers relative orientation, (b) Example of non symmetric curves obtained for out of plane fibers orientation, SMC sample.

2.3. Mechanical characterization methods

2.3.1. Strain measurement

For all types of tests, a contactless image analysis technique using a camera (high speed camera [20-21] or classical camera) allows strain measurement by following the relative displacement of two marked points drawn on the surface of the specimen before testing.

2.3.2. Quasi-static tension behavior and stiffness reduction

Moreover, tensile tests until failure and loading-unloading tests at different increasing applied maximum stresses have been performed on MTS 830 hydraulic machine, in order to

estimate tensile behavior and the macroscopic stiffness reduction during tension respectively. The specimen geometry used for quasi-static tensile test is the same as the optimized one for dynamic tensile tests (see section 2.3.5). The loading speed was 2 mm/min.

2.3.3 Quasi-static compression tests

Compression tests were achieved with the Instron 5881 testing machine with a loading cell of 50 kN, according to the standard NF ISO 6239. The loading speed was 2 mm/min. The LD-SMC specimen is positioned between two jaws as sketched in Fig. 5(a) and used specimen's geometry is shown in Fig. 5(b).

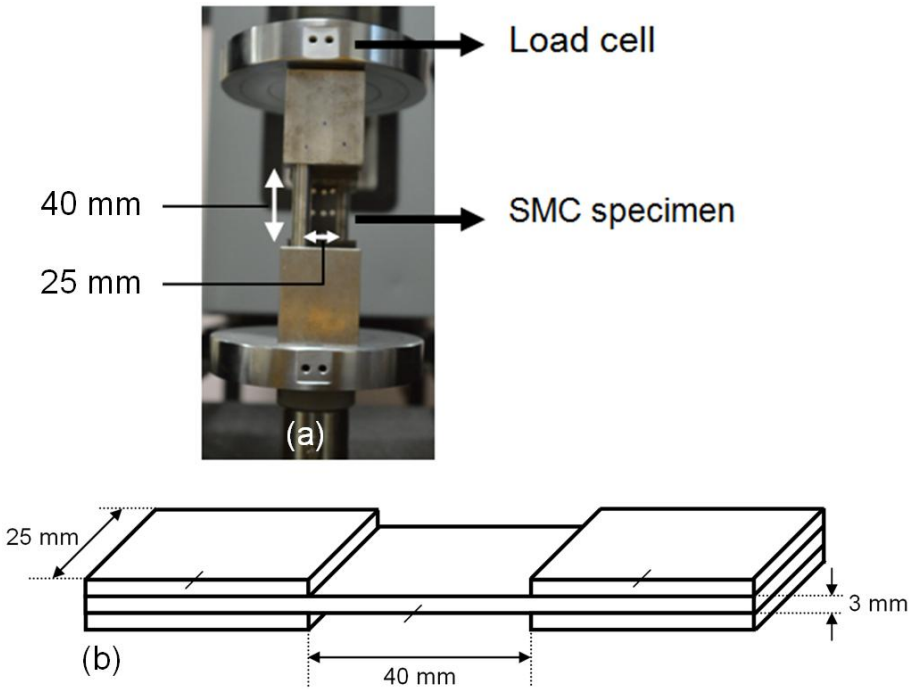

Fig. 5. (a) Experimental setup of compression test and (b) used specimen's geometry

2.3.4. Damage analysis using an in-situ tensile test device

In situ observations were performed by subjecting the specimens into a quasi-static tension load (0.5 mm/min) using a tensile micro-machine (Fig. 6), with a span length of 25 mm, positioned inside a large SEM chamber (HITACHI 4800 SEM). To reduce the relaxation effect in the material, the observation time while maintaining the load was limited to 3 minutes. The observation area corresponded to a polished thickness surface of the composite.

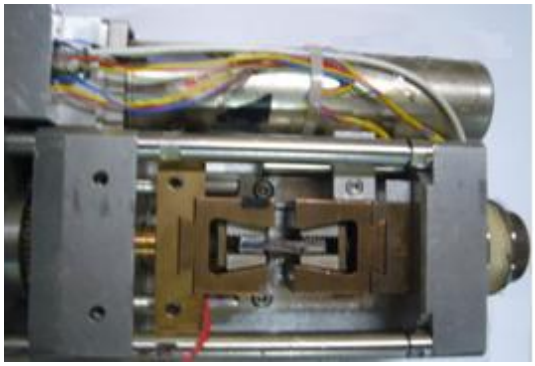

Fig. 6. The micro-machine tensile testing device

2.3.5. High-speed tensile tests

Using a servo-hydraulic test machine (Schenk Hydropuls VHS 5020) which is able to apply a crosshead speed range from quasi-static to 20 m/s, high strain rate tensile tests have been performed. An optimized damping joint consisting of a low impedance material - rubber nitrile (1.5 mm thickness) is placed between the slide and the hydraulic jack in order to attenuate partially the perturbation due to mechanical waves caused by inertial effects and the dynamic shock and also to limit the system ringing related to the hanging mass of the upper fixing system [16-17, 20-21].

Furthermore, in order to reduce the perturbation wave's effect the same optimization procedure used in the previous works [16-17, 20-21] was followed. Therefore, the LD-SMC specimen geometry has been optimized as a result of numerical computations using ABAQUS finite element (FE) code (Fig. 7) in order to reach a homogeneous strain distribution and a rapidly stabilized strain rate within the specimen gauge section at the beginning of the loading stage. Finally the same specimen geometry used in a previous work [20-21] (6 mm radius specimen) appears to be well adapted also for LD-SMC. It can be observed in the consecutive stress profiles that the shock wave vanishes very quickly and the stress distribution becomes rapidly relatively homogeneous (Fig. 8). Experimental strain evolutions confirm the efficiency of the chosen experimental conditions (see Fig. 9).

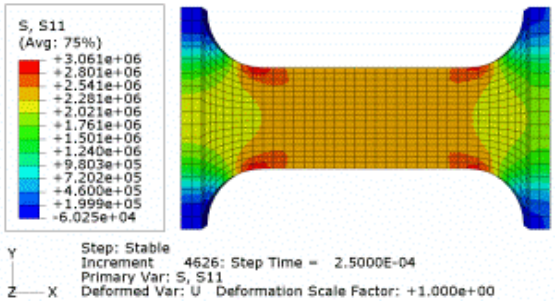

Fig. 7. FE computations optimizing the dumbbell-shaped specimen geometry parameters

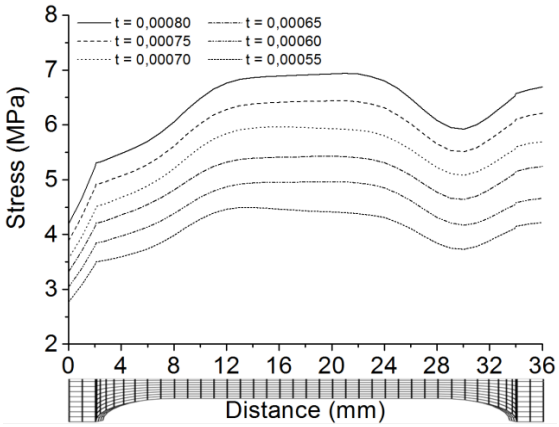

Fig. 8. Spatio-temporal profile of tensile stress calculated along the central line of the LD-SMC specimen. Loading conditions: imposed velocity V = 4 m/s

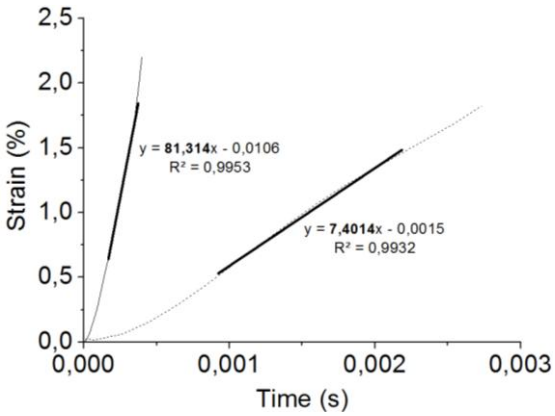

Fig. 9. Experimental strain evolutions at different high strain rates (7.4 s^{-1} and 81.3 s^{-1})

3. Results and discussion

3.1. Specific density

Hollow glass spheres allow reducing the density of sheet molding compound to ~1.3 g/cm^3 compared to the conventional SMC of 1.85 g/cm^3 (i.e. a 30 percent reduction), while maintaining surface quality and mechanical performance. This combination allows the production of lighter parts [15].

3.2. Microstructure analysis

3.2.1. SEM observation

Fig. 10 shows clearly the orientation and distribution of fibers after cutting the plates in different directions (parallel or perpendicular to the Mold Flow Direction). One can note that there are two main differences in the following figures. According to the elliptic forms of the fibers appearing at the observation surface, HO sample show more fibers oriented in the Mold Flow Direction (MFD) compared with randomly-oriented distribution of fibers (RO) [20].

One can note in Fig. 11 that the presence of hollow glass spheres generates out of plane glass fiber orientation during the flowing process. Thus, HO samples show more out of plane oriented bundles which is the inconvenience of using hollow glass spheres compare to standard SMCs which show more regular in-plane orientation.

LD-SMC	Parallel to MFD view	Perpendicular to MFD view
RO	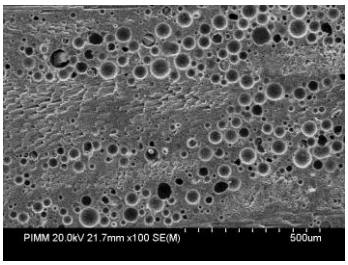	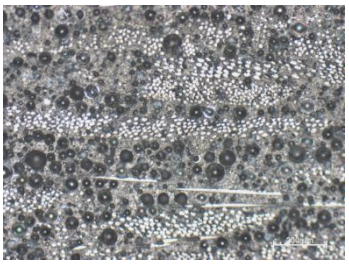
HO	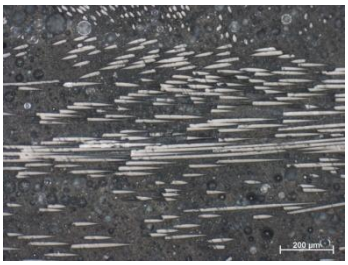	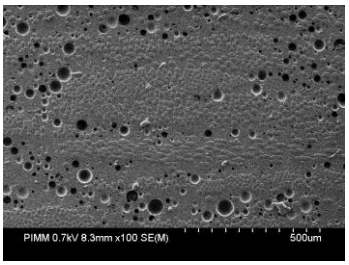

Fig. 10. Microstructure of LD-SMC: Bundle of fibers and hollow glass spheres.

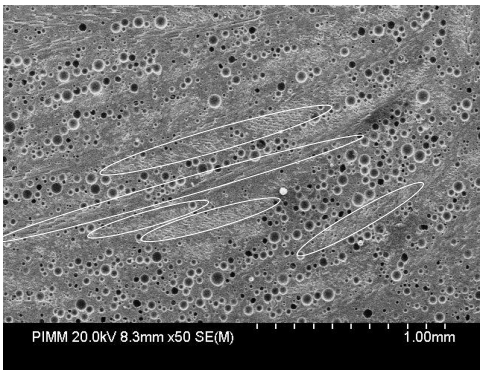

Fig. 11. Out of plane orientation of fiber bundles generated by the presence of hollow glass spheres (HO sample)

3.2.2. Microtomography X analysis

Fig. 12 exhibits the microstructures of LD-SMC RO and HO specimens of using X-ray micro-tomography. Actually, because of the difference of density between the constitutive phases of the composite, the later can be separated as it is shown in this figure. The global 3D spatial distribution of each phase can be analyzed qualitatively.

LD-SMC	Matrix	Glass Fiber	Blank + HGMs
RO	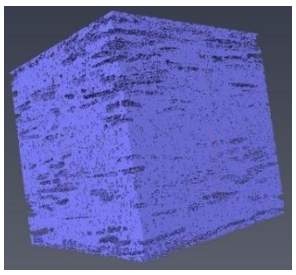	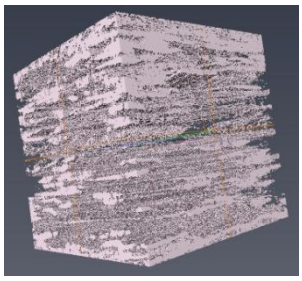	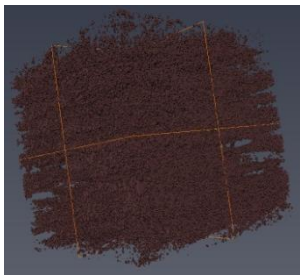
HO	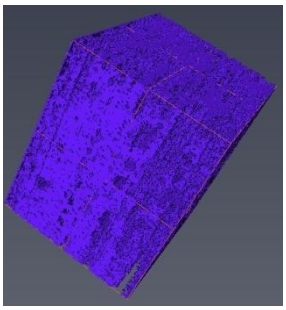	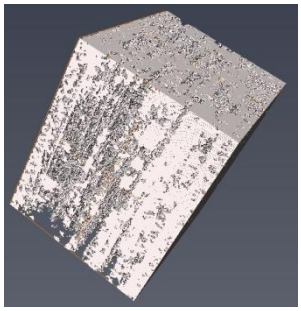	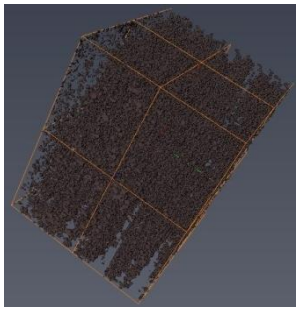

Fig. 12. Micro-tomography results

One can notice that, for both HO and RO samples, the HGMs are homogeneously distributed over the whole volume of the composite. However, HGM content seems to decrease at the surfaces of the plate.

3.2.3. Ultrasonic analysis

Ultrasonic analysis obtained by the methodology introduced in paragraph 2.2.3 leads to typical results shown in Fig. 13. The evolutions of the shear wave velocity for HO SMC specimen (Fig. 13(a) and (b)) emphasize clearly fibers orientation in the mold flow direction (0°) since Fig. 13(c) shows a typical result obtained for a RO sample corresponding to a clearly transversely isotropic SMC microstructure.

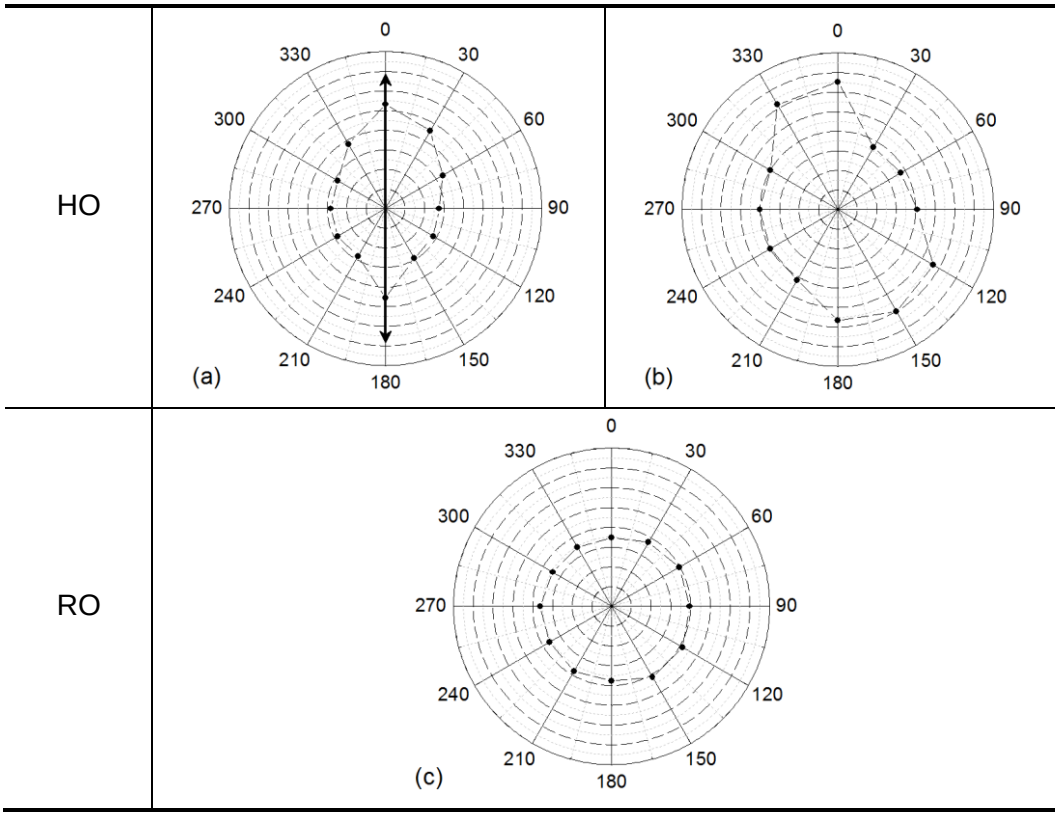

Fig. 13. Ultrasonic results; (a, b) HO plate and (c) RO plate

The majority of samples (more than 80%) of this plate present a main fibers orientation of 0° ± 30°, 0° corresponding to the mold flow direction during process. As mentioned above, the presence of hollow glass spheres forces out of plane glass fibers orientation and as a result the polar curves are not always symmetric (Fig. 13(b)). For randomly oriented plates (Fig.

13(c)), it can be observed that the polar diagrams of velocity are almost circular; which means that there are virtually no preferred direction reinforcements. As a whole, the plate appears rather as an isotropic material.

The propagation velocity of the ultrasonic waves is connected to microstructure and mechanical properties of the material. Coefficient K (%), acoustical birefringence, is defined as:

$$K\,(\%) = \frac{V_{OTmax} - V_{OTmin}}{V_{OTavrage}} x100 \qquad \text{(Eq. 1)}$$

Where V_{OT} is the velocity of the shear waves for a given relative orientation θ of the composite (see Fig. 4). This coefficient characterizes orientation intensity and allows comparing different type of distribution of fibers orientation. Thus, a high value of acoustical birefringence coefficient "K" indicates a main direction of fibers.

Another issue of the ultrasonic measurements is the analysis of the spatial distribution of the fibers. Indeed, high values of density and tensile and shear waves velocities indicate the presence of a high quantity of fibers at the measurement location. The average values of K, V_{OT} and V_{OL} for the 24 samples of two different RO plates and two different HO plates are presented in table 2.

Parameter	RO samples	HO samples
K (%)	3.3	11
ρ (g/cm^3)	1430	1460
V_{OT} (m/s)	1420	1570
V_{OL} (m/s)	2100	2700

Table 2. The average values of K, V_{OT} and V_{OL} after ultrasonic measurement

3.3. Quasi-static mechanical behavior

3.3.1. Overall tension and compression behavior

Tension and compression tests results are superposed in Fig. 14 for both configurations. Five similar tests have been performed for each configuration. The representative curves are presented in a normalized form relative to the tensile RO curve taken as a reference. For both configurations, no significant difference is observed on the linear part of the curves between tension and compression leading to similar Young's modulus.

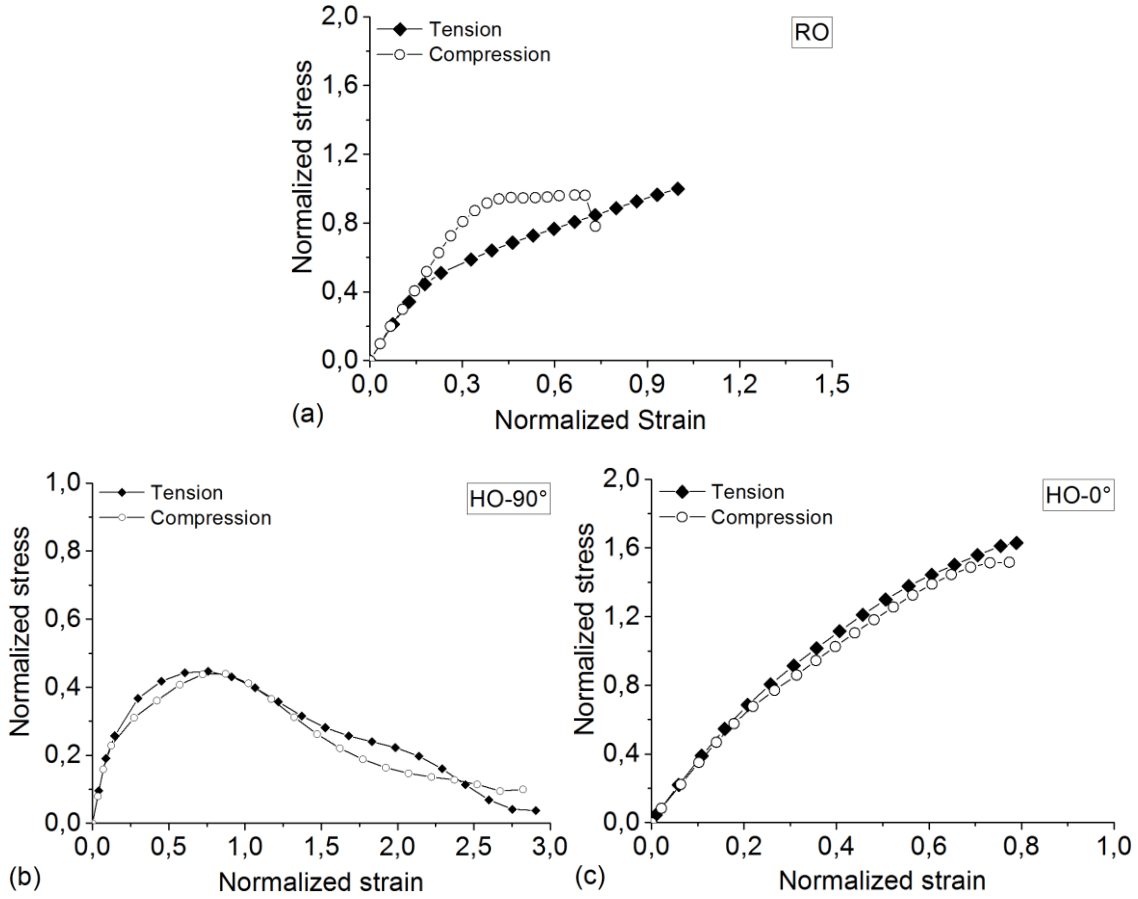

Fig. 14. Tension and compression stress strain curves ; (a) RO, (b) HO-90° and (c) HO-0° (Normalized value = current value / average value obtained for quasi-static tests performed on RO-LD-SMC).

In these curves, the strong effect of the fiber orientation discussed in section 3.2 is clearly emphasized in terms of modulus and inelastic behavior until failure. One can note that both of tension and compression tests, for each kind of specimen, have similar Young's modulus in the firstly linear period. Moreover, except for the RO samples, tension and compression behavior appears to be similar until failure. On the other hand, compression curve of RO configuration presents a longer linear elastic stage followed by a plateau which will be discussed after.

Another specific behavior can be observed in the HO-90° curves. After a maximum value of 0.45 $\sigma_{r(RO)}$ the stress progressively decreases until a very low stress level near to 0,1 $\sigma_{r(RO)}$. This phenomenon has been observed for about 25% of the tested specimens and will

be discussed in section 3.4. The other specimens have been broken for the maximum stress (0.45 $\sigma_{r(RO)}$) as it is illustrated in Figure 14 (b).

3.3.2. Effect of fiber orientation

Fig. 15(a) shows a comparison between the quasi static tensile tests results obtained on on HO-0°, RO and HO-90° samples at room temperature. Note that in the case of HO-90° the curve has been stopped just before the stress decreases described in the previous section. As it can be seen, the value of Young's modulus of HO-0° is about 12 GPa which is higher than those of RO (10 GPa) and HO-90° (9 GPa) samples. The failure stress also highly depends on the fibers orientation. One can note that failure stress of HO-0° is about four times higher than that of HO-90° samples.

In order to emphasize the damage development effect, threshold and kinetic of damage can be characterized by the evolution of the well-known scalar damage parameter [25-26] which is defined as:

$$D_{macro} = 1 - E_D/E_0 \qquad \text{(Eq. 2)}$$

Where E_0 and E_D are the Young's modulus of the virgin and damaged material respectively. The residual Young's modulus after damage, E_D, is measured by a "loading-unloading" procedure in which reached the value of stress increases at each reloading stage. Then, the evolution of the macroscopic damage parameter can be measured and plotted against the stress level for the three kinds of specimen: HO-0°, RO, HO-90° in accordance to their quasi-static tensile curves [21] (Fig. 15(b)).

One can note that HO-0° has the lowest damage parameter evolution. For example, in the case of HO-0° samples, macroscopic damage begins at a stress level of 0.75 $\sigma_{r(RO)}$, significantly higher than those of HO-90° and RO samples (corresponding to 0.25 $\sigma_{r(RO)}$, 0.50 $\sigma_{r(RO)}$, respectively). Moreover, HO-0° damage parameter only grows up until 0.11 for a sharply increasing stress up to 2.10 $\sigma_{r(RO)}$ while this value for HO-90° strongly increases up to 0.22 for a corresponding stress slightly near to 0.50 $\sigma_{r(RO)}$. Moreover, one can note that damage threshold and kinetic are directly correlated to orientation: Increasing fiber orientation in the load direction leads to higher damage threshold and lower kinetic of damage propagation.

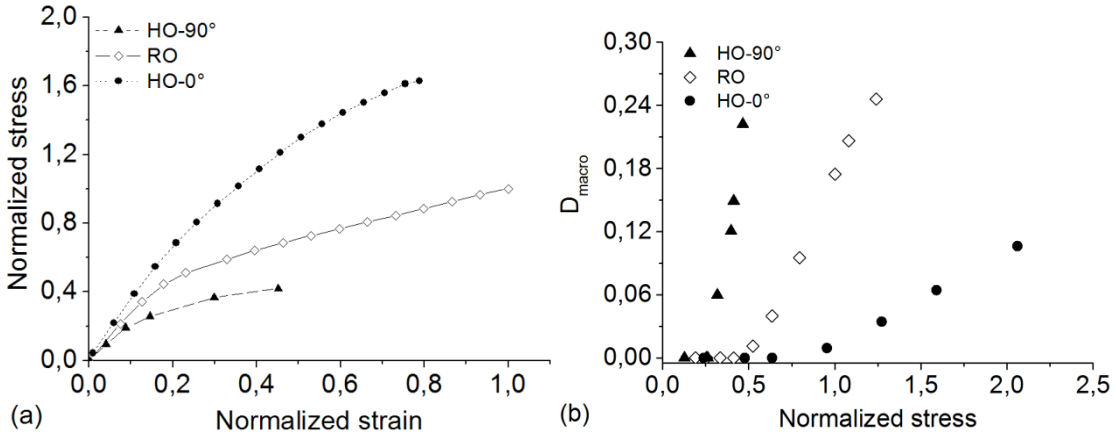

Fig. 15. (a) Quasi-static tensile curves and (b) Macroscopic damage evolution versus normalized applied stress for RO, HO-90° and HO-0° samples (Normalized stress = current value / average value obtained for quasi-static tests performed on RO-LD-SMC)

3.4. Damage mechanism analysis

In section 3.3, the overall mechanical behavior of the LD-SMC in this study has been analyzed at the macroscopic scale. Specific effects have been emphasized. In this section, a damage analysis is performed at the microscopic scale in the case of tensile and compression tests. Microscopic observations are correlated to macroscopic behavior described above in order to determine the specific role played by the presence of HGMs in damage development.

3.4.1. Tensile tests

- In situ SEM tensile tests:

In-situ quasi-static tensile tests have been performed inside the chamber of a SEM as described in section 2.3.4 in order to observe the evolution of damage development at the microstructure scale. HO microstructure has been investigated for two tensile directions: HO-90° and HO-0°. The same representative observation zone was microscopically analyzed at consecutive increasing values of applied stress level: about 3 × 5 mm^2. Preliminary tests showed that this investigation zone is large enough to be qualitatively representative of the damage mechanisms occurring during the tensile loading. Thus, the local investigation presented here can be assumed to be qualitatively representative of the damage accumulation during LD-SMC tensile loading.

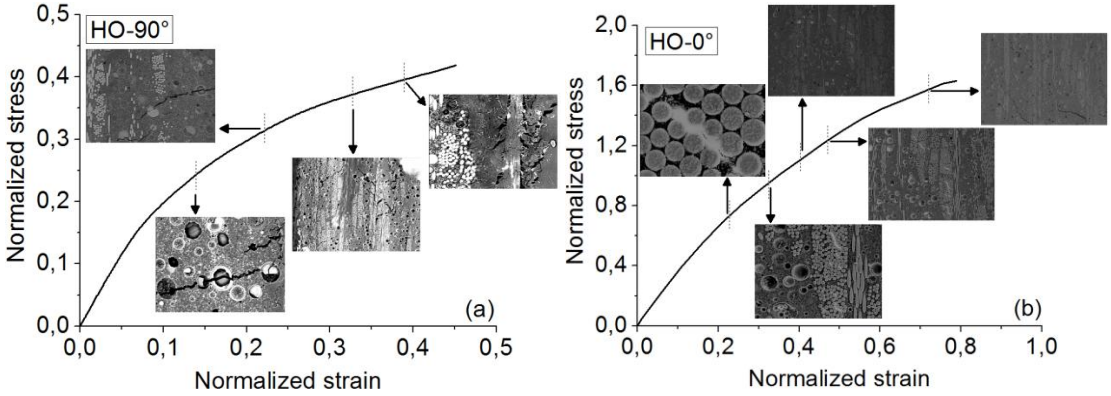

Fig. 16. Experimental in-situ quasi-static tensile tests coupled to microstructure observations for HO-90° and HO-0° samples

In the case of HO-90° samples (see Fig. 16), the first observed damage phenomenon appears together with the first non-linearity of the tensile curve and corresponds to failure or debonding of the HGMs occurring in the fiber depleted zones. This leads to the propagation of micro-cracks perpendicularly to the tensile direction. For a higher value of applied stress, this damage mechanism is spreading through the whole observation zone in a diffuse manner on several HGMs locations. At the same time, the early existing micro-cracks continue growing. By increasing applied stress, fiber-matrix interface failure begins appearing on different bundle locations, especially on the more disoriented fibers versus the loading direction. Furthermore, one can observe coalescence of the two types of micro-cracks which grow simultaneously at higher applied stress values. Finally, when reaching the maximum stress, local shear deformation around the bundles leads to the pseudo-delamination of the bundles near to failure.

The failure stage described above concerns about 75% of the tested specimens for which failure occurs at the maximum stress. However, as mentioned above, for an amount of 25% of HO-90° specimens, the stress value decreases gradually from the maximum stress until a lower stress level near to zero. In order to investigate this phenomenon, some tests have been interrupted during the decreasing stage in order to observe the evolution of the microstructure. Fig. 17 shows clearly a progressive propagation of transverse micro-cracks caused by debonding of HGMs followed by propagation through the polyester matrix. Hence, when most fibers are oriented at 90° versus the loading direction, matrix is submitted to high

stress values in such a way that the diffuse development of this kind of micro-cracks is favored. Moreover, these micro-cracks can easily propagate through 90° oriented bundles (Fig 17b) and can be sometimes deviated or hindered by the presence of a fibers bundle less disoriented. Consequently, for an appropriate distribution of fiber orientation (HO-90°), a progressive “unbuttoning” phenomenon of the HGMs coupled to fiber-matrix interface debonding leads to a wide networks of transverse micro-fractures of the matrix and is accompanied by an overall progressive increase of the strain together with a decrease of the stress as in Fig.14(b). Note that this phenomenon does not occur for microstructures presenting more dispersed distributions of fibers orientations for which the presence of more oriented bundles participates to a more equilibrated local stress distribution between the different phases (matrix and reinforcements). One can also notify that the stress decrease is less frequent in the case of compression tests (only 5% of the HO-90° tested specimen). Indeed, transverse micro-cracking diffusion is not favored by compression loading.

Finally, we must also indicate that this phenomenon has never been observed for high strain rate tensile tests described in section 3.5. Indeed, the HGMs “unbuttoning” phenomenon described above corresponds to a stable propagation on the micro-cracks which is more difficult to obtain at high strain rates.

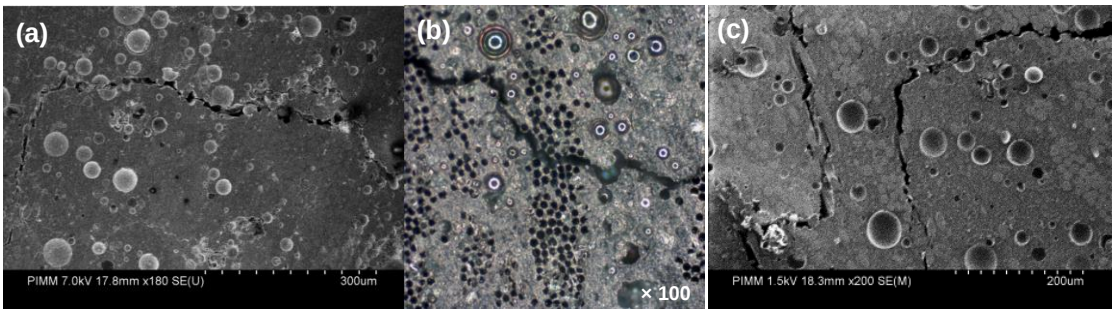

Fig. 17. Matrix microcracking from HO-90° tensile test interrupted during the gradual stress decrease (see Fig.14.b): a) Progressive “unbuttoning” at the HGM-matrix interfaces, b) Easy propagation through 90° oriented bundle, c) Deviation of matrix micro-cracks by more disoriented bundles

On the other hand, damage development observed during a tensile test performed on HO-0° samples is similar to that observed in standard SMC [16-17]. For this configuration,

damage is mostly governed by debonding of fiber-matrix interfaces which still appears at less than 30% of the failure stress in a diffuse manner and preferentially in the more disoriented fibers. Indeed, as a result of the 0° predominant fiber orientation, the load is distributed more homogeneously between bundles and matrix. Thus, apart from fiber-matrix interface failure described above, no other significant damage mechanism has been noticed until 1.60 $\sigma_{r(RO)}$ (just before failure) for which value of matrix breakage appears in the predominant matrix areas. These observations showed that no evident correlation between matrix failure and HGM presence has been pointed out.

- Fracture surface observations:

Post-mortem SEM observations of fracture surfaces have also been used to investigate the role played by HGMs in the final stage of failure (Fig. 18). It can be emphasized that, for all studied fiber direction configurations, HGMs presence is involved in the final failure. Indeed, SEM micrographs highlight both debonding and breakage of the HGMs which always appears in the fracture surfaces together with debonded fiber-matrix interfaces (a, b, d and e). Micro-cracks propagation into the matrix between fibers and fiber bundles and HGMs always precedes final failure (c and f). Moreover, observation of the HO-0° fracture surfaces showed that the presence of HGMs around the more disoriented bundles of fibers promotes the failure process in these areas (d). On the other hand, when they are located around 0° oriented fibers, failure process brings about matrix failure through HGMs interface failure which fosters pull-out of the neighboring bundles of fibers (c). All these observations are in good accordance with the in-situ tensile test results, shown in Fig. 16.

This microstructural damage analysis leads to the general conclusion that damage development and failure during tensile tests performed on LD-SMC is strongly dependent of the interaction between fiber orientation and HGMs presence.

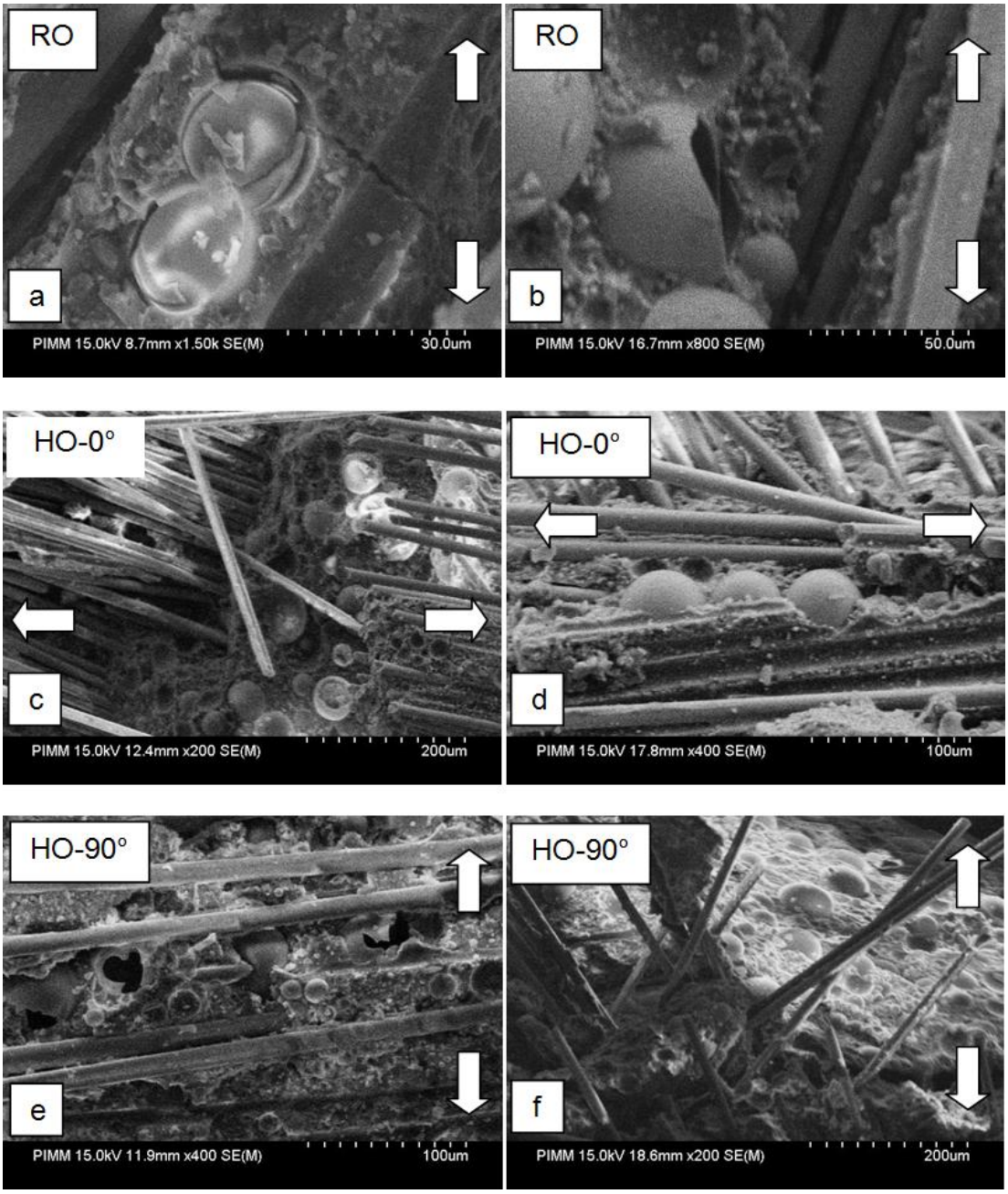

Fig. 18. SEM micrograph of failure surface after quasi-static tensile test

3.4.2. Compression tests

a) Macroscopic observation: One can notice in Fig. 14(a), that in the case of RO samples, damage threshold under compression is more than two times higher than in the case of tensile loading. However, especially for this configuration, the stress-strain curve exhibits a plateau stage which is related to a delamination phenomenon shown in Fig. 19 at macroscopic scale. On the other hand, one can note that compression tests performed on HO-0° samples

lead to wide pseudo-delamination between fiber bundles while HO-90° breakage remains much localized without significant delamination.

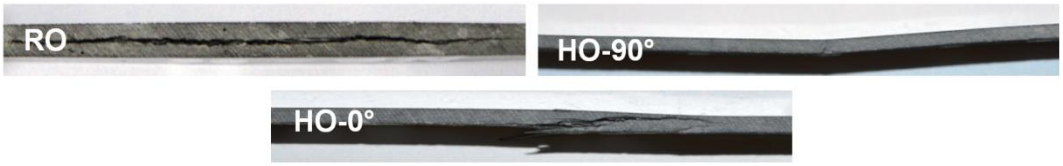

Fig. 19. Macroscopic observation of failure surface after compression test

b) Fracture surface observations: Microscopic observation of RO sample after compression test (Fig. 20) confirms that a macroscopic delamination occurs consecutively to debonding at the hollow glass spheres-matrix interfaces. This appears clearly to be the predominant failure mechanism which is probably due to a higher content of HGM between two LD-SMC sheets during elaboration.

However, this phenomenon is not observed for HO microstructure. Indeed, in the case of HO-0° and HO-90°, compression load is distributed more homogeneously between fiber bundles and matrix. Then, after each damage event, local stresses are redistributed in other locations. Consequently, damage mechanisms propagate in a diffuse manner similarly to those observed under tensile loading.

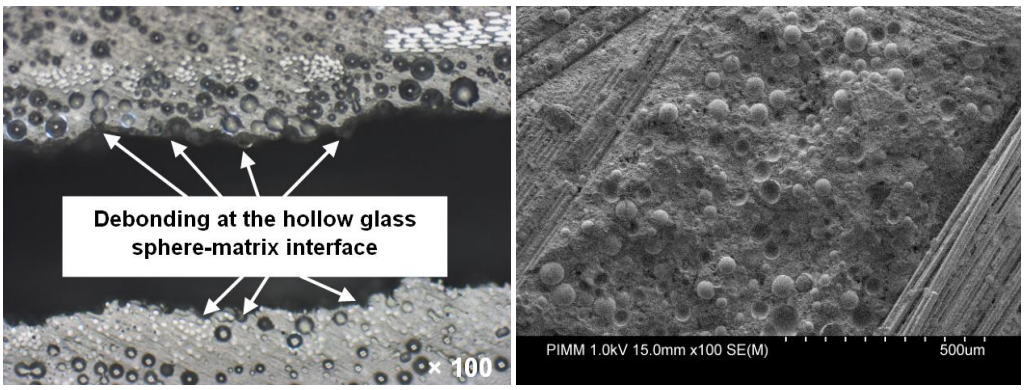

Fig. 20. Microscopic observation of failure surface after compression test of RO sample

3.5. Effects of strain-rate and microstructure on the overall tensile response

LD-SMC automotive structures are frequently submitted to crash events. Thus, in order to complete the overall characterization of LD-SMC mechanical behavior proposed in this

paper, a study of the strain rate effect is needed. Following the procedure described in section 2.3.5, stress-strain (σ-ε) tensile tests curves are plotted for increasing strain rates up to 80 s^{-1} for RO and HO samples. Typical curves are shown in Fig. 21. One can clearly note that the overall behaviors of LD-SMCs is highly load-rate dependent. However, although there are some slight fluctuations due to microstructure dispersion, no significant evolution of the young's modulus is observed (Fig. 22). The elastic behavior can be considered to be insensitive to strain rate in the studied strain rate range. Then, independently one can consider that average values of Young's moduli are 10, 9 and 12 GPa for RO, HO-90° and HO-0° samples, respectively, independently of the strain rate.

Moreover, the evolution of other mechanical characteristics versus strain rate has been estimated. Namely, stress and strain damage thresholds ($\sigma_{threshold}$, $\varepsilon_{threshold}$) and stress and strain ultimate values ($\sigma_{ultimate}$, $\varepsilon_{ultimate}$).

Strain rate effect on LD-SMC brings about a strong damage onset delay. In fact, damage thresholds (Fig. 23(a) and (b)) strongly increase with strain rate for the three kinds of samples. For example, one can note an increase of threshold stress average values from QS to 80 s^{-1}, of 120%, 130% and 114% for HO-0°, R0 and HO-90° samples respectively. Comparatively, failure characteristics are less influenced by strain rate for which moderate increase of ultimate stress average values are observed: 33%, 58% and 55% respectively. On the other hand, observations of fracture surfaces of specimens broken at high loading rate did not reveal significant differences compared to those broken at low or quasi-static rates. Indeed, when increasing strain rate, damage mechanisms initiation and propagation such as debonding at the fiber-matrix or HGM-matrix interfaces might be delayed. A general conclusion of this part of the study is that, similar to SMCs [16-17] and A-SMCs [20-21], high strain rate effect on LD-SMCs brings about the viscous nature of the damage at the local scale and leads to an apparent visco-damageable behavior at the macroscopic scale.

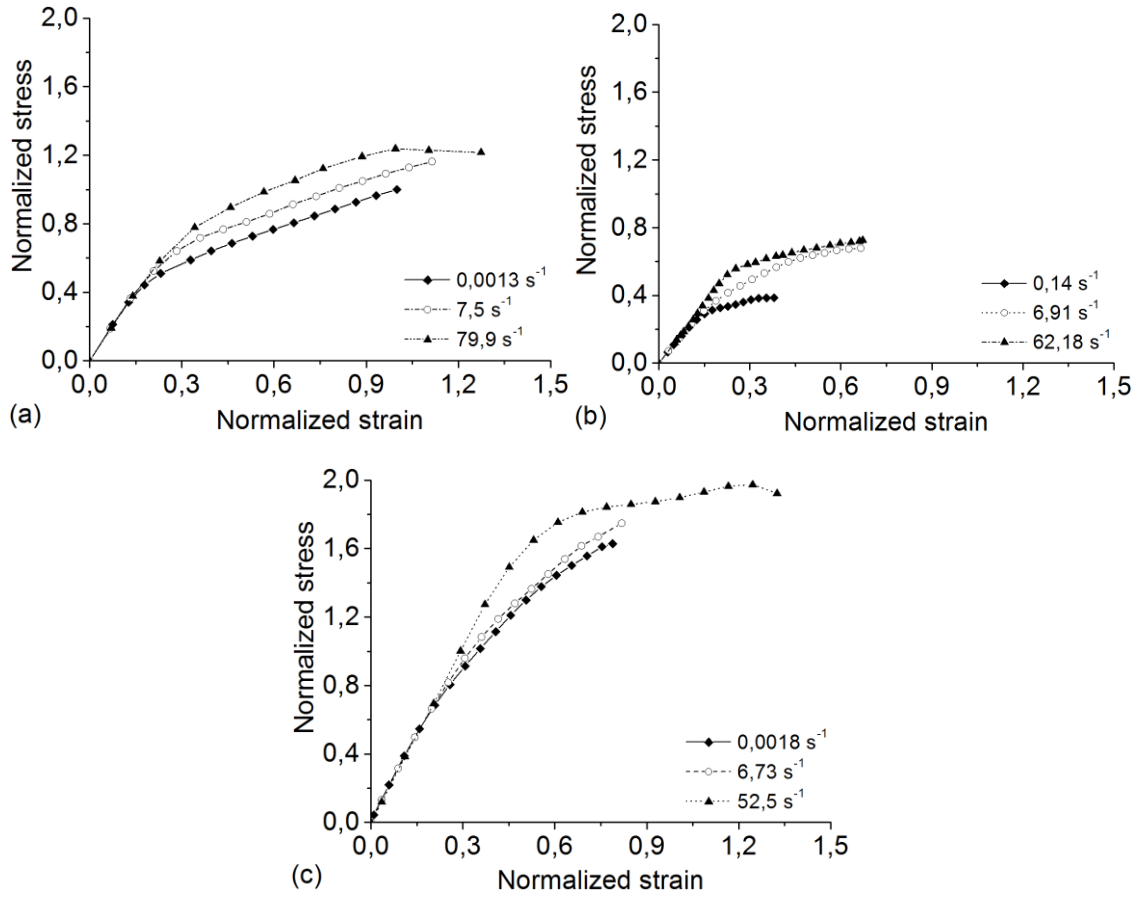

Fig. 21. Experimental high strain rate tensile curves: (a) RO, (b) HO-90° and (c) HO-0° (Normalized value = current value / average value obtained for quasi-static tests performed on RO-LD-SMC)

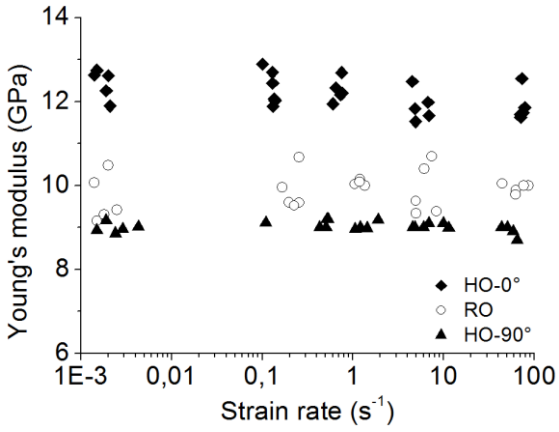

Fig. 22. Evolution of the Young's modulus vs. strain rate

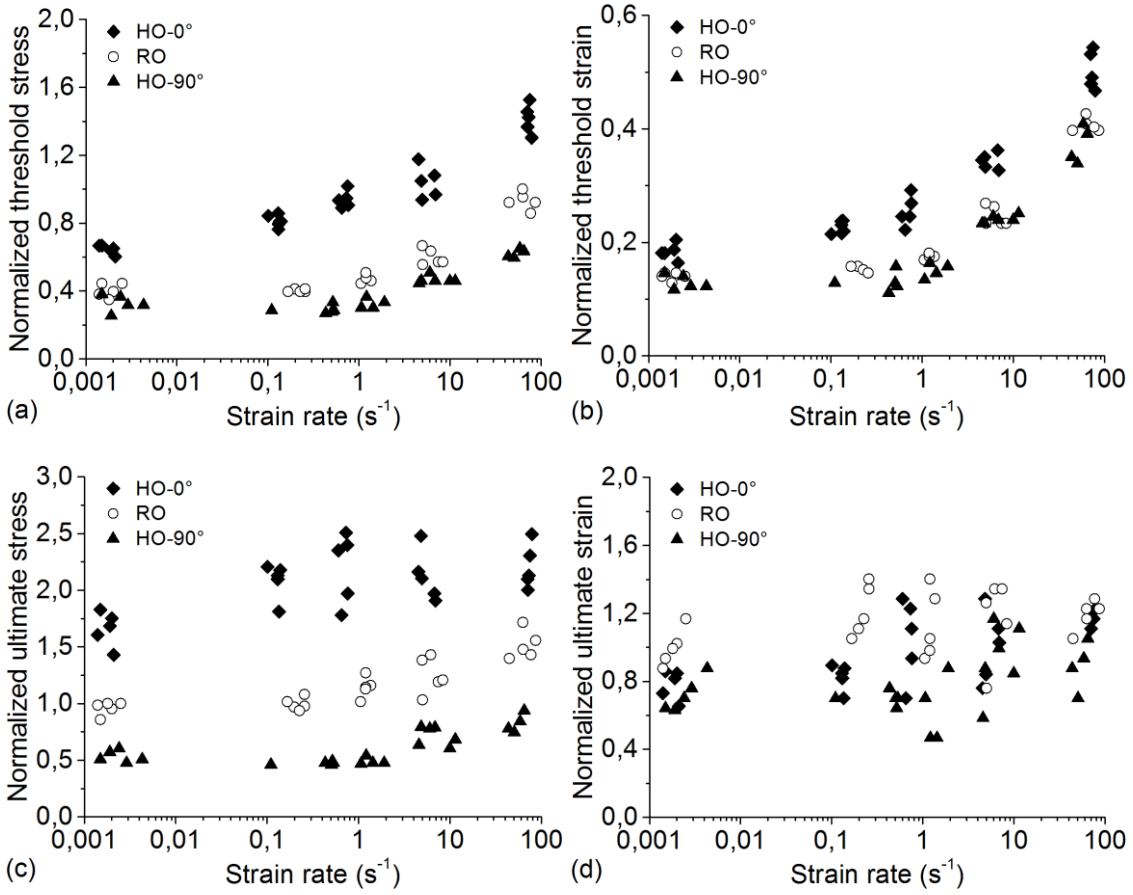

Fig. 23. Influence of strain rate: (a) Normalized threshold strain, (b) Normalized threshold stress, (c) Normalized ultimate strain and (d) Normalized ultimate stress (Normalized value = current value / average value obtained for quasi-static tests performed on RO-LD-SMC)

4. Conclusion

A multi-scale experimental analysis of the influence of HGMs in LD-SMC microstructure has been performed. A general conclusion to be drawn from this work is that the introduction of HGM strongly influences damage development and failure of LD-SMC. Three microstructure configurations of LD-SMCs (RO, HO-90° and HO-0°) were prepared and submitted to tension and compression loading. In order to emphasize the coupled effect of HGMs presence and fiber orientation distribution, damage mechanisms development has been investigated at the microscopic scale. Finally, an evaluation of the strain rate effect concludes this study.

The main conclusions of this work may be specified in various areas as follows:

- HGMs are homogeneously distributed into the overall volume of the material. They are mainly localized around the glass fiber bundles and in the fiber depleted zones.
- Fiber orientation distribution strongly influences the mechanical response of LD-SMC.
- No significant asymmetry has been observed between tensile and compression curves for HO configuration, although compression damage threshold is deleted during compression loading of RO specimens.
- Despite some scattering due to microstructure variations, the elastic modulus is insensitive to strain rate. Strain rate has an obvious influence on the inelastic properties of LD-SMCs samples for all microstructures particularly on the damage threshold (first non-linearity).
- When the fibers are mostly oriented in the loading direction (HO-0° configuration) fiber-matrix debonding appears to be the predominant damage mechanism, when the fibers are mostly oriented perpendicularly to the loading direction (HO-90° configuration), HGM-matrix debonding appears to be the predominant damage mechanism.
- Final failure is always affected by the presence of the HGMs more or less coupled to the fiber-matrix interface debonding depending on the fiber orientation distribution: the more the fibers are oriented perpendicularly to the loading direction, the more HGM debonding drives the final failure.
- Concentration of HGMs between two SMC sheets after processing leads to a macroscopic delamination in compression,
- One may conclude that there is a coupled effect of the viscous nature of HGMs-matrix and fiber-matrix interfaces which leads to a strong influence of the strain rate on the macroscopic behavior of LD-SMCs.

5. References

[1] E. Commission. Further CO_2 emission reduction from cars and vans: a win-win for the climate, consumers, innovation and jobs. Brussels, 2012.

[2] J. Palmer, L. Savage, O. R. Ghita, K. E. Evans. Sheet moulding compound (SMC) from carbon fiber recyclate. Composites Part A: Applied Science and Manufacturing, 2010, 41 (9): 1232-1237.

[3] A. Kraemer, S. Lin, D. Brabandt, T. Böhlke, G. Lanza. Quality Control in the Production Process of SMC Lightweight Material. Procedia CIRP, 2014, 17: 772-777.

[4] M. Fette, P. Sander, J. Wulfsberg, H. Zierk, A. Herrmann, N. Stoess. Optimized and Cost-efficient Compression Molds Manufactured by Selective Laser Melting for the Production of Thermoset Fiber Reinforced Plastic Aircraft Components. Procedia CIRP, 2015, 35: 25-30.

[5] B. Huang, L. Zhao. Bridging and toughening of short fibers in SMC and parametric optimum. Composites Part B: Engineering, 2012, 43(8): 3146-3152.

[6] A. Asadi, M. Miller, A. V. Singh, R. J. Moon, K. Kalaitzidou. Lightweight sheet molding compound (SMC) composites containing cellulose nanocrystals. Composite Structures, 2017, 160: 211-219.

[7] A. Asadi, F. Baaij, H. Mainka, M. Rademacher, J. Thompson, K. Kalaitzidou. Basalt fibers as a sustainable and cost-effective alternative to glass fibers in sheet molding compound (SMC). Composites Part B: Engineering, Available online 9 May 2017, In Press.

[8] P. T. Odenberger, H. M. Andersson, T. S. Lundström. Experimental flow-front visualisation in compression moulding of SMC. Composites Part A: Applied Science and Manufacturing, 2004, 35(10): 1125-1134.

[9] M. S. Kim, W. I. Lee, W. S. Han, A. Vautrin, C. H. Park. Thickness optimization of composite plates by Box's complex method considering the process and material parameters in compression molding of SMC. Composites Part A: Applied Science and Manufacturing, 2009, 40(8): 1192-1198.

[10] P. Dumont, L. Orgéas, D. Favier, P. Pizette, C. Venet. Compression moulding of SMC: In situ experiments, modelling and simulation. Composites Part A: Applied Science and Manufacturing, 2007, 38: 353-368.

[11] M. S. Kim, W. I. Lee, W. S. Han, A. Vautrin. Optimization of location and dimension of SMC pre-charge in compression molding process. Computers & Structures, 2011, 89(15-16): 1523-1534.

[12] D.-K. Kim, H.-Y. Choi, N. Kim. Experimental investigation and numerical simulation of SMC in compression molding. Journal of Materials Processing Technology, 1995, 49(3-4): 333-344.

[13] C. H. Park, W. I. Lee, Y. E. Yoo, E. G. Kim. A study on fiber orientation in the compression molding of fiber reinforced polymer composite material. Journal of Materials Processing Technology, 2001, 111(1-3): 233-239.

[14] J. Grabalosa, I. Ferrer, A. Zúñiga, J. Ciurana. Influence of processing conditions on manufacturing polyamide parts by ultrasonic molding. Materials and Design, 2016, 98: 20-30.

[15] M. Oldenbo, S. P. Fernberg, L. A. Berglund. Mechanical behaviour of SMC composites with toughening and low density additives. Composites Part A: Applied Science and Manufacturing, 2003, 34(9): 875-85.

[16] Z. Jendli, F. Meraghni, J. Fitoussi, D. Baptiste. Micromechanical analysis of strain rate effect on damage evolution in sheet molding compound composites. Composites Part A: Applied Science and Manufacturing, 2004, 35(7-8): 779-785.

[17] Z. Jendli, J. Fitoussi, F. Meraghni, D. Baptiste. Anisotropic strain rate effects on the fibre-matrix interface decohesion in sheet moulding compound composites. Composites Science and Technology. 2005, 65(3-4): 387-93.

[18] F. Fereshteh-Saniee, G. H. Majzoobi, M. Bahrami. An experimental study on the behavior of glass-epoxy composite at low strain rates. Journal of Materials Processing Technology, 2005, 162-163: 39-45.

[19] S. Gurusideswar, R. Velmurugan, N. K. Gupta. High strain rate sensitivity of epoxy/clay nanocomposites using non-contact strain measurement. Polymer, 2016, 86: 197-207.

[20] M. Shirinbayan, J. Fitoussi, F. Meraghni, B. Surowiec, M. Bocquet, A. Tcharkhtchi. High strain rate visco-damageable behavior of Advanced Sheet Molding Compound (A-SMC) under tension. Composites Part B: Engineering, 2015, 82: 30-41.

[21] M. Shirinbayan, J. Fitoussi, M. Bocquet, F. Meraghni, B. Surowiec, A. Tcharkhtchi. Multi-scale experimental investigation of the viscous nature of damage in Advanced Sheet Molding Compound (A-SMC) submitted to high strain rates. Composites Part B: Engineering, 2017, 115: 3-13.

[22] ID19 ESRF. <http://www.esrf.eu/UsersAndScience/Experiments/Imaging/ID19>.

[23] K. Schladitz, A. Büter, M. Godehardt, O. Wirjadi, J. Fleckenstein, T. Gerster, U. Hassler, K. Jaschek, M. Maisl, U. Maisl, S. Mohr, U. Netzelmann, T. Potyra, M. O. Steinhauser. Non-destructive characterization of fiber orientation in reinforced SMC as input for simulation based design. Composite Structures, 2017, 160: 195-203.

[24] M. A. Dupertuis, M. Proctor, B. Acklin. Generalization of complex Snell-Descartes and Fresnel laws. Journal of the Optical Society of America A, 1994, 11 (3): 1159-1166.

[25] D. Krajcinovic, S. Mastilovic. Some fundamental issues of damage mechanics. Mechanics of Materials, 1995, 21 (3): 217-230.

[26] D. Krajcinovic. Selection of damage parameter - Art or science. Mechanics of Materials, 1998, 28(1-4): 165-179.

[27] L. Yang, Z. Wu, D. Gao, X. Liu. Microscopic damage mechanisms of fibre reinforced composite laminates subjected to low velocity impact. Computational Materials Science, 2016, 111: 148-156.

[28] R. M. Bajracharya, A. C. Manalo, W. Karunasena, K. Lau. An overview of mechanical properties and durability of glass-fiber reinforced recycled mixed plastic waste composites. Materials and Design, 2014, 62: 98-112.

[29] V. Feuillade, A. Bergeret, J. C. Quantin, A. Crespy. Relationships between the glass fibre sizing composition and the surface quality of sheet moulding compounds (SMC) body panels. Composites Science and Technology, 2006, 66(1): 115-127.

Article N°5:

Shirinbayan M, Fitoussi J, Meraghni F, Farzaneh S, Surowiec B, Tcharkhtchi A. Post-fatigue residual dynamic behavior of advanced-SMC composites. Article in progress.

Post-fatigue residual dynamic behavior of advanced-SMC composites

M. Shirinbayan[1,*], J. Fitoussi[1], F. Meraghni[2], S. Farzaneh[3], B. Surowiec[4], A. Tcharkhtchi[1]

[1] Arts et Métiers ParisTech, PIMM – UMR CNRS 8006, 151 Boulevard de l'Hôpital, 75013 Paris, France:

E-mails: joseph.fitoussi@ensam.eu, navideh.abbasnezhad@ensam.eu, abbas.tcharkhtchi@ensam.eu;

[2] Arts et Métiers ParisTech, LEM3 – UMR CNRS 7239, 4 Rue Augustin Fresnel, 57078 Metz, France:

E-mail: fodil.meraghni@ensam.eu;

[3] P4 Tech, 94 rue Léon Geffroy, 94440 Vitry Sur Seine, France: E-mail: sedigheh.farzaneh@ensam.eu;

[4] Plastic Omnium Auto Exterior, Sigmatech, Sainte Julie, France:

E-mail: benjamin.surowiec@plasticomnium.com.

Abstract

The paper aims at investigating the effect of an initial pre-damage induced by fatigue loading on the tensile dynamic behavior of Advanced Sheet Molding Compounds (A-SMC). Tension-tension fatigue preloading at a frequency of 30Hz is performed at different applied stress levels prior to subject the A-SMC specimens to tensile tests at different strain rates, namely 10^{-3} s^{-1} (quasi-static), 1 s^{-1} and 60 s^{-1}. The developed experimental approach provided important experimental findings in terms of residual behavior and damage accumulation in relation with the applied pre-fatigue loading conditions. Indeed, it has been shown that the overall quasi-static and the dynamic responses are strongly affected by the level of fatigue number of cycles reached prior applying the high strain loading. The effect of the fatigue pre-damage is found also strongly strain-rate dependent. Experimental results showed that the damage threshold in terms of stress and strain increased with strain rate. However, for a given strain-rate the damage stress threshold depends on the number of cycles applied during the fatigue preloading.

Keywords: Fatigue, Pre-damage, Dynamic, Residual behavior

1. Introduction

In order to protect automobile passengers from injury during a crash, car crash experiments should be performed to simulate the actual accident [1-5]. To obey this matter an optimum combination of body structure with material and also an exact evaluation of fatigue behavior and crash response of materials is highly required [4-5]. Moreover, one can note that

* Corresponding author, mohammadali.shirinbayan@ensam.eu, Tel: +33-144246105

the equipment are not always undamaged materials. In fact, in many applications specially automotive industry, materials are subjected to vibration or oscillation forces [6-8]. Fatigue test can be thought of as simply applying cyclic loading to sample to recognize how it will perform under similar conditions in real usage [6-9]. Thus, for a precise predict of crash events, the study on the behavior of the pre-damage material by fatigue tests under high strain rate loading is appreciated.

An understanding of fatigue behavior is important for any material that experiences repeated loading during service. Fatigue response of composites is usually characterized by an S-N curve, also known as a Wöhler curve [5, 6]. It can be presented as a curve giving the value of cyclic stress amplitude, $\sigma_{max,}$ versus the number of cycles to failure, N. Fiber orientations, applied stresses, temperature, frequency and self-heating effects are main parameters to reliably estimate the cyclic behavior of the materials [10-12]. Wang and Chim [7] have indicated that augmentation of the fatigue stress, σ_{max}, leads to a stiffness reduction rate and shorter fatigue life. The undamaged material constitution is defined in terms of the material elastic modulus, mass density and yield stress.

The classical approach to characterize the crash events is by using high strain rate tensile tests. Mechanical response of materials is sensitive to the rate at which they are loaded. [13-18]. Therefore, for the effective use of materials, their response under various strain rates should be clearly understood.

The question asked in this paper can be formulated as follows: What is the effect of fatigue stress on the residual dynamic behavior of A-SMC material? Answering this question requires defining the scale of the analysis to be proposed. Indeed, one can be interested in this coupling at different scales: macroscopic, microscopic or even nanometric scales. From the macroscopic point of view, we must consider the evolution of the post-fatigue dynamic response, which would allow us to equip ourselves with more representative behavioral laws for the crash dimensioning of real automotive structures. Indeed, the automotive structures are hitherto always dimensioned on the basis of mechanical characterizations made on materials which have not undergone any stress. However, most automobile structures are subjected to stresses of fatigue type before they undergo a crash. On a finer scale - local phenomena of

deformation and damage are at the origin of the macroscopic responses. Is there at these scale specific phenomena developed during fatigue which would modify the expected response under rapid solicitation which follows? For example, in the case of thermoplastic matrix composite materials, it has been shown that repeated stresses may produce a progressive accumulation of plastic deformation and / or specific damage phenomena at the interfaces / interphase fiber-matrix. Finally, on an even finer scale, one can also ask the question of the effect of modifications of the macromolecular architecture in fatigue test.

One can note that the mechanical behavior during subsequent loading appears to be only slightly affected by the type of initial loading mode. Two sequences of tension/fatigue and fatigue/tension tests were performed on copper poly-crystal sheet by Jia et al [19]. The strain rate for the tension tests was in the domain of quasi-static tensile tests, while the fatigue tests were performed under constant plastic strain amplitude control. In the case of fatigue/tension, it was found that fatigue stage had significant influences on the subsequent yield and flow behavior in tension. For tension/fatigue, the strain amount of preloading in quasi-static tensile test clearly affected the initial cyclic loading, while it had almost no effect on the saturation stress of following fatigue test.

An impact fatigue study on 35% jute/vinyl-ester composites [20] showed that, the defect concentration played an important role in the fatigue behavior of the composites under impact loading.

Epaarachchi [21] investigated the effects of static-fatigue interaction on tension-tension fatigue life of glass fiber reinforced plastic (GFRP) composites. Static-fatigue interaction results showed a considerable effect on fatigue behavior of GFRP composites at intermediate and lower applied stress levels possibly due to a longer exposure to applied loads.

What is the impact of these different types of evolution on the residual behavior under rapid solicitation? It is clear that this theme could be the subject of several years of research. In this work, we will only propose a comparison of the post-fatigue dynamic properties with that of the same virgin material. As mentioned above, this comparison is necessary in order to ensure a realistic dimensioning.

SMCs and A-SMCs are high strength glass reinforced thermoset molding materials processed by thermo-compression [22-23], which are ideal for large structural automotive components because of their high strength-to-weight ratio [13]. Vinyl-esters resins used for new Advanced SMCs (A-SMC) exhibit many desirable features, including mechanical properties comparable to those of epoxy. It was reported that fiber-matrix interface debonding, matrix micro cracking, fiber pull-out and breakage, delamination and pseudo-delamination were some of the main damage mechanisms observed under fatigue tests for SMC composites. Tensile curves obtained for A-SMC samples showed clearly that the overall behavior is highly load-rate dependent. Indeed, under rapid tensile load, A-SMC composites exhibit typically a non-linear response. Measuring Young's modulus and material mechanical characteristics such as damage thresholds corresponding to the first non-linearity ($\sigma_{threshold}$; $\varepsilon_{threshold}$) and ultimate stress and strain ($\sigma_{ultimate}$; $\varepsilon_{ultimate}$) as a function of strain rate have been developed for glass fiber reinforced composites, specially A-SMC composites [13-18].

So far no sequential loading study, which is highly related to technical applications, has been performed on SMC composites with fatigue as one of the loading modes and high strain rate as the second loading mode. This test is very remarkable to determine the mechanical characterization of the Advanced SMC (A-SMC).

Randomly Oriented A-SMC (RO-A-SMC) plates have been provided by Plastic Omnium Auto Exterior. In this paper, an experimental procedure is carried-out to investigate the effect of strain rate on the overall behavior of pre-damage RO-A-SMC under fatigue tests. In the coupled loading of fatigue crash, the fatigue procedures with quasi-static and high loading amplitudes perform until defined cycles before failure of samples at the frequency of 30Hz. One can note that, this value of frequency is equal to vehicle vibration while using. After fatigue stage, damaged composite is subjected to quasi-static and high strain rate tensile test to simulate crash events.

After a microstructure presentation of A-SMC composite, the fatigue procedures in certain amplitudes and until defined cycles without failure of samples were presented in the preliminary characterization. All cyclic tests were performed at the frequency equal to 30Hz. After performing the fatigue tests until certain cycles, the tensile tests by varying the staining

rate from the quasi-static to 60 s^{-1} were applied. The results of material characteristics, namely Young's modulus (E); damage thresholds corresponding to the first non-linearity ($\sigma_{threshold}$; $\varepsilon_{threshold}$) and ultimate stress and strain ($\sigma_{ultimate}$; $\varepsilon_{ultimate}$) were discussed.

2. Material description and methods

2.1. Advanced Sheet Molding Compound (A-SMC) composite

Advanced Sheet Molding Compound (A-SMC) composite consists of a vinylester matrix with a high content of glass fibers (50% in mass corresponding to 38.5% in volume, 25 mm length). A-SMC as a thermoset material is a serious candidate for structural parts in the automotive industry. The process of manufacturing has been discussed in the previous paper [13]. The low process time is mandatory in the automotive industry due to the high production rhythm. The composition of A-SMC is shown in Table 1. For the need of this study, Randomly Oriented (RO) plates of A-SMC composite have been provided by Plastic Omnium Auto Exterior.

Product nature	Composition (content in mass percent)
Glass fibers	50 %
Vinyl-ester resin	24 %
Filler	24 %
Other products	2 %

Table 1. A-SMC composition

2.2. Methods

2.2.1. Characterization methods

- X-ray micro-tomography: It allowed a three-dimensional visualization of A-SMC. EasyTom nano setup, which comprises an X-Ray source, a rotating table and an X-ray detector, was used. The studied sample (1 × 1 × 3 cm^3) was placed between the X-ray beam and the camera detector. The principle of operation of the microstructure analysis by X-ray micro-tomography is widely described in [24].

- Microscopic observations: Using Scanning Electronic Microscope (HITACHI 4800 SEM), have been performed with the aim to investigate qualitatively the material microstructure and especially crack propagation during fatigue tests.

- Thermo-mechanical properties: In order to measure the main transitions temperatures due to molecular mobility as a function of temperature, DMTA tests have been performed on RO-A-SMC samples at room temperature using DMA Q800 instrument, from TA Company. The tests have been realized at following condition: alternating bending configuration; temperature range from -100 °C to 250 °C; frequency 1Hz; temperature rate 2 °C/min.

2.2.2. Fatigue tests

Tension-tension fatigue tests have been performed at different applied maximum stress on MTS 830 hydraulic fatigue machine. The minimum applied stress is always chosen to be equal to 10% of the maximum applied stress. In this paper, the results of experiments performed at the frequency of 30Hz are presented. In order to measure precisely the stiffness reduction due to the first loading stage, each fatigue test is preceded by a quasi-static tensile loading-unloading-reloading stage.

During cyclic loading, the temperature rise (due to self-heating) has been measured using an infrared camera (Raynger-MX4) in the specific area (maximum temperature). The evolution of Young's modulus is also determined.

2.2.3. Tensile tests

- Quasi static tensile tests: Quasi static tensile tests by velocity of 2 mm/min have been performed with MTS 830 hydraulic machine.

- High-speed tensile tests: High-speed tensile tests have been performed upon a servo-hydraulic test machine. As specified by the manufacturer (Schenk Hydropuls VHS 5020), the test machine can reach a crosshead speed range from 10^{-4} m/s (quasi-static) to 20 m/s. Moreover, the load level is measured by a piezoelectric crystal load cell having a capacity of a 50 kN. High-strain rate tensile tests were conducted at different strain-rates until the composite specimen total failure. The test machine is equipped with a launching system. The specimen is positioned between the load cell (upper extremity) and the moving device (lower extremity) as

sketched in Fig. 1. A contactless technique [13] was used to measure the local deformation using a high speed camera (FASTCAM-APX RS).

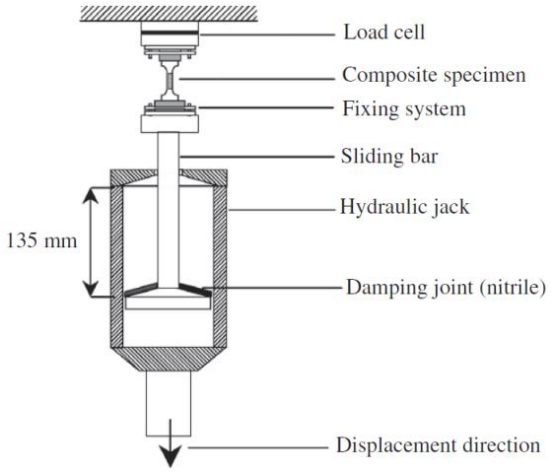

Fig. 1. Experimental device used for high-speed tensile tests

2.2.4. Specimen geometry

In a previous study [13], on the basis of FE simulations and assuming that the specimen behaves like an elastic anisotropic solid, a recursive optimization procedure results in the determination of optimal geometrical parameters for high speed tensile tests: L_1, L_2, L_3 and R (Fig. 2). These parameters are optimized in such a way of reducing the stress wave effects in the overall response and of generating homogeneous stress/strain field during high strain rate tensile tests. The experimental coupled loading of fatigue crash was performed on the same geometry of sample.

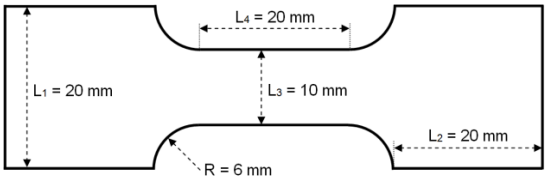

Fig. 2. Obtained specimen dimension from optimization procedure results

3. Experimental results and discussion

3.1. Microscopic characterization

For three-dimensional visualization of A-SMC composite (Fig. 3), X-ray tomography technique was used. Actually, it can be observed not only microstructures of the skin, but also those of the shell and core. Indeed, fibers are initially randomly oriented before compression molding. The complete characterizations of A-SMC composite provided by Plastic Omnium Auto Exterior have been presented in the previous paper [13].

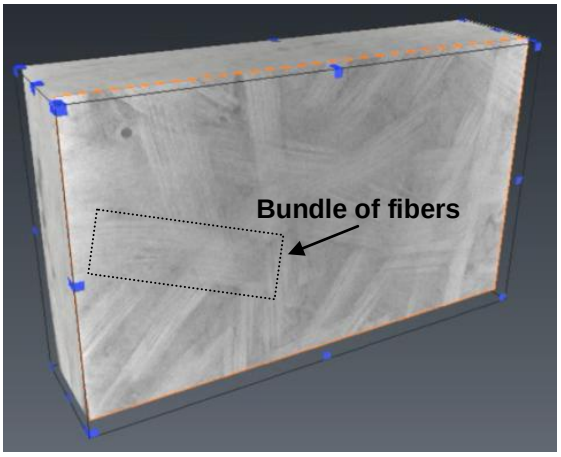

Fig. 3. Three-dimensional visualization of A-SMC composite

3.2. Thermo-mechanical properties

In order to measure the main transitions temperatures due to molecular mobility as a function of temperature, DMTA tests have been performed on RO-A-SMC samples at room temperature. Fig. 4 shows the evolution of the storage modulus and the loss modulus versus temperature obtained by DMTA test.

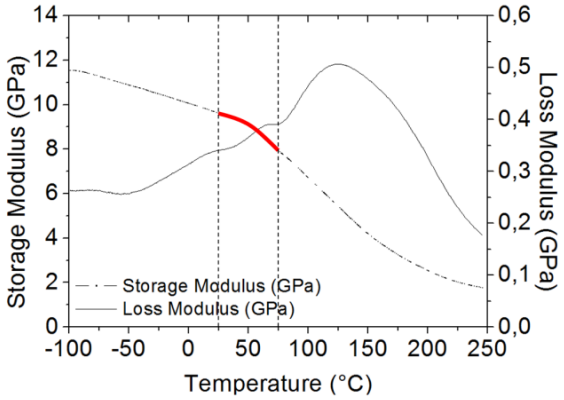

Fig. 4. DMTA test performed on RO-A-SMC

A-SMCs present a vitreous transition temperature lying between 60 and 200 °C. It can be assumed that the glass transition temperature is about 130 ºC. Although the temperature range from 25 °C to 75 °C corresponds to the zone of the β transition known in amorphous polymers as being the ductile-brittle transition. This zone relates to the scale of the macromolecules with sufficient thermal agitation to activate the movement of the radicals at the periphery of the carbon chain. This zone can be considered as centered around 45 °C.

3.3. Fatigue behavior analysis

3.3.1. Wöhler curve and self-heating phenomenon

Fig. 5(a) shows the Wöhler curve of A-SMC samples at frequency of 30Hz. It shows a bilinear form defining two different zones related to the high and low loading amplitude fatigue behavior. In this case, high loading amplitude zone corresponds to fatigue life less than 2000 cycles for loading amplitude up to 0.62 σ_r. At the end of the high loading amplitudes, the curve starts deviating. It can be noticed that in this case for a maximum applied stress equal to 0.45 σ_r, the fatigue life is about 10^5 cycles whilst the fatigue life is about 2×10^6 cycles for a maximum applied stress of 0.38 σ_r. Therefore, an applied stress variation of 15% leads to a fatigue life 20 times higher.

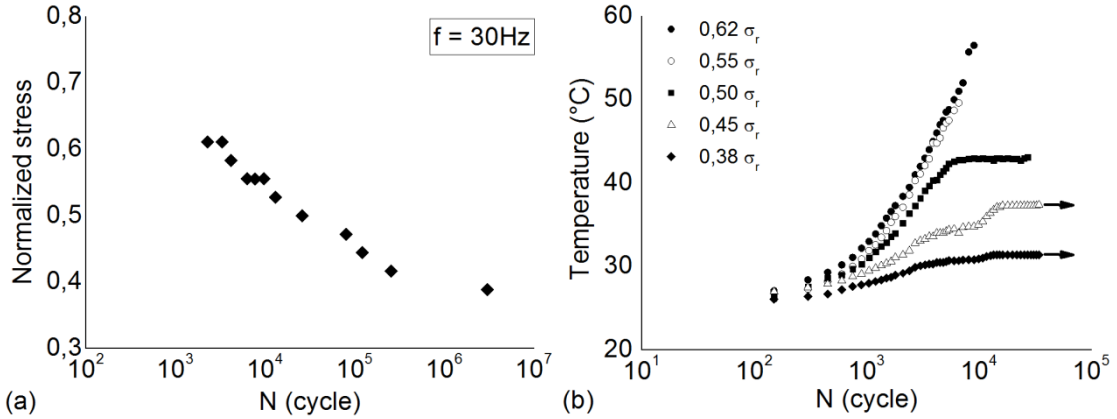

Fig. 5. (a) Normalized Wöhler curve at frequency of 30Hz, (b) Temperature variation at different amplitudes and frequency of 30Hz (Normalized value = current value / average ultimate stress value (σ_r) obtained for tests performed on RO-A-SMC)

Fig. 5(b) illustrates the variation of temperature during fatigue tests at different amplitudes (f = 30 Hz). One can observe there is not a significant change in the temperature up to 200 cycles. In the case of fatigue tests at 0.62 σ_r, the temperature increases rapidly from room temperature to 50°C up to 2000 cycles while temperature variation is low for fatigue tests of 0.38 σ_r. Self-heating depends directly on the viscoelastic behavior of the polymer. It was shown that, this behavior is related to the applied loading. So it can logically be supposed that by increasing the applied loading, the self-heating temperature increases during fatigue test but the viscosity of the matrix decreases [13, 25-26]. Therefore, to study the effect of strain rate on the overall behavior of pre-damage A-SMC, the fatigue procedures with applied stresses of 0.38 σ_r, 0.45 σ_r (low loading amplitudes) and 0.55 σ_r (high loading amplitudes) were chosen until defined cycles before failure of samples at frequency of 30Hz. One can note that, these amplitudes of applied stress and defined cycles haven't a significant effect on temperature rise. This means self-heating phenomenon can't be greatly influence on the coupled loading of fatigue dynamic.

3.4. Methodology to analyze dynamic post-fatigue

In order to demonstrate the specific effect of fatigue on dynamic behavior of A-SMC composite, we need to define a reference state to which we will compare post-fatigue dynamic behavior. Since it has been demonstrated that damage is the driving force behind the behavior of A-SMC composites, it is possible to fix the change in stiffness as an indicator of damage. From a phenomenological point of view, the relative stiffness (E/E_0) evolves during the loading for both types of loading: fatigue and tensile test (increasing monotone quasi-static or dynamic). Consider a loading-unloading test performed on a composite A-SMC up to a stress value σ_1. If the non-linearity threshold is exceeded, σ_0, micro-cracks develop at the local scale defining a damaged state characterized by a lesser Young's modulus. If we reload again, a new value of the nonlinearity threshold will be observed close to σ_1 and a break for a value equivalent to that of the virgin material (see Fig. 6). Thus, regardless of the strain rate, the non-linearity threshold will always correspond to a value close to the maximum stress previously achieved. Moreover,

the rupture should always occur for a value close to the rupture stress of the virgin material (Fig. 6).

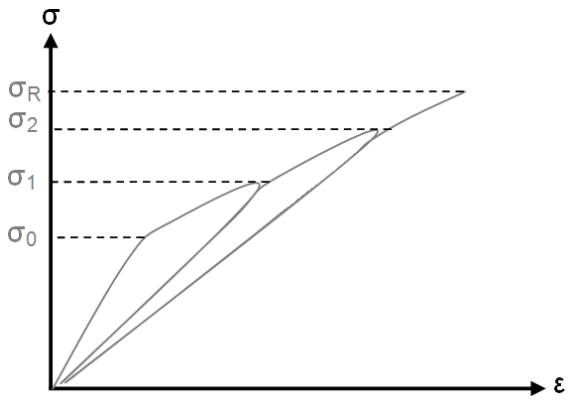

Fig. 6. Evolution of the threshold of apparent damage during the stress

Let us now consider tensile curves at different strain rates as well as a given damaged state of the material characterized by a modulus E lower than the modulus of the virgin material E_0. If this reference damage state (module E) is considered to be that obtained in monotonic tension, the evolution of the damage threshold for this reference state can be plotted by construction as in Fig. 7. This curve, evolution of the damage threshold as a function of the strain rate, can be plotted for different states of damage (different modules E).

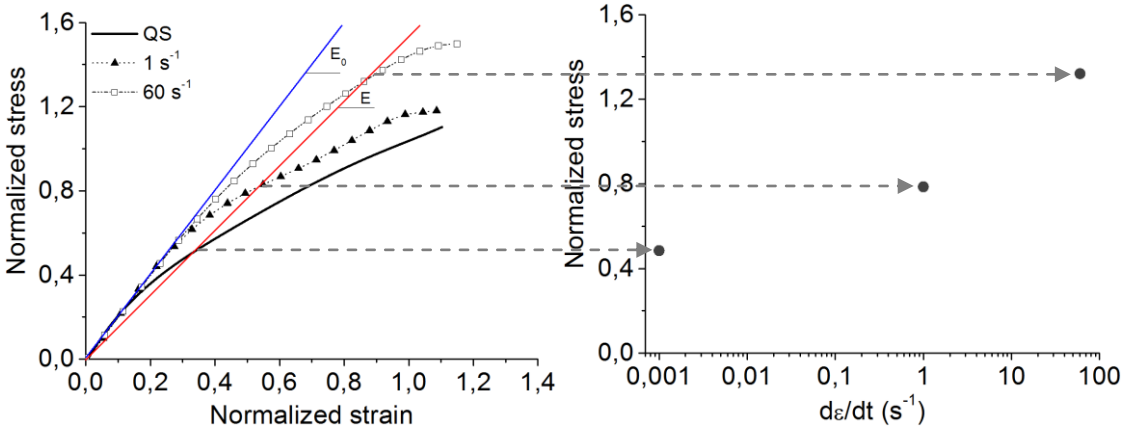

Fig. 7. Evolution of the apparent damage threshold as a function of the strain rate for a given damage state

It is therefore possible to define a reference curve of the evolution of the threshold as a function of the strain rate per state of considered damage.

However, this state of macroscopic damage (module E) can also be achieved by a partial stress of fatigue type (Figs. 8 and 9). The methodology proposed in this study consists in comparing the iso-damage evolution curves (modulus E) obtained from post-fatigue dynamic tests to those which can be obtained in monotonic dynamic traction (as in figure 7). The comparison will be made on successive equivalent E damage states corresponding to different values of the lifetime fraction, N/N_r. The remaining potential of a pre-damaged sample is then compared with the pre-damaged monotonic tension at different strain rates. The differences observed between the post-fatigue and the monotonic tensile evolutions will be attributed to the specific phenomena developed in fatigue. For example, the deviation observed on the damage threshold may be calculated for different conditions (Amplitude, N/N_r, ε̇) by the following expression:

$$\mathrm{Ecart}_{\sigma_{threshold}} = \frac{\sigma_{threshold}^{reference} - \sigma_{threshold}^{post-fatigue}}{\sigma_{threshold}^{reference}} \qquad (9)$$

This methodology therefore makes it possible to demonstrate, for macroscopic damage states (E) equivalent, differences in the structural state of the damaged material. In other words, this study attempts to answer the following question: has a pre-damage performed in monotonic tension produce, from the view point of the macroscopic properties under rapid loading, the same effects as the same level of pre-damage that would be obtained in fatigue? In other words, what would be the effect of fatigue on the remaining potential at different loading strain rates?

The selected variability parameters will be the fatigue lifetime fraction N/N_r which is directly related to the damage state characterized by fatigue due to the decrease in relative stiffness E/E_0 (Figs. 8 and 9). Another parameter is the amplitude of the applied stress in fatigue. Three values of applied stress were defined: 0.38 σ_r, 0.45 σ_r and 0.55 σ_r (σ_r: ultimate stress obtained for quasi-static tensile tests serving as a reference). The fatigue tests were interrupted at different values of the lifetime fraction, N/N_r, i.e. around 3%, 15%, 35% and 50% according to the table 2.

The correct repeatability of the interrupted fatigue tests is checked on the curves of decrease of relative stiffness (Fig. 8).

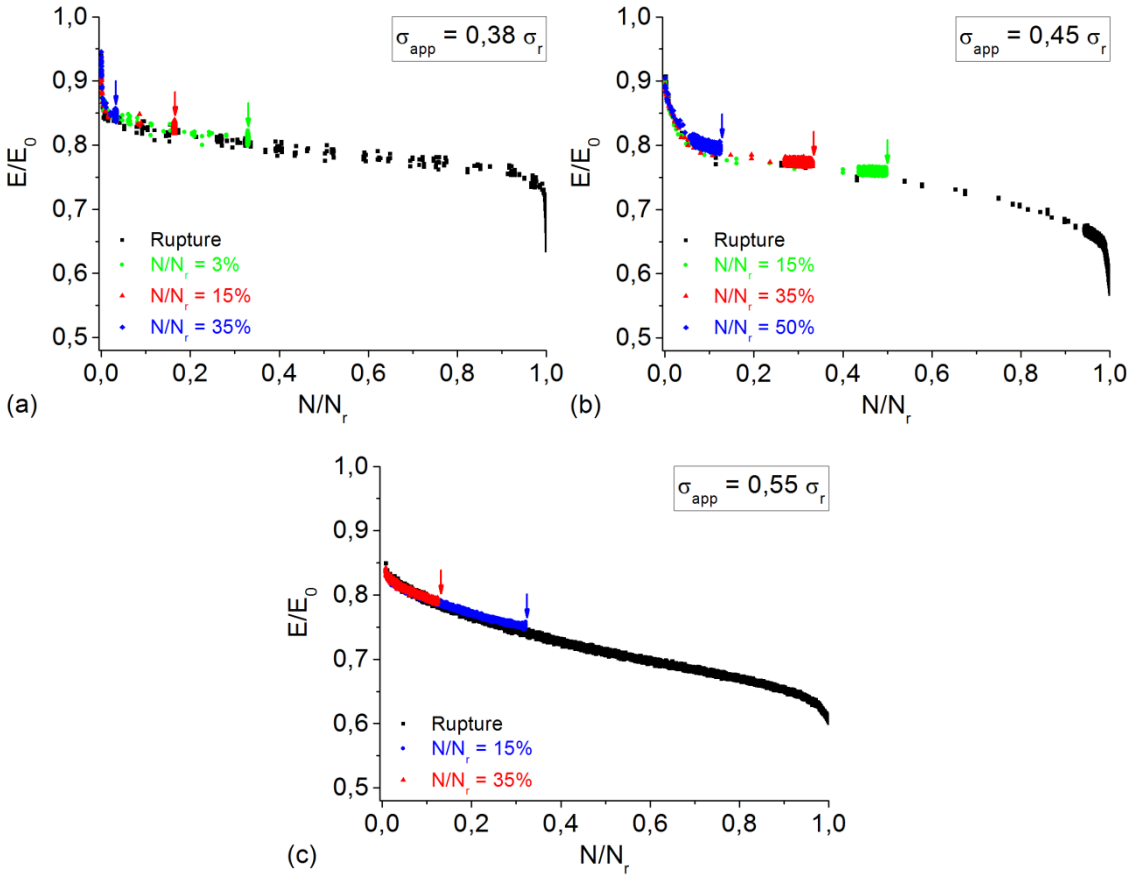

Fig. 8. Evolutions of the relative Young's modulus for different applied stresses and certain defined cycles; (a) 0.38 σ_r, (b) 0.45 σ_r and (c) 0.55 σ_r

The representative curves $E/E_0 = f(N/N_r)$ are grouped in Fig. 15 for the three applied amplitudes.

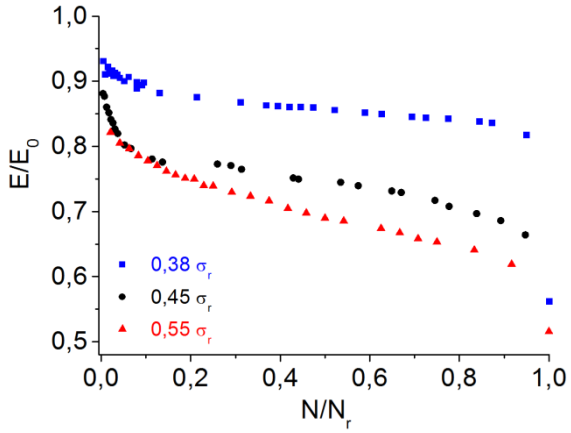

Fig. 9. Evolution of the relative stiffness as a function of the lifetime fraction

Following the interruption of the fatigue test (Figure 8), monotonic tensile tests are carried out around three strain rates: 10^{-3} s^{-1}, 1 s^{-1} and 60 s^{-1}. The details of this procedure are shown in table 2. For each of the test conditions of this procedure (Amplitude, N/N_r, ε̇), the tests were carried out four times. All the tests were carried out on the optimized sample geometry (Fig. 2) in order to ensure a good quality of the dynamic tests.

Fatigue test			Tensile test		
Applied stress	Defined cycles	N/N_r (%)	Strain rate		
0.38 σ_r	100 000 500 000 1 000 000	3 15 35	quasi-static	1 s^{-1}	60 s^{-1}
0.45 σ_r	15 000 40 000 60 000	15 35 50	quasi-static	1 s^{-1}	60 s^{-1}
0.55 σ_r	1 000 2 500	15 35	quasi-static	1 s^{-1}	60 s^{-1}

Table 2. Loading parameters in trials for the study of coupling fatigue-dynamic

3.4.1. Thermal and damage effects

In order to correspond with the conditions of use of the automobile structures, the fatigue tests were carried out at a frequency of 30Hz. In Fig. 10, the changes in the temperature increase measured during the fatigue tests were reported for applied stresses of 0.38 σ_r, 0.45 σ_r and 0.55 σ_r.

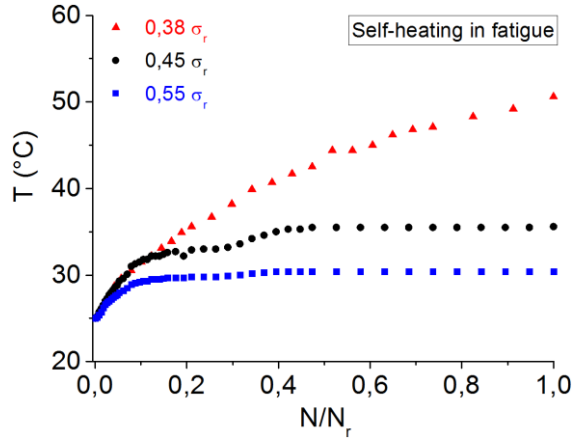

Fig. 10. Temperature variation during fatigue tests at different amplitudes (f = 30Hz)

A temperature which can exceed 50 °C is noted. However, DMTA analysis (Fig. 4) shows no insignificant variations in this temperature range. Consequently, part of the decrease in stiffness measured in Figs. 8 and 9 are linked to the self-heating phenomenon. Our approach being based on the analysis of the decreases in stiffness due to damage, we must extract the evolution of the relative modulus in the temperature range from 25 °C to 75 °C which corresponds to the zone of the transition β (around 45 °C). It should be remembered that the applied strain amplitude in DMTA test is extremely low and are not able to produce self-heating whatever the frequency.

Our methodology is based on the follow-up of the decreases in stiffness linked to the damage, it is necessary to be freed from the part of the decrease of relative stiffness which is related to the increase of the temperature by self-heating. It is therefore necessary to extract this contribution from the curves in Fig. 9. In order to evaluate this curve, we have used the curves of Fig. 4 and 10 by extracting the thermal part induced by the self-heating $(E/E0)_T$ in considering that:

$$\frac{E}{E_0} = 1 - (\frac{E}{E_0})_T - (\frac{E}{E_0})_D \qquad (10)$$

Or $(\frac{E}{E_0})_D$ corresponds to the decrease in stiffness due only to damage. This treatment is illustrated in the case of the amplitudes of 0.38 σ_r, 0.45 σ_r and 0.55 σ_r on the curves of Fig. 11. It should be noted that for this frequency, the thermal part remains relatively limited except for the amplitude of 0.55 σ_r.

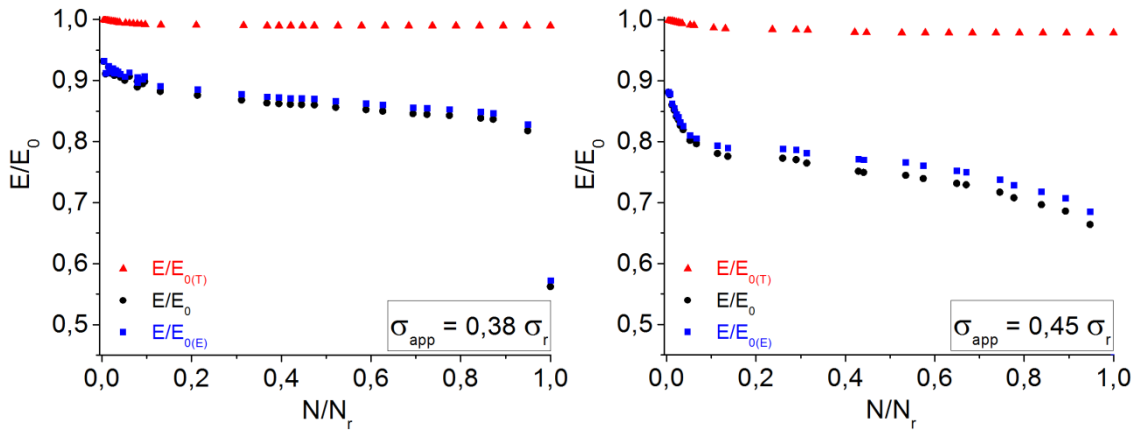

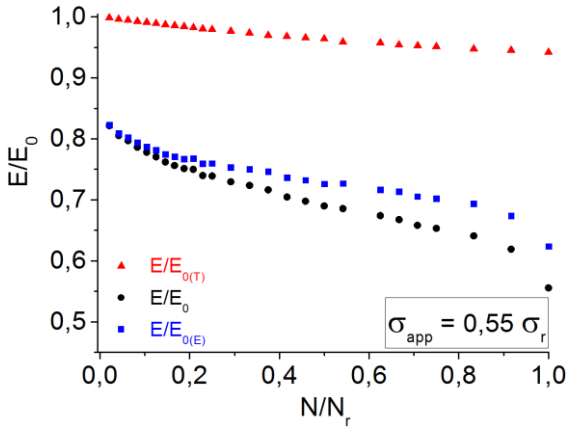

Fig. 11. Decomposition on the thermal part and on the part related to the damage;

(a) 0.38 σ_r, (b) 0.45 σ_r and (c) 0.55 σ_r

3.5. Tensile curves of dynamic post-fatigue loading

Tensile tests at different strain rates (from QS to 60 s^{-1}) were performed on the pre-fatigued RO-A-SMC samples with three stress amplitudes of 0.38 σ_r, 0.45 σ_r and 0.55 σ_r, according to the protocol presented in table 2. By way of example, the stress-strain curves (σ-ε) plotted for different strain rates and different lifetime fraction values (N/N_r) for stress amplitudes of 0.38 σ_r are shown in Fig. 12. It should be noted that for all the pre-damaged curves, the curves of monotonic traction tests are established for each strain rate. It is clear that after the coupling fatigue dynamic tests, the pre-damaged samples have a lower modulus of elasticity, failure stress and strain than the virgin samples. One can notice that normalized stress (respectively strain) = stress (respectively strain) / ultimate stress (respectively strain) obtained for quasi-static tensile tests serving as a reference.

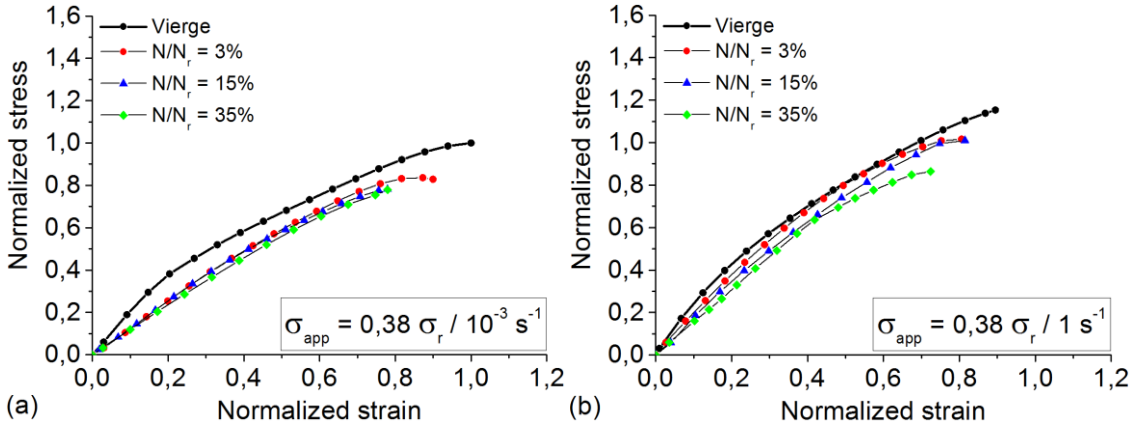

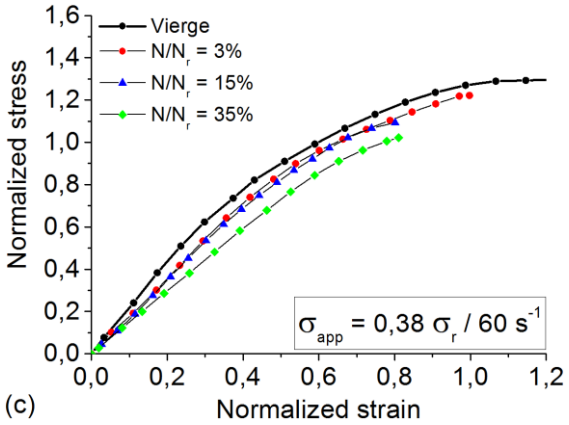

Fig. 12. Experimental stress-strain curves for coupled loading of fatigue crash at applied stress of 0.38 σ_r and distinct values of lifetime fraction (N/N_r): (a) quasi-static, (b) 1 s^{-1} and (c) 60 s^{-1}

3.6. Effects of rapid (dynamic) post-fatigue loading on residual stiffness

Prior to tensile stage (after fatigue stage) the elastic modulus (initial slopes of the stress-strain curves) of all tests were measured by quasi-static tensile tests with the force equivalent to 50% of maximum applied stress during fatigue stage. These values are helpful to compare with the elastic moduli after tensile tests at different strain rates. Results show the values are similar. Fig. 13 shows E/E_0 for pre-damaged A-SMC obtained from tensile test as a function of strain rate for different fatigue loading conditions. Tensile results of pre-damaged A-SMCs show the elastic modulus remains insensitive to strain rate.

For the tensile tests at different strain rates (from QS to 60 s^{-1}) performed on fatigued samples under different conditions (amplitude and cycle numbers), we plotted the evolution of the relative modulus (E/E_0) as a function of lifetime fraction (N/N_r) in Fig. 14.

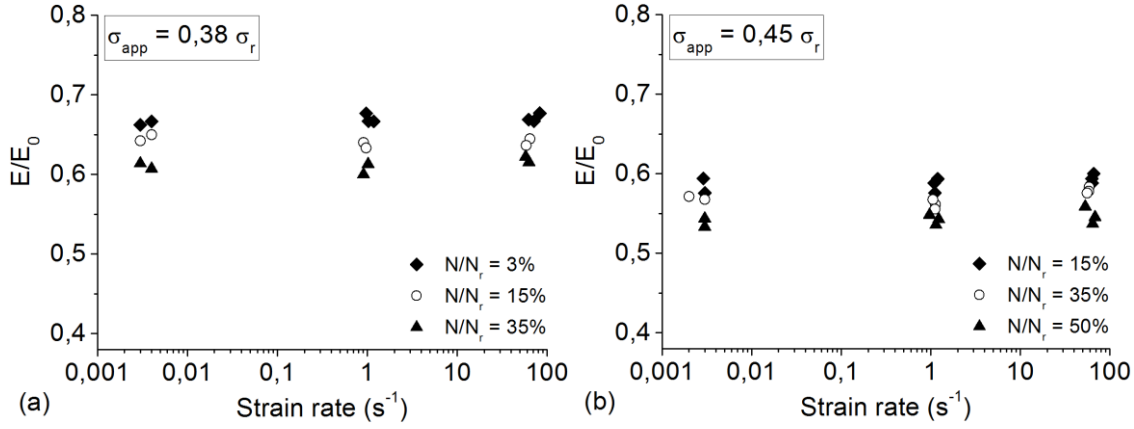

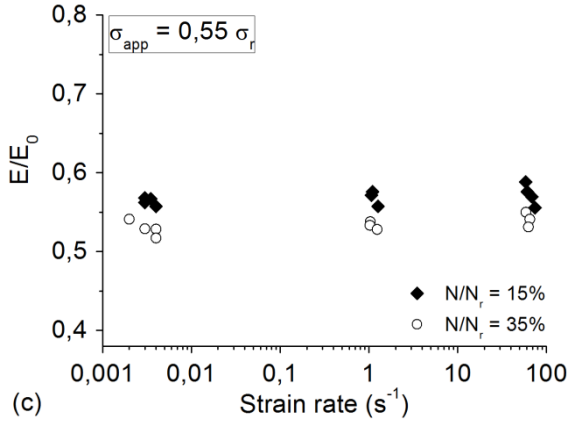

Fig. 13. Influence of strain rate on the elastic modulus:

(a) σ_{app} = 0.38 σ_r, (b) σ_{app} = 0.45 σ_r, (c) σ_{app} = 0.55 σ_r

The results show that the amplitude of loading plays an important role in the evolution of Young's modulus. When the applied stress is 0.55 σ_r with the lifetime fraction (N/N_r) of 15%, the modulus of elasticity decreased about 43%; whereas this value is similar to that of a fatigued sample with an applied stress of 0.45 σ_r and a lifetime fraction (N/N_r) of 35%. The curves also show that the decrease of Young's modulus of the pre-damaged sample with amplitude of 0.38 σ_r is less than that of fatigue with amplitude of 0.55 σ_r. This is true for all samples at different lifetime fractions (N/N_r). In other words, the curve of the modulus of the fatigued samples of 0.38 σ_r remains above two other obtained curves.

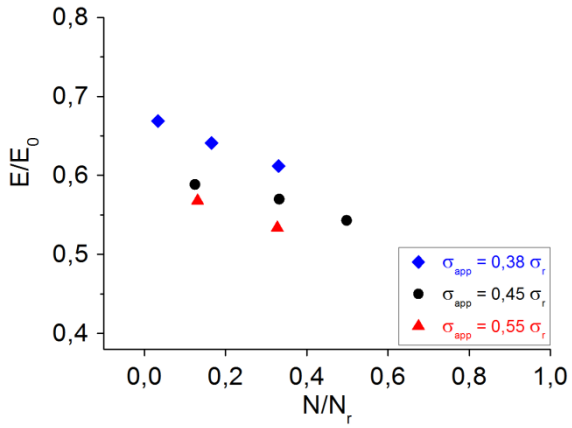

Fig. 14. Evolution of Young Modulus of fatigued samples under different conditions

(tensile tests are carried out at the rate of 60 s^{-1})

3.7. Effect of the strain rate on the characteristics of the pre-damaged material in fatigue

Material characteristics, namely damage thresholds corresponding to the first non-linearity ($\sigma_{threshold}$; $\varepsilon_{threshold}$) and ultimate stress and strain ($\sigma_{ultimate}$; $\varepsilon_{ultimate}$) as a function of strain rate are shown in Figs. 15-17. Normalized stress (respectively strain) = stress (respectively strain) / ultimate stress (respectively strain) obtained for quasi-static tensile tests serving as a reference. Note that the ultimate characteristics correspond to the maximum stress level (before delamination when it occurs). However, the non-linear overall response of the A-SMCs and pre-damage A-SMCs composites are drastically influenced by strain rate. Moreover, the damage threshold, in terms of stress and strain, is increased with strain rate in all tests.

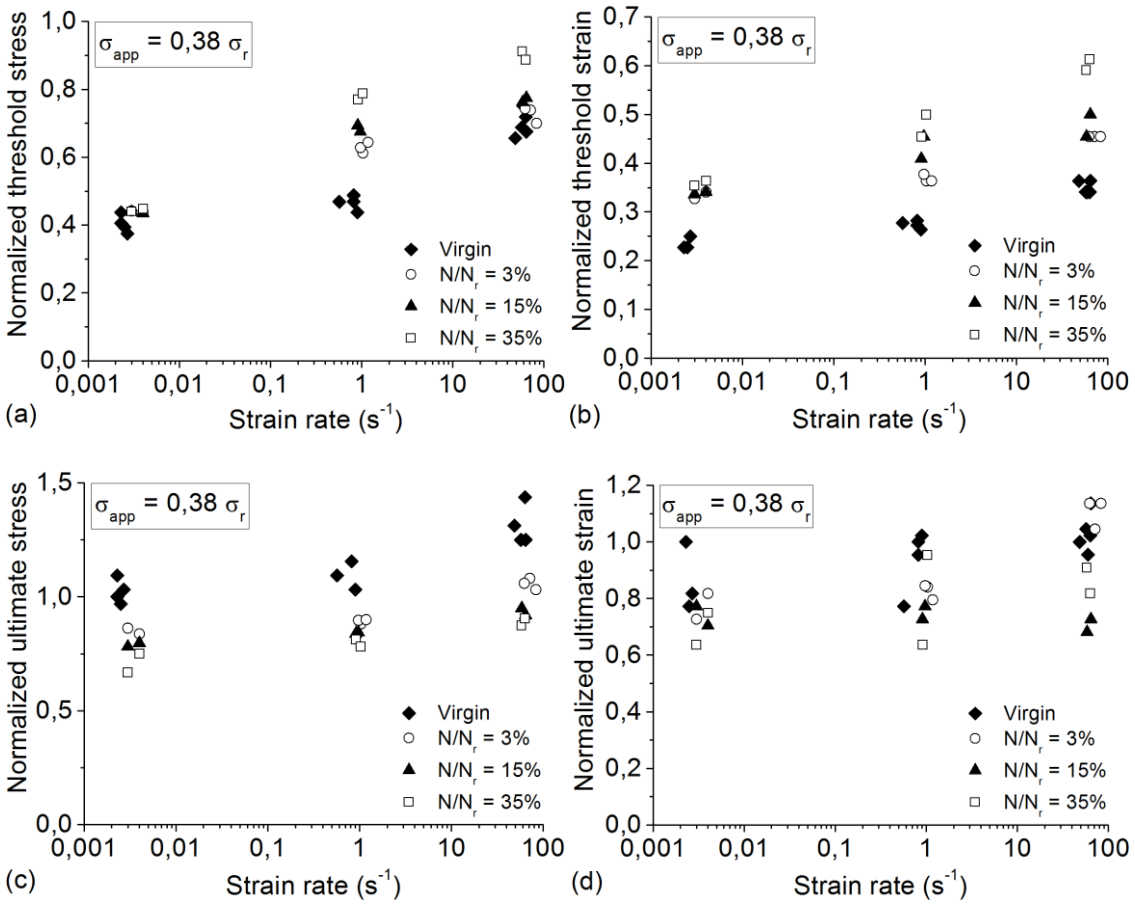

Fig. 15. Influence of strain rate on: (a) Normalized threshold stress, (b) Normalized threshold strain, (c) Normalized ultimate stress and (d) Normalized ultimate strain; (σ_{app} = 0.38 σ_r)

One can note that for all tests, no significant strain rate effect is noticed on the ultimate strain.

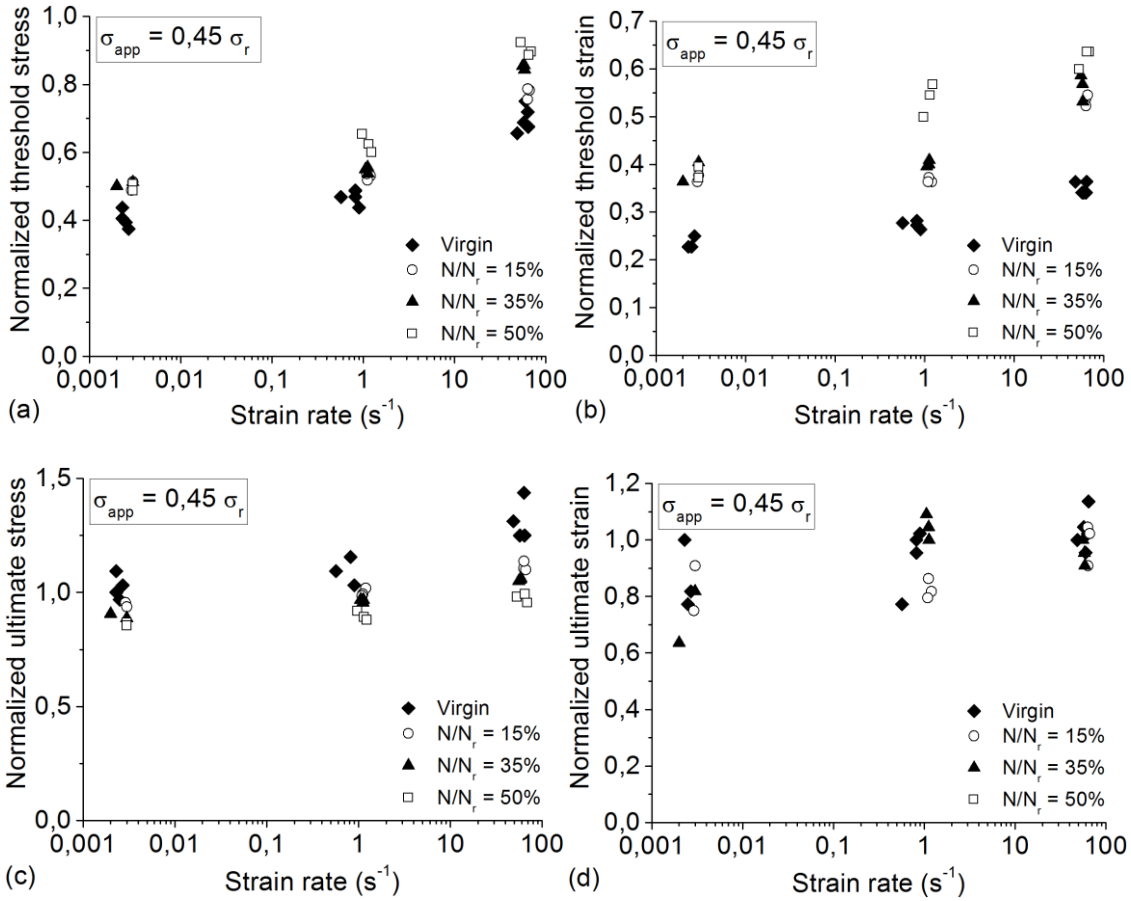

Fig. 16. Influence of strain rate on: (a) Normalized threshold stress, (b) Normalized threshold strain, (c) Normalized ultimate stress and (d) Normalized ultimate strain; (σ_{app} = 0.45 σ_r)

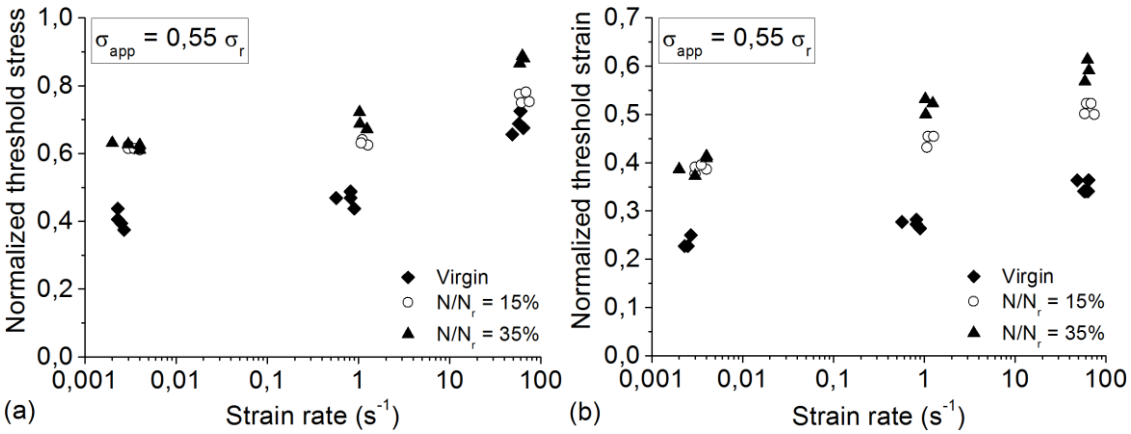

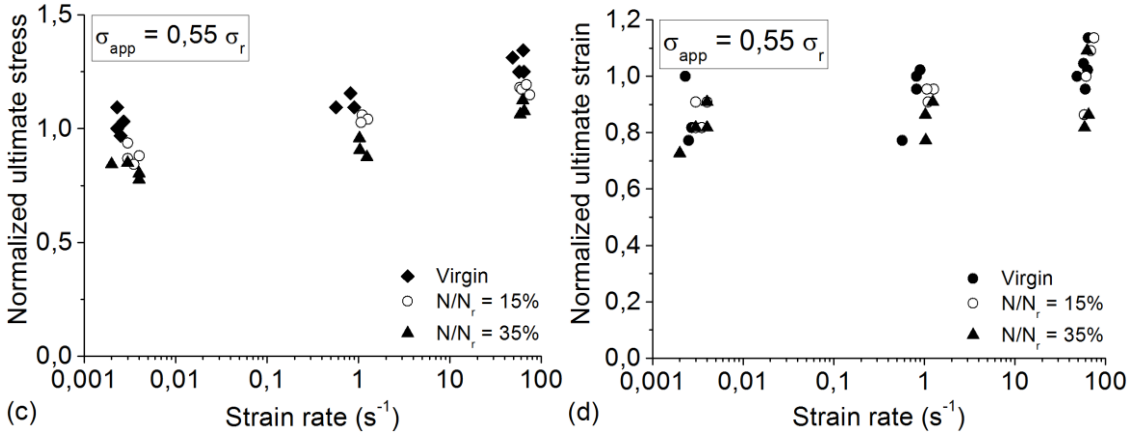

Fig. 17. Influence of strain rate on: (a) Normalized threshold stress, (b) Normalized threshold strain, (c) Normalized ultimate stress and (d) Normalized ultimate strain; (σ_{app} = 0.55 σ_r)

3.7.1. Evolution of the ultimate properties

As mentioned above, according to the curves of Fig. 12 for applied stress of 0.38 σ_r, it is observed that the pre-damaged samples have a remaining mechanical potential, lower than the virgin samples: For example, the ultimate stress of the virgin sample is about 50% more than pre-damaged sample up to 10^6 cycles.

It can also be seen that the fatigued samples undergo the impact of the strain rate with the same intensity whatever the degree of imposed lifetime fraction. Indeed, the curves of the failure stress as a function of the strain rate remain to parallel whatever the considered fraction of lifetime. This is shown on the evolution curves of the relative value $\frac{\sigma^{r(\dot{\varepsilon})}}{\sigma^{r}_{QS}}$ (Fig. 18) which indicates a single curve as a function of the strain rate whatever the loading amplitude and the imposed lifetime. This allows us to conclude that there is no significant effect of fatigue on sensitivity to strain rate at the level of local phenomena which leads to rupture.

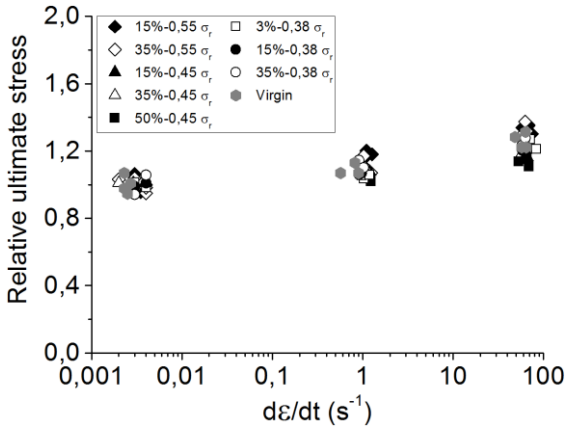

Fig. 18. Relative value of the ultimate stress for different values of the imposed amplitudes and the lifetime fractions

3.7.2. Evolution of the damage threshold

The effect of strain rate on the damage threshold of the post-fatigue samples is much more important. It is more marked when the fraction of lifetime increases. The evolution of the relationship $\frac{\sigma^{seuil}(\dot{\varepsilon})}{\sigma_{QS}^{seuil}}$ for two values of the lifetime fractions (15% and 35%) highlights (figure 19) that, regardless of the degree of damage affected in fatigue, sensitivity to the strain rate decreases when the applied stress increases in fatigue test. Indeed, when the applied stress in fatigue is important, structural changes associated with the accumulated local micro deformation can contribute to decrease the delay effect of the visco-damageable. On the other hand, for lower amplitudes, the structural changes of the matrix and areas close to the fiber-matrix interface are more limited. Moreover, it can be noted that when the degree of damage affected in fatigue is important, sensitivity to strain rate increases (see figure 20). This points out that the viscous effect of damage is strongly related to the propagation of micro-cracks pre-existing in fatigue test. The propagation of cracks initiated at the fiber-matrix interface is predominant damage mechanism for A-SMC composite. Note that the delay effect observed on the initiation of new cracks in the fiber-matrix interface can also participate in a greater sensitivity to the strain rate.

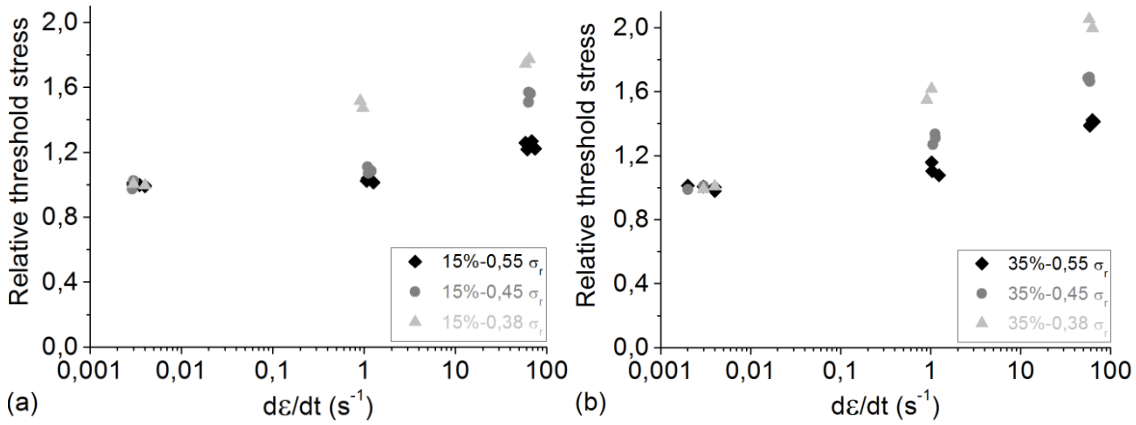

Fig. 19. Relative threshold stress in post-fatigue samples depending on the strain rate for different values of the lifetime fraction: (a) 15% and (b) 35%

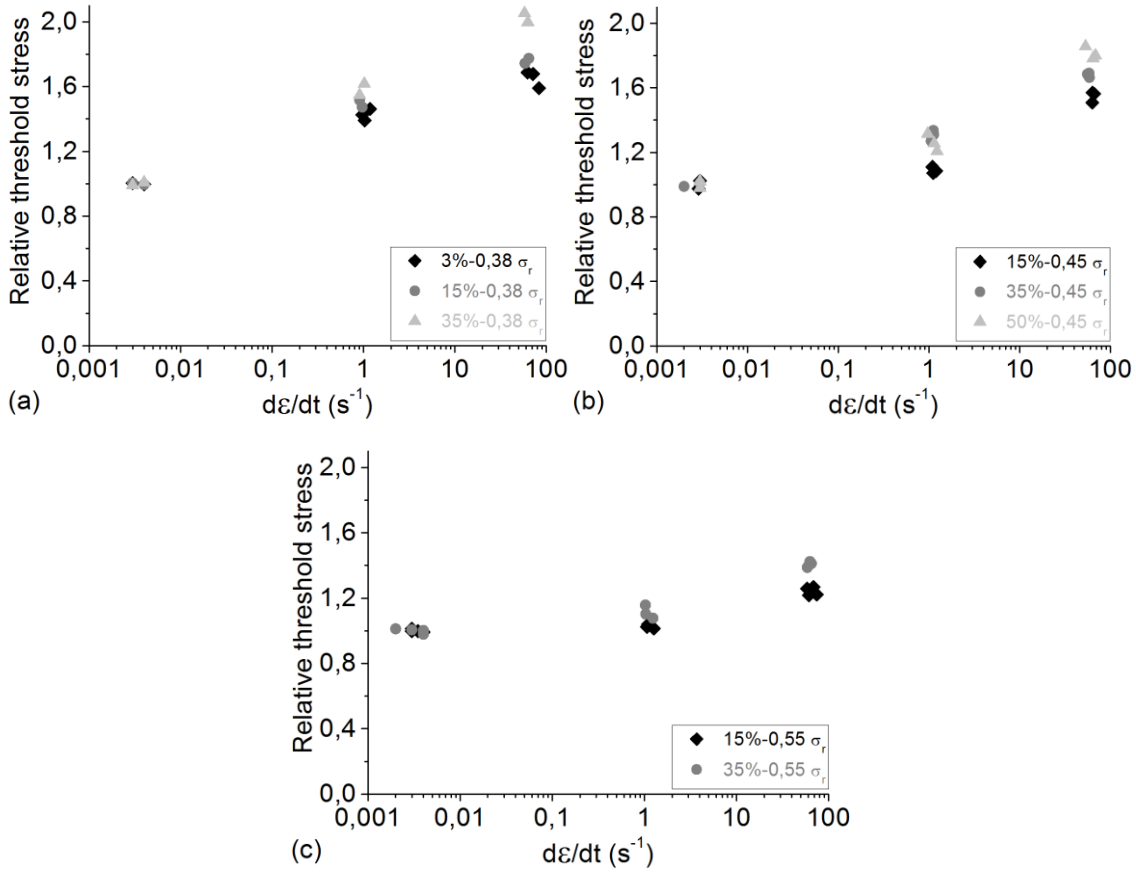

Fig. 20. Sensitivity to strain rate for post-fatigue samples with varying degrees of damage: (a) $\sigma_{app} = 0.38\ \sigma_r$, (b) $\sigma_{app} = 0.45\ \sigma_r$, (c) $\sigma_{app} = 0.55\ \sigma_r$

3.7.3. Evolution of the deviation related to the fatigue loading

A way to quantify the specific residual effect of dynamic post-fatigue behavior is to analyze the evolution of the gap between the measured post-fatigue properties and those of reference corresponding to an equivalent pre-damaged made under monotonous tensile test (see figure 21).

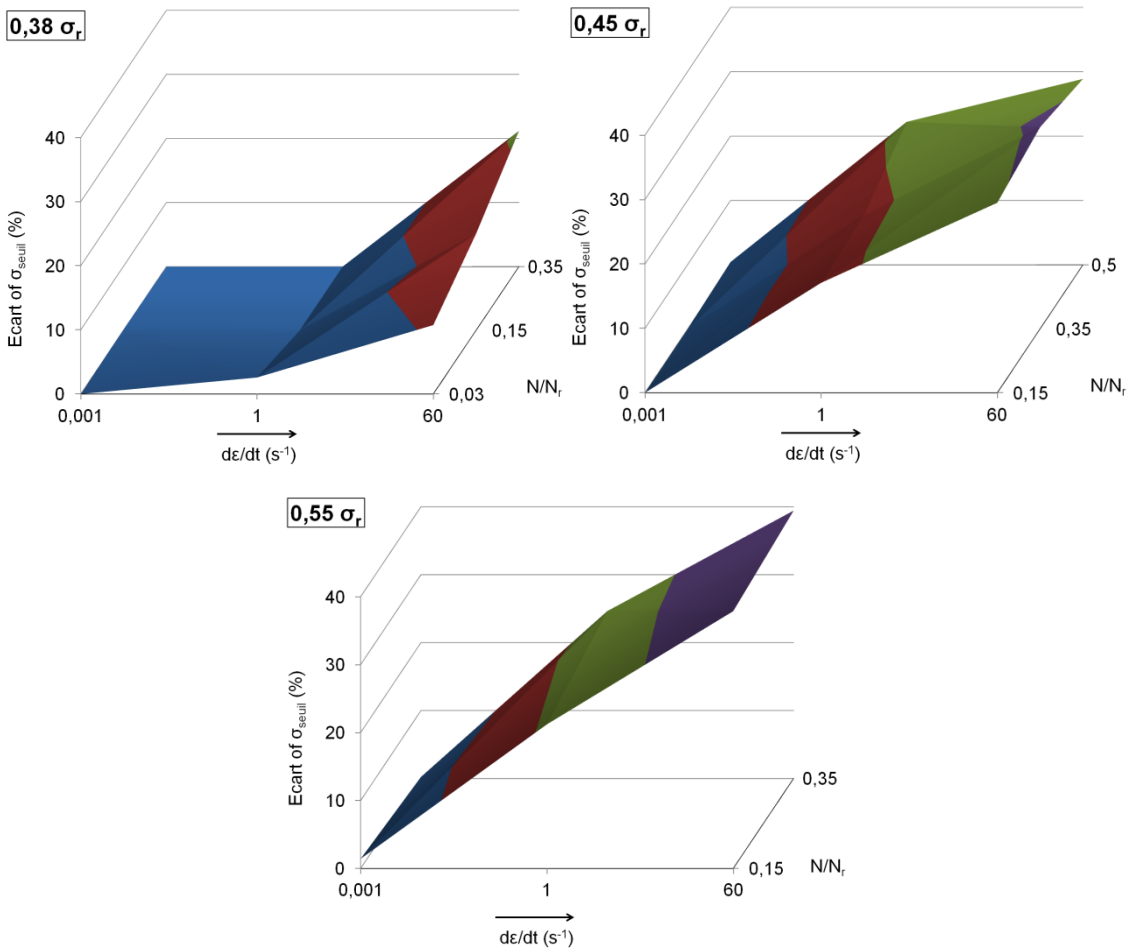

Fig. 21. Evolution of the gap between the measured post-fatigue properties and those of reference at different strain rates; (a) σ_{app} = 0.38 σ_r, (b) σ_{app} = 0.45 σ_r, (c) σ_{app} = 0.55 σ_r

It was stated that the origin of the observed gap between post-fatigue curves and those of monotonous tensile tests is attributed to specific phenomena developed in fatigue. This gap is presented in figure 20 in terms of damage threshold. Overall, we can conclude that the effect of a solicitation of type fatigue on the threshold in quasi-static tensile test is low, even negligible, and becomes important at high strain rate. This effect is specially marked at high applied

amplitude and more affected lifetime fraction in fatigue test. Indeed, for larger values of fraction of lifetime, one can note that the gaps reach of the values on the order of 20%, 30% and 40% for the amplitude values of 0.38 σ_r, 0.45 σ_r and 0.55 σ_r, respectively. These developments confirm the analysis made above.

4. Conclusion

Based on the results, the following conclusions may be drawn:

- A-SMC Fatigue behavior at frequency of 30Hz shows that at maximum applied stress equal to 0.45 σ_r, the fatigue life is about 10^5 cycles when the fatigue life is about 2×10^6 cycles for a maximum applied stress of 0.38 σ_r. Therefore, an applied stress variation of 15% leads to a fatigue life 20 times higher.
- The methodology proposed in this paper consists in comparing the iso-damage evolution curves (modulus E) obtained from post-fatigue dynamic tests to those which can be obtained in monotonic dynamic traction. The comparison has been made on successive equivalent E damage states corresponding to different values of the lifetime fraction, N/N_r. The remaining potential of a pre-damaged sample is then compared with the pre-damaged monotonic tension at different strain rates. The differences observed between the post-fatigue and the monotonic tensile evolutions will be attributed to the specific phenomena developed in fatigue.
- Tensile results of pre-damaged A-SMCs show the elastic modulus remains insensitive to strain rate.
- The experimental results show in the case of applied stress of 0.55 σ_r after 15% of the lifetime fraction in fatigue test, the value of elastic modulus is decreased about 31% while this value is equal to post-fatigue dynamic test after 50% of the lifetime fraction in the case of applied stress equal to 0.45 σ_r. One can note the effect of applied amplitude and lifetime fraction for A-SMC behavior during post-fatigue dynamic test is significant.
- It is observed that the pre-damaged samples have a remaining mechanical potential, lower than the virgin samples: For example, the ultimate stress of the virgin sample is about 50% more than pre-damaged sample up to 10^6 cycles.

- There is no significant effect of fatigue on sensitivity to strain rate at the level of local phenomena which leads to rupture.
- In spite of the degree of damage affected in fatigue, sensitivity to the strain rate decreases when the applied stress increases in fatigue test. When the applied stress in fatigue is important, structural changes associated with the accumulated local micro deformation can contribute to decrease the delay effect of the visco-damageable. This points out that the viscous effect of damage is strongly related to the propagation of micro-cracks pre-existing in fatigue test.
- It was stated that the origin of the observed gap between post-fatigue curves and those of monotonous tensile tests is attributed to specific phenomena developed in fatigue. This effect is specially marked at high applied amplitude and more affected lifetime fraction in fatigue test.

5. References

[1] Thornton PH, Edwards PJ. Energy absorption in composite tubes. Journal of Composite Materials. 1982;16(6): 521-45.

[2] Uenishi A, Kuriyama Y, Yoshida H, Takahashi M. Material Characterization at High Strain Rates for Optimizing Car Body Structures for Crash Events. Nippon Steel Technical Report. 2003;88.

[3] Obradovic J, Boria S, Belingardi G. Lightweight design and crash analysis of composite frontal impact energy absorbing structures. Composite Structures. 2012;94(2): 423-30.

[4] Alia RA, Cantwell WJ, Langdon GS, Yuen SCK, Nurick GN. The energy-absorbing characteristics of composite tube-reinforced foam structures. Composites Part B: Engineering. 2014;61: 127-35.

[5] Jacob GC, Fellers JF, Simunovic S, Starbuck JM. Energy absorption in polymer composites for automotive crashworthiness. Journal of Composite Materials. 2002;36(7): 813-49.

[6] Guster C, Pinter G, Mosenbacher A, Eichlseder W. Evaluation of a Simulation Process for Fatigue Life Calculation of Short Fibre Reinforced Plastic Components. Procedia Engineering.10(0): 2104-9.

[7] Wang SS, Suemasu H, Chim ESM. Analysis of fatigue damage evolution and associated anisotropic elastic property degradation in random short-fiber composite. Engineering Fracture Mechanics. 1986;25(56): 829-44.

[8] Mortazavian S, Fatemi A. Fatigue behavior and modeling of short fiber reinforced polymer composites including anisotropy and temperature effects. International Journal of Fatigue.2015; 77: 12-27.

[9] Atodrais D.R, Putatundaa S.K, Mallick P.K. Fatigue crack growth model and mechanism of a random fiber SMC composite. Polymer Composites. 20(2): 240-9.

[10] Bellenger V, Tcharkhtchi A, Castaing P. Thermal and mechanical fatigue of a PA66/glass fibers composite material. International Journal of Fatigue. 2006;28(10): 1348-52.

[11] Esmaeillou B, Ferreira P, Bellenger V, Tcharkhtchi A. Fatigue behavior of polyamide 66/glass fiber under various kinds of applied load. Polymer Composites.33(4): 540-47.

[12] Esmaeillou B, Fitoussi J, Lucas A, Tcharkhtchi A. Multi-scale experimental analysis of the tension-tension fatigue behavior of a short glass fiber reinforced polyamide composite. Procedia Engineering.10(0): 2117-22.

[13] Shirinbayan M, Fitoussi J, Meraghni F, Surowiec B, Bocquet M, Tcharkhtchi A. High strain rate visco-damageable behavior of Advanced Sheet Molding Compound (A-SMC) under tension. Composites Part B: Engineering, 2015;3670(82): 30-41.

[14] Fitoussi J, Guo G, Baptiste D. A statistical micromechanical model of anisotropic damage for S.M.C. composites. Composites Science and Technology. 1998;58(5): 759-63.

[15] Fitoussi J, Bocquet M, Meraghni F. Effect of the matrix behavior on the damage of ethylene-propylene glass fiber reinforced composite subjected to high strain rate tension. Composites Part B: Engineering. 2013;45(1): 1181-91.

[16] Fitoussi J, Meraghni F, Jendli Z, Hug G, Baptiste D. Experimental methodology for high strain-rates tensile behaviour analysis of polymer matrix composites. Composites Science and Technology. 2005;65(14): 2174-88.

[17] Jendli Z, Meraghni F, Fitoussi J, Baptiste D. Micromechanical analysis of strain rate effect on damage evolution in sheet molding compound composites. Composites Part A: Applied Science and Manufacturing. 2004;35(7-8): 779-85.

[18] Jendli Z, Fitoussi J, Meraghni F, Baptiste D. Anisotropic strain rate effects on the fibre-matrix interface decohesion in sheet moulding compound composites. Composites Science and Technology. 2005;65(3-4): 387-93.

[19] WP Jia, JV Fernandes. Mechanical behaviour and the evolution of the dislocation structure of copper polycrystal deformed under fatigue–tension and tension–fatigue sequential strain paths. Materials Science and Engineering: A, 2003.

[20] D Ray, B.K Sarkar, N.R Bose. Impact fatigue behaviour of vinylester resin matrix composites reinforced with alkali treated jute fibres. Composites Part A: Applied Science and Manufacturing. 2002;33(02): 233-41.

[21] J Epaarachchi. Effects of static–fatigue (tension) on the tension–tension fatigue life of glass fibre reinforced plastic composites. Composite Structures. 2005;74(04): 419-25.

[22] Le TH, Dumont PJJ, Orgéas L, Favier D, Salvo L, Boller E. X-ray phase contrast microtomography for the analysis of the fibrous microstructure of SMC composites. Composites Part A: Applied Science and Manufacturing. 2008;39(1): 91-103.

[23] Palmer J, Savage L, Ghita OR, Evans KE. Sheet moulding compound (SMC) from carbon fibre recyclate. Composites: Part A: Applied Science and Manufacturing. 2010;41(9): 1232-7.

[24] ID19 ESRF. <http://www.esrf.eu/UsersAndScience/Experiments/Imaging/ID19>.

[25] M. Shirinbayan, J. Fitoussi, M. Bocquet, F. Meraghni, B. Surowiec, A. Tcharkhtchi. Multi-scale experimental investigation of the viscous nature of damage in Advanced Sheet Molding Compound (A-SMC) submitted to high strain rates. Composites Part B: Engineering, 2016, Article in press.

[26] M. Shirinbayan, J. Fitoussi, F. Meraghni, M. Laribi, B. Surowiec, A. Tcharkhtchi. Coupled effect of loading frequency and amplitude on the fatigue behavior of Advanced Sheet Molding Compound (A-SMC). Journal of Reinforced Plastics and Composites, Article in press.

[27] Ye L. On fatigue damage accumulation and material degradation in composite materials. Composites Science and Technology. 1989;36(4):339-350.

[28] Fleckenstein J, Jaschek K, Büter A, Stoess N. Fatigue design optimization of safety components made of SMC. Procedia Engineering.10(0):390-396.

[29] D. R. Atodaria, S. K. Putatunda, P. K. Mallick. Fatigue Crack Growth Model and Mechanism of a Random Fiber SMC Composite, 1999, 20(2): 240-9.

[30] D. Krajcinovic, S. Mastilovic. Some fundamental issues of damage mechanics. Mechanics of Materials, 1995, 21(3): 217-230.

[31] D. Krajcinovic. Selection of damage parameter - Art or science. Mechanics of Materials, 1998, 28(1-4): 165-179.

ÉTUDE DU COMPORTEMENT MÉCANIQUE ET DE L'ENDOMMAGEMENT DE DIVERS MATÉRIAUX COMPOSITES SMC SOUMIS À DES CHARGEMENTS DE TYPE DYNAMIQUE, FATIGUE ET DYNAMIQUE POST-FATIGUE

RESUME : Le dimensionnement au crash des structures automobiles en matériaux composites à renforts discontinus tels que les SMC est généralement réalisé sur la base de données expérimentales recueillies sur des matériaux vierges n'ayant subi aucun chargement depuis leur mise en œuvre. Or, les accidents proviennent après quelques années de mise en service durant lesquelles la structure composite est soumise généralement à des sollicitations de type fatigue à plus ou moins grande amplitude. La prise en compte d'un pré-endommagement éventuel en fatigue devient alors essentielle si l'on veut rester réaliste. Par ailleurs, de nouvelles formulations de matériaux composites SMC ont été récemment développées. Leur comportement en fatigue et sous sollicitation rapide étaient jusqu'à lors inexplorés. Cette étude à caractère fortement expérimentale a donc pour but d'apporter la connaissance nécessaire au dimensionnement de structures en matériaux SMC de diverses formulations, notamment le A-SMC et le LD-SMC. Le premier correspond à une matrice vinylester fortement renforcée de mèches de fibres de verre (50%). Le second correspond à une formulation proche de celle d'un SMC standard dans laquelle on a rajouté un fort taux de billes de verre creuse afin de réduire la densité. Une analyse multi-échelle permet de mettre en évidence l'influence de la microstructure sur les phénomènes d'endommagement sous sollicitation quasi-statique, dynamique et fatigue. Des méthodes originales d'analyse expérimentale sont développées afin de corréler ces mécanismes aux comportements macroscopiques observés. Les essais dynamiques rapides optimisés sont réalisés jusqu'à des vitesses de déformation de l'ordre de 80 s^{-1} et mettent en évidence un comportement visco-endommageable pour les deux matériaux SMC étudiés. Le décalage du seuil d'endommagement et la baisse de la cinétique d'endommagement observés à l'échelle macroscopique sont directement corrélés au seuil et cinétique des mécanismes d'endommagement observés à l'échelle locale telles que la rupture à l'interface fibre-matrice ou bille-matrice, la microfissuration de la matrice et le pseudo-délaminage entre les mèches de fibres de verre. Par ailleurs, une analyse multi-échelle du même type est également réalisée sous sollicitation de type fatigue dans laquelle les fréquences varient de 10 à 100 Hz. Une étude de l'influence des phénomènes d'auto-échauffement sur l'endommagement et le comportement du A-SMC est proposée. Enfin, une analyse originale des propriétés résiduelles sous sollicitation rapide d'échantillons préalablement fatigués à différents niveaux de fraction de durée de vie met en évidence une forte influence de l'histoire du chargement sur la sensibilité du A-SMC à la vitesse de sollicitation. L'ensemble des résultats de cette étude, de par son apport de compréhension des phénomènes mis en jeu, constitue la base expérimentale nécessaire à la construction d'outils de dimensionnement adaptés aux structures SMC sous sollicitations cycliques et dynamiques.

Mots clés : Comportement Mécanique, Endommagement, Composite SMC, Dynamique, Fatigue.

STUDY OF MECHANICAL AND DAMAGE BEHAVIOR OF SMC COMPOSITE MATERIALS SUBJECTED TO DYNAMIC, FATIGUE AND POST-FATIGUE DYNAMIC LOADINGS

ABSTRACT: Classically, crash design of automotive composite structures made of discontinuous reinforcements such as SMC is usually based on experimental data obtained from virgin materials without any history of loading. However, crash events always occur after a few years of use during which composite structure is generally subjected to more or less important fatigue loading. Taking into account of a potential pre-damage in fatigue becomes essential if we want to stay realistic. Moreover, new formulations of SMC composites have been developed recently. Up to now, their fatigue and dynamic behavior were never being explored. This study, of a mostly experimental nature, aims to provide the knowledge necessary for design of structures made of various SMC formulations including A-SMC and LD-SMC. The first one is a vinylester matrix reinforced with a high content of glass fibers (50%). The second corresponds to a standard SMC formulation in which we added a high content of hollow glass micro-sphere in order to reduce density. A systematic multi-scale analysis allows to highlight the influence of the microstructure on damage phenomena under quasi-static, dynamic and fatigue loading. Original experimental methods are developed to correlate these mechanisms to the observed macroscopic behavior. Optimized dynamic tests are performed at strain rate up to 80 s^{-1} and highlight a visco-damageable behavior for the two SMC materials in study. Damage threshold delay and reduction of damage kinetics observed at the macroscopic scale are directly correlated to the threshold and kinetic of damage development observed at the local scale such as fiber-matrix or matrix-microsphere interfaces, matrix micro-cracking and pseudo-delamination between the bundles of glass fiber. Moreover, a similar multi-scale analysis is also performed under fatigue loading in which the frequency ranges from 10 to 100 Hz. A study of the influence of the self-heating phenomenon on the fatigue damage behavior of A-SMC is proposed. Finally, an original analysis of the remaining dynamic properties of samples which were previously submitted to fatigue loading until different levels of lifetime highlights a strong influence of the history of the loading on the strain rate sensitivity of the A-SMC. Considering the high contribution of this study in term of comprehension of the phenomena involved in the mechanical response of SMC materials, all of the experimental findings of this study provide the physical background crucial to build structural design tools for SMC subjected to cyclic and dynamic loading.

Keywords: Mechanical behavior, Damage, SMC composite, Dynamic, Fatigue.

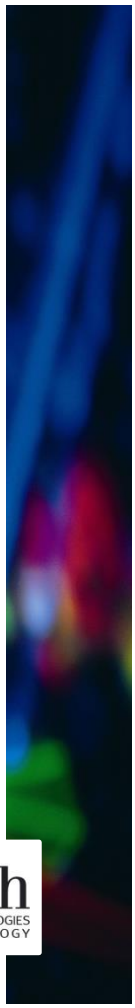

ARTS ET MÉTIERS ParisTech

ParisTech INSTITUT DES SCIENCES ET TECHNOLOGIES PARIS INSTITUTE OF TECHNOLOGY